DYNAMIC AND MASS TRANSFER PHENOMENA OF SPHERICAL CAPPED BUBBLES

A Thesis
presented for the Degree of
Doctor of Philosophy

by

RODERICK IAN LAWRENCE GUTHRIE

Department of Metallurgy,
The Royal School of Mines,
May, 1967.

ABSTRACT

The velocities of single bubbles in the size range 1.1 to 2.5 cm equivalent radius (5 to 65 cm^3 volume) rising in various liquids including molten silver, have been measured. The dynamic behaviour of large bubbles in molten metals was found to be similar to that in other liquids.

Velocities and shapes of spherically capped bubbles in aqueous systems were studied in an 18" I.D. column to minimise Wall Effects, and were inter-related by a simple model based on potential flow around a spherical segment.

A study of the 'enclosed' wakes carried behind large bubbles (rising in liquids of various viscosities) has shown flow patterns to be similar to those established behind bluff bodies. An approximate mass transfer coefficient, (between the wake and the bulk) has been obtained for bubbles rising in water.

Instantaneous rates of mass transfer of carbon dioxide between single bubbles and liquids have been measured. Rates of absorption and desorption were observed to be similar. The damping of ripples on bubble surfaces by surface active agents markedly reduced rates of transfer. Bubbles whose equivalent radii exceeded about 1.3 cm absorbed at an unsteady rate.

A technique for the measurement of rates of transfer between single bubbles and liquids at high temperature has been developed. Instantaneous rates of mass transfer between oxygen bubbles in the size range of 1 to 1.5 cm equivalent radius and molten silver are slightly less than those predicted by unsteady state diffusion theory. This discrepancy indicates the possibility of surface active effect or chemical control.

TABLE OF CONTENTS

CHAPTER 1.

1.0 INTRODUCTION

Gas Bubble Systems in Metallurgy.

Many metallurgical processes involve interactions between gas bubbles and liquids. Examples include the removal of carbon as carbon monoxide in steelmaking, blowing air through copper matte to remove sulphur in copper refining, and the removal of hydrogen from steel during vacuum degassing in a ladle.

General Purpose of Present Programme of Investigation.

In many of the processes involving gas bubbles rising in metals, the thermodynamics are insufficiently well known to enable a precise estimate to be made of equilibrium conditions. However, it is far more difficult to predict the rates at which such processes occur. Consequently, the investigation covered in this thesis is part of a programme designed to obtain a better understanding of the important factors influencing mass transfer between gases and liquids in metallurgical systems.

In particular, information is required on the rate of decarburisation of iron by the reaction [C] + [O] → CO gas, as well as the removal of gaseous elements, such as hydrogen, which are in solution in iron.

1.1 FACTORS GOVERNING THE RATE OF PROCESSES

The overall rate at which a reaction proceeds depends upon the rates at which the individual steps in the sequence occur. In the

case of the transfer of dissolved carbon and oxygen from molten iron into a rising bubble, the following steps are involved.

1) transport of dissolved carbon and oxygen atoms from the bulk liquid to the interface,
2) adsorption of the atoms at sites on the interface,
3) reaction at the interface to form a CO molecule,
4) desorption of the product CO from the interface into the gas phase,
5) transport of the CO into the bulk of the gas bubble. (In the event of transport taking place to a pure CO bubble, this step is not relevant).

The removal of hydrogen by vacuum degassing is an analogous process to that described above. In this case, step 1 consists of transport of hydrogen atoms, step 3 forms H_2 molecules. Step 5 may be important if the gas/metal interface is provided by purging with an inert gas.

In many cases (e.g. CO formation in steelmaking), estimated chemical reaction rates at typical steelmaking temperatures are far higher ($\sim 10^5$ times) than observed process rates (1, 34.). Also provided rates of adsorption and desorption are very rapid, as would be expected on the basis of hydrogen adsorption and effusion in Alpha Iron [63], steps 1 or 5 will determine the rate of mass transfer, and the process may be considered to be transport controlled.

1.1.1. The Mass Transfer Coefficient

In the case of liquid phase transport control, the rate of gas absorption into the liquid phase from rising bubbles may be expressed in terms of a mass transfer coefficient defined by the equation

$$\dot{n} = k_L A_e (C_I - C_B) \qquad 1.1 - 1.$$

Where $\dot{n}$ = flux of diffusing species (Gm. Atoms or moles/sec.)

k_L = mass transfer coefficient of diffusing species (cm sec^{-1})

C_I = interfacial concentration of dissolved species (Gm. Atoms or moles/cc of liquid)

C_B = bulk liquid concentration of dissolved species (Gm. Atoms or moles/cc of liquid)

A_e = Surface Area of an equivalent volume sphere.

Throughout this work, k_L is defined as in equation 1.1. -1.

1.2. GENERAL PLAN OF EXPERIMENTAL WORK

Because of experimental difficulties, it is not yet possible to carry out experiments on liquid iron, and systems which might offer useful analogies were considered. Furthermore, though many metallurgical processes involve a multiplicity of bubbles (bubble swarms), it was decided to conduct these experiments on single bubbles. These give a better opportunity of studying the basic phenomena (for example mass transfer can be more readily related to the gas/liquid interfacial area than with swarms of bubbles). Also, observations of bubbles in the open hearth process indicate that the size range corresponds to that associated with spherical cap bubbles in water. Thus, the

present work relates specifically to large bubbles rising singly through liquids. From the point of view of simulating liquid phase transport control in steelmaking, two systems were chosen for this work.

1) Aqueous systems

2) Molten silver

Aqueous Systems

Experimental evidence strongly indicates [45] that the mass transfer from a pure CO_2 bubble into water is liquid phase transport controlled. Thus, provided the fluid dynamic conditions of a CO_2 bubble in aqueous solution reproduce those of bubbles in metals, the rate of mass transfer of CO_2 should give some indication of oxygen and/or carbon transfer to CO bubbles in molten iron. In addition, the low temperature systems provided an opportunity of perfecting experimental techniques and procedure prior to high temperature experiments. Since bubbles in metallurgical systems may have to pass through slags of moderate to high viscosity, the aqueous systems studied included polyvinyl alcohol solution, which gave a viscosity range of 1.4 to 730 cp.

Molten Silver

It was deisrable to carry out some experiments on metallurgical systems since extrapolation to gas/metal reactions in steelmaking is less than similar extrapolations from aqueous systems.

Of all the high temperature systems considered for simulating liquid phase transport control, the oxygen-silver system appeared the most satisfactory;

(1) The work of Mizikar, Grace and Parlee indicates that the transport of dissolved oxygen through silver determines the rate of gas absorption [48].

(2) The solution of oxygen in molten silver is typical of many other diatomic gas/metal systems. The solubility of the diatomic gases (H_2, N_2, O_2) in molten metals at pressures less than that at which a second phase is formed, is given by the experimental relation

$$C_B = qP^{1/2}$$

q = Sieverts constant, C_B = concentration of dissolved species (in bulk of silver)(Gm. Atoms/cc liquid)

The above relation indicates that gas is dissociated into atoms during the solution process, and that the reaction between oxygen and silver, for example, may be written as

$$O_2 \rightleftarrows 2[O \text{ in silver}]$$

Similar equations may be written for H_2 in Al, Cu, Fe, Mg; N_2 in Fe, Cr, Mo and O_2 in Cu.

(3) The solubility of oxygen is in the useful range for making measurements of bubble volume changes. As the rate of oxygen transfer can be measured from these volume changes, the need of sampling and analysing the contents of the vessel after each test is avoided. Also, since silver oxides are unstable at 1000°C (1 Atmos), there will be no resistance to oxygen transfer due to the presence of an interfacial oxide phase.

(4) The density and surface tension of silver (9.26 gm/cc and 920 dynes/cm) appreciably extended the range of liquid properties covered by the low temperature work. In addition, the temperature, although high, is manageable, and silver may be contained within a Ni-Cr alloy vessel.

1.3 PREVIOUS WORK IN THIS LABORATORY

A previous investigation on mass transfer in similar systems was carried out by W. G. Davenport [32]. Experiments on aqueous systems were carried out in a 6" I.D. column, where overall mass transfer coefficients, calculated from initial and final volumes, were measured. In addition, since the surface area and shape of bubbles may influence mass transfer these were studied in the aqueous systems and in mercury.

Preliminary experiments on oxygen solution in molten silver were carried out, in which pressure changes within the container were measured by a mercury manometer. However the inertia of the manometer was such that the mass transfer results were of limited accuracy and not reproducible. Also, due to the design of the apparatus, difficulties were encountered in releasing single bubbles from the rotating cup at the bottom of the apparatus, due to silver leakage and solidification along the drive shaft set in the side of the Ni-Cr alloy container.

1.4 PRINCIPLE OBJECTIVE OF PRESENT WORK

CO_2 - Aqueous Systems

A number of outstanding questions left by Davenport's investigation were studied in the present case. These were as follows:

1) Since the previous work was confined to a 6" I.D. column, it was important to find out what effect, if any, was caused by the proximity of the walls on
   a) rising velocities in water and viscous P.V.A. solutions.
   b) shape
   c) mass transfer coefficients.

2) Previous measurements were confined to overall mass transfer coefficients, and results suggested that the transfer rate decreased with time. The present experiments were therefore carried out measuring instantaneous mass transfer coefficients, and investigating any variations with column height.

3) It was hoped that these results would indicate what effect, if any, surface active agents could have on large bubbles, for which there was limited information.

4) With high viscosity P.V.A. solutions, (250 cp) large bubbles had been observed to trail long gas skirts. These had not previously been reported in the literature and it was necessary to ascertain whether they could be due to 'wall effects' in the 6" I.D. column.

   It was also desirable to ascertain whether these skirts became more pronounced at still higher viscosities, whether they were observed in other highly viscous liquids, and to what extent they increased mass transfer rates.

5) A preliminary study of wakes carried behind large bubbles was initiated as a step towards the understanding of mixing processes in systems such as the O - H. Process.

Oxygen-Silver System

6) The mercury manometer used by Davenport for measuring rates of pressure change was of limited accuracy so that the measurement of velocities and mass transfer coefficients required confirmation using an improved method of pressure measurement.

CHAPTER 2.

PREVIOUS WORK

2.1. SHAPE AND VELOCITY OF BUBBLES IN LIQUIDS

A large amount of data has been collected for bubbles rising through liquids at room temperature. Most of the early work is summarised in the report by Haberman and Morton (2).

They presented their results in terms of the following dimensionless numbers:-

$$Re = \frac{\rho U d_e}{\mu}$$ the Reynolds Number

$$Cd = \frac{4gd_e}{3U^2}$$ a Drag Coefficient

$$M = \frac{g\mu^4}{\rho\sigma^3}$$ the Morton Number

$$W = \frac{\rho U^2 d_e}{\sigma}$$ the Weber Number

They found that as the size of the bubbles was increased, a change in shape from spherical to ellipsoidal to spherical cap was observed in all liquids. The volumes at which these transitions occurred however, varied with the properties of the liquid.

For spherical bubbles of given volume, the viscosity of the liquid was the most important property describing the rate of rise. Rising velocities lay between those

predicted by Stoke's Law for rigid spheres i.e.

$$U = \frac{2gr^2}{9\mu} (\rho_L - \rho_G) \qquad 2.1.-1.$$

and those predicted by Hadamard and also Rybczynski for fluid spheres

$$U = \frac{1gr^2}{3\ \mu} (\rho_L - \rho_G) \qquad 2.1.-2.$$

They suggested that surface activity and bubble diameter determined the actual relationship.

In the case of ellipsoidal bubbles, the surface tension of the liquid assumed greater importance. For liquids of low M number ($<10^{-3}$) a minimum in the drag curve was obtained for Reynolds Numbers $\sim$250 ($d_e \sim 0.3$ cm). These minima occurred near the transition from spherical to ellipsoidal shape (W$\sim$2.2) but were not obtained for liquids of high M value.

In the case of spherical capped bubbles, rising velocities were independent of liquid properties. They obtained a constant drag coefficient of 2.6. The transition to spherical caps was completed at Weber Numbers of approximately 20 in all liquids studied.

D. W. Moore (3, 4) suggested on theoretical grounds that for small distorted bubbles rising through liquids of low viscosity, Morton Number ($<10^{-7}$), a minimum drag coefficient would occur in the curve of Cd vs Re at W=2.2,

and that the flow of liquid around the bubble was steady. Hartunian and Sears (5) found that transition to ellipsoidal bubbles was complete at W=30. They showed theoretically, for low M liquids, ~~possible~~ instability of the gas envelope resulting from the interaction of surface tension and inertial forces would account for the sharp rise in drag coefficient, and also explain the bubble's zig-zagged motion.

LARGE SPHERICAL-CAP BUBBLES

Davies and Taylor (6) were the first to investigate the dynamics of large bubbles (>5 cc). They found that, within experimental error, the front surface of the bubble was spherical and that its average radius, $\bar{r}$, was related to the bubble's rising velocity by the expression

$$U = 0.652\ (g\bar{r})^{\frac{1}{2}} \qquad 2.1.-3.$$

Rosenberg (7) also studied instantaneous shapes and velocities of S.C. bubbles and obtained a constant of 0.645 in the above expression. Figure 2.1.a. represents an idealised model of a S.C. bubble suggested by Davies and Taylor, i.e. a spherical segment. Various dimensions are defined on the diagram.

Davies and Taylor showed that assuming potential flow, the requirement of constant pressure within the bubble gives

the relationship (Bernculli),

$$q^2 = 2gr\ (1 - \cos\theta) \qquad 2.1.-4.$$

Also, assuming the flow to be the same as that for irrotational flow over the forward part of a sphere,

$$q = \frac{3}{2} U \sin\theta$$

Hence,

$$U = 0.667\ (gr)^{\frac{1}{2}} \times \left[\frac{2}{1 + \cos\theta}\right]^{\frac{1}{2}}$$

$$= \frac{2}{3}\ (gr)^{\frac{1}{2}}, \quad \theta = 0 \qquad 2.1.-5.$$

In order that U should be constant, it is evident that the above equation can only hold for $\theta = 0$. However, the coefficient of 0.667 is very similar to experimental values indicating that near potential flow around the front part of S.C. bubbles actually occurs.

Collins (8) extended the theory by obtaining a second approximation to the shape required for potential flow. His solution showed that an axisymmetric shape given by the equation

$$r_\theta = r\ (1 - \xi \sin^4\theta)$$

where $\xi = 0.0785$, closely satisfied the condition of constant pressure for $\theta \geq 20^\circ$. Taking an averaged radius, $\bar{r}$, between $\theta = 0^\circ$ and 36.5°, he found $\bar{r} = 0.953r$ which led to a velocity vs average radius relationship of

$$U = 0.652\ (g\bar{r})^{\frac{1}{2}} \qquad 2.1.-6.$$

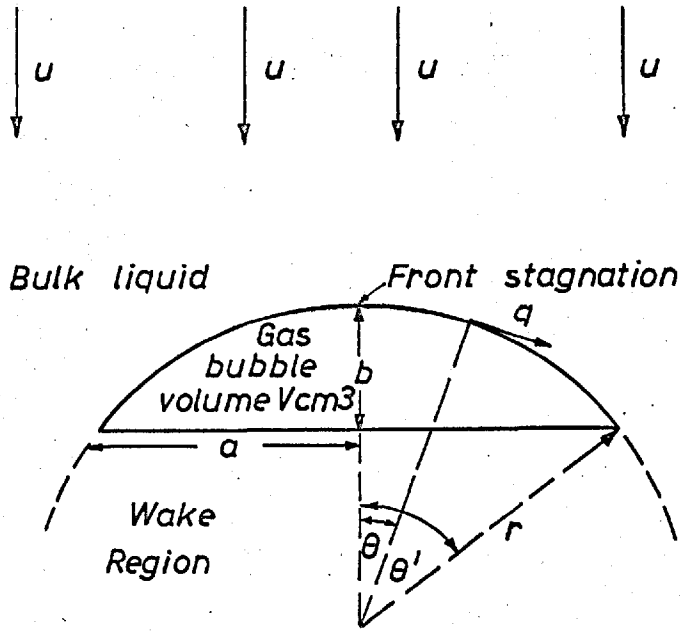

Bubble held stationary by imposing a downwards velocity u on system

u ; The terminal velocity of the bubble (cm. sec^{-1})

a , Basal radius. (cm.)

b , Bubble height. (cm.)

r , Radius of spherical cap (cm.)

r_e , " " Equivalent volume sphere (cm.)

d_e, Diameter " " " (cm.)

q , Tangential velocity of liquid at interface (cm. sec^{-1})

θ', Angle subtended at bubble edge

FIG. 2.1.a IDEALISED MODEL OF SPHERICAL CAP BUBBLE

This constant agrees slightly more closely with experimental data.

In a more recent paper (40), Collins considered the dynamics of a cycloidal cap bubble in potential flow and showed that the predicted rising velocity was again in close agreement with experimental values. He pointed out that the model predicted zero drag, although it allowed the velocity to be related to bubble volume. He calculated that the angle θ' subtended by the cap was 52.5°.

A different model, proposed by Davidson and Rippin (9), assumed potential flow around a bubble trailing a stagnant wake that extended to infinity. This model does not predict zero drag, whilst it enables the rising velocity to be related to the bubble volume. ($\theta' = 50^{\circ}$). However, the relationship obtained:-

$$U = 0.79\ (g\bar{r})^{\frac{1}{2}}$$

predicts velocities some 30% above those observed experimentally. They attributed this discrepancy to the fact that real wakes were turbulent and involved a pressure recovery of $0.38\rho gb$, (10). This would produce a lower pressure just behind the bubble, a higher drag coefficient and hence a lower terminal velocity.

All the above theories either assume or predict cap shapes very close to that of a true spherical cap.

2.1.1. Wakes Behind Submerged Bluff Bodies

Owing to the optical anisotropy of nitro-benzene, Davies and Taylor (6) were able to distinguish a region of turbulence of approximately spherical dimensions present behind S.C. bubbles. Maxworthy (41) has made similar observations. This represents the existing knowledge of wake patterns established behind large S.C. bubbles rising through liquids. However, a large amount of data has been obtained on fluid flow past submerged bodies of various geometry e.g. circular cylinders, spheres, circular discs and flat plates.

For geometrically similar bodies, a Reynolds Number, Re, may be used to correlate flow patterns and resulting drag coefficients to a common basis independent of body size. Low values of Re indicate a preponderance of viscous drag forces over inertial drag forces and laminar flow, whilst high values of Re indicate large inertial drag forces (form drag) and turbulent flow.

The flow pattern established around such objects passes through a series of transitions as the Reynolds Number is increased. In the case of circular cylinders, approximate fore and aft symmetry of the streamlines around the body is observed at $Re < 2.0$. Above this value, the symmetry is gradually destroyed due to breakaway of the main fluid flow from the body at $\theta' = 85^{\circ}$ (the bulk flow

pattern reforms further downstream). At the same time, two standing vortices are formed immediately behind the cylinder. The resulting enclosed wake gradually becomes more elongated with increasing Re, until at Re≈40, it can no longer maintain stability.

Thereafter, alternate breakaway of the two vortices results in a periodic wake of similar width to the body, extending far downstream and is known as the Von Karmen Vortex Street.

Similar transitions were observed by Moeller (12) for flow past a sphere. At lower Reynolds Numbers an enclosed laminar wake containing an annular vortex was observed. At Re>200, material was shed from the periphery of the annular vortex, resulting in a periodic wake structure extending far behind the obstacle. The oscillations increased with Re (as for a cylinder) and were still evident when the wake became turbulent at Re≈1,000. The oscillation of the wake was zig-zagged rather than spiral.

Marshall and Stanton (13) investigated non-turbulent flow past circular discs, observing an enclosed laminar wake containing an annular vortex for Re<200. At Re>200, they observed periodic discharge of vorticity from the wake in the form of vortex loops, which were shed obliquely to the axis of symmetry.

The fluid within recirculating wakes behind three dimensional bodies normally become turbulent at Re>1,000.

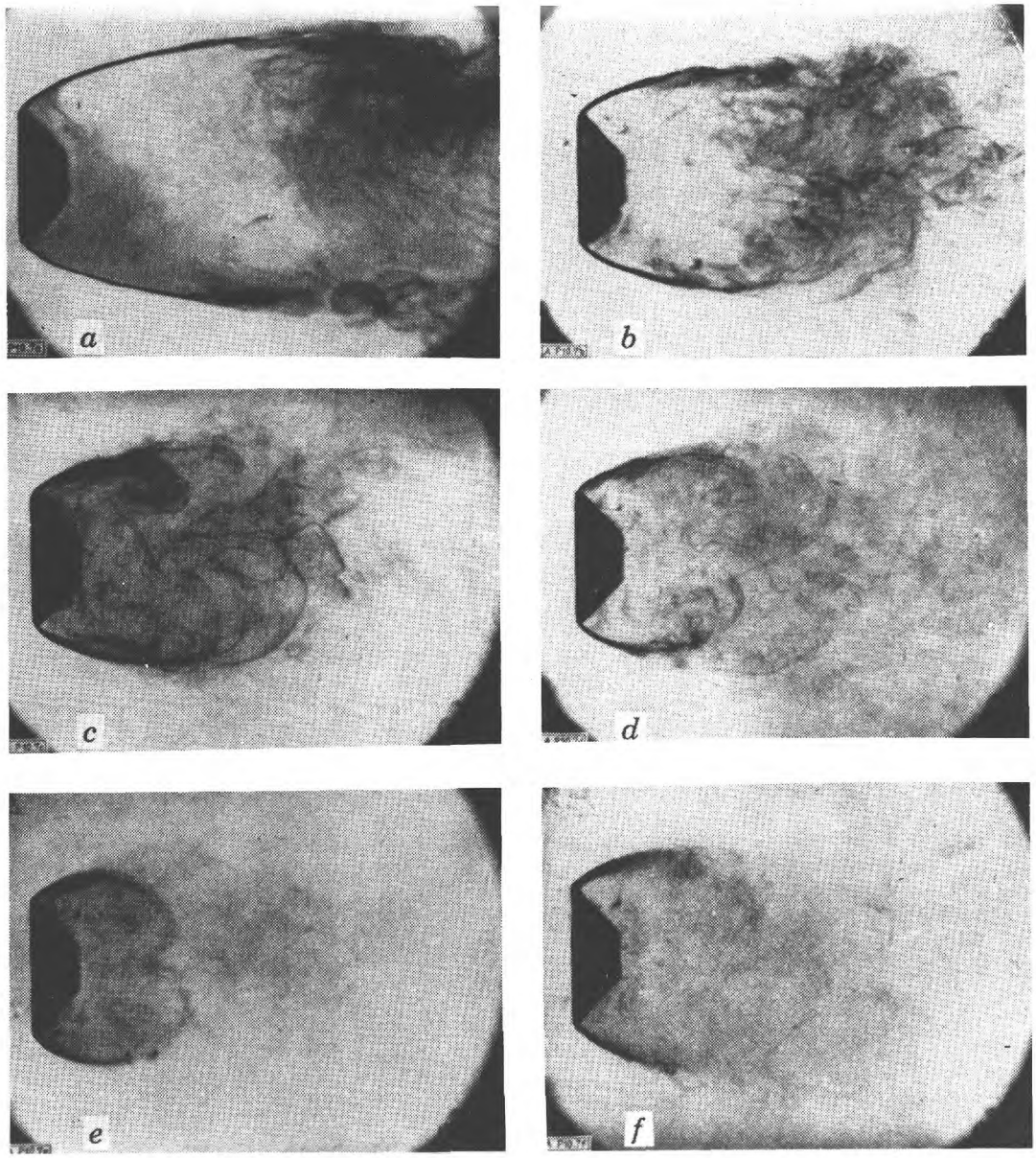

Plate a, Re = 820 Plate f, Re = 1750

Fig.2.1.b. Air flow past a Flat Plate at various Reynolds Numbers.

Also turbulent interactions with the bulk result in an illdefined mixing zone. However, the annular vortex may still be observed (11). Photographs taken by O. Flachsbart (14) in Figure 2.1.b. show the transformation from laminar to turbulent flow within the wake very clearly and exhibit similar flow patterns to those observed behind S.C. bubbles.

2.2. THEORIES OF MASS TRANSFER BETWEEN PHASES

Mass Transfer problems are usually formulated by considering an idealised mathematical model for the process.

The mechanism by which solute is transferred from one fluid phase to another has been considered by a number of workers. Their theories are based upon models which may be divided into two categories:-

a. Boundary layer type.

b. Surface renewal type.

In their boundary layer theory, Lewis and Whitman (15, 16) proposed that steady state mass transfer of solute occurred across a 'film' of fluid near to the interface which was in laminar or streamline flow. They supposed that the turbulence created in the main body of a stirred fluid was damped out in the neighbourhood of the interface. Thus solute, 'a', was transferred from a region of constant solute concentration ($C_{a,B}$), to the interface by molecular diffusion through a laminar boundary layer of effective

thickness Δ. The theory as originally proposed, resulted in equations of the type

$$\dot{n}_a = \frac{D_a}{\Delta} A (C_{a,B} - C_{a,I}) \qquad 2.2.-1.$$

The theory as such gives no indication of the value for Δ and it has also been shown that Δ is a function of solute diffusivity, D_a. Thus, the equation is more conveniently written as

$$\dot{n}_a = k A (C_{a,B} - C_{a,I}) \qquad 2.2.-2.$$

where k is a mass transfer coefficient (cm sec^{-1}).

Although the boundary layer approach may sometimes lead to solutions for transfer rates provided hydrodynamic conditions are known, it is unsuccessful when applied to many practical problems, and lead to the devlopment of the penetration theories.

The first of these was proposed by R. Higbie (17) who studied the rate of gas absorption from elongated CO_2 bubbles rising through water contained in a vertical glass cylinder. He observed that for such short contact times between the two phases, the Lewis Whitman film mechanism was not a valid basis for theory. By considering unsteady state mass transfer of gas into a laminar film of water, he obtained an analytical solution for Ficks second law of diffusion, which lead to a ~~definitional~~ solute mass transfer

coefficient, k_L, of the form

$$k_L = 2\left[\frac{D_L}{\pi t}\right]^{\frac{1}{2}} \qquad 2.2.-3.$$

where t is the time of contact of the liquid film with the gas.

Danckwerts (18) subsequently adapted the Higbie penetration theory to deal with transfer between turbulently stirred fluids. He considered that the existence of a laminar layer close to the interface was unlikely in industrial systems such as gas absorption in packed towers. Eddies were considered to arrive randomly at the interface from the bulk fluid, replacing 'old' surface with new material.

During the time of exposure of these macro-molecular units, transfer proceeded at a rate predicted by Higbie's Penetration Theory. The mean transfer rate was obtained by integration of transfer into all these units. This lead to a mean mass transfer coefficient of the form.

$$k_L = (D_L S)^{\frac{1}{2}} \qquad 2.2.-4.$$

where S = fraction of surface replaced/sec.

Harriott (19) extended Danckwerts work by considering a random distribution of distances and a random distribution of eddy lifetimes (or contact times). His theory, which predicts a gradual increase in the effect of diffusivity, D_L on k_L, as the diffusivity is decreased, can allow for the exponent of D_L to vary between 0.5 and 1.0.

2.2.1. Theory of Mass Transfer from Bubbles

When a pure gas dissolves in a liquid such that chemical equilibrium exists at the interface, its rate of solution is governed by the rate of diffusion of the solute from the interface into the bulk of the liquid. In such cases, the diffusional flux may be written as in equation (1.1.-1.). page 5,

i.e. $$\dot{n} = k_L A_e (C_I - C_B)$$

where A_e is the area of a sphere having a volume equal to that of the bubble.

Various Penetration Theories have been proposed which predict values of k_L. They assume that the gas/liquid interface is in potential (20, 21) or laminar flow (17) and that velocity gradients within the liquid may be neglected for short penetration distances of the solute gas

For a spherically shaped bubble, Higbie (17), proposed that the time of exposure of liquid elements was equal to the time taken for the bubble to rise through one diameter. Substitution for t in equation (2.2.-3.) gives

$$k_L = 2\left[\frac{D_L U}{\pi d_e}\right]^{\frac{1}{2}} \qquad 2.2.-5.$$

Baird and Davidson (20) derived an expression for diffusion through a film of fluid moving in potential flow around a spherically shaped interface. They showed that

in general the total absorption rate from a moving spherical surface film into the bulk fluid was given by

$$\frac{dn}{dt} = 4\pi^{\frac{1}{2}} (C_I - C_B) r^{3/2} D_L^{\frac{1}{2}} \left[\int_{\theta=o}^{\theta=\theta'} q \sin^2\theta \, d\theta \right]^{\frac{1}{2}} \qquad 2.2.-6.$$

Assuming that q is equal to that predicted by potential flow theory around a sphere;

$$q = \frac{3}{2} U \sin\theta \qquad 2.2.-7.$$

Integration of 2.2.-6. between 0 and π yields:-

$$\dot{n} = 4\pi r^2 \left[\frac{2D_L U}{\pi r} \right]^{\frac{1}{2}} (C_I - C_B) \qquad 2.2.-8.$$

where $$k_L = 2 \left[\frac{2D_L U}{3\pi d} \right]^{\frac{1}{2}} \text{ cm sec}^{-1} \qquad 2.2.-9.$$

Thus k_L is similar to that predicted by Higbie's original theory which did not consider dilation effects.

Baird and Davidson obtained a solution of 2.2.-6. for the case of gas absorption from a spherically capped bubble into a liquid. Substituting the Bernoulli equation for flow round a spherical surface of a constant pressure object eqtn. 2.1.-4., and assuming the shape of the bubble to be a spherical segment subtending an angle of 50° at its edge, they finally obtained the expression

$$k_L = 0.975 D_L^{\frac{1}{2}} \left[\frac{g}{d_e} \right]^{\frac{1}{4}} \qquad 2.2.-10.$$

Where k_L is based upon the area of an equivalent volume sphere.

Similarly Davidson and Harrison (10) obtained

$$k_G = 0.975 D_G^{\frac{1}{2}} \left[\frac{g}{d_e}\right]^{\frac{1}{4}} \qquad 2.2.-11.$$

for transfer of solute gas from the interface into the bulk gas phase of a S.C. bubble.

Lochiel and Calderbank (21) obtained a similar expression though their transfer coefficient was different, since their calculations were based upon the actual cap area of the bubble, instead of on the area of an equivalent volume sphere. In their analysis they assumed that the tangential velocity was given by equation 2.2.-7.

All the above theories neglect radial expansion (or contraction) of the interface during bubble rise. Beek and Kramers (22) attempted to obtain a general expression for mass transfer from an expanding interface, but were unsuccessful. Also no theory exists for transfer from the rear surface of a S.C. bubble as the dynamics of wakes are unknown.

2.2.2. Low Temperature Interactions between Bubbles and Liquids - Experimental

The importance of bubble-liquid interactions in many chemical operations has lead to a considerable number of mass transfer investigations. The majority of this work has been centred upon small bubbles of less than 1 cc volume ($d_e < 1.2$ cm). However, some investigators (20, 30,

31, 32) have covered part of the size range of present interest.

Table 2.2.a. gives a synopsis of the more important investigations. All mass transfer coefficients quoted are based upon areas of equivalent volume spheres.

Most workers have studied the solution of CO_2 bubbles in water and it is apparent that many discrepancies exist between their results. For bubbles of equivalent diameter $d_e < 0.3$ cm, transfer coefficients ranging from 0.005 to 0.035 cm sec^{-1} are reported. However, it is generally accepted (27, 28, 29, 30) that contamination of bubbles' surfaces by surface active materials accounts for the very low transfer coefficients sometimes obtained. In the range (d_e = 0.3.-0.6. cm), the bubble changes from a spherical to ellipsoidal shape and this seems to coincide with a maximum transfer coefficient of 0.036 cm/sec. approx. This coefficient may remain constant during bubble rise, or, depending upon the degree of contamination within the system, may decrease more or less rapidly. (28, 29).

In the range (d_e = 0.6-2.5 cm) the bubble changes from ellipsoidal to spherical cap shape and all workers agree that k_L remains virtually constant during bubble rise. Baird (20) and Davenport (32) both obtained a value of 0.026 cm/sec^{-1} approx. for bubbles in the size range 1.8-2.5 cm. However, Lochiel's values were considerably

higher, and ranged from 0.042 cm/sec^{-1} at d_e = 1.8 cm. to 0.033 cm/sec^{-1} at d_e = 2.5 cm. (31). In the latter's case, reported transfer coefficients were based upon the surface area of a S.C. bubble of eccentricity equal to 3, where $E = \frac{2a}{b}$. Consequently, in order to compare their results with other workers, adjustments have been made to express their results in terms of coefficients based upon areas of equivalent volume spheres.

In the range (d_e = 2.5 - 4.2 cm), Baird found that initial transfer coefficients of CO_2 bubbles in water increased markedly with bubble size, decaying to a value of approx. 0.026 cm/sec^{-1} after 6 seconds of bubble rise. Results obtained by Davenport over this size range, (32) showed similar time effects; <u>overall</u> mass transfer coefficients were found to decrease with column height, especially at large bubble volumes. Surface active solutions of 0.5% polyvinyl alcohol caused a drop in overall values of k_L from 0.026 cm/sec in distilled water to 0.012 cm/sec. This decrease coincided with the suppression of rippling surfaces observed in water, although velocities and shapes (i.e. linear dimensions) were not affected. Baird studied the effect of liquid surface tension - time variations on gas absorption:- surface ageing solutions of 0.1% n-hexanol, (freshly exposed surfaces of which, take several hundredths of a second to obtain constant surface tension) suppressed ripples, and k_L was similar to that predicted for frontal transfer alone, (eqtn. 2.2.-10), indicating stagnation of the rear surface of bubbles. CO_2 bubbles in non-ageing solutions of 0.1% n-butanol absorbed more rapidly and bubble surfaces were rippling.

TABLE 2.2.-a.

SYSTEM	RANGE d_e (cm)	METHOD AND RESULTS All k_L based upon A_e	AUTHORS & YEAR
CO_2/H_2O	0.41	Single Bubbles (0.036 cc.) held stationary by downflow of water at 25°C through 2 cm I.D. glass column. Instantaneous volumes recorded by movement of Mercury thread in capillary connected with sealed apparatus. Transfer rates decreased with time $k_L \approx 0.02$ cm/sec.	LEDIG & WEAVER 1924 (23)
CO_2/H_2O	0.2 - 0.4	Stream of CO_2 bubbles rising through 3 cm I.D. column, 100 cm high. Input and output gas measured to give overall values of $k_L \sim 0.02$ to 0.03 cm/sec at 20°C (bubble frequency and size estimated).	GUYER & PFISTER 1946 (24)
CO_2/H_2O	0.26 - 0.58	Single CO_2 bubbles rising through 10 cm I.D. column. Transfer over various heights ranging from 60-456 cm from release point. Average values of $k_L \sim$ 0.02 to 0.03 cm/sec.	DATTA NAPIER & NEWITT 1950 (25)

TABLE 2.2.-a (continued)

O_2/H_2O	0.3 - 0.66	Streams of O_2 bubbles rising in 8 cm I.D. glass column, 120 cm high at 20°C. Water analysed for oxygen. Overall k_L~0.028 to 0.055 cm/sec	COPPOCK & MEIKLEJOHN 1951 (26)
CO_2, O_2, H_2, C_2H_4, $/H_2O$ CO_2/glycerol	0.2 - 0.8	Single bubbles rising through 12 cm I.D. glass column at 11-20°C. Instantaneous volumes recorded by method similar to (23). At d_e<0.3, non-circulation of bubbles through contamination with grease led to very low values of k_L. A maxm. k_L of 0.039 cm/sec observed in CO_2, O_2 and C_2H_4/H_2O systems at 0.3 cm dia. Hydrogen transfer indicated $k_L \propto D^{\frac{1}{2}}$.	HAMMERTON & GARNER 1954 (27)
CO_2/H_2O	0.15 - 0.55	Square perspex column, 20°C. Photographic measurement of bubble volume with time. Inst. values of k_L; rates decayed rapidly with time approaching those for solid spheres. Also, below d_e = 0.3, overall values of k_L decreased with size. Initial k_L~0.055 cm/sec at d_e>0.3 cm.	DEINDORFER HUMPHREY 1961 (28)

TABLE 2.2.-a. (continued)

CO_2/H_2O + glycerol	0.05 - 0.4	Inst. volume measurement. Peak k_L of 0.035 cm/sec at d_e = 0.3 cm in H_2O, k_L decreased with time at all volumes, but at $d_e < 0.3$ cm values decreased rapidly to that for solid spheres. With increasing viscosity of glycerol, rates of decay became less marked, finally becoming constant at ~ 20 cp.	CLARKE 1962 (29)
CO_2, N_2O C_2H_4, C_2H_6, / H_2O, HNO_3.	0.3 - 2.0	Overall values of k_L over various sections of the 9 cm I.D. pyrex column, 180 cm long. Inst. volumes measured similarly to (23). k_L decreased with size for $d_e < 0.5$ cm, at $d_e > 0.5$ cm, k_L ~ 0.030 for all systems, decreasing with time slightly.	LEONARD & HOUGHTON 1963 (30)
CO_2/H_2O	0.5 - 2.5	4" I.D. P.V.C. column 10' long at 17-23°C. Inst. shapes photographed, volume measurements recorded from changes in gas pressure in top space above liquid. Great precautions taken to eliminate contamination. Little or no decay observed k_L ~ 0.028 at d_e = 0.75 cm and 0.033 cm/sec at d_e = 2.5.	LOCHIEL & CALDERBANK 1964 (31)

TABLE 2.2.-a. (continued)

CO_2/H_2O + S.A. Agents	0.4 - 4.2	Pyrex column 6" I.D. 10' high. Expts. at 20°C. Inst. volumes using soap-film meter + cine camera. At d_e = 2.5, k_L = 0.026 cm/sec and const. thereafter initial rates increased with size decaying to ~0.026 cm/sec after 6 secs. S.A. solutions of 0.1% n-butanol reduced overall values of k_L to ~0.016 cm/sec.	BAIRD & DAVIDSON 1962 (20)
CO_2/H_2O, CO_2/C_2H_5OH CO_2/aq.P.V.A.	0.4 - 4.2	Perspex column 6" I.D. 10' high, Expts. 15-21°C. Overall values of k_L obtained from initial and final volumes using soap film meter technique. k_L ~ 0.026 at d_e = 2.5 cm, whilst at d_e > 2.5, k_L showed a decay with distance from release. Overall transfer rates in P.V.A. solns. were initially low, k_L ~ 0.012 cm/sec, at small P.V.A. conc. (0.5%) but began to rise as the P.V.A. conc. was increased.	DAVENPORT 1963 (32)

2.2.3. High Temperature Work

Although little is known of chemical reaction rates at steelmaking temperatures, workers (1, 33, 34) agree that the chemical kinetics of most reactions are too rapid to account for observed rates of reaction and have concluded that the majority of processes in steelmaking must be transport controlled.

Several workers have investigated the Open-Hearth Steelmaking reaction in which oxygen is transported through gas/slag/ and liquid metal phases to react with dissolved carbon in the metal.

Larsen and Sordahl (33) carried out investigations on a pilot plant process and found that transport of oxygen through a nitrogen rich layer of gas at the gas/slag interface limited the rate of carbon drop in the metal. Darken (34) concluded that the transport of dissolved oxygen across the slag/metal interface by the reaction

$$(FeO)_{slag} \rightleftarrows Fe + (O)_{Fe}$$

was transport controlled; he calculated that expected rates of reaction on the basis of chemical control were 10^5 times those observed in practice.

Richardson (1) considered the reaction between dissolved carbon

$$(C)_{Fe} + (O)_{Fe} \rightarrow (CO)_{gas}$$

and oxygen species to form carbon monoxide at the interface

of rising bubbles of carbon monoxide. On the basis of transport control between the gas, slag and metal phases, and from operational observations he concluded that the mass transfer coefficient for the above reaction was 0.05 cm/sec.

Carbon elimination in steelmaking is now generally considered to be controlled by a series of oxygen transport steps between the high oxygen potential in the atmosphere above the slag (oxidising flame in the O-H process, oxygen in the L.D.) and the low oxygen potential CO bubble/metal interface.

It should be noted that the rate of chemical reaction is a function of the concentrations of the reacting species. Thus gas/metal processes involving very small solute gas concentrations may well be chemically controlled. A. G. Szekely (35) has calculated that the removal of hydrogen from steel at low hydrogen concentrations is slower than transport control would suggest.

Apart from calculations based upon operational processes, little work has been done in the study of gas/metal interactions. Davenport (32) examined the shape and dynamics of S.C. N_2 bubbles rising in mercury.

Comparatively few results on gas/metal transfer have been obtained, and the majority of these are of limited accuracy. Niwa et al (38) studied the CO steelmaking reaction and obtained $k_L \sim 10^{-1}$ to 10^{-2} cm sec^{-1}.

Pehlke and Bement (37) studied the desorption of hydrogen from molten aluminium at 700°C into rising argon bubbles and estimated a transfer coefficient, k_L, of 0.04 rising to 0.07 cm/sec with increased bubbling rate, (30-60 bubbles/sec, $\bar{r}_e \sim 0.35$ cm).

Davenport (32) carried out an investigation of oxygen absorption by molten silver at 1,000°C and estimated a transfer coefficient of 0.05 cm/sec.

CHAPTER 3.

EXPERIMENTAL EQUIPMENT AND PROCEDURE USED IN ROOM TEMPERATURE INVESTIGATION

3.1. EXPERIMENTAL EQUIPMENT

The low temperature investigation was carried out using 18" and 6" I.D. clear perspex columns, both with a maximum height of approximately 10'.

The arrangement of the larger column, together with its accessories, is shown in Figs. 3.1.a. and b. Two alternative methods were used for filling the dumping cup; either through a capillary tube situated below the cup in the bottom flange of the column, or through a stainless steel capillary tube leading directly into the base of the cup via the rotating shaft (Fig. 3.1.b.).

The second method was necessary with solutions of polyvinyl alcohol, since the surface active agents produced a stable froth in the cup when the first method of filling was used. On rotating the cup full of foam, a shower of small bubbles were released instead of a single large one.

This alternative method of passing gas directly into the cup was also used for experiments on the desorption of carbon dioxide from CO_2 saturated water into rising nitrogen bubbles. In these experiments it was necessary to know

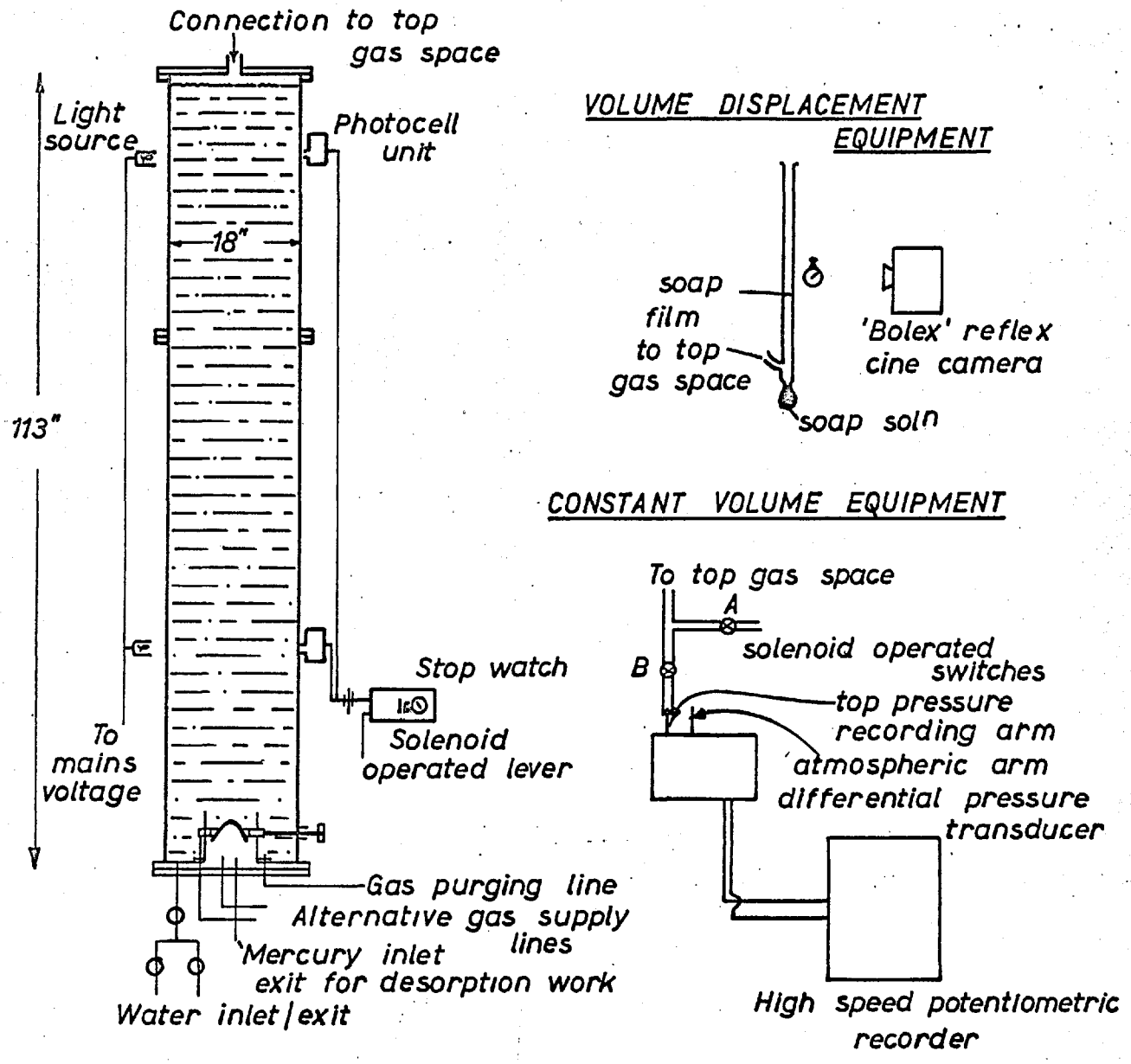

FIG. 3.1.a DIAGRAM OF LOW TEMPERATURE APPARATUS
(18" dia. PERSPEX COLUMN)

FIG.3.1.b DIAGRAM OF LOWER SECTION OF COLUMN (18" dia.)

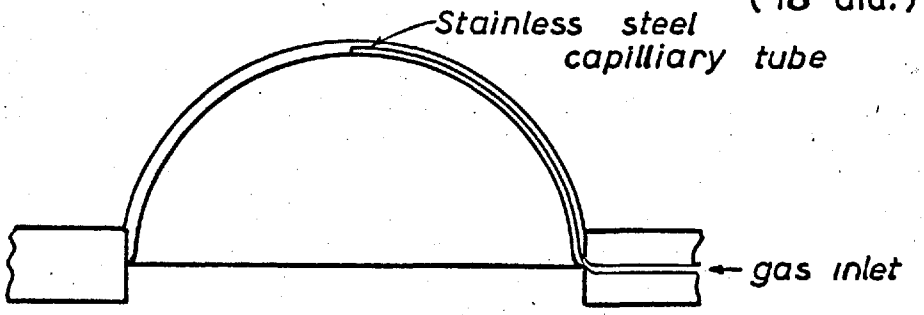

CUP No.2.

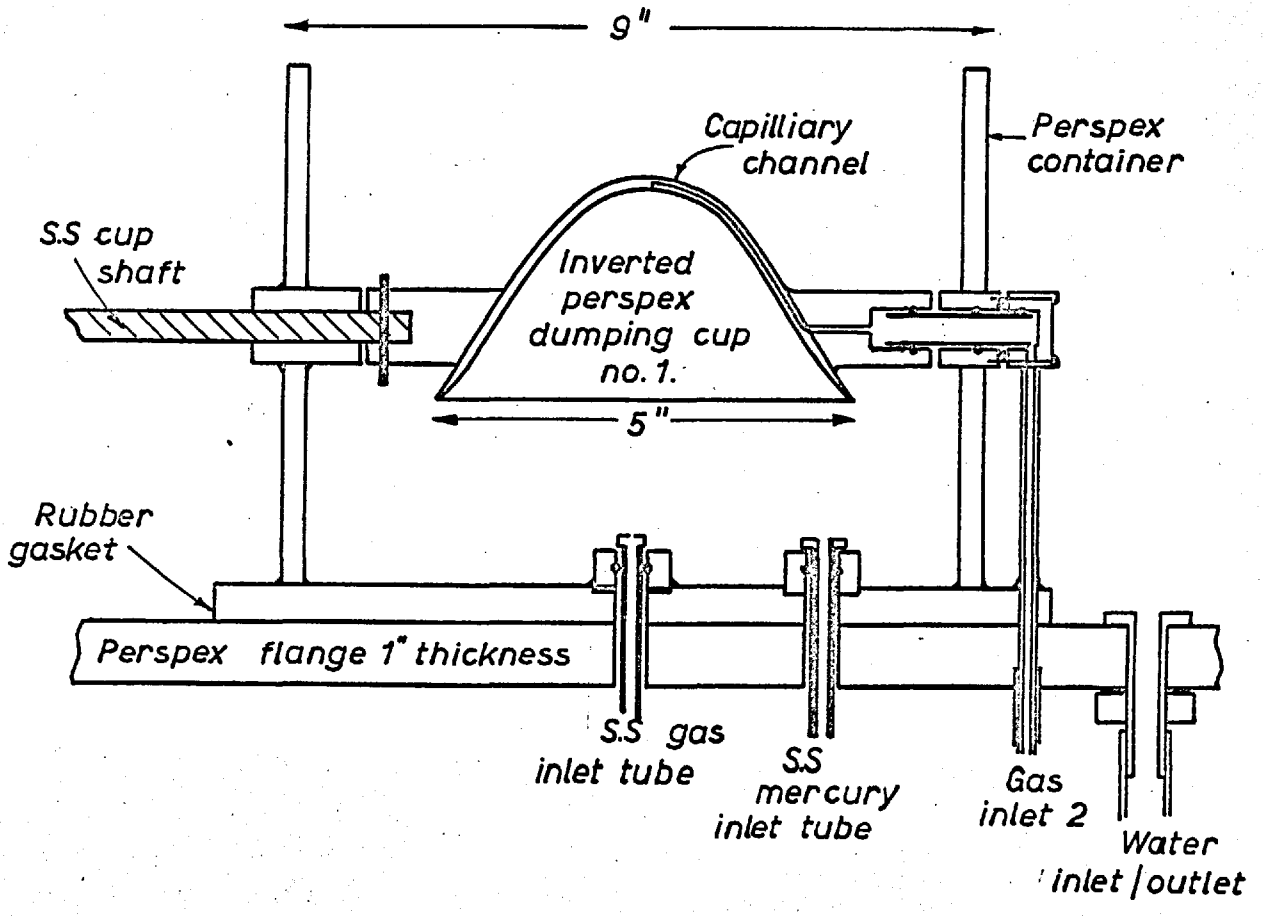

the concentration of CO_2 in the bubble at the moment of release. This was best achieved by preventing any CO_2 absorption before the bubble was released; the level of mercury in the small perspex container (see Fig. 3.1.b.) was raised until it was above the level of the cup. The cup was rotated to ensure that any aqueous solution or gas was removed. The cup was then inverted and the mercury level in the container was lowered to a predetermined level depending on the size of gas bubble required. Nitrogen was then passed through the base of the cup to displace the mercury within it. After adjustment of the mercury level in the cup to the level in the container, the cup was rotated to release a bubble of pure nitrogen. This method could only be used for relatively small bubbles of less than 15 cc in water. Large bubbles broke up due to disturbances at the water/mercury interface when the bubble was released. Presumably it is difficult for the normal wake pattern observed behind S.C. bubbles, to become established. When the bubble is released from a water-mercury interface, the disturbance caused by the entrainment of aqueous liquid into the wake of such a bubble is apparently sufficient to cause its disintegration.

The 6" I.D. column used in the investigation was of similar design to the larger one, but without the small mercury container.

3.1.1. Cup Design

Perspex was used in preference to metal, so that gas in the dumping cup should be readily visible. Two designs of cup were found to be necessary to cover the range of bubble volumes and liquids used in the investigation.

The first perspex cup (see Fig. 3.1.b.) was employed for bubbles rising in water, and was successfully operated to form bubbles of up to 70 cc. Great difficulty was experienced in producing perfect bubbles larger than 30 cc.

The second cup was in the shape of a hemisphere rotating about its basal diameter. This shape was found to be essential for the production of perfect bubbles in high density liquids such as mercury. Other cup designs apparently caused sufficient disturbance in high density liquids to break up the released gas.

An interesting observation made during the course of the low temperature investigation was that perfect bubbles greater than 15 cc. were either extremely difficult or impossible to form in liquids of low surface tension and viscosity, (e.g. alcohol and 0.10% aqueous polyvinyl alcohol). At the other end of the scale, bubbles in liquids of high viscosity (e.g. 4 - 8% P.V.A. solution) could be perfectly formed up to 200 cc. and probably greater.

3.2. MATERIALS

The gases and liquids used in the investigation, together with relevant details and properties are listed in Table 3.2.a.

The high viscosity aqueous liquids were prepared from 'Alcotex 88-40' polyvinyl alcohol powder. The large quantities required to fill the 18" I.D. column were prepared in large tanks (53 cm high, 44 cm I.D.). These were firstly filled with preheated distilled water (60°C), which was vigorously stirred using a 7 cm dia. x 3 cm paddle rotating at 1200 r.p.m. and driven by 1/4 h.p. electric motor. The powder was sprinkled into the vortex and rapidly dissolved. The liquid prepared (8% P.V.A.) was allowed to stand for 24 hours to allow the tiny air bubbles (drawn into the system during mixing) to disperse.

The N_2 and CO_2 gases used in this investigation contained less than 50 parts per million of impurities, apart from moisture.

TABLE 3.2.a.

LIQUID	TEMP.	SURFACE TENSION	VISCOSITY	DENSITY	BUNSEN SOLUBILITY COEFF. (CO_2)	DIFFUSIVITY
	°C	dynes/cm	cp	gm/cc	cc/cc	$cm^2 sec^{-1}$
TAP WATER	18.8	73	1.1	1.0	0.90 (46)	1.39×10^{-5} (45) (15°C)
Aqueous P.V.A. solutions					Solubility as % of CO_2.	
Conc. Wt. %					Solubility in water (32)	CO_2 Diffusivity (32)
0.10	19.6	50	1.4	1.00	99.8	$1.4 (\pm 0.15) \times 10^{-5}$
4.19	20.1	47.7	46	1.01	93.8	$1.4 (\pm 0.15) \times 10^{-5}$
5.64	21.5	46.9	130	1.01	93.1 $\pm$ 1%	$1.4 (\pm 0.15) \times 10^{-5}$
6.65	21.3	46.5	276	1.01	92.8	$1.3 (\pm 0.15) \times 10^{-5}$
8.40	18.3	46.0	735	1.02	92.5	
					Solubility of [O] in Silver (62)	[O]/Ag.
Silver (47)	1020	920	3.89	9.26	1.72×10^{-3} gm Atoms [O]/cc Ag.	9×10^{-5}
99.95% purity before and after expts. (49)						(48,61)

3.3. MEASURING TECHNIQUES

The various methods employed in the measurements of shape, velocity and mass transfer rates of S.C. bubbles are described in the following sections.

3.3.1. Measurement of Bubble Shapes

Bubble shapes were determined photographically. Only height and basal width were measured as these are sufficient to fix the geometry of a truly S.C. bubble.

The best method for aqueous polyvinyl alcohol solutions was found to be cine-photographic measurement, employing back lighting of the column. A 16 mm Bolex Reflex Cine Camera, using a fine grain black and white film was employed. A Flat Box Section was fitted to the outside of the upper part of the column to eliminate radial distortion of the photographs.

Absolute measurements of bubble dimensions were calculated by photographing an accurately machined grid consisting of 1/4" dia. holes spaced at $\frac{1}{2}$" centres in 1/4" thickness aluminium plate. The plate was suspended along the axis of bubble rise.

3.3.2. Measurements of Bubble Velocities

The mean velocity of a bubble rising in the 18" I.D. column was calculated from the time required for the bubble to traverse a measured distance. (See Fig. 3.1.a.).

Two sets of light sources (usually 60 watt light bulbs) were placed diametrically opposite two photo-electric cells, at selected levels in the column. The sensitivities of the photocells were adjusted so as to respond to the interruption in light caused by a rising bubble. When the light beam was interrupted, a solenoid-operated lever started or stopped the stopwatch. Errors arising from inertial effects in the lever mechanism were minimised by having identical circuits and mechanical connections for both the start and stop operations.

The scale on the stopwatch could be read to 0.01 seconds, and the accuracy of the watch was specified as within 0.01 seconds for operating times up to 10 seconds.

3.3.3. Measurement of Bubble Volumes

Two methods have been employed, the 'Volume Displacement' technique and the 'Constant Volume' technique.

3.3.3.1. 'Volume Displacement' Technique

The method adopted in the investigation is similar to that described by Baird and Davidson (20). The small gas space above the liquid at the top of the column was connected to the atmosphere through a soap-film meter. The movement of the soap film indicated the volume change which occurred within the bubble.

The initial volume of the bubble was measured by noting the movement of the soap film when filling the cup. Similarly, the final volume of the bubble at the top of the column was again read visually from the meter. These two measurements were sufficient to calculate an overall mass transfer coefficient as described by Davenport (32).

Instantaneous volume changes of rising bubbles were measured by taking a cine photograph of the moving soap film and an adjacent stopwatch. Frequently, the instant of release of the bubble could be detected from a sudden change in volume of the soap film meter. However, in the case of small bubbles (~5 cc.), this was insufficient to pinpoint the starting times precisely. As an added precaution the stopwatch was started automatically when the tipping cup had rotated through an angle of 45 degrees. This was accomplished by means of a flap, attached to the cup shaft, interrupting a light beam to a photocell. Comparison of the starting times for large inert bubbles obtained from the sudden change in volume with that given by the stopwatch, showed precise agreement.

Size Effects

Several difficulties were encountered with the large diameter column, which were not so marked for the 6" I.D. column.

Firstly, owing to the ~~greater surface area of perspex and~~ much greater mass of liquid, thermal equilibrium between the column and its surroundings was often not obtained until two days after filling. Experiments were only commenced when the soap film meter was steady.

The second difficulty resulted from the greater volume of the top gas space above the liquid (nine times the volume of the 6" I.D. column). Response to volume changes of the gas within the column were found to be sluggish unless wide bore, 1/4" I.D., P.V.C. tubing was used to connect the soap film with the top space. Further methods to speed up response time involved the use of 1/4" bore stopcocks and the elimination of all sharp bends. These precautions made the measuring system virtually independent of the top gas space volume and the length of connecting tubes.

3.3.3.2. 'Constant Volume' Technique

In this technique, the top gas volume was connected to a differential pressure transducer which measured changes in top pressure existing between the top space and the atmosphere outside. Changes in top pressure were caused by the volume changes of bubbles rising in the column.

The differential pressure transducer used in the investigation was of the diagphragm type, manufactured by

Hilger I.R.D. Ltd. The ratio of E.M.F. output to applied pressure was checked and found to be constant over the whole pressure range of the instrument (-2" H_2O-0-.2"H_2O).

Changes in volume of the transducer due to slight movement of the diaghragm were negligible ($<10^{-3}cm^3$) compared with top gas volumes of ~3,000 cc.

The instrument had a rated response time of 50 c/s, an accuracy within 2% for full scale deflection and it incorporated a fully adjustable zero between -10-0- +10mV output.

The E.M.F. signal from the pressure transducer was fed into a high speed, single point Leeds and Northrup potentiometric recorder. The recorder could respond to a full scale deflection signal (20mV) within 0.25 seconds and mV readings were accurate to within 1% for F.S.D. A number of chart speeds were incorporated, including 1 and 4 inches per second (accuracy within 3%).

Procedure

Initially, the gas space above the liquid at the top of the column was connected to one of the arms of the differential manometer, while the other arm was left open to the atmosphere (see Fig. 3.1.a.). The gas line connecting the top space with the instrument, initially open to the atmosphere via solenoid switch 'A', was closed

and gas bubbled into the inverted cup. This caused compression of the top space, resulting in an E.M.F. output from the transducer directly proportional to the change in top gauge pressure. The volume of the gas in the cup could then be calculated from a knowledge of the initial volume (v_i), initial pressure (p_i) and final pressure (p_o) of the top gas space. If the compression of the gas in the top space is isothermal, the bubble volume, V, is given by

$$V = v_i \left[1 - \frac{p_i}{p_o} \right] \qquad 3.3.-1.$$

When the bubble was released, the variation of pressure with time was measured by the transducer and registered on the recorder.

Before starting the next experiment, the top space was returned to atmospheric pressure by operating switch 'A'.

In order to pinpoint the starting time of the bubble at the moment of release, a cam wheel was placed on the cup shaft and closed a microswitch when the cup had turned 45°. This switched on the recorder chart which immediately moved at the rated speed.

In some cases, a light and photo-electric cell were used to accurately set the position of the bubble in the column with the corresponding pressure reading on the chart.

In these experiments, the interruption of the light beam caused the cell to transmit a small E.M.F. signal to the recorder and superimpose a small 'blip' on the pressure-time curve.

Measurement of Top Gas Volume

In order to relate the pressure changes measured to the bubble volume, it was necessary to know the initial volume of the top space above the liquid. The initial volume was determined by discharging liquid from the bottom of the column into a burette and, at the same time, measuring the change in pressure at the top of the column. If Δv is the volume run out (cc) and p_i and p_f are the initial and final pressures, the initial top volume is given by

$$v_i = \frac{\Delta v \; p_f}{(p_i - p_f)} \qquad 3.3.-2.$$

Three independent measurements for each top space volume used ~~normally~~ agreed within a percent.

This method of measuring top space volume may be equally well applied to the system when under vacuum, and has the advantage of automatically accounting for the distortion of the top and bottom flanges that occurs when the present apparatus is evacuated. If the pressure at the bottom of the column is less than atmospheric, it would be preferable to introduce a measured quantity of liquid into the column.

Non-Isothermal Behaviour

Preliminary experiments indicated that the stagnant gas space at the top of the column did not necessarily behave isothermally. This problem, mainly encountered with the 6" I.D. column was solved by increasing the area available for heat transfer by suspending strips of damp filter cloth or copper gauze within the gas space.

The increase in surface area and in thermal capacity of the container was sufficient to reduce non-isothermal behaviour to a minimum. The results of these experiments are discussed in the following chapter.

CHAPTER 4.

4.0. EXPERIMENTAL RESULTS

The results obtained on shapes velocities and mass transfer rates together with relevant theory and calculations are presented below.

4.1. INVESTIGATION OF CONSTANT VOLUME MEASURING TECHNIQUE

Preliminary work on the rise of nitrogen bubbles in water using the 6" I.D. column showed that the expected rise in pressure of the gas in the top of the column due to the expansion of a rising nitrogen bubble was less than that obtained experimentally. Furthermore, it was found that the final pressure recorded when the bubble broke surface, dropped to the expected value after a small time lapse (~4 seconds). After ensuring that the recording system was not underdamped, that the apparatus and connections were leak tight and that similar discrepancy was observed when the liquid level in the column was changed by other means, it was concluded that the gas in the top space did not necessarily respond isothermally to volume changes within the column. In order to study the magnitude of this departure from isothermal conditions, the volume of the top space was altered either by bubbling gas into the cup at predetermined rates or by running out

liquid from the column into a burette. In the first case, the resulting rise in liquid level compressed the gas in the top space, and the pressure vs time was recorded. In all cases, the rate of bubbling was controlled to maintain a constant value of $\frac{dp}{dt}$, furthermore it was continued until the reduction in volume was $\geq 1\%$ that of the original top volume (i.e. $\frac{\Delta v}{v_i} \simeq 0.01$). The final pressure, $p_{1,ad}$, obtained immediately after filling was measured in addition to the final pressure $p_{1,is}$, after thermal equilibrium had been obtained. The latter pressure is the one which would have been directly measured had the compression been isothermal.

Theory

Under isothermal conditions with steady change in pressure

$$\left(\frac{dp}{dt}\right)_{is} = \frac{-p_o v_o}{v^2} \frac{dv}{dt} \qquad 4.1.-1.$$

whereas under non-isothermal conditions, during which the gas is assumed to obey the relationship.

$$pv^n = \text{constant} \qquad \text{where } 1 \leq n \leq \gamma$$

$$\left(\frac{dp}{dt}\right)_{ad} = \frac{-n\, p_o v_o^n}{v^{n+1}} \frac{dv}{dt} \qquad 4.1.-2.$$

Equations 1 and 2 may be integrated between v_1 and v_o over time t, so that at constant rates of pressure change,

$$\left(\frac{dp}{dt}\right)_{is} = \frac{p_{1,is} - p_o}{t} = \frac{p_o\, v_o}{t}\left[\frac{1}{v_1} - \frac{1}{v_o}\right] \qquad 4.1.-3.$$

similarly,

$$\left(\frac{dp}{dt}\right)_{ad} = \frac{p_{1,ad} - p_o}{t} = \frac{p_o\, v_o^n}{t}\left[\frac{1}{v_1^n} - \frac{1}{v_o^n}\right] \qquad 4.1.-4.$$

The departure from isothermal conditions may be shown by,

$$\frac{\left(\frac{dp}{dt}\right)_{ad} - \left(\frac{dp}{dt}\right)_{is}}{\left(\frac{dp}{dt}\right)_{is}} = \frac{p_{1,ad} - p_{1,is}}{p_{1,is} - p_o} = \frac{v^*\left[v^{*n-1} - 1\right]}{\left[v^* - 1\right]}$$

where $v^* = \frac{v_o}{v_1}$ 4.1.-5.

Equation 4.1.-5. shows that the departure from isothermal conditions will depend upon values of v^* and n. However, as the experiment was carried out only for a short time period and consequently the initial top space volume, v_o, was large compared with volume changes ($v_o \not\approx 1.01\ v_1$), the right hand side of the equation 4.1.-5. may be evaluated as $v^* \to 1$ by application of 'de l'Hospital's rule',

$$\lim_{v^* \to 1} \frac{\left(\frac{dp}{dt}\right)_{ad} - \left(\frac{dp}{dt}\right)_{is}}{\left(\frac{dp}{dt}\right)_{is}} = \frac{p_{1,ad} - p_{1,is}}{p_{1,is} - p_o} = (n - 1) \qquad 4.1.-6.$$

As previously stated $\frac{v_o}{v_1} \approx 1.01$, and in this case the right side of equation 4.1.-5. will not be more than 1% greater

than the value of (n-1).

On the above basis, the graph, (Fig. 4.1.-a), of

$$\left[\frac{p_{1,ad} - p_{1,is}}{p_{1,is} - p_o}\right] \text{ vs} \left(\frac{dp}{dt}\right)_{ad}$$

represents the variation of (n-1) vs $\left(\frac{dp}{dt}\right)$ad. Furthermore since $1 \leq n \leq 1.4$, these values represent the limits of the graph for any value of $\left(\frac{dp}{dt}\right)$ad.

Fig. 4.1.-a shows that the behaviour of gas in the top space was far from isothermal (curve A), the value of n rising to 1.11 at values of $\frac{dp}{dt}$ equal to 0.3" H_2O/second. In order to ensure conditions were more nearly isothermal, modifications were made to the top space as described in section 3.3.3.2., so as to give a ratio of top space surface area to volume of approx. 1.4 $cm.^{-1}$ This resulted in curve B, which shows that typical experimental values of $\left(\frac{dp}{dt}\right)$ad between 0 and 0.4" H_2O/second were within 1.5% of the isothermal value.

Owing to the high ratio of water surface area to gas volume, results obtained using the 18" I.D. column followed curve B, without any modifications to the top gas space being necessary.

The previous analysis has neglected the effect of water vapour on the equations, and is only valid under present experimental conditions provided the water vapour in the top gas space behaves as an ideal gas.

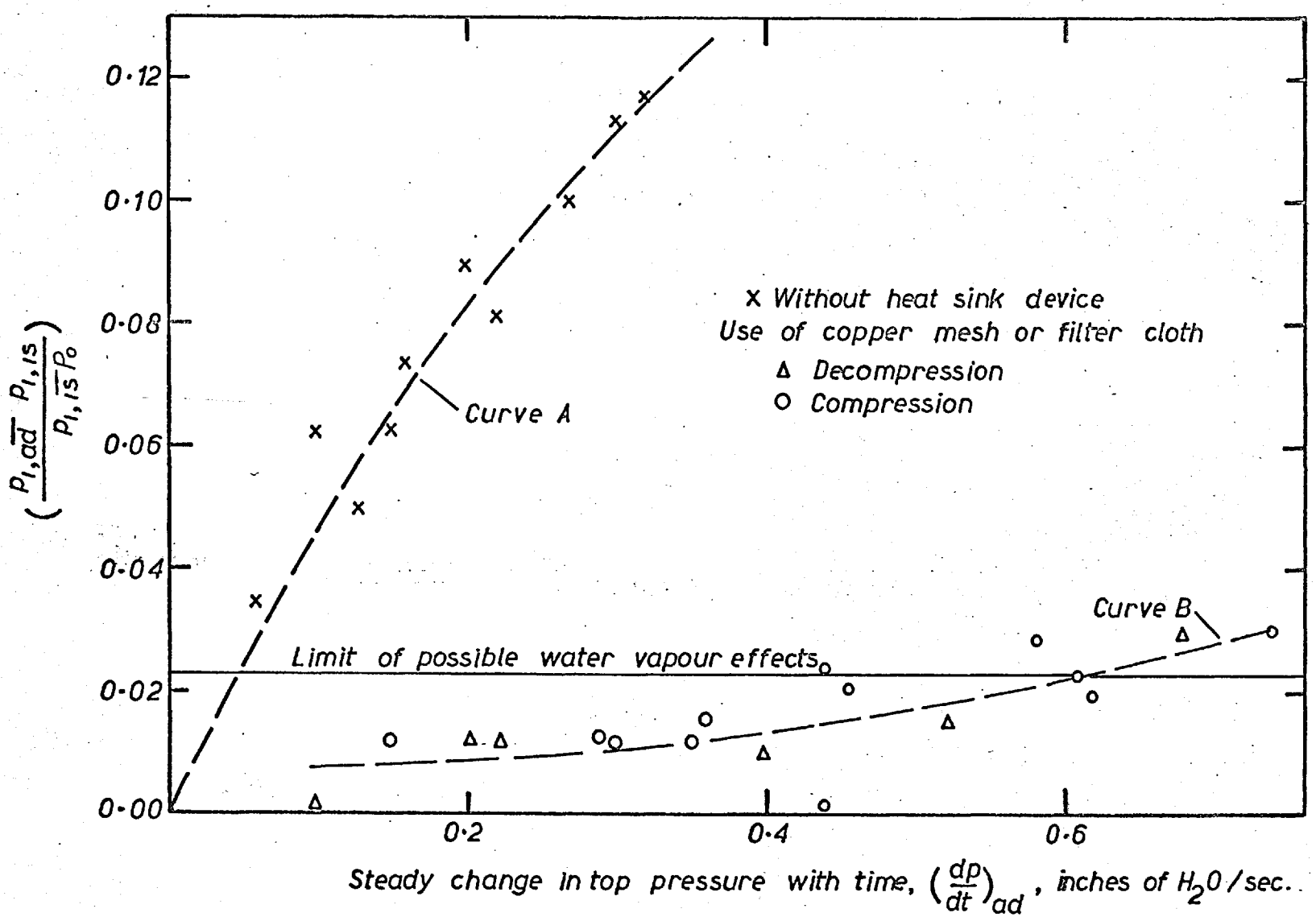

FIG. 4.1.a NON-ISOTHERMAL BEHAVIOUR OF GAS IN TOP SPACE OF 6" I.D COLUMN

Thus small compressional changes in the top volume may cause slight supersaturation of the vapour which may or may not lead to partial condensation.

One likely possibility is that the water vapour becomes supersaturated during ~~adiabatic~~ non-isothermal compression of the top space, but condenses during the longer time period as the system is returning to equilibrium.

In this case, a similar analysis as before may be applied to the top gas space.

Under isothermal compression, but with no supersaturation, equation 4.1.-1. becomes

$$\left(\frac{dp}{dt}\right)_{is,c} = (p_o - p_{H_2O})\, v_o \left[\frac{1}{v_1} - \frac{1}{v_o}\right] \qquad 4.1.-7.$$

c = condensation occurring, which leads to an equation similar to 4.1.-5. i.e.

$$\frac{\left(\frac{dp}{dt}\right)_{ad} - \left(\frac{dp}{dt}\right)_{is,c}}{\left(\frac{dp}{dt}\right)_{is,c}} = \frac{p_{1,ad} - p_{1,is,c}}{p_{1,is,c} - p_{o,is}} \qquad 4.1.-8.$$

$$= \left[\frac{p_o}{p_o - p_{H_2O}}\right]\left[\frac{v^{*n} - 1}{v^* - 1}\right] - 1$$

The limit of this equation as $v^* \rightarrow 1$, is

$$\frac{\left(\frac{dp}{dt}\right)_{ad} - \left(\frac{dp}{dt}\right)_{is,c}}{\left(\frac{dp}{dt}\right)_{is,c}} = \left[\frac{p_o}{p_o - p_{H_2O}}\right] n - 1 \qquad 4.1.-9.$$

From this equation, it is seen that as $n \rightarrow 1$, i.e. fully isothermal conditions within the gas, the right hand side

becomes $\frac{p_{H_2O}}{p_o - p_{H_2O}}$

This shows that there could be a slight additional pressure drop due to condensation of water vapour, the numerical ratio being $\frac{1.7}{74.3} = 0.023$. Thus values between 0 and 0.023 on the ordinate of Fig. 4.1.a. could be explained in terms of non-equilibrium partial condensation of water vapour.

As previously stated, experimental values fell within this range after modification had been made.

4.2. INERT BUBBLE RESULTS USING CONSTANT VOLUME TECHNIQUE

The rise of inert nitrogen bubbles through water in the 18" I.D. column provided a means of comparing experimental top pressure time curves with those predicted theoretically.

Thus, curve A of Fig. 4.2.a. represents two similar pressure time curves (one incorporating two timing blips). Appendix 4.2 gives experimental readings of pressure with time for Runs 1 and 2, used in the construction of curve A. Curve B is that predicted on the basis of isothermal expansion of the bubble. Point O marks the instant of bubble release, and also of chart movement, whilst points X and Y correspond to the time instants at which the bubble

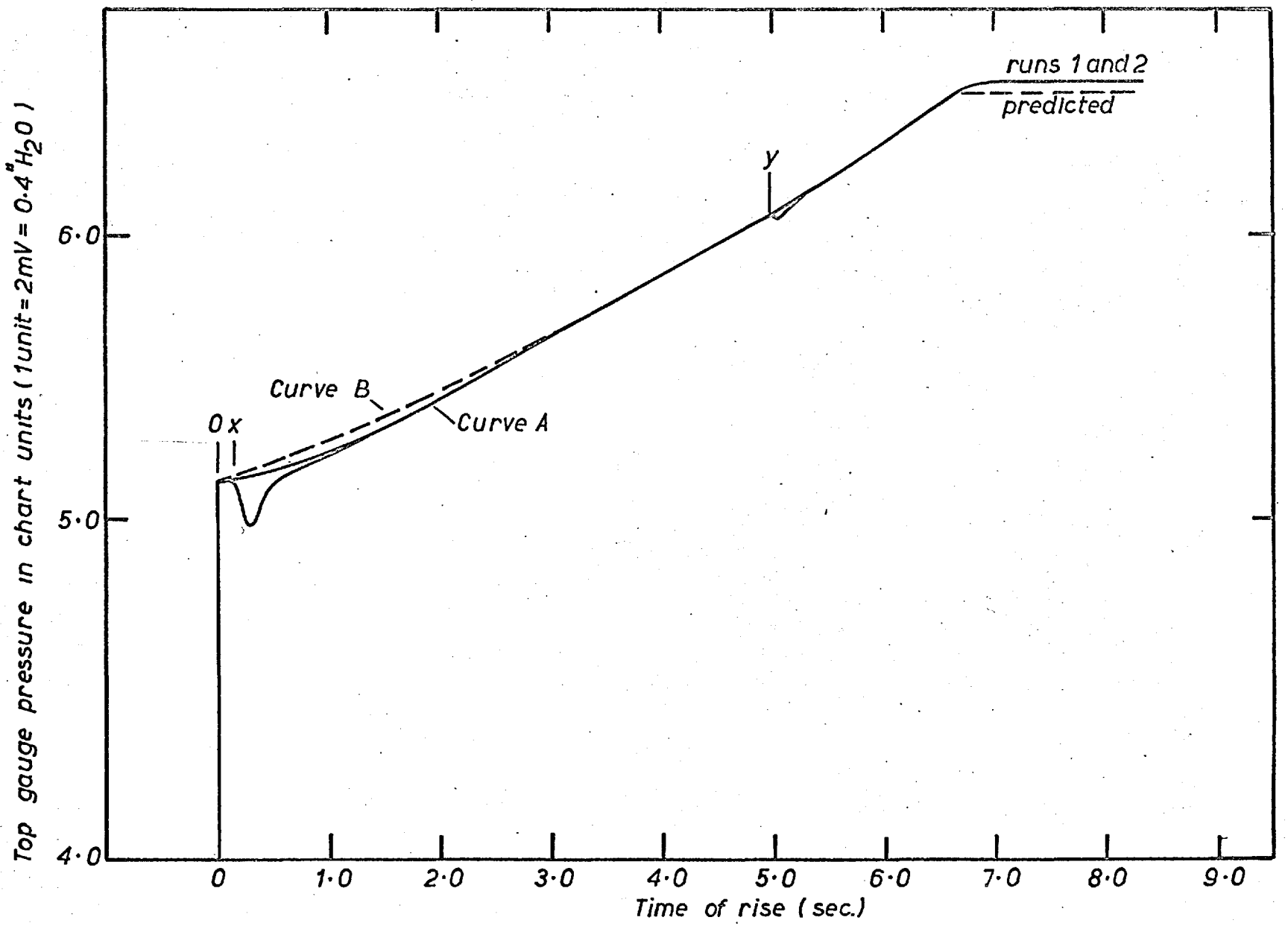

FIG. 4.2.a COMPARISON BETWEEN TYPICAL EXPERIMENTAL PRESSURE-TIME CURVES FOR N_2 BUBBLES IN WATER (CURVE A) & THAT PREDICTED FOR ISOTHERMAL EXPANSION (CURVE B)

passed the light-photocell stations, distances 6.0 cm and 202.3 cm above the inverted cup.

Neglecting the stagnation pressure term ($\frac{1}{2}\rho U^2$), the pressure within the bubble is taken to equal to static pressure within the water at the nose of the bubble i.e.

$$P = p + \rho g\ (H-h) \qquad 4.2.-1.$$

whilst the bubble volume, V, is related to the pressure, p, within the top gas space by the equation presented in 3.3.3.2.

$$V = v_i \left[1 - \frac{p_i}{p}\right] \qquad 4.2.-2.$$

The latter assumes isothermal compression of the top gas space and neglects possible water vapour effects.

Assuming that the gas within the bubble expands isothermally,

$$PV = P_o\ V_o \qquad 4.2.-3.$$

Substituting appropriate values for bubble pressure and volume from 4.2.-1. and 4.2.-2. respectively, in 4.2.-3. gives

$$\left[1 - \frac{p_i}{p}\right]\left[p + \rho g\ (H-h)\right] = \left[1 - \frac{p_i}{p_o}\right]\left[p_o + \rho g H\right] \quad 4.2.-4.$$

Putting h = H in 4.2.-4, the final top pressure, p_1, after bubble rise is given by

$$p_1 = p_o + \rho g H \left[1 - \frac{p_i}{p_o}\right] \qquad 4.2.-5.$$

Also, neglecting to a first approximation the small differences between p and p_o in the term $p + \rho g (H-h)$, the top pressure, p, y seconds after bubble release is related to known constants in the expression

$$\left[1 - \frac{p_i}{p}\right] = \left[1 - \frac{p_i}{p_o}\right] \frac{p_o + \rho g H}{p_o + \rho g (H-h)} \qquad 4.2.-6$$

Calculations based upon 4.2.-5 and 4.2.-6 are given in Appendix 4.2. Curve B was constructed on the basis of equation 4.3.-6, derived in the subsequent section, and resulted in a better approximation of p vs t to that given in 4.2.-6, over the first part of the curve.

As seen, p_y coincides with curves A and B, whilst the final top pressures agree closely with that predicted by equation 4.2.-5, the error in $\frac{(p_1 - p_{predicted})}{(p_1 - p_o)} 100$ being within +3%. It may be concluded from the results that bubbles expanded isothermally, and that the measuring technique was reliable.

4.3. INERT BUBBLE RESULTS USING 'VOLUME DISPLACEMENT' TECHNIQUE

After the necessary modifications to the apparatus described in section 3.3.3.1. had been made, a series of tests on nitrogen bubbles were performed to test the accuracy of the measuring system.

The response of the soap film meter in measuring actual

changes of bubble volume was determined by comparing experimental volume - time measurements with theoretical relationships. Similarly, since subsequent experiments in the measurements of mass transfer coefficients involve estimations of the derivative of the curve showing bubble volume as a function of time, the theoretical relationship for inert bubbles was compared with that found by experiment.

Theory

The rates of change of volume and pressure with respect to time for an inert bubble expanding isothermally is given by

$$P\frac{dV}{dt} + V\frac{dP}{dt} = 0 \qquad 4.3.-1.$$

Also, $$P = P_o - \rho gh \text{ and } \frac{dP}{dt} = -\rho gU \qquad 4.3.-2,3.$$

Furthermore, the instantaneous rising velocity of a bubble is given by

$$U = KV^{1/6} \qquad 4.3.-4.$$

where $K = 25.0\ cm^{\frac{1}{2}}sec^{-1}$ for water, from present results described in section 4.4.

Substitution for U and P in equation 4.3.-1 yields

$$\frac{dV}{dt} = \frac{\rho gKV^{13/6}}{(P_oV_o)} \qquad 4.3.-5.$$

which on inegrating between bubble volumes V_o and V_t, corresponding to t = 0 and t = t,

gives

$$V_t = \left[\frac{V_o}{1/V_o^{1/6} - \frac{7 \rho g K t}{6 P_o}} \right]^{6/7} \qquad 4.3.-6.$$

Table 4.3.-a. gives predicted values of V and $\frac{dV}{dt}$ at time t seconds after the release of known volumes of gas, whilst experimental results are given in Appendix 4.3. A typical volume vs time result (W.23) is presented in Fig. 4.3.a. Bubble volumes agreed within 1.5% of those predicted. i.e. $\frac{V - V_{predicted}}{V_{predicted}}$ 100.

Fig. 4.3.b. gives a plot of smoothed values of $\frac{dV}{dt}$ obtained for 10, 15 and 20 cc bubbles respectively. Two series of experiments on each size of bubble were carried out; a, using a top volume space of 1,000 cc and the meter connected directly to the column with minimum (30cm) length of piping, and b, using a top volume of 2,500 cc and a 300 cm length of 1/4" I.D. tubing connecting the burette beside the bottom of the column to the top gas space. The results showed no difference between the two sets of conditions.

Fig. 4.3.b. shows that apart from an initial time lag which was independent of bubble size, curves of $\frac{dV}{dt}$ accurately follow the relationship given by equation 4.3.-6.

TABLE 4.3.-a.

Given; Height of water above cup, H = 273 cm

P atmospheric = 76 cm Hg

$K = 25.0\ cm^{\frac{1}{2}} sec^{-1}$, $\frac{7}{6}\frac{\rho g K}{P_o} = 0.0223$

TIME sec	INITIAL VOLUME, V_o cm^3	VOLUME, V cm^3	$\frac{dV}{dt}$ $cm^3\ sec^{-1}$
0	10.0	10.00	0.280
1	10.0	10.29	0.299
2	10.0	10.59	0.318
3	10.0	10.92	0.340
4	10.0	11.28	0.363
5	10.0	11.65	0.391
6	10.0	12.06	0.421
7.31	10.0	12.64	0.469
0	15.0	15.00	0.451
1	15.0	15.46	0.446
3	15.0	16.50	0.554
5	15.0	17.69	0.645
6.84	15.0	18.96	0.749
0	20.0	20.00	0.631
1	20.0	20.69	0.676
3	20.0	22.10	0.783
5	20.0	23.81	0.920
6.51	20.0	25.28	1.048

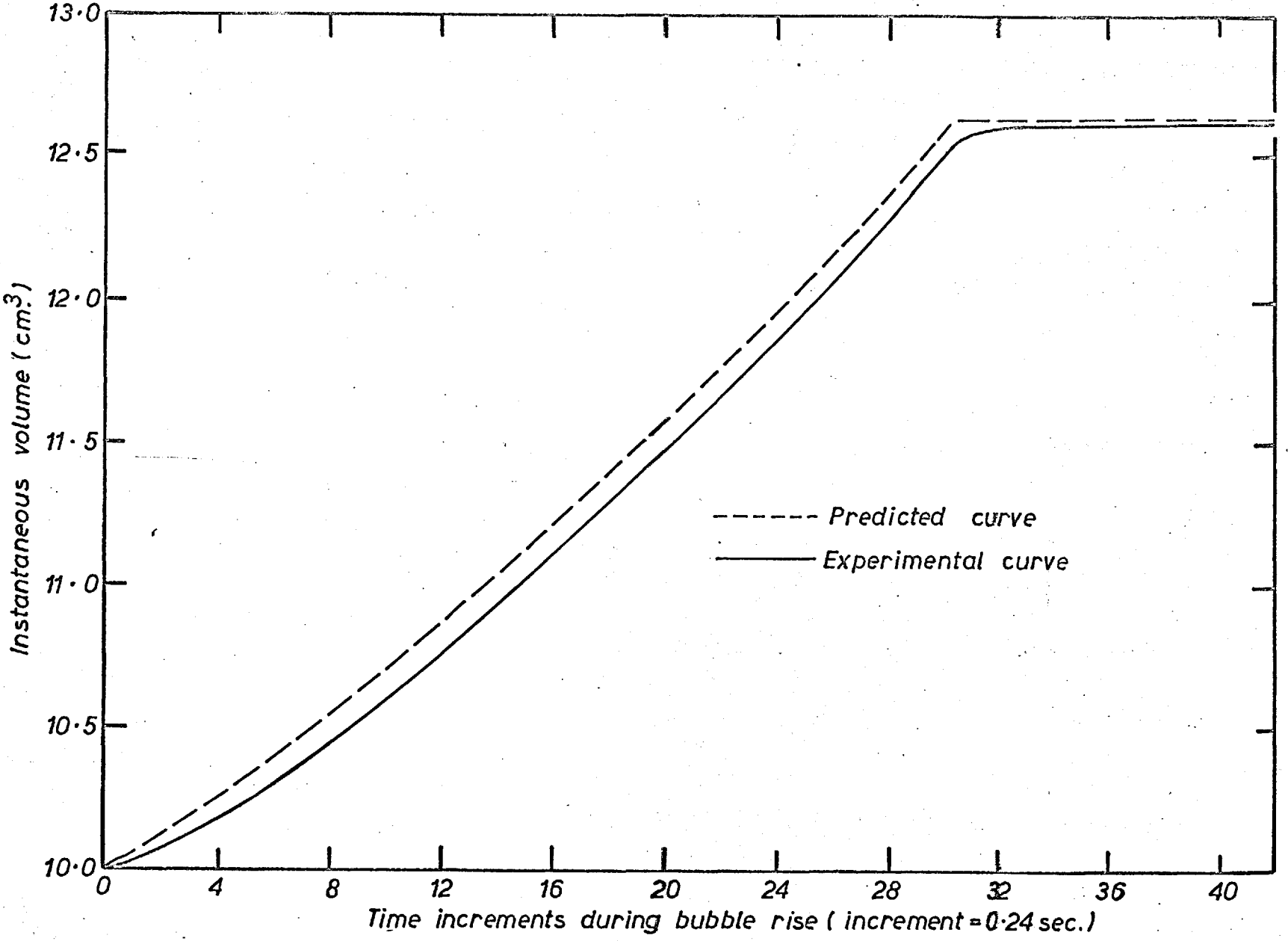

FIG. 4.3.a TYPICAL PLOT OF BUBBLE VOLUME TIME RELATIONSHIP FOR N_2 BUBBLE IN WATER (RUN 23) COMPARED WITH THEORETICAL CURVE

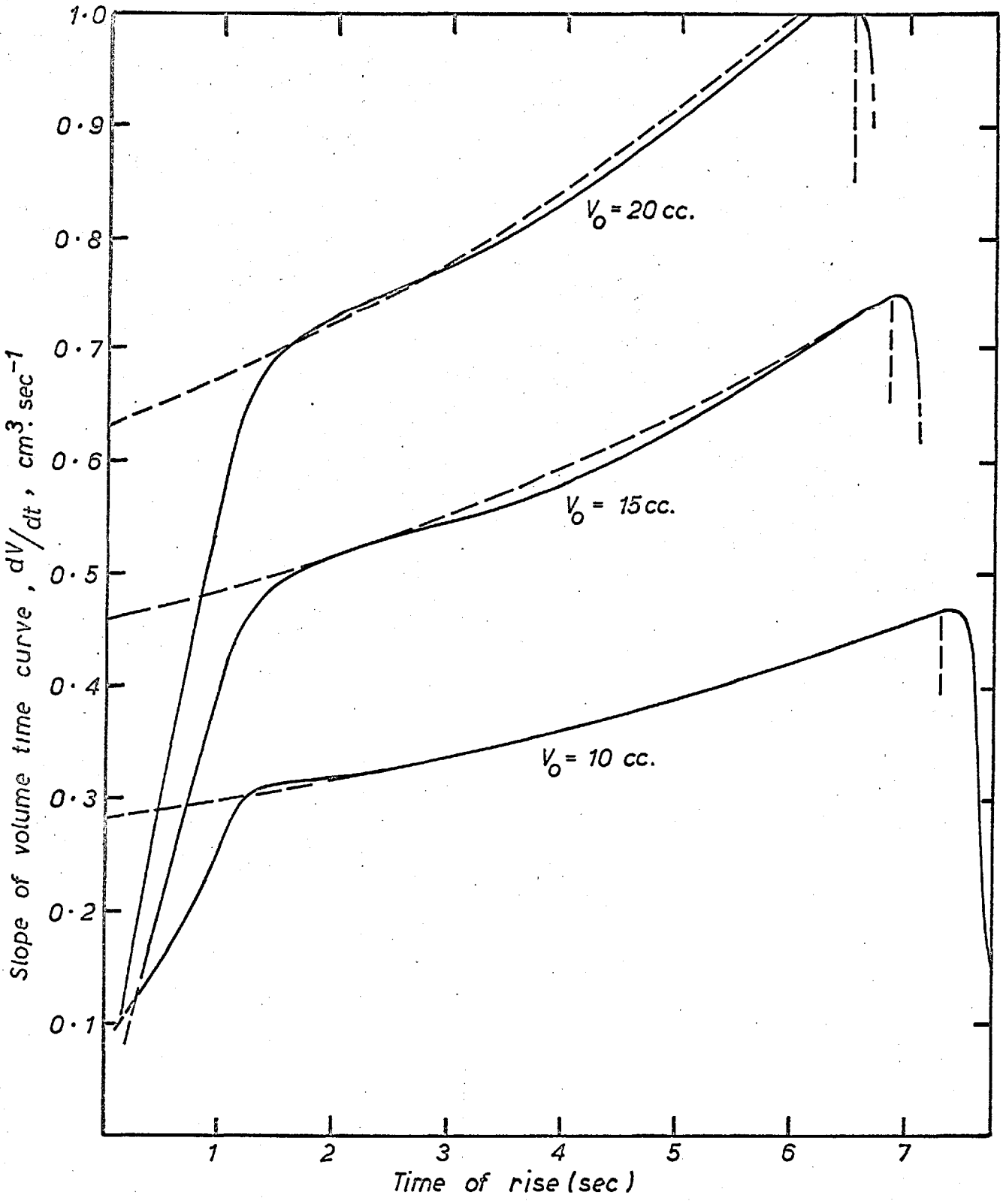

FIG. 4.3.b COMPARISON OF THEORETICAL AND EXPERIMENTAL VALUES OF dV/dt. FOR INERT BUBBLES RISING THROUGH 18" I.D COLUMN

Experimental values of $\frac{dV}{dt}$ were obtained by taking the difference in volume readings of the filmed soap film meter over a small period of time, Δt, and plotting the value of $\frac{\Delta V}{\Delta t}$ as equal to $\frac{dV}{dt}$ at the mid-point position. Smoothed values of $\frac{dV}{dt}$ vs time for individual results gave a close fit to the predicted line, with departures not greater than $\pm$ 0.03 $cm^3/sec.$ for all bubble sizes studied, after the first initial time lag.

In order to confirm that the present approximate method of obtaining curves of $\frac{dV}{dt}$ was justified, a different method, developed for the mass transfer work, was used for RUN W.23. Thus curve A of Fig. 4.3.c. shows a plot of $\frac{dV}{dt}$ obtained by differentiation of a fifth degree polynomial equation which was fitted by the method of least squares to the experimental volume-time relationship shown in Fig. 4.3.a. Curve B was obtained by the present method. As seen, little error was introduced. The results of these calculations, together with experimental results are presented in Appendix 4.3.

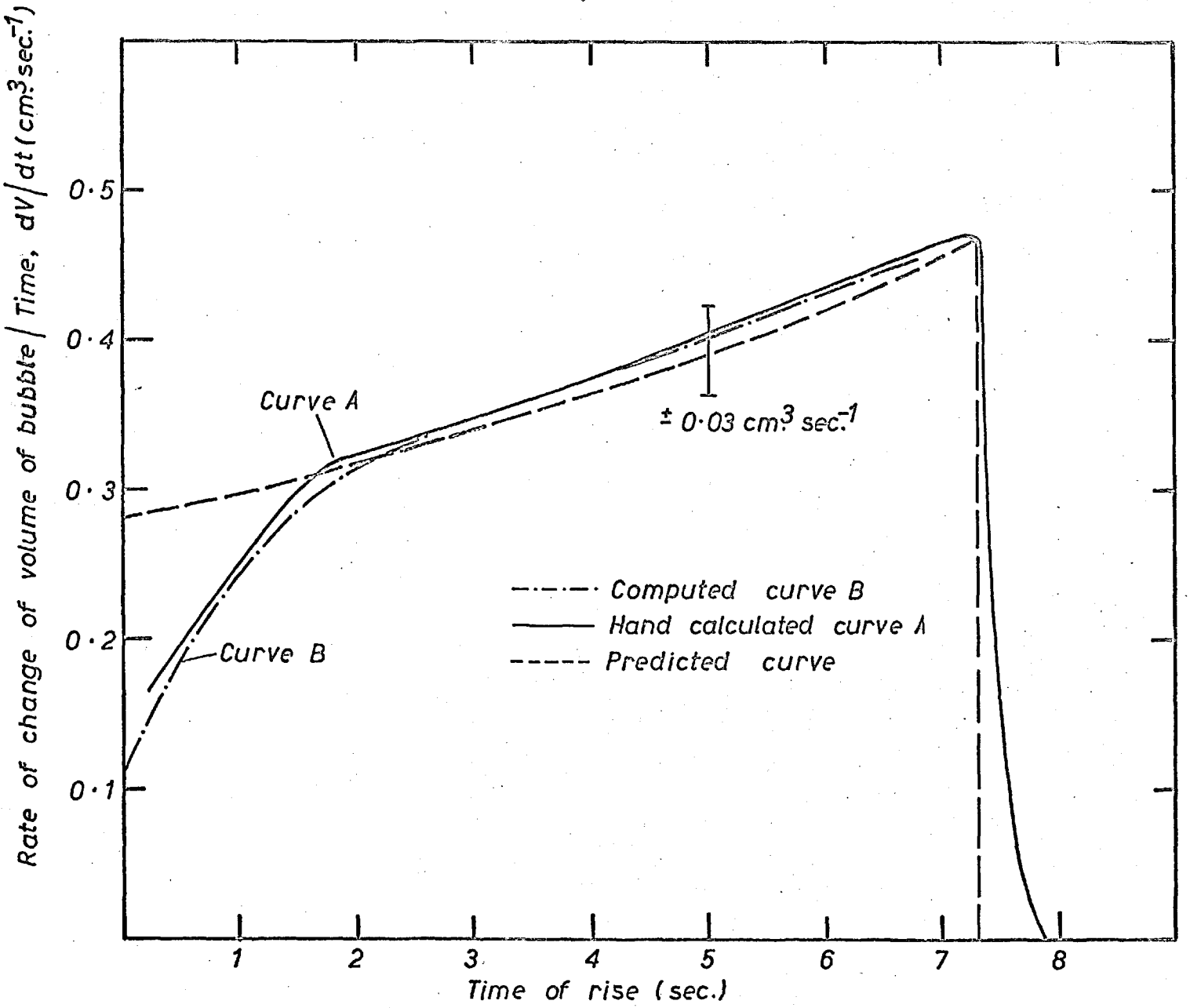

FIG.4.3.c COMPARISON OF THE THEORETICAL & EXPERIMENTAL RATES OF VOLUME CHANGE WITH TIME FOR INERT BUBBLE INITIAL VOLUME 10 cm^3. RUN 23.

4.4. VELOCITIES OF RISING GAS BUBBLES

Using the methods described in Chapter 3, section 3.3.2., velocities of nitrogen bubble rising in tap water and various P.V.A. liquids were obtained. The 18" I.D. column was used to reduce the effect of wall proximity on bubbles up to 100 cc in volume.

Initial work aimed at confirming the relationship obtained by Davies and Taylor (6) between instantaneous values of bubble volume and velocity in tap water. The present results are given in terms of velocity vs average volume of bubble to one sixth power. Fig. 4.4.a. summarises results for bubble rising in tap water. Velocities were measured over two different distances i.e. 140 and 215 cm. Within experimental error, both sets of results fall on the line drawn on the graph, representing the equation

$$U = KV^{1/6} \qquad 5 \text{ cc} \leq V \leq 45 \text{ cc} \qquad 4.4.\text{-}1.$$

where $K = 24.99 \pm 0.15 \text{ cm}^{\frac{1}{2}}\text{sec}^{-1}$.

Alternatively, equation 4.4.-2 may be used to relate the terminal velocity to the radius of the equivalent volume sphere

$$U = C\,(g\,r_e)^{\frac{1}{2}} \qquad 5 \leq V \leq 45 \text{ cc} \qquad 4.4.\text{-}2.$$

where $C = 1.013 \pm 0.006$.

Fig. 4.4.b. summarises the results of rising velocities obtained with various aqueous polyvinyl alcohol

FIG. 4.4a TERMINAL VELOCITIES OF NITROGEN BUBBLES IN TAP WATER vs. ONE SIXTH POWER OF BUBBLE VOLUME

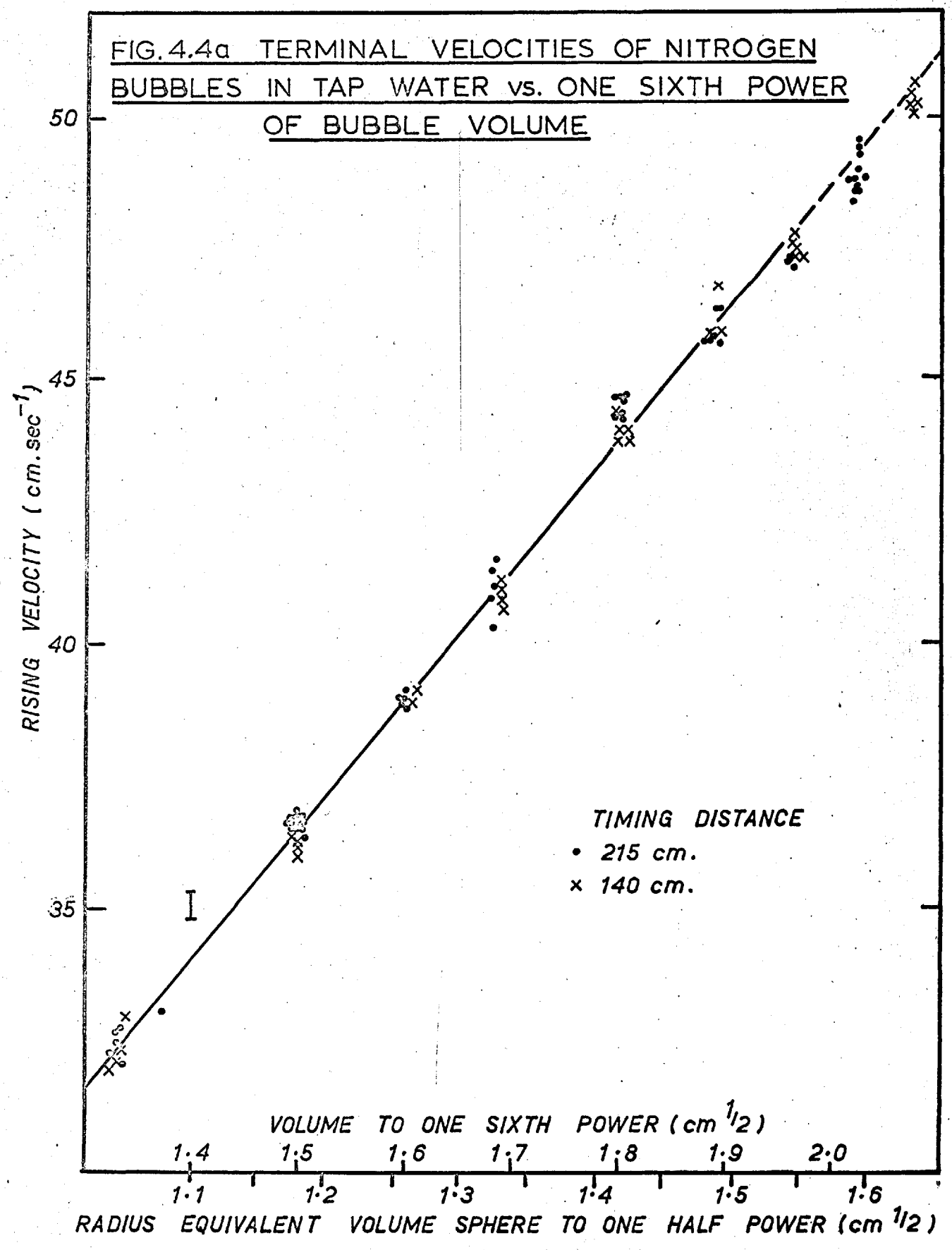

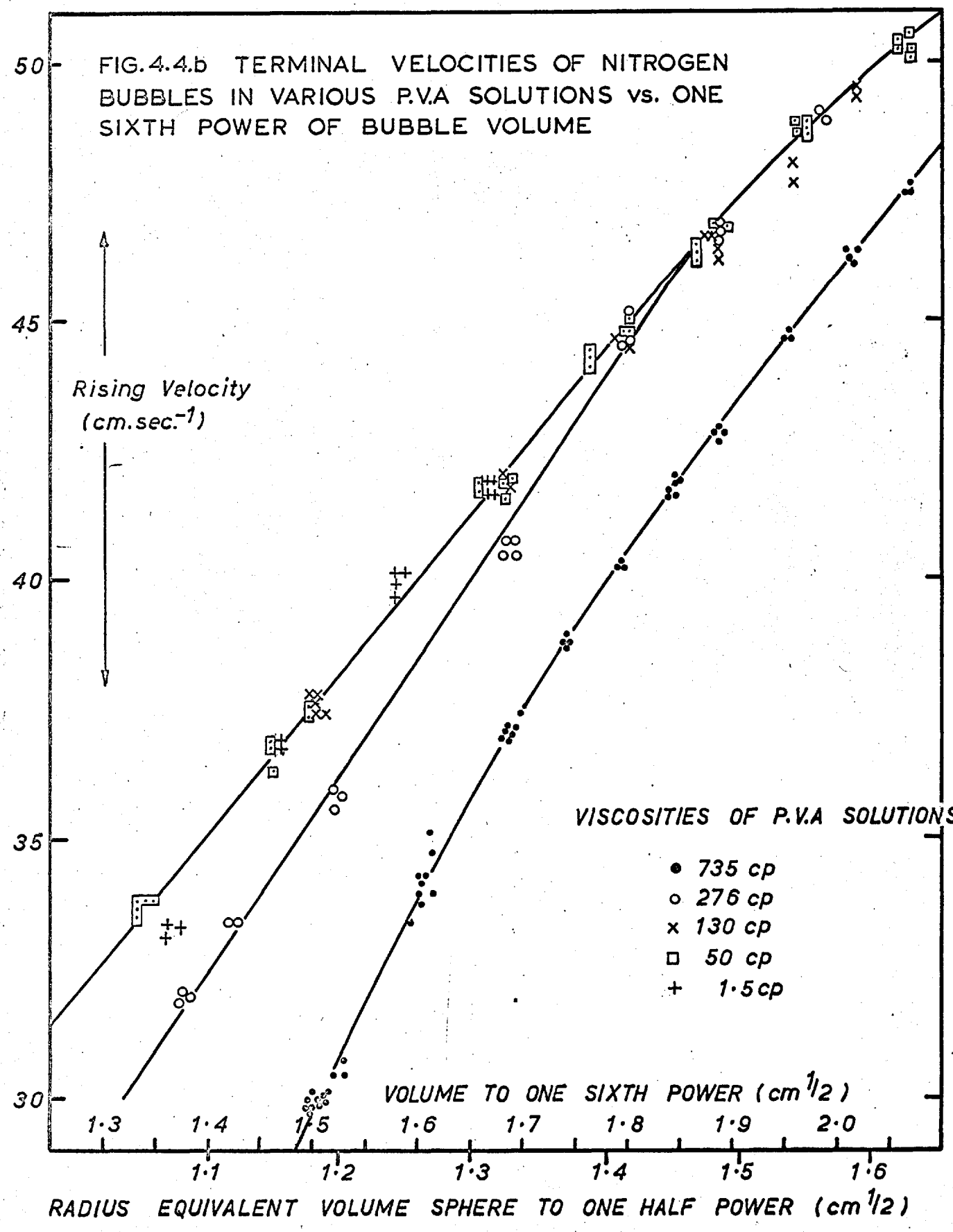
FIG. 4.4.b TERMINAL VELOCITIES OF NITROGEN BUBBLES IN VARIOUS P.V.A SOLUTIONS vs. ONE SIXTH POWER OF BUBBLE VOLUME
Rising Velocity (cm.sec.-1)
50
45
40
35
30
VISCOSITIES OF P.V.A SOLUTIONS
735 cp
276 cp
130 cp
50 cp
1·5 cp
VOLUME TO ONE SIXTH POWER (cm 1/2)
1·3
1·4
1·5
1·6
1·7
1·8
1·9
2·0
1·1
1·2
1·3
1·4
1·5
1·6
RADIUS EQUIVALENT VOLUME SPHERE TO ONE HALF POWER (cm 1/2)

solutions. The value of the slope obtained for liquids with viscosities in the range 1.5 cp. to 130 cp. was

$$K = 24.94 \pm 0.20 \text{ cm}^{\frac{1}{2}}\text{sec}^{-1} \qquad 5 \leq V \leq 45 \text{ cc}$$

or $C = 1.011 \pm 0.008$ "

The final value of K chosen for water and low viscosity liquids was 25.0 $\text{cm}^{\frac{1}{2}}\text{sec}^{-1}$. At higher viscosities, bubble velocities were depressed, especially at low bubble volumes.

The empirical equations representing the curves were:-

276 cp. P.V.A. soln.

$$U = 30.4V^{1/6} - 10.4 \qquad 5 \text{ cc} < v < 40 \text{ cc} \qquad 4.4.-3.$$

735 cp. P.V.A. soln.

$$U = 35.3V^{1/6} - 30.0 \qquad 5 \text{ cc} < V < 30 \text{ cc} \qquad 4.4.-4.$$

$$U = 26.4V^{1/6} - 7.06 \qquad 30 \text{ cc} < V < 100 \text{ cc} \qquad 4.4.-5.$$

4.4.1. Use of Average Volume in Determination of K

The constant, K, in equation 4.4.-1. has been evaluated from the relation found between the average velocity, U, and the arithmetic average volume, $\bar{V}$, of a bubble rising up the column from positions 1 and 2, distance H' cms apart.

In order to correlate present values of K with those reported in the literature, (2, 6), which were evaluated from instantaneous values of volume and velocity, it is necessary to ascertain the ratio of V^*/V. V^* is

defined as that volume of bubble having an instantaneous velocity equal to U, where $U = \frac{H'}{t}$. It has been shown (32) that V* is given by the relationship

$$\left[\frac{V^*}{V_o}\right]^{1/6} = \frac{7\ \rho g H'\ P_o^{1/6}}{6\left(P_o^{7/6} - P_1^{7/6}\right)} \qquad 4.4.-6.$$

where P_o and P_1 represent the fluid pressures at the first and second light-photocell positions respectively. Rearranging 4.4.-6. in terms of $V^*/\bar{V}$, where $\bar{V} = \frac{V_o + V_1}{2}$, gives;

$$\left[\frac{V^*}{\bar{V}}\right]^{1/6} = \frac{7\left[1 - P_1/P_o\right]}{6\left[1 - \left(P_1/P_o\right)^{7/6}\right]} \left(\frac{2}{1 + \left(P_1/P_o\right)^{-1}}\right)^{1/6} \qquad 4.4.-7.$$

A typical experimental value of 0.85 for the ratio of P_1/P_o gives $\left[\frac{V^*}{\bar{V}}\right]^{1/6} = 0.996$.

Substitution for $\bar{V}^{1/6}$ in equation 4.4.-1. in terms of V*, gives $K_{instantaneous} = 25.06 \pm 0.15\ cm^{\frac{1}{2}}sec^{-1}$ compared with the experimental value of $24.99 \pm 0.15\ cm^{\frac{1}{2}}sec^{-1}$. Thus both methods are equivalent, and $\bar{V}$ has been replaced by V in the velocity volume relationships given previously.

4.5. SHAPES OF BUBBLES

Shapes of S.C. bubbles rising in water and various P.V.A. solutions were obtained using the experimental techniques discussed in Chapter 3, section 3.3.1. These measurements were carried out in the 18" I.D. column, in

conjunction with velocity and mass transfer measurements for each concentration of aqueous P.V.A. solution prepared.

Fig. 4.5.a. presents typical photographs obtained, whilst Fig. 4.5.b. gives plots of height and basal radius vs radius of equivalent volume sphere, r_e, for bubbles rising in water, and various P.V.A. solutions.

Although the accuracies of bubble dimensions are not directly estimable due to the scattering effect of P.V.A. on incident light, a plot of bubble volumes calculated from the linear dimension data normally agreed within $\pm$ 10 per cent of measured displacement volumes (Fig.4.5.c.). This indicated linear dimension variations of approximately $\pm$ 3%. Experimental results are given in Appendix 4.5.

4.5.1. Visual Observations

Bubbles of volume greater than 5 cc rose rectilinearly in spherical cap form in all liquids investigated. Bubbles rising in tap water and distilled water exhibited rippling surfaces. At larger volumes (~20 cc), it was noticeable that a marked amount of rippling occurred on the lower portions of the frontal surfaces of the bubble, together with larger scale rippling of the bottom planar surfaces.

Bubble rising in aqueous polyvinyl alcohol, although

15cc.
H_2O,1 cp.

30 cc.
H_2O,1 cp.

20 cc.
130 cp. P.V.A.

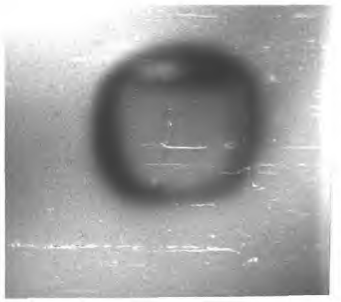

25 cc.
735 cp. P.V.A.

40 cc.
735 cp. P.V.A.

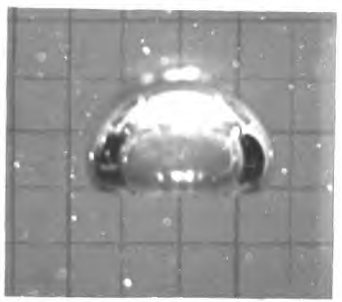

7.5 cc.
Glycerol/H_2O

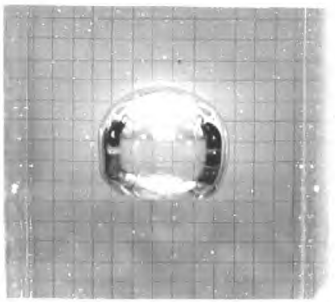

25 cc.
Glycerol/H_2O

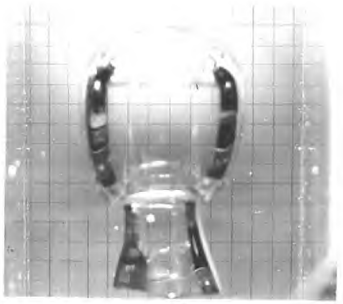

50 cc.
Glycerol/H_2O

Fig.4.5.a. Nitrogen Bubbles rising through various liquids.

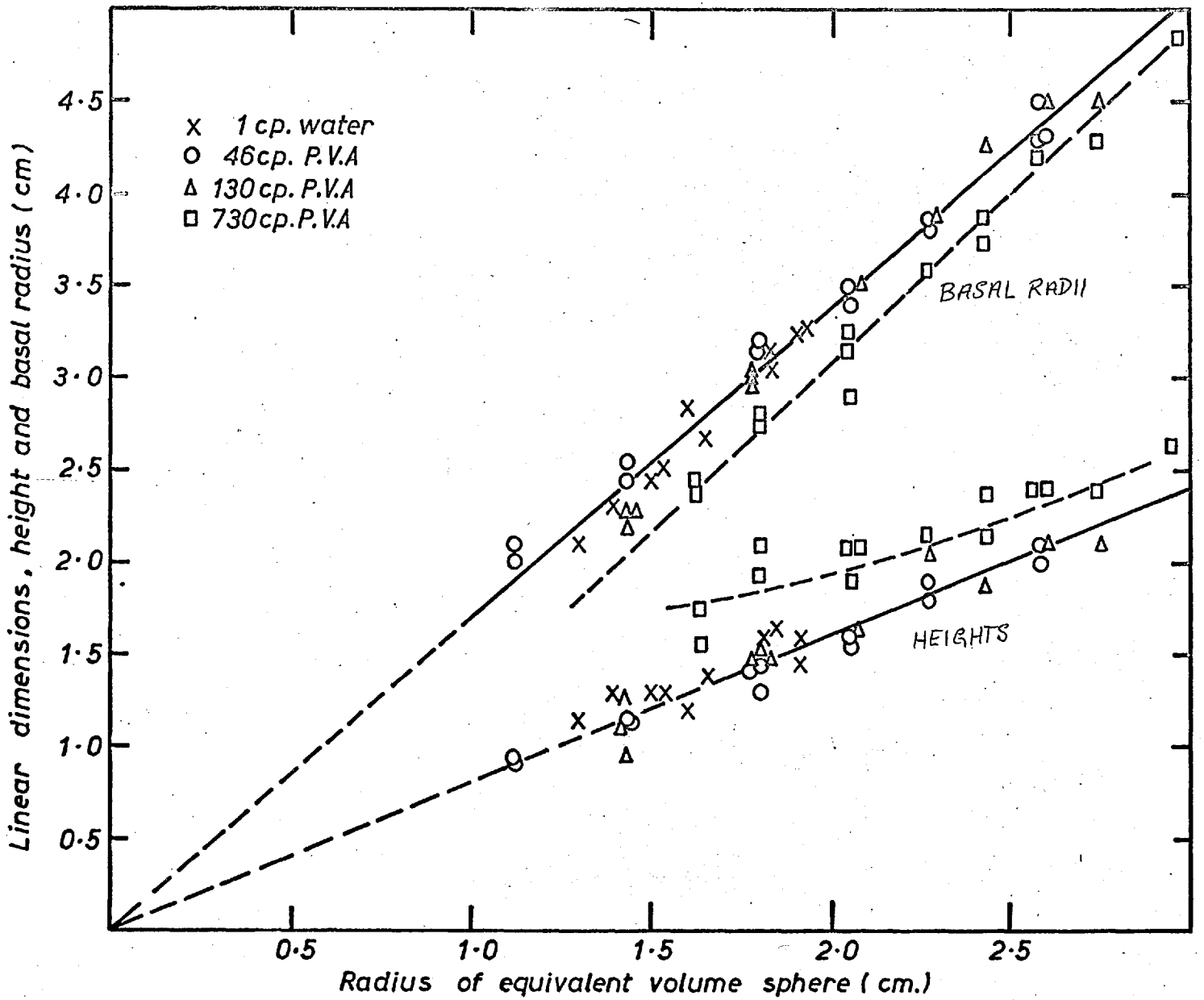

FIG.4.5.b HEIGHTS & BASAL RADII OF BUBBLES RISING IN P.V.A SOLUTIONS OF VARIOUS VISCOSITIES

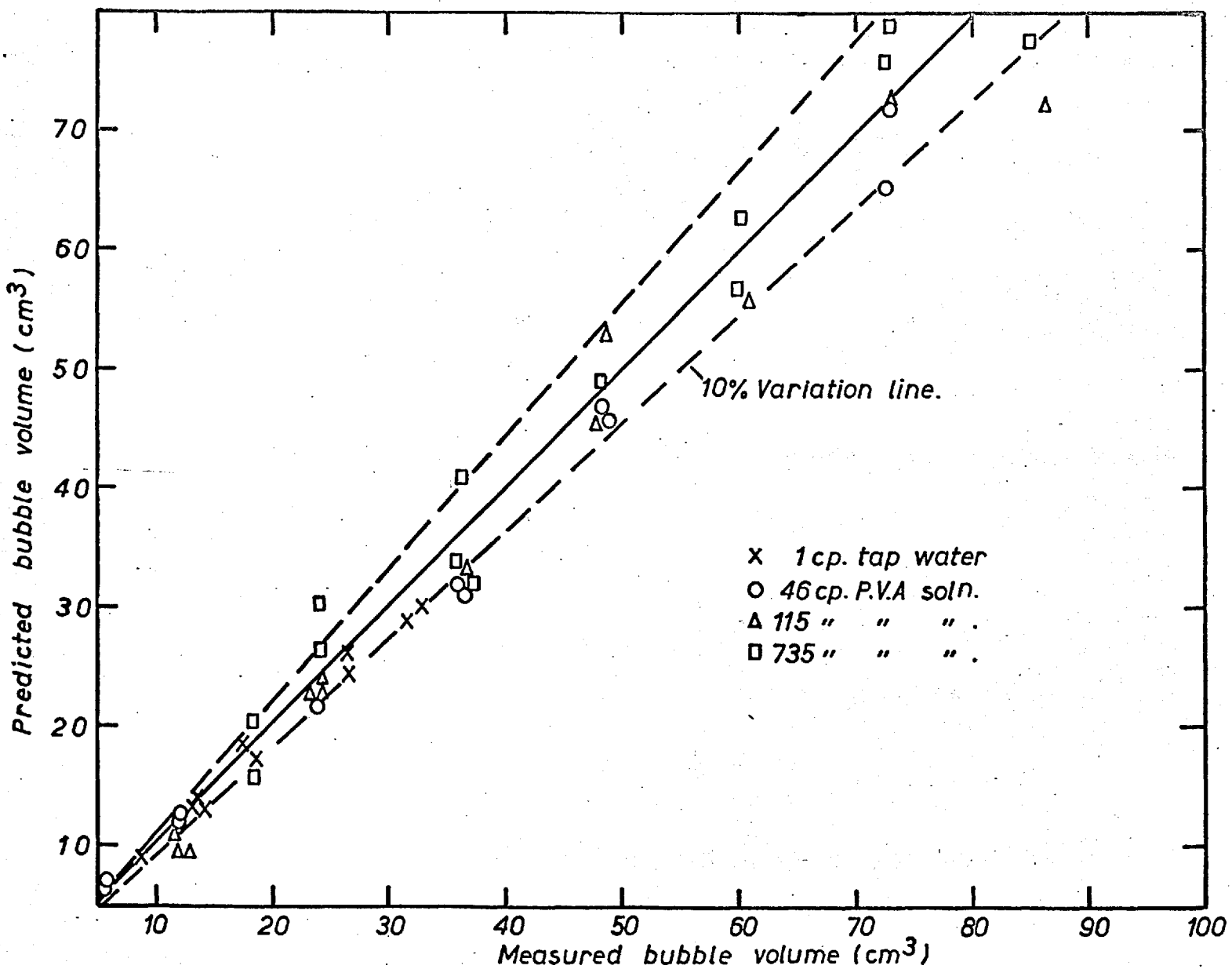

FIG.4.5.c COMPARISON OF MEASURED DISPLACEMENT VOLUMES WITH THOSE CALCULATED FROM PHOTOGRAPHIC LINEAR DIMENSION DATA

of spherical cap shape, were much different in appearance. Even at small concentrations (0.1% P.V.A.), the front surface was perfectly smooth, whilst rippling of the bottom surface was noticeably damped. Ripples were completely absent in more concentrated solutions (130 cp) but a small concave impression could be observed on the rear surface. As the viscosity of the P.V.A. solution was further increased, bubbles greater than approximately 20 cc in volume streamed a thin film of gas from their trailing edge, partially separating the wake fluid from the bulk. The effect was first noticed at viscosities of approximately 200 cp., whilst the gas films or 'skirts' became more stable with increasing viscosity. A similar phenomenon was observed for bubbles rising through 1,000 cp glycerol/water solution. (Fig. 4.5.a.).

In the case of the larger bubbles (40 cc), portions of this gas film sometimes broke away. These films rapidly collapsed to form very small bubbles.

4.5.2. Shape of Wakes

The shapes of wakes carried up behind S.C. bubbles rising in water may be seen from typical photographs presented in Figs. 4.5.2. a and b. These show the sequence of events following the emergence of a bubble through a 6" diameter aperture set in a flange separating

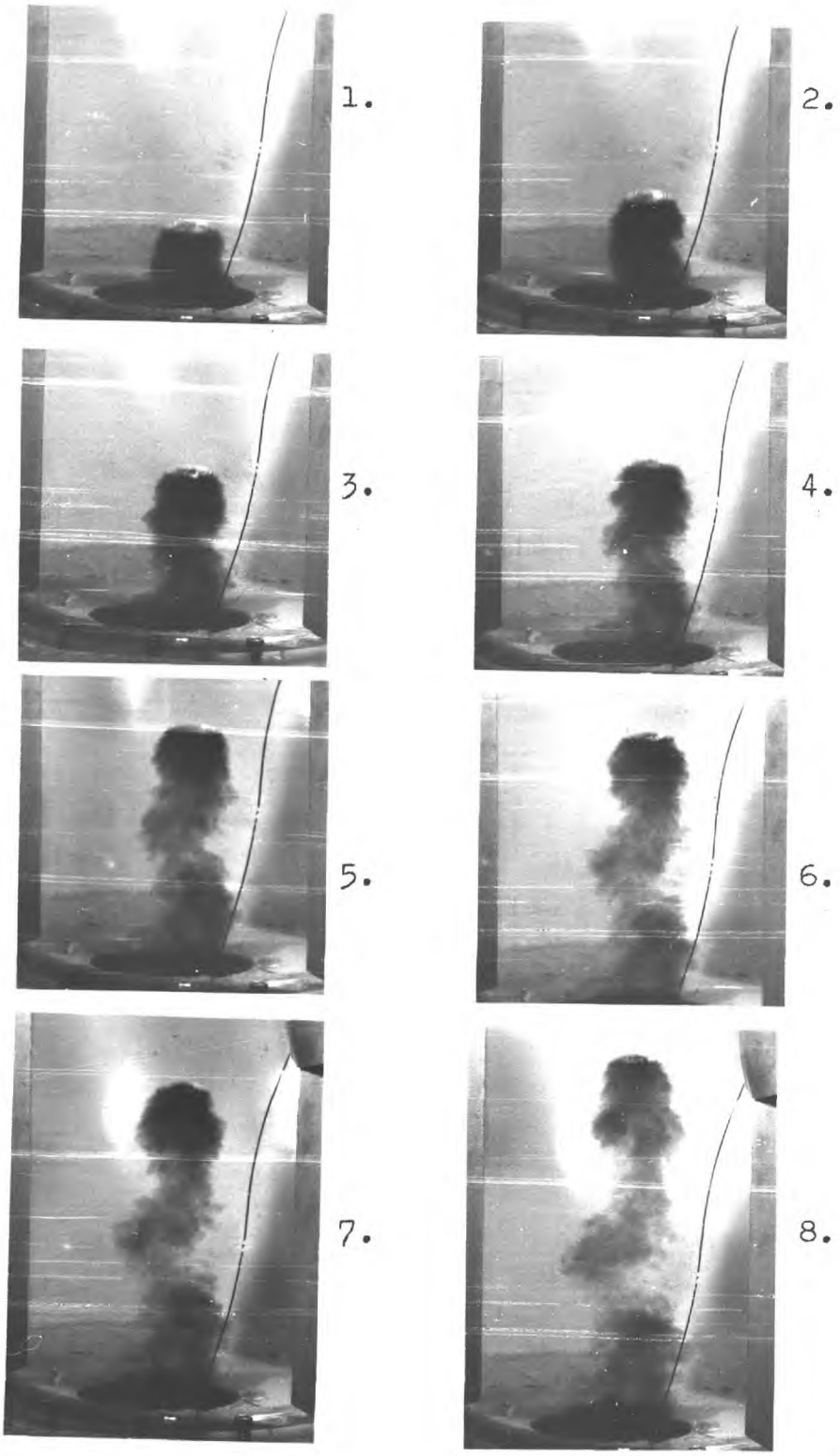

Fig.4.5.2.a. Wake behind S.C. bubble in H_2O (Δt = 0.13 secs.)
V = 23 cc.

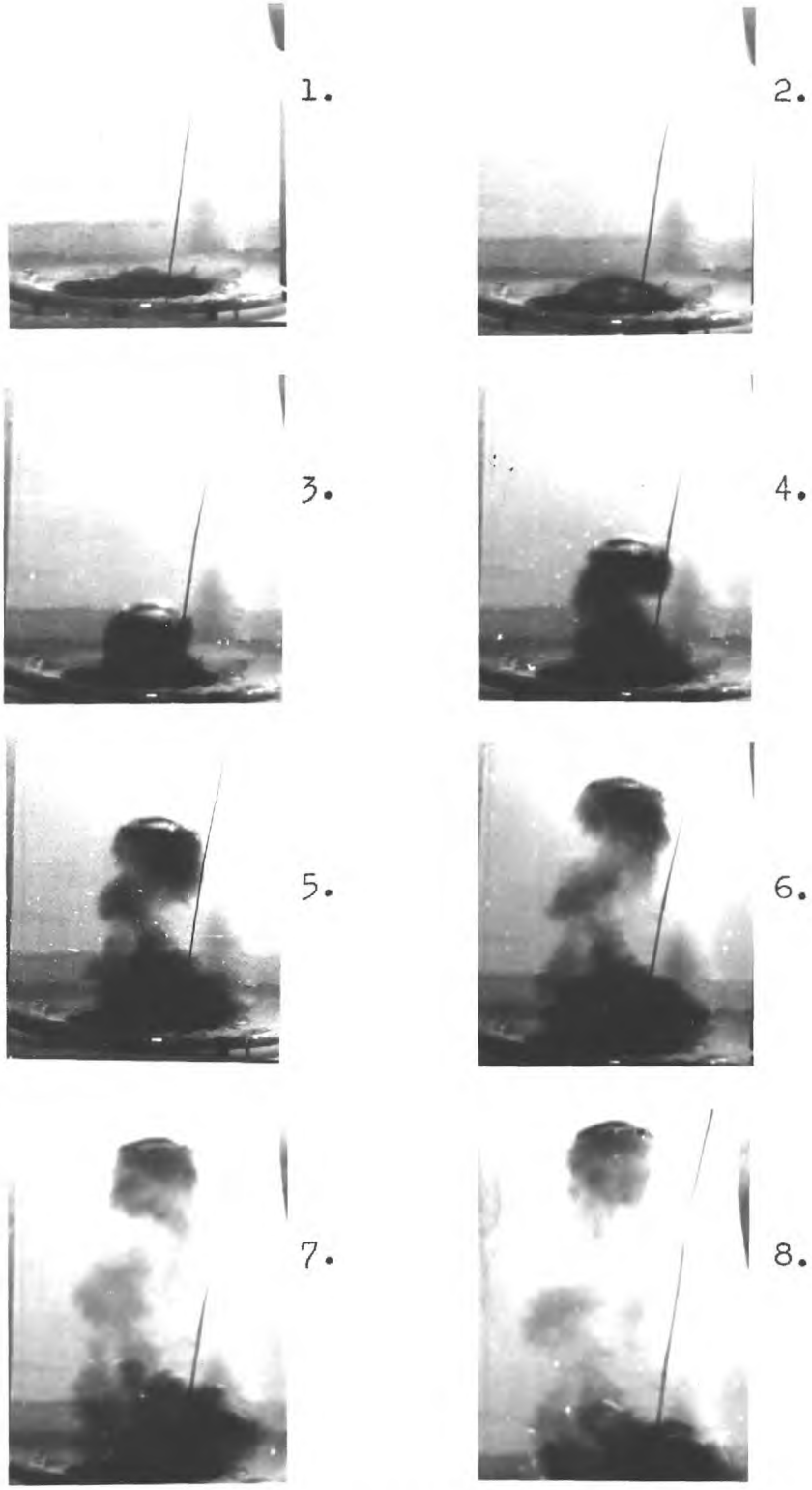

Fig.4.5.2.b. Wake behind S.C. bubble in H_2O (Δt = 0.17 secs.)
V = 34 cc.

the top and bottom parts of the 18" I.D. column. The water in the lower section of the column, which was coloured black by the addition of a few grains of water soluble nigrosine dye, was separated from the top section by a plane, moveable shutter.

Generally, it is apparent that a S.C. bubble entrains a large amount of fluid behind its base. The original material within this 'enclosed wake' is gradually diluted by turbulent mixing with the surrounding fluid. The discarded material is deposited behind the moving bubble in the form of a relatively quiescent spout or wake with a cross section similar to the basal width of the bubble. As seen from the photographs, this spout is tortuous in appearance.

The enclosed wake contains an annular vortex of recirculating wake fluid. The limits of this wake are well defined just behind the bubble, but become more diffuse in the lower regions and finally disappear in the lowest parts of the 'enclosed wake' where turbulent mixing with the bulk fluid is greatest.

Although precise measurements of wake dimensions are impossible, tentative outlines have been drawn around the 'boundaries' and extrapolated into the diffuse region at the bottom of the enclosed wake. The overall shape of the bubble and its associated wake approximates to an

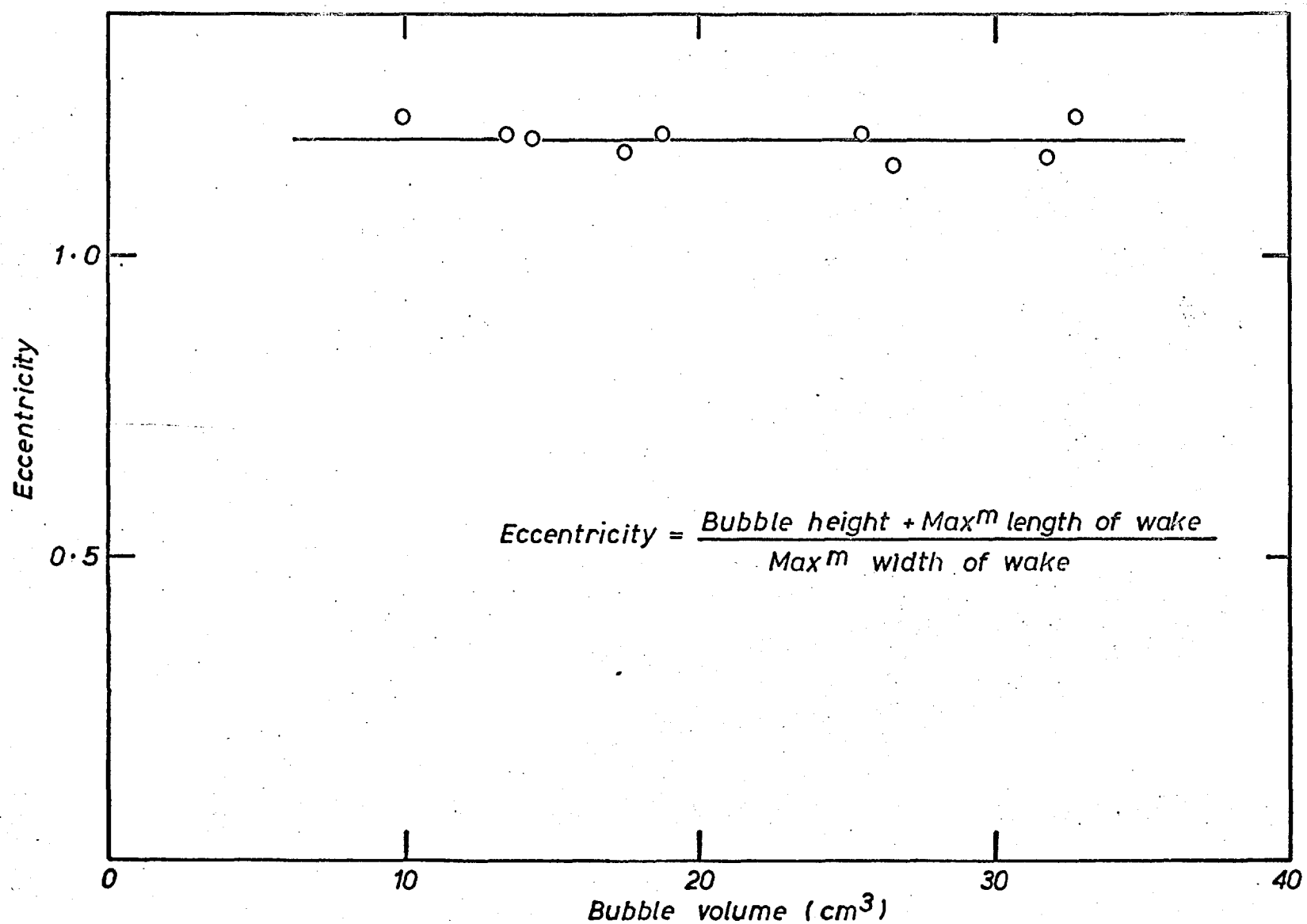

FIG.4.5.2c SHAPES OF 'ENCLOSED WAKES' CARRIED BEHIND S.C BUBBLES IN WATER.

ellipsoid, of major axis equal to the maximum height of the bubble and wake, and of minor axis equal to the maximum width of the wake. As seen from Fig. 4.5.2.c., the eccentricity is independent of bubble volume in the range studied, with a value of 1.20 ± 0.05.

Wakes in Highly Viscous Liquids

The wakes contained behind S.C. bubbles rising in more viscous P.V.A. liquids (>200 cp) are accurately outlined by the thin skirts of gas separating the wake from the bulk of the liquid. Again, extrapolation was necessary close to the lower stagnation region of the wake, since the skirts did not totally enclose the wake. The wake boundaries are extremely stable for bubble volumes up to approximately 35 cc in 730 cp P.V.A. solutions, above which slight instabilities become evident in the lower parts of the skirt, increasing with bubble volume. Similarly, at 350 cp, skirts were less stable, wavering of the lower parts being evident.

The results for inert bubbles rising in 730 cp solution are presented in Fig. 4.5.2.d.

At low volumes, the eccentricity of the bubble and its associated wake is less than unity but at volumes greater than approximately 35 cc eccentricity becomes independent of the volume with a value of 1.25 ± 0.075.

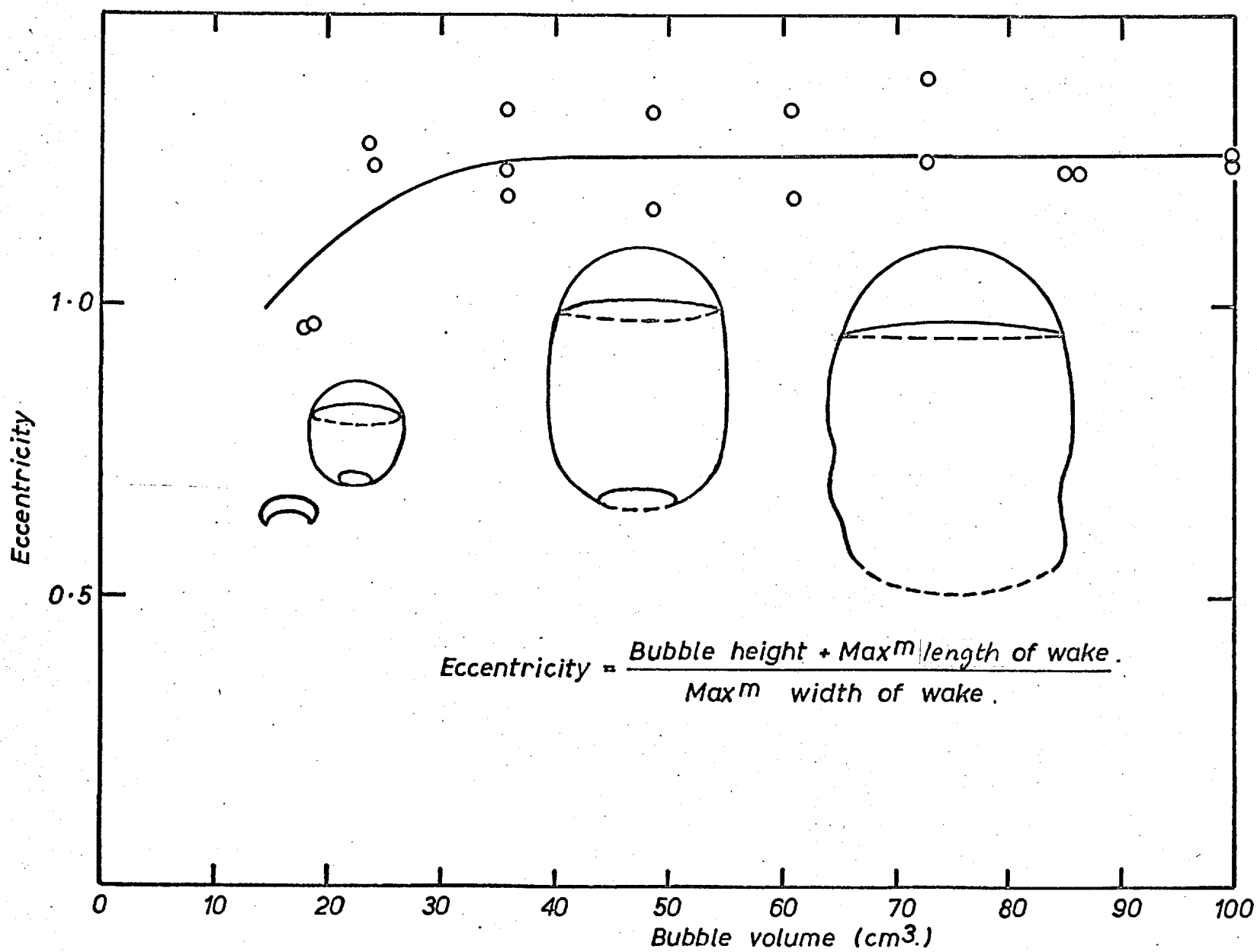

FIG. 4.5.2.d SHAPES OF 'ENCLOSED WAKES' CARRIED BEHIND BUBBLES IN 735 cp P.V.A SOLUTION

4.6. MEASUREMENT OF TRANSFER RATES

Since the present work is concerned mainly with instantaneous mass transfer rates, these have been described in terms of a mass transfer coefficient, k_L, first defined in section 1.1.1.

$$\dot{n} = k_L A_e (C_I - C_B) \qquad 4.6.-1.$$

This basic equation must be adopted to describe k_L for a rising bubble in terms of known or directly measurable properties of the system under investigation.

4.6.1. Theory of Measurement

1. Absorption from CO_2 bubble by volume displacement method

a. The area of a sphere, A_e, whose volume is equal to the bubble's volume, V, may be replaced using the equation

$$A_e = SV^{\frac{2}{3}} \qquad 4.6.-2.$$

where S = Shape Factor of a Sphere, 4.837.

b. Over the present range of experimental liquid pressures (1-2 Atmos), the solution of CO_2 in water is known to follow Henry's Law. (55). Thus, the interfacial solute concentration of CO_2 may be related to the CO_2 partial pressure within the bubble by the equation

$$C_I = \frac{\beta P_{CO_2}}{273 R} \qquad 4.6.-3.$$

where β = Bunsen Solubility Coefficient, equal to the volume of gas (cc) [corrected to 273°K and 1 Atmos of CO_2]

dissolved in 1 cc of liquid.

P_{CO_2} = partial pressure of CO_2 in atmospheres.

R = ideal gas constant in Atmos cc/°K/gm mole.

C_I = number of gm. moles dissolved in 1 cc of liquid.

Equation 4.6.-3. assumes interfacial chemical equilibrium between CO_2 in the gas and liquid phases. C_B was maintained at zero by purging the liquid phase with nitrogen prior to transfer experiments.

c. $\dot{n}$, the number of moles of CO_2 transferred per second from the bubble, may be related to the volume and pressure of the gas within the bubble, assuming isothermal conditions, by

$$\dot{n} = -\frac{1}{R\theta}\left[P\frac{dV}{dt} + V\frac{dP}{dt}\right] \qquad 4.6.-4.$$

Substitution of $\dot{n}$, A_e and C_I in equation 4.6.-1. leads to

$$-\frac{1}{R\theta}\left[P\frac{dV}{dt} + V\frac{dP}{dt}\right] = k_L\, S V^{\frac{2}{3}}\left[\frac{\beta P}{273R} - 0\right] \qquad 4.6.-5.$$

where $P_{CO_2} = P$, for a bubble of pure CO_2.

Also,

$$P = P_o - \rho g \int_{o}^{t} U\,dt \qquad 4.6.-6.$$

If the bubble velocity between 0 and t is assumed to be constant and given by

$$U = K\,\bar{V}^{\,1/6}$$

where

$$\bar{V} = \frac{V_o + V_t}{2}$$

this expression may be rewritten as

$$P = P_o - \rho g K \bar{V}^{1/6} t \qquad 4.6.-7.$$

from which it follows that

$$\frac{dP}{dt} = -\rho g K \bar{V}^{1/6} \qquad 4.6.-8.$$

In the case of bubbles rising through highly viscous P.V.A. liquids, the appropriate equations given in section 4.4. were used for velocity relationships. Equation 4.6.-7 becomes

$$P = P_o - \rho g (A + B \bar{V}^{1/6} t) \qquad 4.6.-7a.$$

Substitution for P and $\frac{dP}{dt}$ in 4.6.-5. from 4.6.-7. and 4.6.-8. respectively, gives a differential equation expressing k_L in terms of V, $\frac{dV}{dt}$ and known constants.

$$k_L = -\frac{273}{S\beta\theta}\left[\frac{1}{V^{\frac{2}{3}}}\frac{dV}{dt} - \frac{V^{\frac{1}{3}}}{\frac{P_o}{\rho g K \bar{V}^{1/6}} - t}\right] \qquad 4.6.-9.$$

Provided that U and k_L are assumed to be constant this equation may be integrated from V_o to V_1 to give

$$\frac{(P_o V_o)^{\frac{1}{3}} - (P_1 V_1)^{\frac{1}{3}}}{P_o^{4/3} - P_1^{4/3}} = \frac{k_L}{4}\frac{S\beta\theta}{\rho g K \bar{V}^{1/6}} \qquad 4.6.-10.$$

P_1 is the final pressure in the bubble, and is equal to $(P_o - \rho g U t_1)$.

2. Desorption of CO_2 by volume displacement technique

The derivation of the desorption equation follows a similar procedure, with the additional consideration of bulk concentrations of CO_2 in the bubble and liquid taken into account.

The mole fraction of CO_2 in an initially pure bubble of nitrogen is given by

$$X_{CO_2} = \frac{n_{total} - n_{N_2}}{n_{total}} = \frac{P\,V - P_o V_o}{P\,V} = 1 - \frac{P_o V_o}{P\,V} \qquad 4.6.\text{-}11.$$

Assuming that there is no resistance in the gas phase, the solute concentration of CO_2 at the interface is related to the bulk partial pressure of CO_2 within the bubble by equation 4.6.-3.

$$C_I = \frac{\beta\, P_{CO_2}}{R273} = \frac{\beta\, P X_{CO_2}}{R273}$$

Substitution for X_{CO_2} from 4.6.-11 gives

$$C_I = \frac{\beta\, P}{R273}\left[1 - \frac{P_o V_o}{P\,V}\right] \qquad 4.6.\text{-}12.$$

Since the liquid was saturated with streams of small bubbles of CO_2 prior to desorption runs, one possible assumption would be that the solute concentration of CO_2 throughout the column was related to the hydrostatic pressure according to Henry's Law, so that

$$C_B = \frac{\beta\, P}{R273} = \frac{\beta\left(P_o - \rho g h\right)}{R273}$$

Substituting these expressions in equation 4.6.-4. where $\dot{n}$ is now positive since gas is transferred into the bubble, and rearranging as in 4.6.-9. gives

$$k_L = \frac{273\ \rho g\ (K\bar{V}^{1/6})\ V^{\frac{1}{3}}}{S\beta\theta\ \ (P_o V_o)}\left[\left\{\frac{P_o}{\rho g K\bar{V}^{1/6}} - t\right\}\frac{dV}{dt} - V\right] \qquad 4.6.\text{-}13.$$

which may be integrated between V_o and V_1 assuming k_L and U are constant, to give

$$\frac{[P_1V_1]^{4/3} - [P_oV_o]^{4/3}}{P_o^{4/3} - P_1^{4/3}} = \frac{k_L\ S\beta\theta\ P_oV_o}{273\rho g K\bar{V}^{1/6}} \qquad 4.6.\text{-}14.$$

3. Absorption from CO_2 bubble using constant volume technique

In this case, bubble volume changes were measured in terms of equivalent pressure changes in the top gas space, and are related by equation 4.2.-2.

$$V = v_i\left[1 - \frac{p_i}{p}\right]$$

from which it follows that

$$\frac{dV}{dt} = \frac{p_i v_i}{p^2}\frac{dp}{dt} \qquad 4.6.\text{-}15.$$

subscript i, refers to initial conditions existing within the top gas space, i.e. before the introduction of gas into dumping cup.

The pressure in the bubble is given by

$$P = p + \rho g\left[H - \int_o^t KV^{1/6}\,dt\right] \qquad 4.6.\text{-}16.$$

from which it follows that

$$\frac{dP}{dt} = \frac{dp}{dt} - \rho g K V^{1/6} \qquad 4.6.-17.$$

In order to obtain a general solution for the mass transfer equation, the assumption of constant rising velocity was not made. In the case of present results, changes in bubble volume were small and lead to variations in U of not more than 2%, so that negligible error would have resulted from considering U to be constant as in 4.6.-8. However, when bubbles are rising in liquids in which the top space is under partial vacuum, bubble volumes may change appreciably (e.g. 500%), so that changes in velocity must be considered. (Eqtn. 4.4.-1. assumed valid).

Substitution of V, $\frac{dV}{dt}$, P and $\frac{dP}{dt}$ in equation 4.6.-5. and rearrangement yields,

$$k_L = -\frac{273}{S\beta\theta}\left[\left[\left(\frac{p}{(p-p_i)v_i}\right)^{\frac{2}{3}}\frac{p_i v_i}{p^2} + \left(\frac{(p-p_i)v_i}{p}\right)^{\frac{1}{3}}\frac{1}{p+\rho g(H-\int_o^t KV^{1/6}dt)}\right]\frac{dp}{dt}\right]$$
$$+\frac{273}{S\beta\theta}\left[\frac{\rho g K v_i^{\frac{1}{2}}(1-p_i/p)^{\frac{1}{2}}}{p+\rho g(H-\int_o^t KV^{1/6}dt)}\right] \qquad 4.6.-18.$$

Thus k_L may be computed from changes in top pressure, p, and other known constants.

4.6.2. Calculations Involving Mass Transfer Equations

a. Calculation of k_L by Constant Volume Equation

Substitution in the appropriate differential equation (4.6.-9., 4.6.-13. or 4.6.-18.) of known experiment constants, together with value of V and $\frac{dV}{dt}$ (or p and $\frac{dp}{dt}$) at time t seconds after bubble release leads to the solution of k_L.

In order to show a typical calculation using equation 4.6.-18, an example of absorption of CO_2 from a bubble rising in water has been chosen. The method of measurement was by the constant volume technique and table 4.6.2.-b. shows observed values of gauge pressure at successive time intervals after the release of a 17.6 cc bubble. (See second column).

These values of Δp have been plotted in Fig. 4.6.2.a. Two curves have been drawn so as to smooth the data, one estimated visually, the other representing a polynomial of the fifth degree in time i.e.

$$\Delta p = a_o + a_1 t + a_2 t^2 + a_3 t^3 + a_4 t^4 + a_5 t^5 \quad 4.6.-19.$$

The coefficients of this polynomial were determined by the method of least squares and formed part of a computor programme prepared for the calculation of instantaneous mass transfer coefficients using a form of equation 4.6.-18.

In order to ease computation of k_L, equation 4.6.-18. has been restated in terms of a system of units relevant

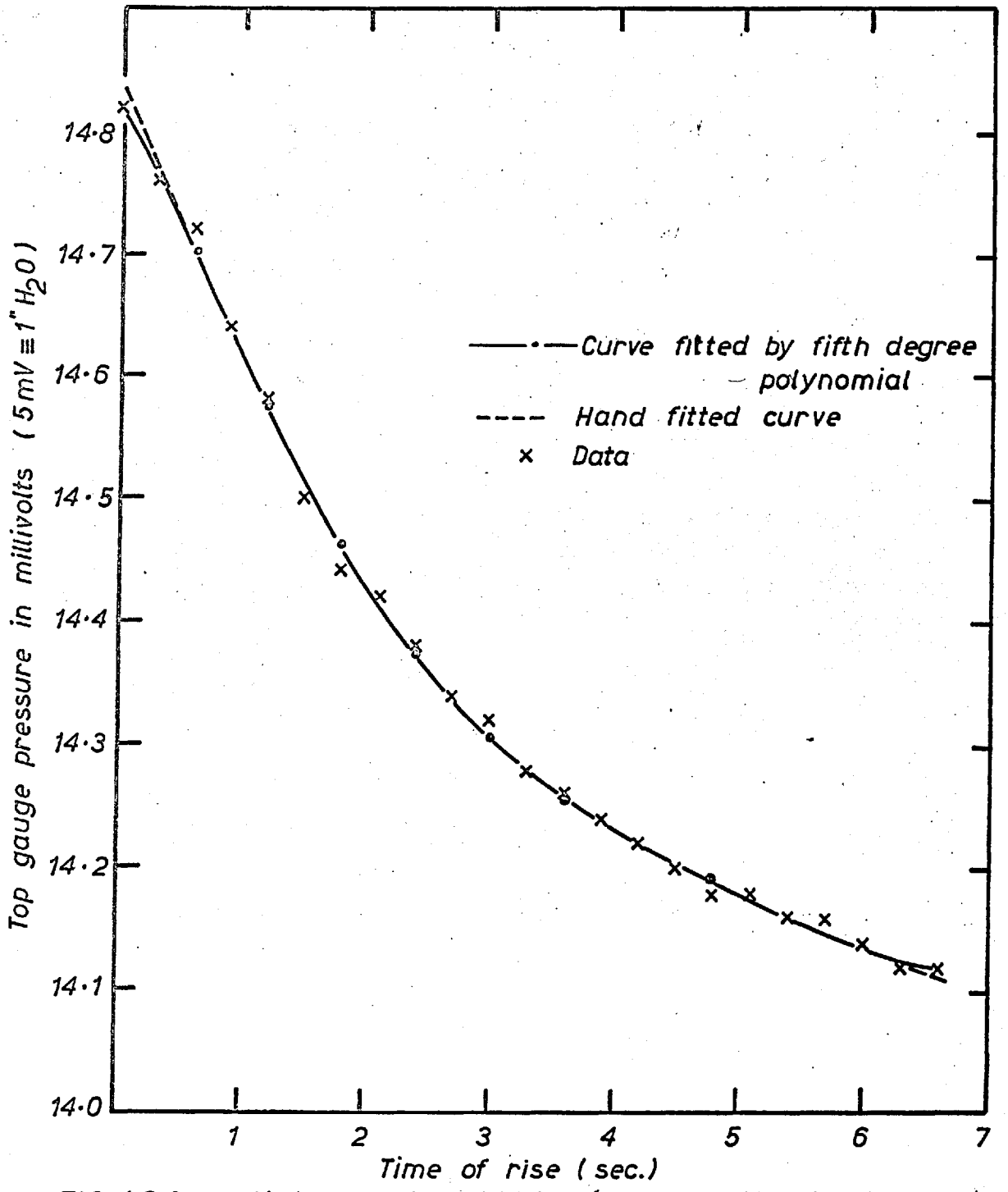

FIG. 4.6.2a EXAMPLE OF SMOOTHED CURVES TO FIT DATA OF TOP GAUGE PRESSURE WITH TIME.

HAND CALCULATED EXAMPLE FOR CO_2 ABSORPTION IN TAP WATER BY CONSTANT VOLUME TECHNIQUE

TABLE 4.6.2.-b

Time Interval 0.3 sec. Temperature 21.4°C. INITIAL TOP PRESSURE 1 ATMOS (2035 mV), N = 21

TIME (sec) t	CHART UNITS $\frac{mV}{2}$	TOTAL PRESSURE (mV) e	BUBBLE VOLUME $\frac{(e-e_i)}{e} v_i$ (cc)	de/dt mV sec^{-1}	1st BRACKET IN 4.6.-18B cm sec^{-1}	2nd BRACKET IN 4.6.-18B	TRANSFER COEFF. cm sec^{-1}
0.0	7.41	2049.82	17.63	-0.240	-0.0420	0.0784	0.0275
0.3	7.38	2049.77	17.58				
0.6	7.36	2049.71	17.50	-0.206	-0.0364	0.0806	0.0267
0.9	7.32	2049.64	17.42				
1.2	7.29	2049.57	17.34	-0.173	-0.0307	0.0815	0.0256
1.5	7.25	2049.51	17.26				
1.8	7.22	2049.45	17.20	-0.145	-0.0258	0.0831	0.0248
2.1	7.2.	2049.41	17.16				
2.4	7.19	2049.37	17.10	-0.120	-0.0215	0.0846	0.0242
2.7	7.17	2049.34	17.07				
3.0	7.16	2049.31	17.03	-0.100	-0.0181	0.0860	0.0238
3.3	7.14	2049.29	16.99				
3.6	7.13	2049.26	16.97	-0.082	-0.0149	0.0878	0.0234
3.9	7.12	2049.24	16.95				
4.2	7.11	2049.22	16.92	-0.067	-0.0122	0.0889	0.0231
4.5	7.10	2049.20	16.90				
4.8	7.09	2049.19	16.89	-0.053	-0.0096	0.0912	0.0230
5.1	7.09	2049.17	16.87				
5.4	7.08	2049.16	16.85	-0.039	-0.0071	0.0931	0.0228
5.7	7.08	2049.14	16.84				
6.0	7.07	2049.13	16.83	-0.029	-0.0053	0.0950	0.0228
6.3	7.06	2049.12	16.82				
6.6	7.06	2049.11	16.79	-0.019	-0.0035	0.0968	0.0228

to the measuring technique.

Differential top space pressures were recorded by equivalent changes in E.M.F. output, Δe, from the transducer. This E.M.F. was traced out on the moving chart of the potentiometric recorder, 1 chart unit representing 2 mV.

Also 1 mV = 1/5 inches Water Gauge.

Thus p dynes/cm^2 $= \left[\frac{2.54}{5} \times \rho_{H_2O} \times g\right]$ e, where e is the appropriate value of pressure in terms of mV.

Substituting for p in equation 4.6.-18. in terms of e, one obtains the relation

$$k_L = -\frac{273}{S\beta\theta}\left[\frac{1}{\left[(1-e_i/e)v_i\right]^{\frac{2}{3}}}\,\frac{e_i v_i}{e^2} + \frac{\left[(1-e_i/e)v_i\right]^{\frac{1}{3}}}{e+\frac{5\rho H}{2.54\rho_{H_2O}} - \frac{5\int_0^t U dt}{2.54\rho_{H_2O}}}\right]\frac{de}{dt}$$

$$+\frac{273}{S\beta\theta}\left[\frac{\frac{5\rho K}{2.54\rho_{H_2O}}\left[(1-e_i/e)v_i\right]^{\frac{1}{2}}}{e+\frac{5\rho H}{2.54\rho_{H_2O}} - \frac{5\rho\int_0^t U dt}{2.54\rho_{H_2O}}}\right] \qquad \text{4.6.-18B.}$$

For the present example, the symbols in the above equation take the values listed below:-

e_i, the equivalent value in mV of the initial top space pressure, (1 Atmos), i.e. 2035 mV.

$e = e_i + \Delta e$ where Δe is the differential gauge pressure in mV at time t after bubble release.

ρ = 1.0 gm/cc, β = 0.844 cc CO_2/cc H_2O . . . .

ρ_{H_2O} = 1.0 gm/cc, S = 4.837, θ = 273 + 21.4°K.

K = 25.0 $cm^{\frac{1}{2}}sec^{-1}$, v_i = 2439 cc, H = 266 cm.

Referring to table 4.6.2.-b, the first column indicates the time after bubble release at which chart readings were taken (tabulated in column 2). The third column represents the total pressure within the top space in terms of mV and was obtained from the summation of e_i and the graphically smoothed values of Δe. The fifth column was constructed from point values read from a smoothed curve of $\frac{d(\Delta e)}{dt}$. First order differences only were used in the construction of the latter curve.

The last column gives calculated instantaneous values of k_L and these are compared with computerised values in Fig. 4.6.2.d.

Calculation of k_L by Volume Displacement Equation

Because the top pressure remained virtually constant with time in the previous example, it was possible to re-calculate values of k_L by using equation 4.6.-9.

Since the top pressure changes during the bubble's ascent were <0.2% the hydrostatic pressure change, equation 4.6.-17. may be rewritten as

$$\frac{dP}{dt} = - \rho g U$$

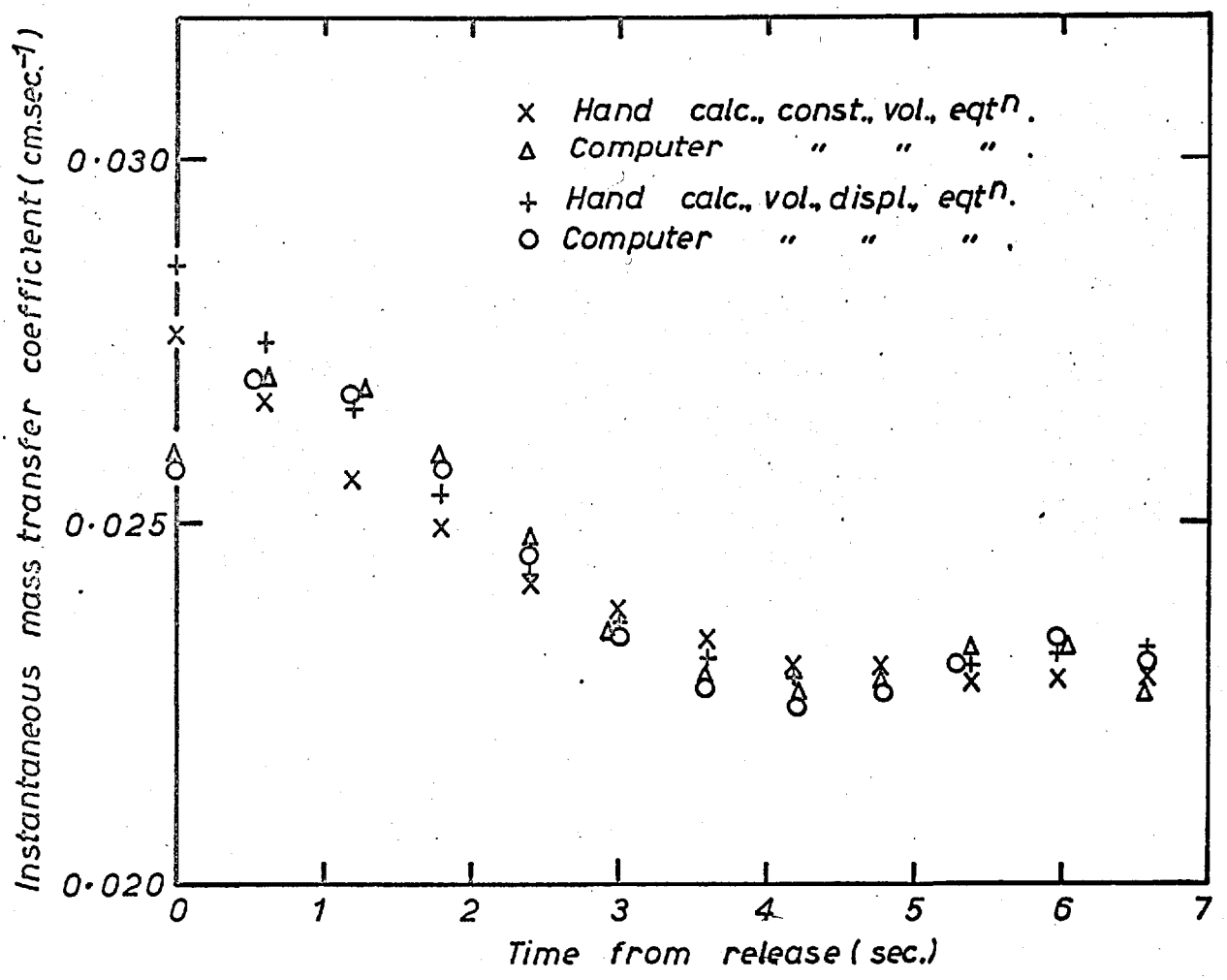

FIG. 4.6.2.d COMPARISON OF FOUR DIFFERENT METHODS OF CALCULATION OF $\bar{k}_L$ vs. TIME FOR TYPICAL ABSORPTION RESULT. INITIAL VOLUME OF CO_2 BUBBLE IN TAP WATER 17·6cc.

and equation 4.6.-16. as

$$P = p_o + \rho g(H - K\bar{V}^{1/6}t)$$

Equation 4.6.-18, then reduces to 4.6.-9. when rewritten in terms of pressure and volume changes of the bubble.

The change in volume of the bubble with time was derived from column 2 of the previous table of results, using equation 4.2.-2.

Similar visually smoothed curves of volume vs time and of $\frac{dV}{dt}$ vs time were used in the calculation of k_L using a form of the volume displacement equation presented below. Incidentally, the computed curve fitted by the method of least squares to the volume - time graph took the form,

$$V = b_o + b_1t + b_2t^2 + b_3t^3 + b_4t^4 + b_5t^5 \quad 4.6.-20.$$

and formed part of a computor programme prepared for the calculation of instantaneous mass transfer coefficients.

The volume displacement equation was adapted to:-

$$k_L = -\frac{273}{S\beta\theta}\left[\frac{1}{V^{\frac{2}{3}}}\frac{dV}{dt} - \frac{V^{\frac{1}{3}}}{\frac{P_o 76 \times 13.6}{\rho K\bar{V}^{1/6}} - t}\right] \quad 4.6.-9.B.$$

In this equation P_o represents the total pressure on the bubble sitting in cup in Atmospheres and is equivalent in this instance to

$$P_o \equiv \frac{p_o + \rho gH}{76 \times 13.6 \times g} \text{ Atmos}$$

TABLE 4.6.2-c

HAND CALCULATED EXAMPLE FOR CO_2 ABSORPTION IN TAP WATER BY VOLUME DISPLACEMENT TECHNIQUE

TIME	SMOOTHED BUBBLE VOLUME (see column 4, 4.6.2.a)	dV/dt SMOOTHED	$\frac{1}{V^{2/3}}\frac{dV}{dt}$	$\frac{P_o}{\rho g K V^{1/6}} - t$	$\frac{V^{1/3}}{P_o/\rho g K V^{1/6} - t}$	k_L
sec.	cm^3	$cm^3\ sec^{-1}$	$cm\ sec^{-1}$	sec	$cm\ sec^{-1}$	$cm\ sec^{-1}$
0.0	17.63	-0.310	-0.0457	32.65	0.0800	0.0286
0.3	17.58	-0.302				
0.6	17.50	-0.266	-0.0395	32.10	0.0810	0.0275
0.9	17.42	-0.250				
1.2	17.34	-0.226	-0.0337	31.20	0.0830	0.0266
1.5	17.26	-0.204				
1.8	17.20	-0.186	-0.0279	31.05	0.0833	0.0254
2.1	17.16	-0.167				
2.4	17.10	-0.145	-0.0218	30.48	0.0846	0.0243
2.7	17.07	-0.127				
3.0	17.03	-0.114	-0.0172	29.88	0.0860	0.0236
3.3	16.99	-0.100				
3.6	16.97	-0.890	-0.0135	29.30	0.0878	0.0231
3.9	16.95	-0.835				
4.2	16.92	-0.740	-0.0112	28.70	0.0895	0.0230
4.5	16.90	-0.690				
4.8	16.89	-0.600	-0.0091	28.13	0.0914	0.0229
5.1	16.87	-0.570				
5.4	16.85	-0.520	-0.0079	27.53	0.0933	0.0231
5.7	16.84	-0.480				
6.0	16.83	-0.460	-0.0070	26.95	0.0950	0.0232
6.3	16.82	-0.420				
6.6	16.79	-0.420	-0.0064	26.35	0.0974	0.0236

In the present calculation, P_o is numerically equal to 1.27 Atmos; $\frac{2581mV}{2035mV}$.

Other quantities appearing in 4.6.-9B. are the same as those for the previous calculation. Referring to table 4.6.2.-c. the second column gives smoothed bubble volumes at times tabulated in column 1., whilst the third column presents smoothed values of $\frac{dV}{dt}$. The calculation of k_L in the seventh colmn follows by appropriate substitutions in 4.6.-9B.

Comparison of k_L obtained by equations 4.6.-9B and 4.6.-18B. are given in Fig. 4.6.2.d. together with computed values.

4.6.3. Experimental Mass Transfer Results

The results of CO_2 absorption and desorption in tap water, and of CO_2 absorption in various aqueous P.V.A. solutions are presented in Figs. 4.6.3. a to j. Results generally refer to work carried out in the 18" I.D. column, using the volume displacement technique.

A few runs of CO_2 absorption in tap water in the 18" I.D. column and 6" I.D. column (e.g. Fig. 4.6.2.b.) were carried out using the constant volume technique, and resulted in similar curves to those given in Fig. 4.6.3.c.

The graphs showing curves of instantaneous mass transfer coefficients vs time represent smoothed curves

of a number of results at each bubble volume. As a typical example, the construction of curve No. 4 of Fig. 4.6.3.f. is shown in Fig. 4.6.3.a. Four experiments on bubbles of 19.45 cc (± 0.1 cc) initial volume were carried out, resulting in four smoothed curves of k_L vs. time. Point values of k_L obtained from each curve have been plotted at 12 time instants in the diagram. Averaged values of k_L at each time interval were calculated, and a smoothed curve drawn through the resulting plot. In addition, typical maximum variations in k_L at one second intervals are shown as bars across some of the averaged curves of k_L vs time. Standard errors in k_L for the curves are given on pages 104 a and b.

The graphs representing time averaged (or overall) values of the mass transfer coefficient, $\overline{k}_L$ vs $\overline{r}_e$ (Figs. 4.6.3 b and e), were obtained by integration of the individual curves of instantaneous mass transfer coefficients over the time intervals corresponding to the bubble rising 240 cms from the inverted cup,

$$\text{i.e.} \quad \overline{k}_L = \frac{\int_o^t k_L \, dt}{t}$$

The $\overline{r}_e$ values in these graphs are based on the arithmetic average bubble volumes between o and t, i.e. $\frac{3\pi}{4}\left[\frac{V_o + V_t}{2}\right]^{1/3}$. This value differed from the time averaged radius, $\frac{3\pi}{4}\left[\frac{\int_o^t V dt}{t}\right]^{1/3}$, by less than 0.6%.

Furthermore, it has been shown by Davenport (32) that if the velocity is proportional to $V^{*\,1/6}$ (p.67), where V* is the instantaneous volume corresponding to the velocity, the errors in using the arithmetic average volume will be negligible, whilst plots of U vs $\overline{V}^{1/6}$ were independent of measuring distance (Fig. 4.4.a.).

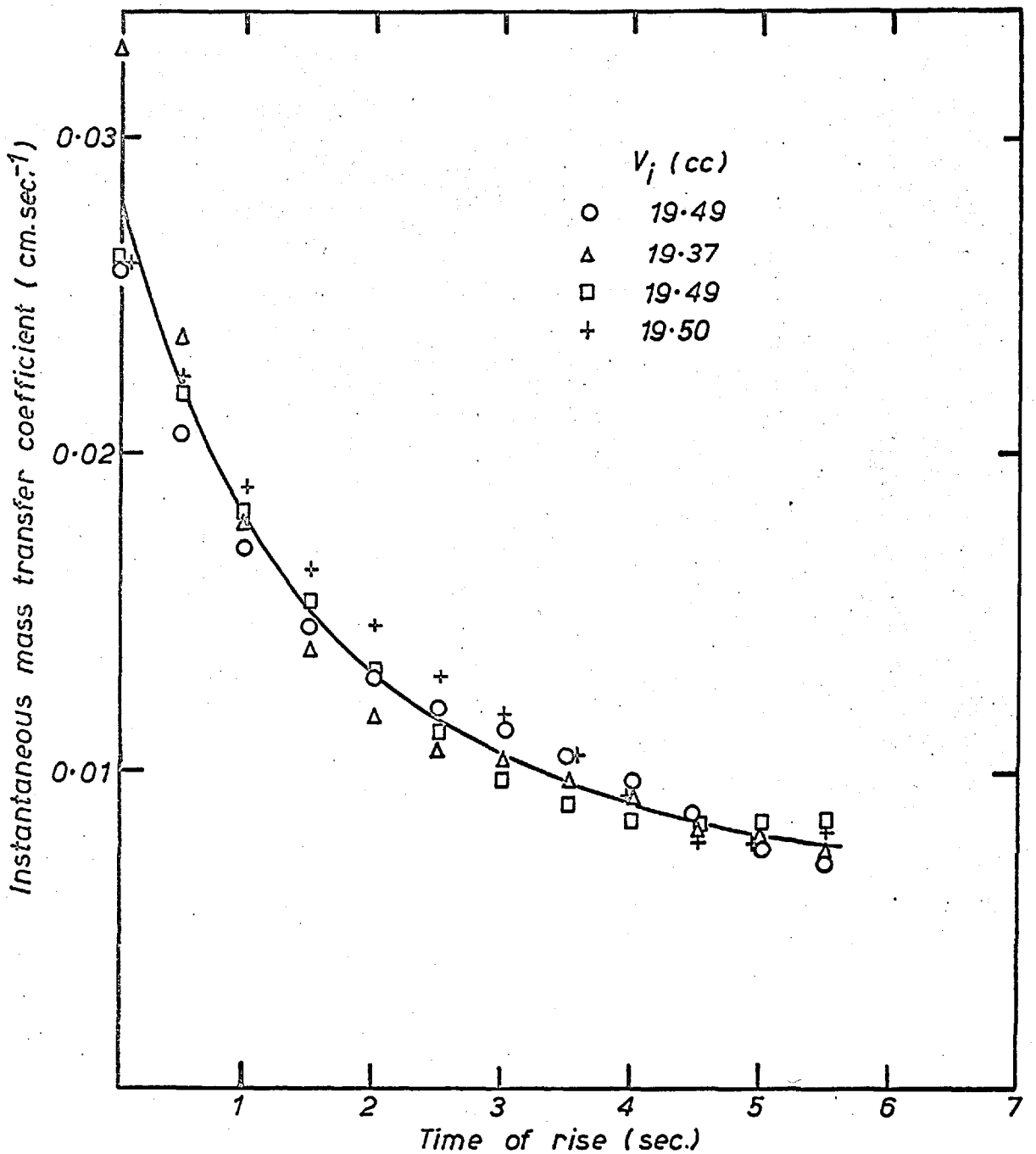

FIG.4.6.3a PLOTS OF INDIVIDUAL CURVES OF k_L vs TIME USED IN THE CONSTRUCTION OF CURVE 4 OF FIG.4.6.3.f

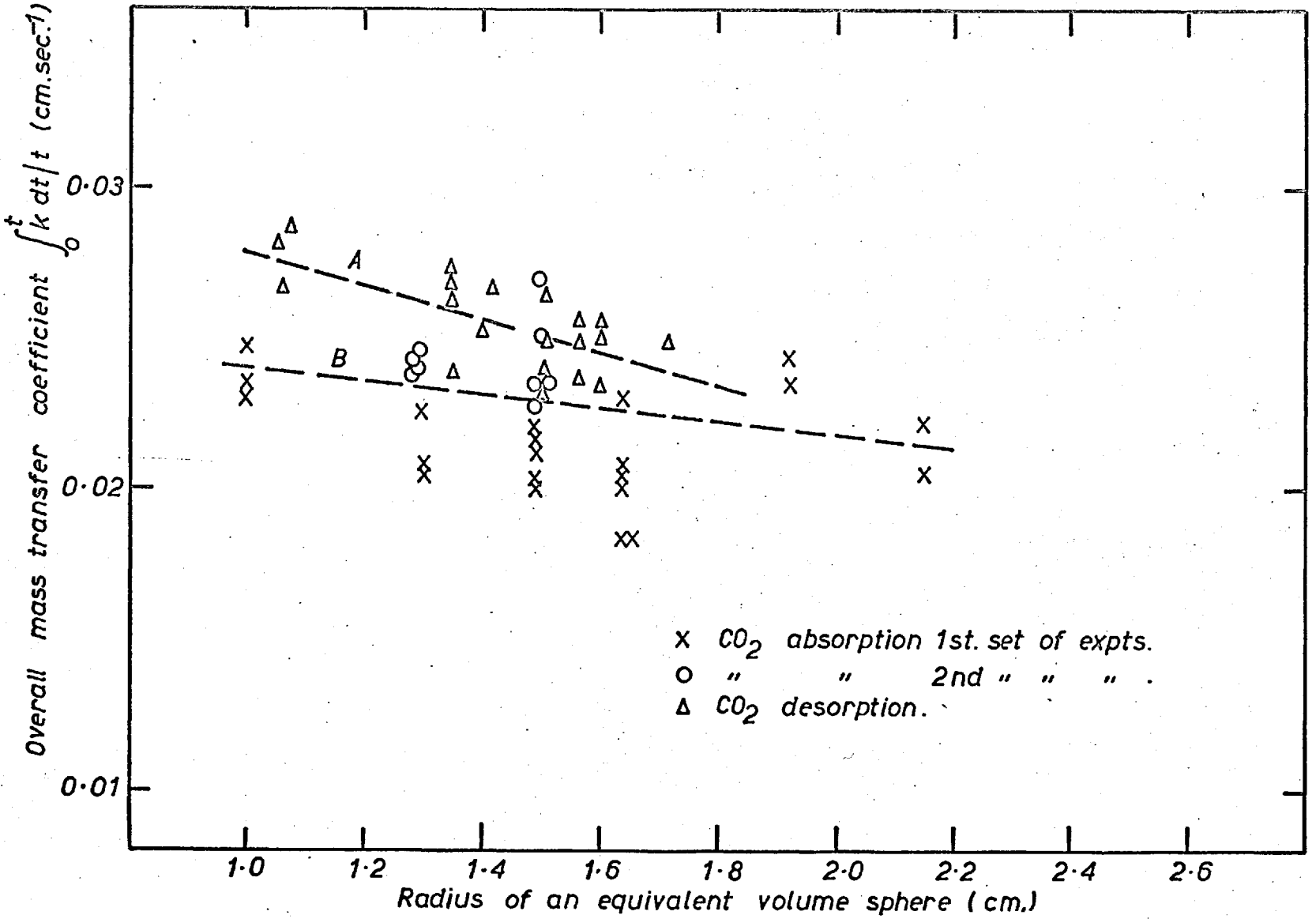

FIG.4.63b PLOT OF OVERALL MASS TRANSFER COEFFICIENT vs. RADIUS OF EQUIVALENT SPHERE (MEAN VOLUME) FOR CO_2 ABSORPTION & DESORPTION IN TAP WATER
18" dia. COLUMN 240 cm.

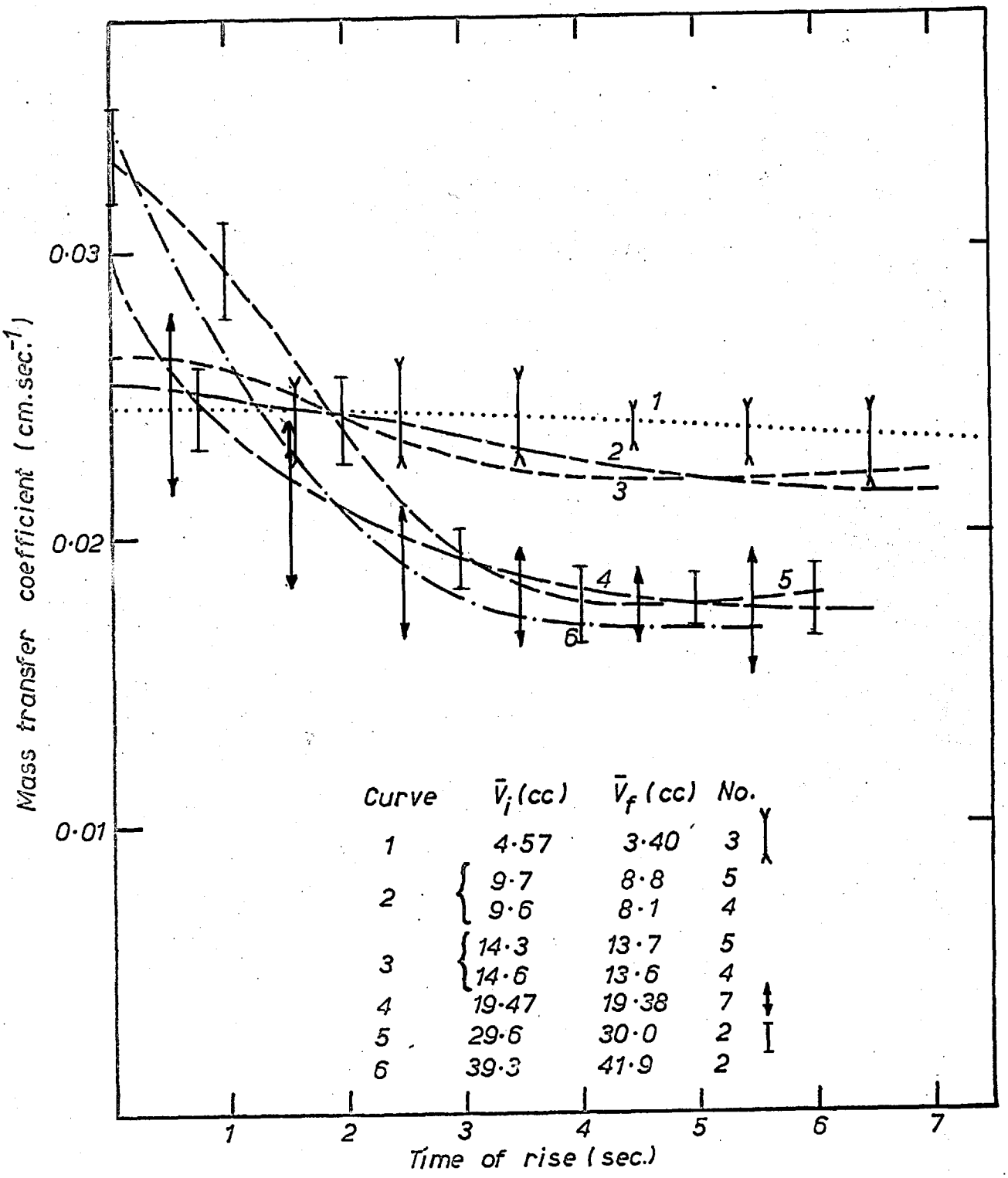

FIG. 4.6.3c INSTANTANEOUS MASS TRANSFER COEFFICIENT vs. TIME FOR ABSORPTION OF CO_2 FROM PURE BUBBLE INTO TAP WATER 18 dia. COLUMN

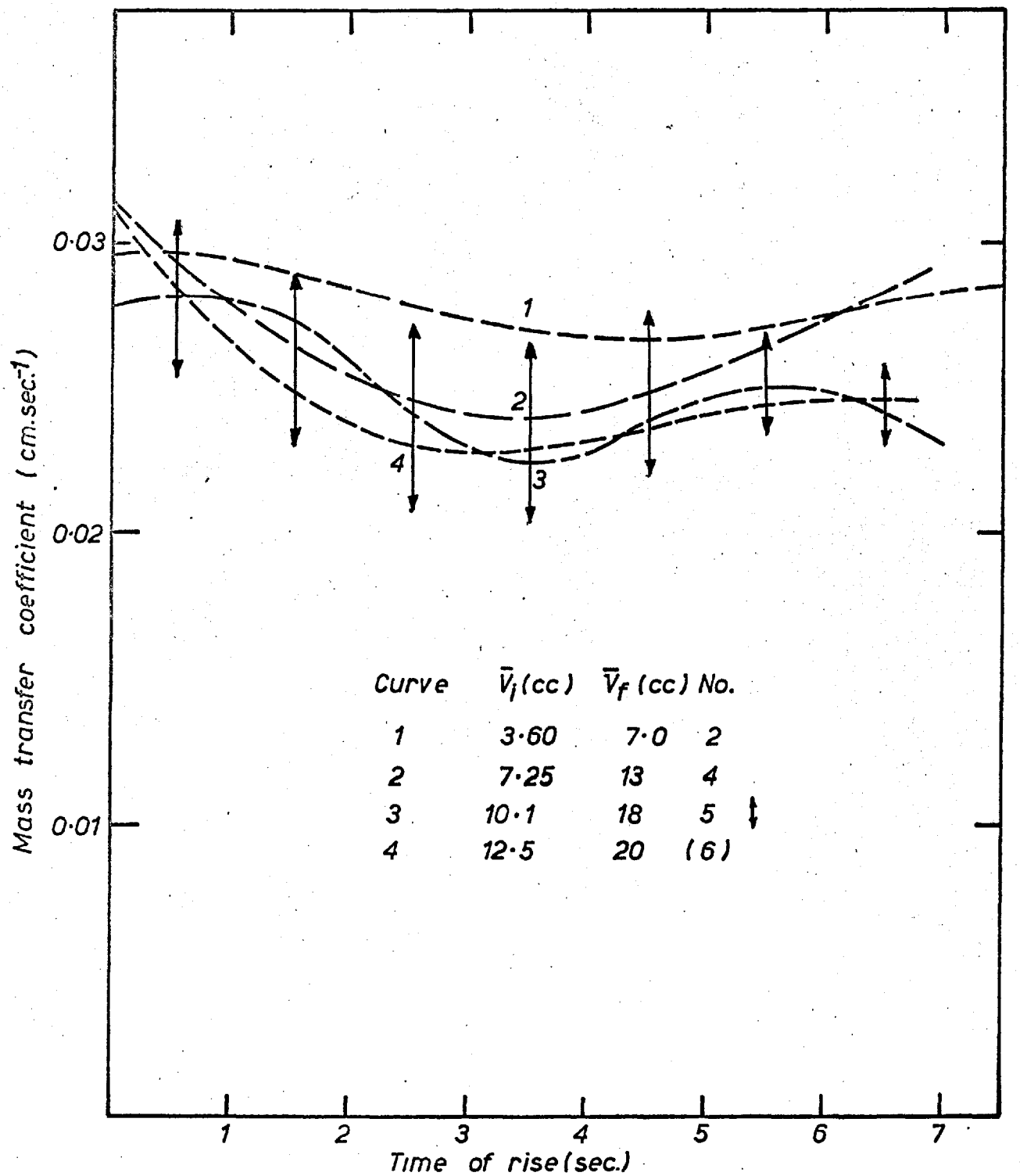

FIG.4.6.3d INSTANTANEOUS MASS TRANSFER COEFFICIENT vs. TIME OF RISE FOR DESORPTION OF CO_2 FROM TAP WATER INTO AN INITIALLY PURE BUBBLE OF NITROGEN-18" dia. COLUMN.

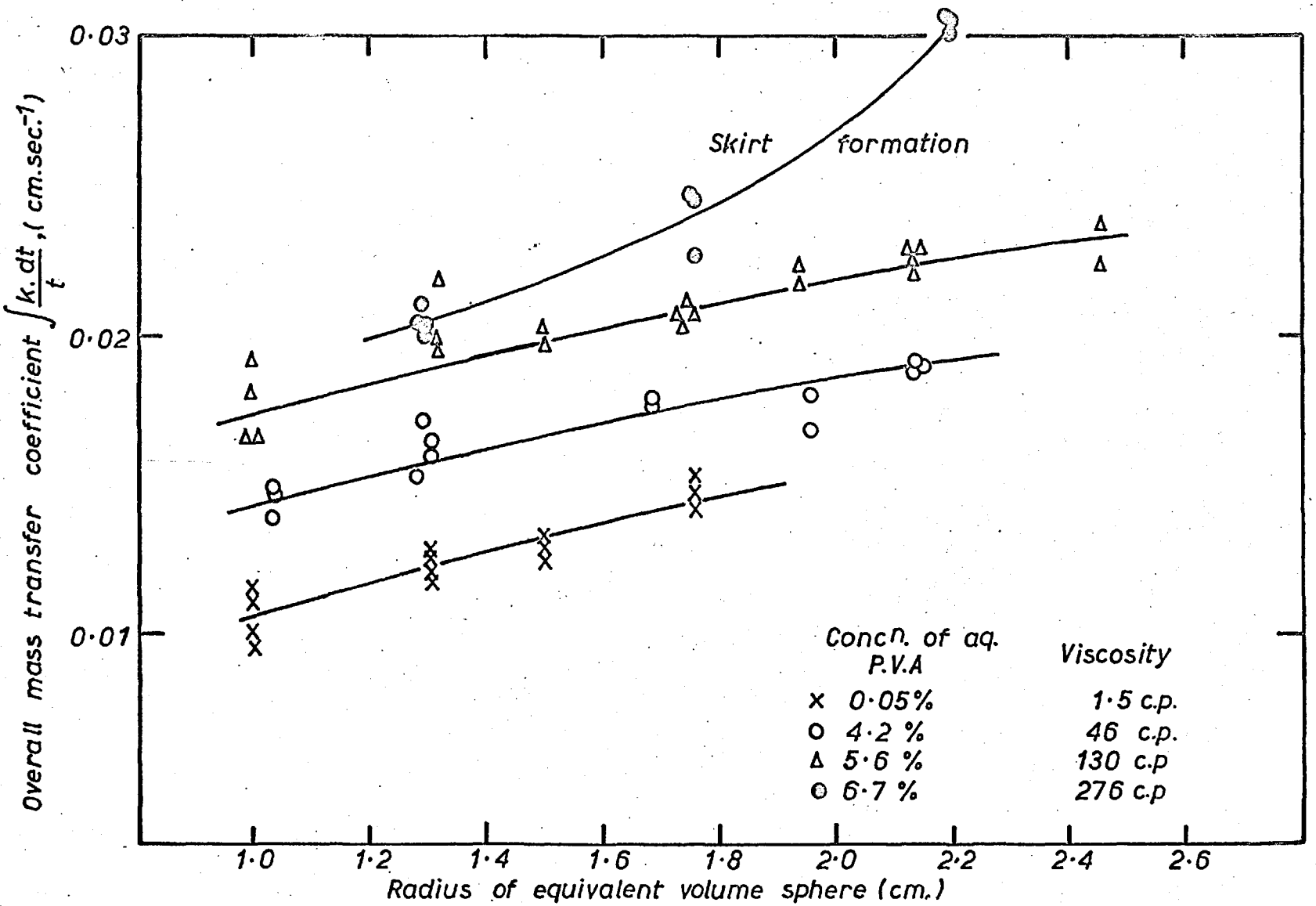

FIG. 4.6.3.e PLOT OF OVERALL MASS TRANSFER COEFFICIENT vs. RADIUS OF EQUIVALENT VOLUME SPHERE (MEAN VOLUME) FOR CO_2 ABSORPTION FROM PURE BUBBLES IN VARIOUS AQUEOUS P.V.A SOLUTIONS. 18" i.d COLUMN, 240 cm. LENGHT.

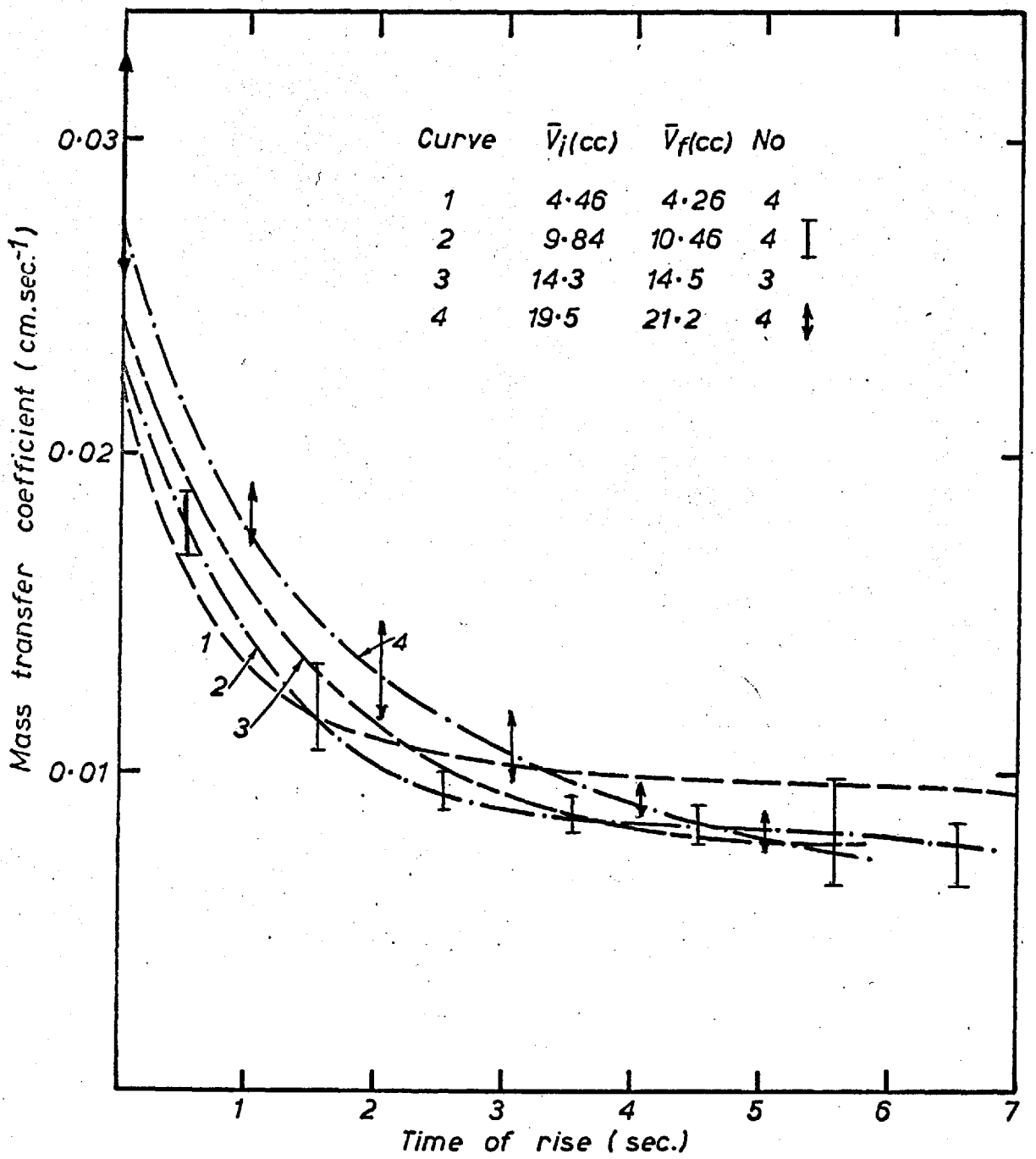

FIG.4.6.3.f PLOT OF INSTANTANEOUS MASS TRANSFER COEFFICIENT vs. TIME FOR ABSORPTION OF CO_2 FROM PURE BUBBLE INTO 0·05% AQUEOUS P.V.A SOLUTION

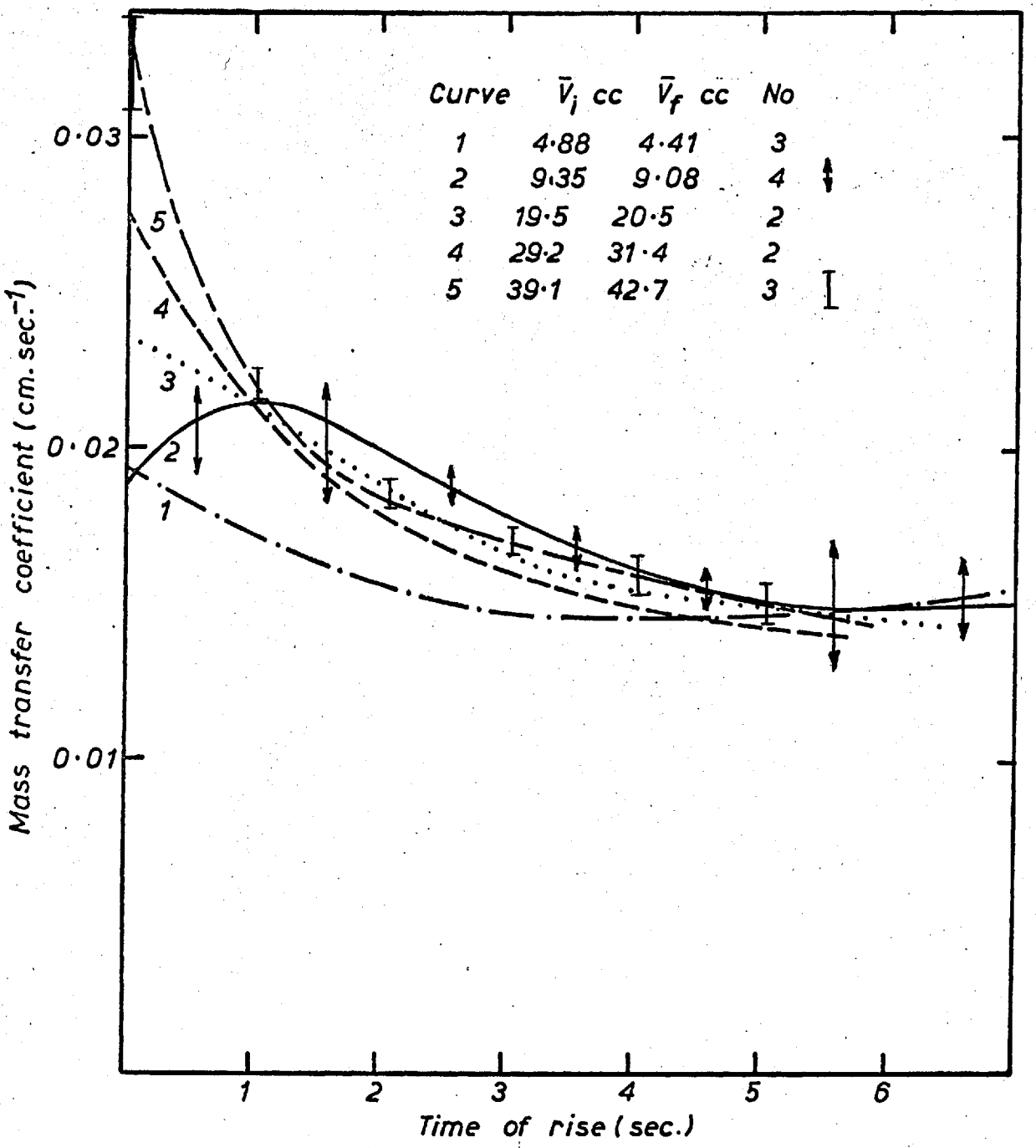

FIG.4.6.3.g PLOT OF INSTANTANEOUS MASS TRANSFER COEFFICIENT vs TIME FOR ABSORPTION OF CO_2 FROM PURE BUBBLE INTO 4·2% P.V.A 46 cp

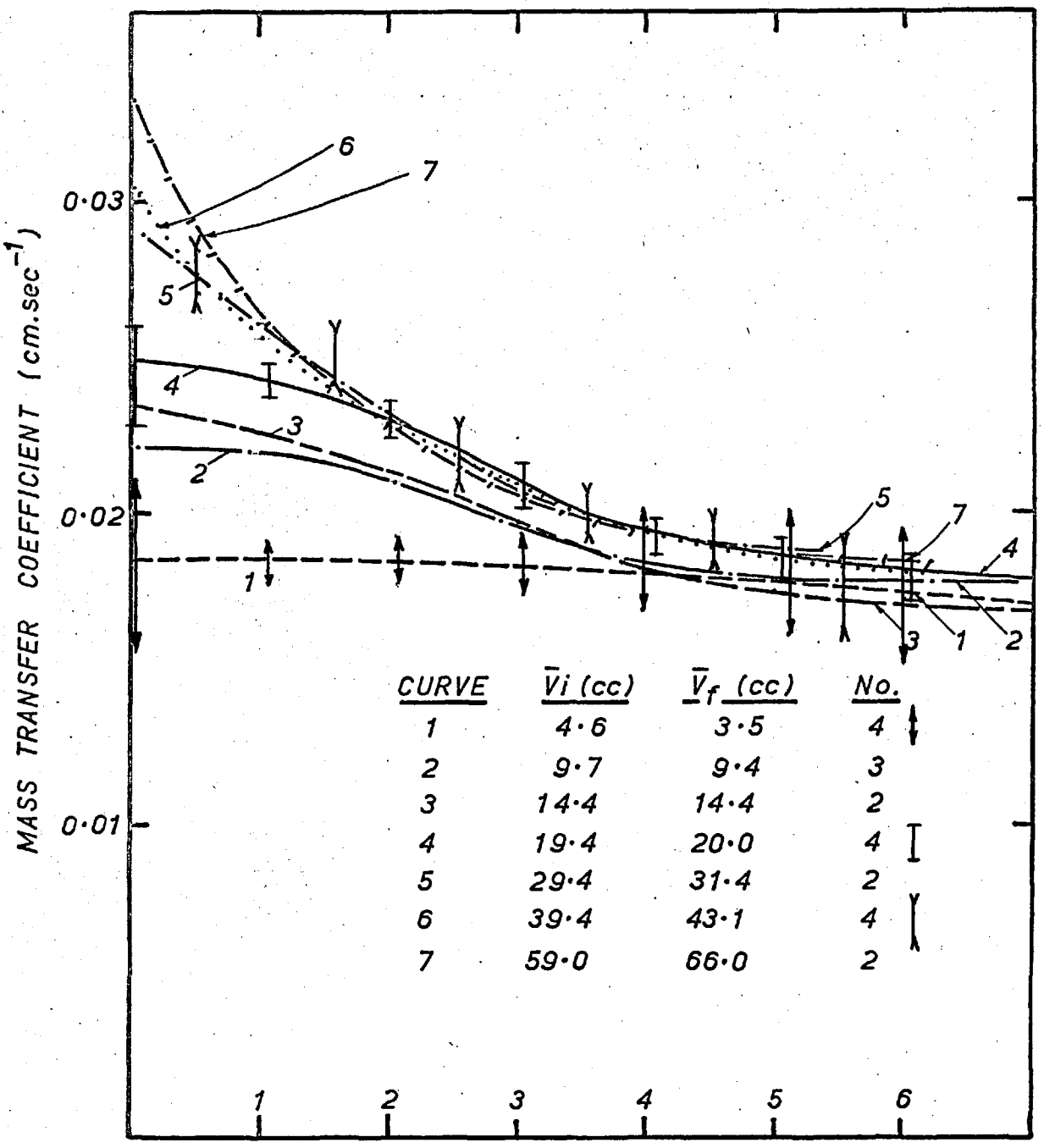

CURVE	$\bar{V}i$ (cc)	$\bar{V}_f$ (cc)	No.
1	4·6	3·5	4
2	9·7	9·4	3
3	14·4	14·4	2
4	19·4	20·0	4
5	29·4	31·4	2
6	39·4	43·1	4
7	59·0	66·0	2

FIG. 4.6.3h

PLOT OF INSTANTANEOUS MASS TRANSFER COEFFICIENT vs TIME FOR ABSORPTION OF CO_2 FROM PURE BUBBLE INTO A 5·6% P.V.A SOLUTION. VISCOSITY 130 cp TEMP. 21·5°C

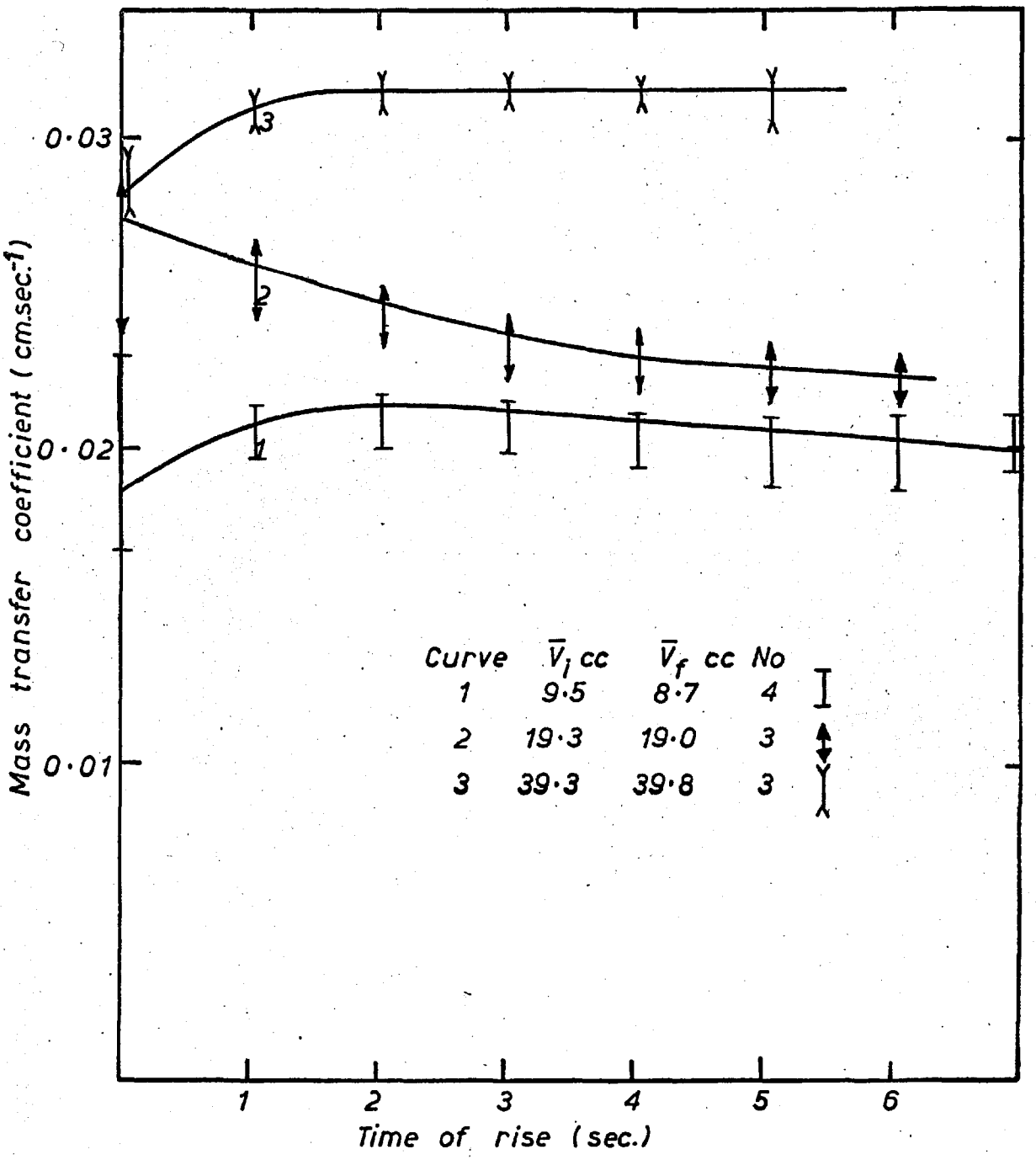

FIG.4.6.3.i PLOT OF INSTANTANEOUS MASS TRANSFER COEFFICIENT vs TIME FOR ABSORPTION OF CO_2 FROM PURE BUBBLE INTO 6·7% AQUEOUS P.V.A SOLUTION 276 c.p

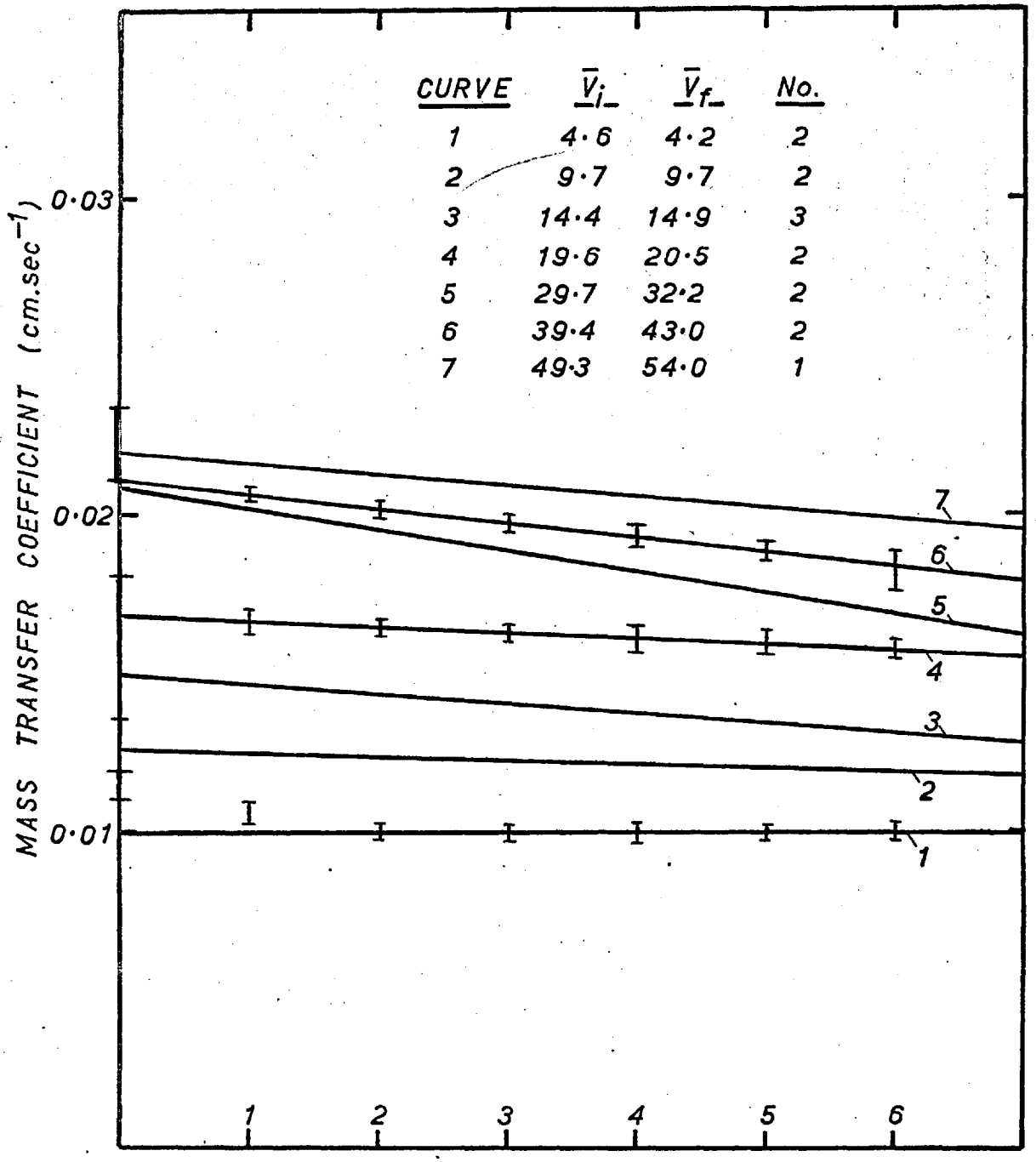

FIG.4.6.3.j

PLOT OF INSTANTANEOUS MASS TRANSFER COEFFICIENT vs. TIME FOR ABSORPTION OF CO_2 FROM PURE BUBBLE INTO AN 8·4% P.V.A SOLUTION VISCOSITY 735 cp TEMP. 19·6°C

The standard errors, s, of the averaged curves of k_L vs time for aqueous sustems are given in the table. Since errors in time were small ($\sim$ 0.01 secs) these have been ignored in comparison with variations in k_L, and the standard errors have been evaluated using the expression

$$s = \left[\frac{\sum_{1}^{n} \left[\sum_{i=1}^{i=N} \left(k_L - \underline{k_L} \right)^2_{i,t} \right]}{n(N-1)} \right]^{1/2}$$

where, N = no. of curves of k_L vs time for a given initial bubble volume

n = no. of time instants examined (1/2 second intervals, 11 $11 \leqslant n \leqslant 15$)

k_L = point value of each result at each time instant considered (cm sec^{-1})

$\underline{k_L}$ = point value of averaged curve " " " " "

Table of Standard Errors in Averaged Curves of k_L vs Time

Curve No.		Figure Numbers						
		4.6.3.c	4.6.3.d	4.6.3.f	4.6.3.g	4.6.3.h	4.6.3.i	4.6.3.j
1	s	0.0016	0.0031	0.0025	0.0019	0.0016	0.0013	0.0008
	k_L*	0.0240	0.0280	0.0107	0.0145	0.0175	0.0206	0.0100
2	s	0.0029	0.0027	0.0012	0.0017	0.0019	0.0017	0.0015
	k_L	0.0214	0.0260	0.0125	0.0164	0.0208	0.0240	0.0123
3	s	0.0031	0.0021	0.0010	0.0012	0.0016	0.0006	0.0011
	k_L	0.0210	0.0248	0.0128	0.0178	0.0200	0.0305	0.0140
4	s	0.0027	0.0020	0.0013	0.0017	0.0008		0.0009
	k_L	0.0196	0.0246	0.0148	0.0175	0.0208		0.0162
5	s	0.0019			0.0009	0.0013		0.0007
	k_L	0.0240			0.0190	0.0222		0.0186
6	s	0.0017				0.0014		0.0009
	k_L	0.0214				0.0226		0.0196
7	s					0.0017		
	k_L					0.0230		

* k_L as previously defined on P 94 i.e. $\frac{\int_0^t k_L \, dt}{t}$ em sec^{-1}.

4.6.4. Estimation of Errors (Volume Displacement Technique)

Initial bubble volumes were accurate to within 0.1 cc during volume displacement experiments, whilst plots of instantaneous volumes, V, vs time for rising inert bubbles indicated similar accuracy in V (Figs. 4.2.a. and 4.3.a.). Also smoothed curves of $\frac{dV}{dt}$ for individual results obtained in the construction of Fig. 4.3.b. were within ± 0.030 cm^3/sec of the predicted curves for N_2 bubbles (e.g. Fig. 4.3.c.), after an initial time lag of approximately one second.

Thus, taking a typical example of CO_2 absorption in tap water, described in section 4.6.2., the bubble volume changed from 17.6 cc to a final value of 16.8 cc, resulting in a variation in velocity from 40.4 to 40,0 cm/sec. Thus the assumption of constant velocity leads to an error of less than a percent. Also, K was accurate to $\pm\frac{1}{2}\%$ and starting times were accurate to 0.1 seconds or better.

Using the volume displacement equation as a basis for estimation of errors, it is evident from the foregoing remarks that the coefficient of variation ($100\,\frac{s}{\bar{x}}$, where s = standard deviation, $\bar{x}$ = arithmetic mean value of quantity considered) in the sixth column of Table 4.6.2.c.

$$\frac{\frac{V^{1/3}}{P_o}}{\rho g K V^{1/6}} - t \qquad 4.6.4.\text{-}1.$$

will not be more than ±2% in this case, whilst that in the fourth column ie.

$$\frac{1}{(V)^{\frac{2}{3}}} \frac{dV}{dt} \qquad 4.6.4.-2.$$

will be accurate to within $\pm \frac{0.030}{V^{\frac{2}{3}}}$ cm/sec. Inserting numerical values in 4.6.4.-1. and 2., 1.8 seconds after bubble release, shows that

$$k_L = \frac{273}{S\beta\theta} (0.0279 \pm (0.0045) + 0.0833 (\pm 0.0016))$$

$$= 0.0243 \pm 0.001 \text{ cm/sec.}$$

For smaller bubbles, estimated accuracies become slightly less.

Individual results of k_L vs time in aqueous P.V.A. solutions generally fell within ± 0.0015 cm/sec of the averaged curves of k_L vs time (e.g. Fig. 4.6.3.a.), and this accuracy is reflected in the small variations in the values of $\bar{k}_L$ plotted in Fig. 4.6.3.e. In the case of transfer experiments in tap water variations in k_L were somewhat greater (± 0.0025 cm/sec and this led to larger variations in $\bar{k}_L$ (Fig. 4.6.3.b.) compared with those recorded in P.V.A. solutions. Davenport (32) has considered the maximum error in $\bar{k}_L$ due to water vapour effects, and has shown that this error is of the order of ± 0.001 cm/sec.

Effect of Initial Time Lag on k_L

In the case of expanding nitrogen bubbles, variations between observed and predicted values of $\frac{dV}{dt}$ were large during the first second of rise. Referring to RUN W.23 and assuming that the gas within the bubble was CO_2 (and not N_2), it is possible to apply equation 4.6.-9. and evaluate k_L. Theoretically, if no time lag existed, k_L would be zero since the fictitious CO_2 bubble would have expanded as an inert bubble. This example is illustrated in Fig. 4.6.4.a. where it is seen that k_L was initially + 0.008 cm/sec^{-1} but rapidly fell to zero after 1 second approximately, thereafter remaining nearly zero as expected. Assuming similar time lags in true absorption experiments, initially expanding bubbles will have true values of k_L below those observed, whilst initially contracting bubbles will have true values of k_L above those observed, during this short time period.

Thus, in the case of CO_2 absorption in water and P.V.A. solutions, bubbles up 15-20 cc initially contracted, leading to higher, initial true values of k_L to those observed, whilst bubbles greater than 20 cc expanded continuously, leading to lower true values of k_L to those observed.

The magnitude of the initial discrepancies in k_L cannot be directly evaluated, but they are unlikely to be very large since errors in k_L resulting from errors in $\frac{dV}{dt}$ are substantially decreased by the numerical value of 4.6.4.-1.

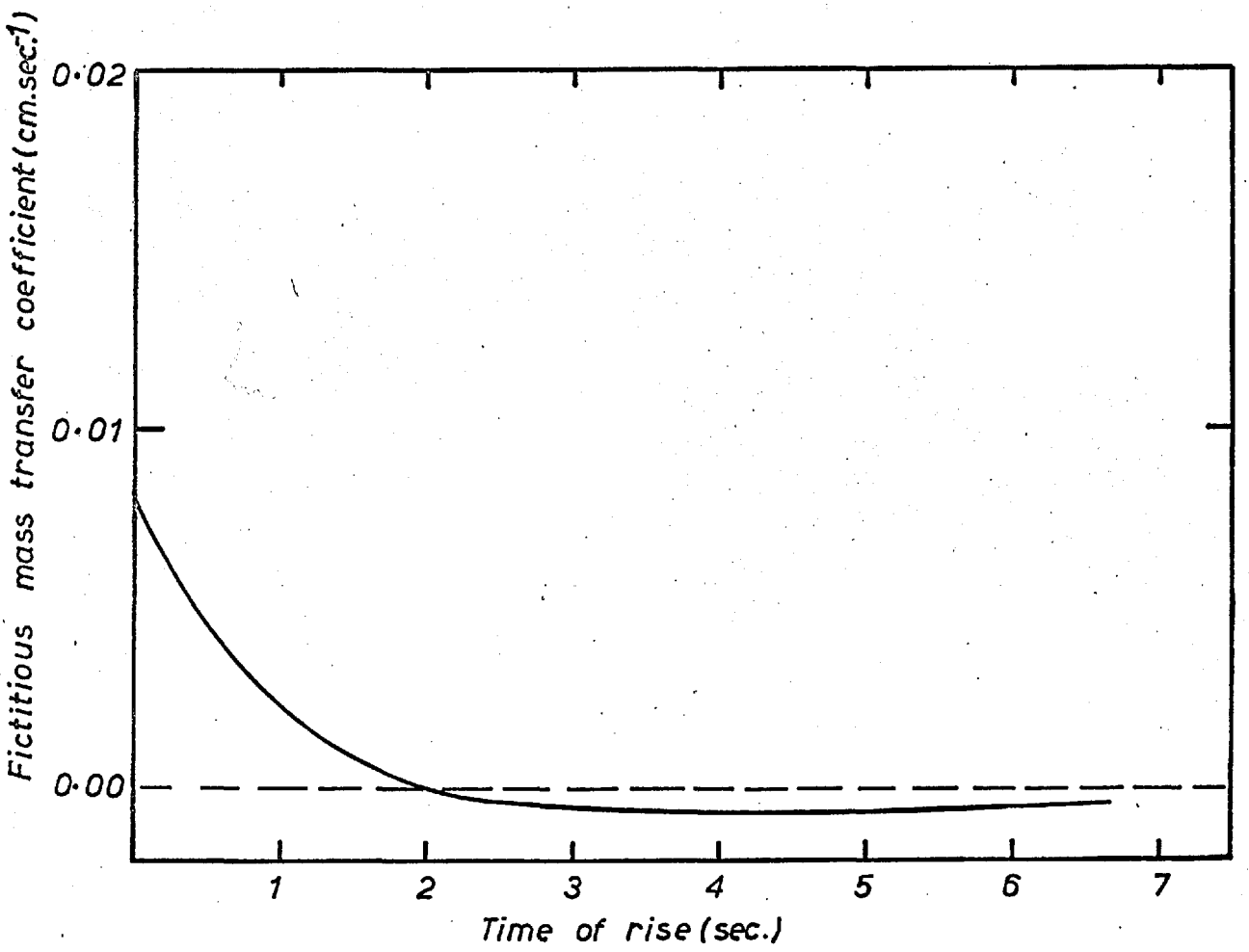

FIG.4.6.4.a PLOT OF FICTITIOUS MASS TRANSFER COEFFICIENT FOR RISE OF INERT BUBBLE (RUN 23) TO ILLUSTRATE EFFECT OF TIME LAG

4.7. MASS TRANSFER FROM WAKES

The rate of mass transfer of fluid between the 'enclosed wakes' of bubbles rising in water and the bulk was estimated from measurements made during the course of the coloured dye experiments previously described. The original dye concentration within the wake, $C_{w,o}$ gradually decreased as the bubble passed through the clear water in the top section of the column. An estimate of the time taken, t_1, for the dye concentration to drop to half its original value was made by comparing the colour intensity of the wake with that of a prepared sample (half the original concentration). This sample was contained within a thin glass vessel of similar dimensions to the bubble's wake, and was photographed in the column at various heights so as to allow direct photographic comparison of the colour intensities.

Theory

Assuming the enclosed wake to be well mixed, the amount of dye within the wake t seconds after passing into the clear water is given by

$$N = C_w V_w \qquad 4.7.-1.$$

where C_w = bulk dye concentration in wake.

V_w = Volume of enclosed wake.

Taking V_w = constant, it follows that

$$\frac{dN}{dt} = V_w \frac{dC_w}{dt}$$

Writing an equation (similar to that in 1.1.1.) which defines a wake mass transfer coefficient, K_w, i.e.

$$\frac{dN}{dt} = - K_w A_w (C_w - C_B) \qquad 4.7.-2.$$

where A_w = peripheral area of enclosed wake.

C_B = Bulk dye concentration in top section of column (=0).

Putting $C_B = 0$, and combining 4.7.-1 and 2 gives

$$\frac{dC_w}{C_w} = K_w \frac{A_w}{V_w} dt$$

B.C. $C_w = C_{w,o}$, $t = 0$. and $C_w = C_w$ at $t = t$.

Intergrating the above expression between $t = 0$ and $t = t$, (taking K_w to be constant) gives

$$K_w = \frac{V_w}{A_w t} \ln\left[\frac{C_{w,o}}{C_w}\right] \qquad 4.7.-3.$$

Equation 4.7.-3. was simplified by considering the wake to be spherical, with a radius r equal to that of the cap of its bubble. Thus, putting $C = C_o/2$ in 4.7.-3. finally gives

$$K_w = 0.23 \; r \; t_{\frac{1}{2}}^{-1}$$

where $t_{\frac{1}{2}}$, is the time taken for the dye concentration to decrease to half its original value. Fifteen observations on bubbles ranging from 10 to 30 cc resulted in an average mass transfer coefficient K_w of 0.4 $\pm$ 0.1 cm/sec.

CHAPTER 5.

5.0. EXPERIMENTAL EQUIPMENT AND PROCEDURE USED IN HIGH TEMPERATURE INVESTIGATION.

The velocity and mass transfer techniques used together with the relevant equipment are described below.

5.1. APPARATUS

The apparatus containing the molten silver was basically similar to those used in the low temperature investigation and provided for the release of single bubbles from an hemispherical cup. The apparatus was constructed from Nimonic 75 alloy since the material has good machinability, excellent high temperature mechanical properties and remains uncorroded in the presence of molten silver and oxidising atmospheres (O_2).

Fig. 5.1.a. shows the apparatus used. The container, 28" high, 4" I.D. with a 1/4" wall thickness, was pre-heated to 1050°C and filled by slow additions of granular silver through a $\frac{1}{2}$" diameter filling tube. A run-off tube was provided in the bottom flange for withdrawal of the silver, whilst as an added precaution, the whole of the apparatus could be tilted to pour the silver out through the filling tube. Since reliable high temperature seals at 1000°C were found to be impracticable, the filling tube extended outside the enclosing furnace and was sealed

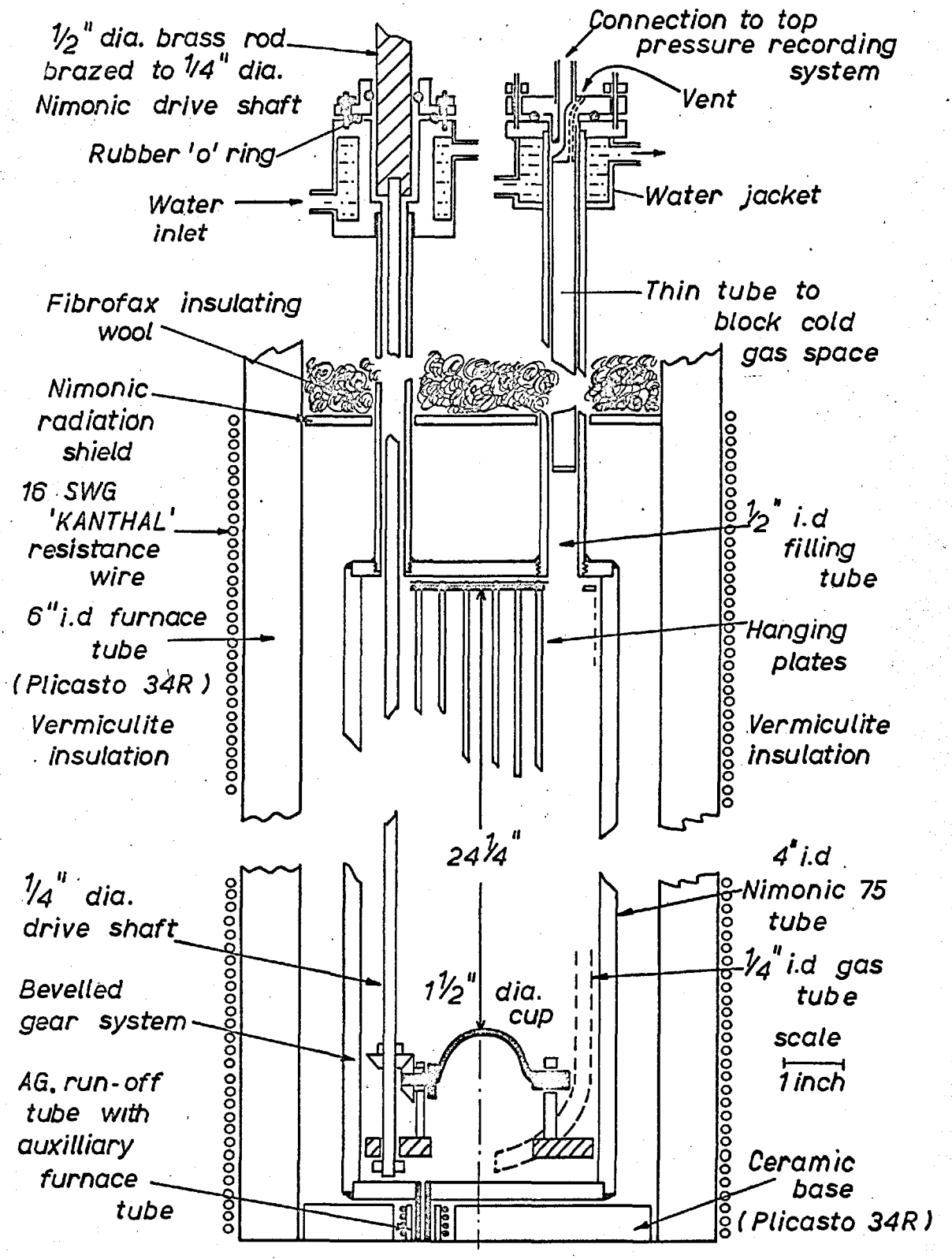

FIG. 5.1.a HIGH TEMPERATURE SILVER APPARATUS

by means of a rubber O. ring as shown in the diagram. Similarly, the vertical shaft of the cup rotating mechanism was sealed by means of an easily removable rubber O. ring. The hemispherical cup, situated at the bottom of the column, was turned by translating the rotation of the shaft through 90°. This was accomplished by the use of a bevelled gear system, and smooth drive was provided from the lubricating action of the silver.

Gas could be bubbled into the inverted cup from two thin bore 1/4" I.D. Nimonic tubes which were passed down the inside of the apparatus so as to preheat the gas to the temperature of the silver. A third tube was provided for temperature traverses.

The internal parts of the apparatus were connected to the top plate of the column by three 1/4" diameter rods, in order to allow easy removal in case of breakdown. Fortunately this was not necessary

The Nimonic tube was contained within a 3.5 K.W. resistance wire tube furnace insulated with vermiculite (expanded mica). The heating was provided by 16 S.W.G. Kanthal A furnace wire which was wound by lathe around the 1" thick, 6" I.D. cast tube of Plicasto 34R. The furnace was split-wound, incorporating a centre and two end tappings on the windings. The Pt - Pt, 13% Rh

thermocouple placed close to the furnace windings was connected to a temperature controller which regulated the power supplied (± 10%) from the 20A Variac. A steady temperature of 1020°C ± 2°C was maintained within the silver during experiments whilst temperature traverses indicated vertical variations of ⩾15°C within the gas phase.

5.2. MEASUREMENTS OF BUBBLE VOLUME

Bubble volumes were measured using the constant volume technique originally developed for room temperature studies, and were related to changes in top space pressure from atmospheric ($p - p_i$) by the usual equation

$$V = v_i \left(1 - \frac{p_i}{p}\right) \qquad 5.2.-1.$$

A top space volume of approximately 1000 cc was chosen, so that the volume of gas outside the hot zone in the connecting tube to the differential pressure transducer comprised only 2% of the total volume.

The constant volume method was preferred to the volume displacement technique, as it eliminated the possibility of spurious volume changes resulting from gas displacement along the non-isothermal connecting tube. Suitable precautions were taken to minimise possible adiabatic behaviour of the gas within the top space (see 4.1.). Thus, high experimental rates of pressure change

with time, $(\frac{dp}{dt})$ were avoided by using the suitably large top gas volume, whilst a high surface area to gas volume ratio ($\sim$2) was provided by hanging seven thin Nimonic plates from the top of the container(Fig. 5.1.a.). No departure from isothermal conditions was subsequently detected during the experiments.

The apparatus used to record differences between atmospheric and top space pressure with time was the same as that used in the low temperature investigation. However, the pressure range of the differential pressure transducer was increased to $\pm$ 10" H_2O by changing the pressure diaphragm head, whilst the chart speed of the potentiometric recorder was increased to 4"/second by changing the gear ratio.

Measurements of Top Space Volume, v_i

An electrical contact device attached to a micro-manometer was used to record the difference in height between the silver surface and the container top. The volume of the top space could be measured to an accuracy of approximately 2%. Allowance was made for the volume of the plates and rods within the top space and the volume within the gas line to the transducer.

5.3. THE BULK OXYGEN CONCENTRATION

During the mass transfer work involving the absorption of oxygen in Ag, it was found that the high solubility of oxygen in silver (90 cc O_2/cc Ag at 1020°C) resulted in such a rapid rate of oxygen absorption in pure silver, that no gas could be collected in the dumping cup. Consequently, it was found necessary to partially saturate the silver with oxygen so as to reduce absorption rates.

Oxygen was rapidly bubbled into the silver from the two gas lines for about 6 hours. Provided the silver had remained stagnant during that time, and no oxygen desorption from the silver surface had occurred, the oxygen concentration finally established at equilibrium would have been distributed according to Sieverts Law; the increasing argentostatic head of silver ensuring an increasing bulk oxygen concentration with depth. A similar effect has been considered in the CO_2 desorption studies described previously.

However, present work on wakes has shown that a considerable amount of material is carried up as a wake behind large S.C. bubbles. This, added to the effect of a small diameter column, must inevitably lead to recirculation and mixing of the silver. Thermal convection currents must also have an added mixing effect. In view

of these considerations, the presence of an oxygen concentration gradient within the silver was considered undesirable and the silver was, therefore, well mixed by releasing large S.C. bubbles at frequent intervals from the dumping cup during saturation with oxygen.

Measurement of Bulk Oxygen Concentrations

When steady state conditions had become established, the top space was sealed from the atmosphere by closing the solenoid switch A. (Fig. 5.3.a.). The partial pressure of oxygen within the top space then adjusted itself so as to reach equilibrium with the bulk oxygen concentration through absorption or desorption of oxygen at the gas/liquid interface. The total pressure was recorded by connecting the top space to a mercury manometer, and the equilibrium partial pressure of oxygen was then related to the absolute pressure finally obtained by the equation

$$p_{O_2} = p_{total} - {}^{X}N_2 \, p_i \qquad 5.3.-1.$$

where ${}^{X}N_2$ = mole fraction of nitrogen in saturating gas and p_i = initial top pressure (i.e. 1 Atmos.). Since oxygen solution in silver follows Sieverts Law (56), the bulk oxygen concentration was related to the oxygen partial pressure within the top gas space by the equation.

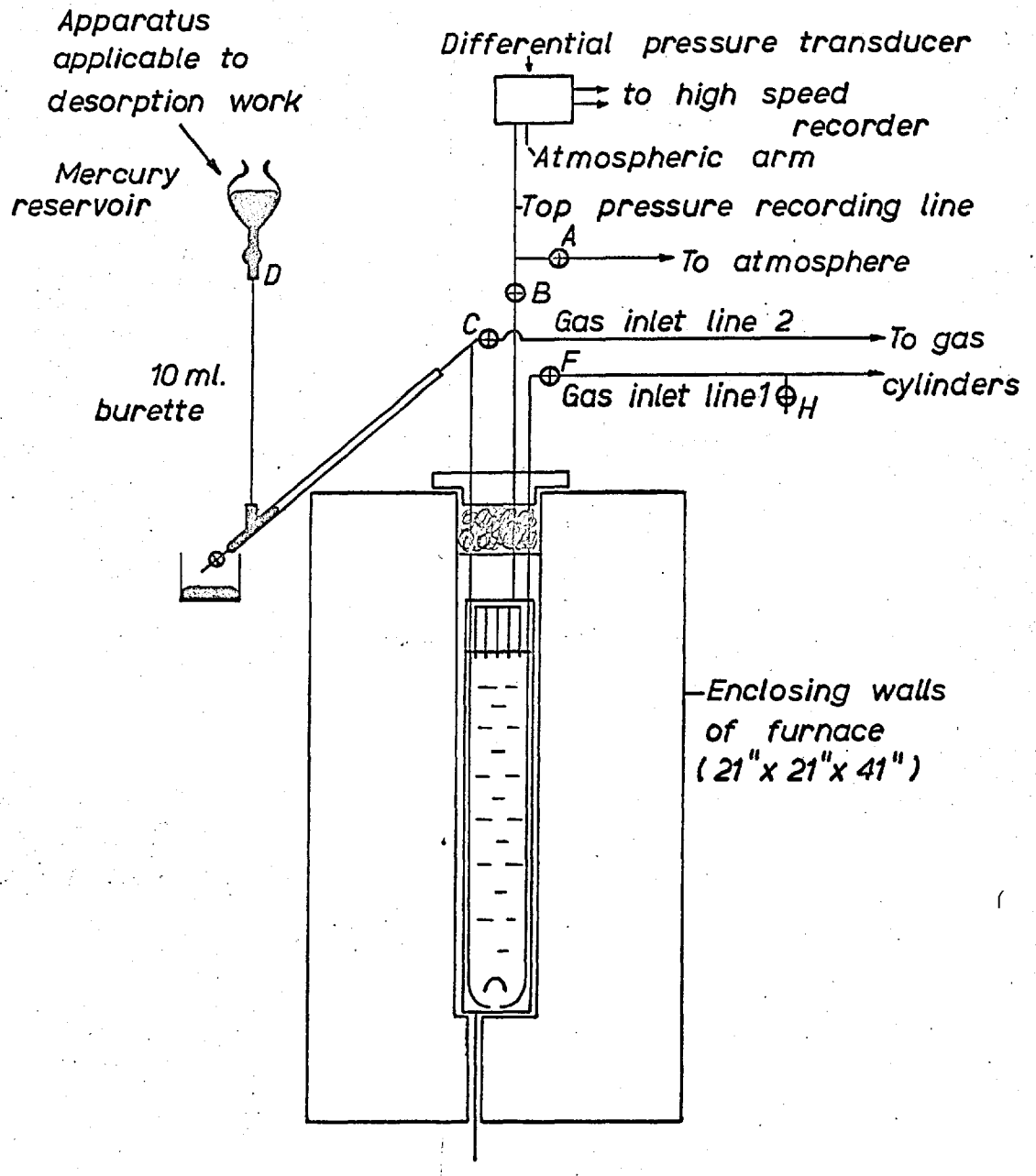

FIG. 5.3.a HIGH TEMPERATURE MEASURING SYSTEM

$$C_{[O]} = q\,(p_{O_2})^{\frac{1}{2}}$$

where $C_{[O]}$ = number of gm atoms oxygen/cc of silver and q = constant, gm atoms/cc/Atmos.$^{\frac{1}{2}}$.

Since the rate of attainment of equilibrium was fairly slow (~10 mins.), it was found useful, after closing switch A. to the atmosphere, to release oxygen bubbles from the cup so as to stir the liquid interface. In these cases the rate of attainment of equilibrium was much swifter. (N.B. In some cases when the top space became supersaturated, the pressure dropped down to the equilibrium value).

The equilibrium partial pressure was found to remain substantially constant during each series of runs.

5.4. GAS INJECTION TECHNIQUES

In order to calculate mass transfer coefficients for the absorption of oxygen from O_2/N_2 bubbles into saturated silver, and for the desorption of oxygen from partially saturated silver into bubbles containing nitrogen, it is necessary to know the nitrogen concentration within the bubble. Accordingly, a technique was developed by which a known quantity of nitrogen was injected into the dumping cup. A 10 ml burette, graduated in 0.02 cc intervals, was connected to the gas inlet system as shown

diagrammatically in Fig. 5.3.a. Tap C was initially opened and nitrogen/oxygen gas mixture allowed to bubble slowly through into the silver. It was then closed, the dumping cup inverted, and tap D was opened, and The volume of mercury displaced, Vc, displaced gas into dumping cup. Assuming no accumulation of nitrogen within the gas line, and no change in pressure, it follows from the ideal gas law that the number of moles of nitrogen, n_{N_2}, injected at 1020°C into the cup is given by

$$n_{N_2} = \frac{Pc\ Vc}{R\theta c} X_{N_2} \qquad 5.4.-1.$$

where X_{N_2} = mole fraction of nitrogen in injected gas mixture.

c = cold (i.e. at Room Temperature).

5.5. EXPERIMENTAL PROCEDURE

a. Absorption Runs

After bubbling through vigorously with the saturating gas via inlet line No. 1. tap H was opened to allow the silver to run back up to the line, after which tap F was closed. A small amount of oxygen was bubbled through the second gas line to ensure no run back had occurred, after which the empty cup was inverted. Switch A was then operated to isolate the system from the atmosphere, and the recorder started immediately. Oxygen desorption

from the top space resulted in a steady rate of increase in top pressure. After approximately two seconds, gas was introduced into the cup as rapidly as possible, allowed to settle, and the cup swiftly turned. After the bubble reached the surface (~1.7 seconds from release), the pressure continued to rise at the original steady rate due to continuing oxygen desorption from the top space. Top pressure changes resulting from bubble volume changes were obtained after allowing for the pressure changes caused by desorption from the top surface.

b. Desorption Runs

A similar procedure was carried out for desorption work, but in this case the bulk oxygen concentration was chosen so that no desorption from the silver interface occurred. Thus, no allowance was necessary in these cases and equation 5.2.-1. was directly applicable.

CHAPTER 6.

6.0. EXPERIMENTAL RESULTS

The results obtained on velocities and mass transfer rates of bubbles rising through molten silver at 1020°C, together with relevant theory and calculations are presented below.

6.1. INERT BUBBLE EXPERIMENTS

The passage of inert gas bubble of nitrogen up with 4" I.D. column provided a means of determining the accuracy of the pressure measuring system. The final top pressure, p_1, after the rise of an inert bubble is given by

$$p_1 = p_o + \rho g H \left[1 - \frac{p_i}{p_o}\right] \qquad 6.1.-1.$$

where p_o = top pressure with gas in cup

p_i = top pressure prior to gas introduction

H = height of silver above cup

Fig. 6.1.a. presents a typical inert gas bubble pressure-time result and is similar to those observed during room temperature investigations. As seen, the final top space pressure after bubble rise closely agrees with that predicted in Fig. 6.1.a. The experimental error, defined as $\left(\frac{p_1 - p_{1,\,\text{predicted}}}{p_1 - p_o}\right)100$, was + 3% in this case, whilst the errors on all inert runs were within this order of

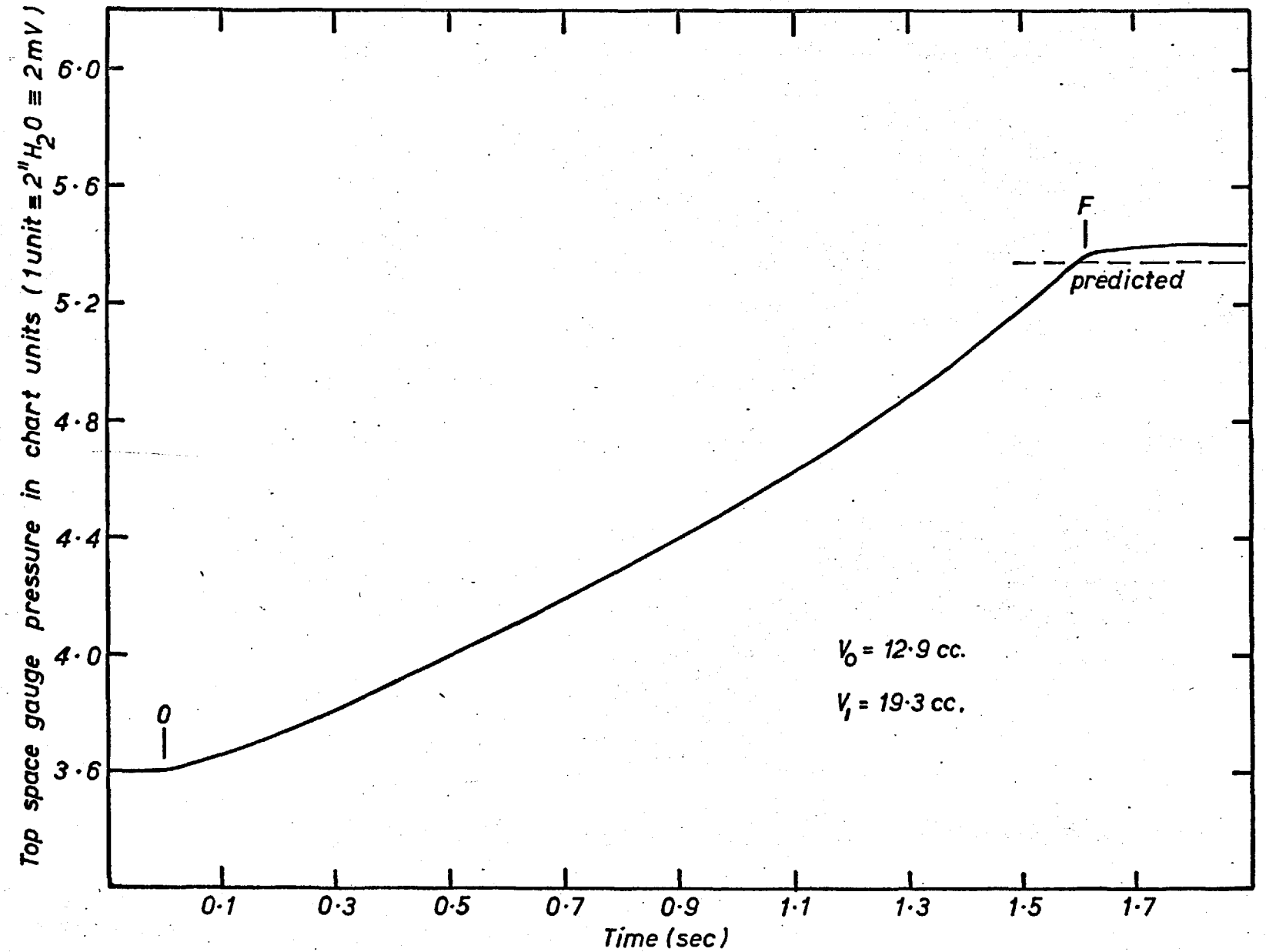

FIG. 6.1.a TYPICAL PRESSURE-TIME CURVE FOR INERT BUBBLE RISING THROUGH MOLTEN SILVER AT 1020°C Run 60

magnitude (i.e. $\pm$ 5%), and the mean error of the series was within a percent.

In another set of inert experiments, the accuracy of the injection technique was tested by slowly bubbling pure nitrogen through unsaturated silver into the dumping cup. The volume of gas, V, injected into the cup was calculated on the basis of equation 5.4.-1. putting X_{N_2} = 1, it follows that

$$n_{N_2} = \frac{Pc\ Vc}{R\ \theta c} = \frac{P\ V}{R\ \theta}$$

or

$$V = \frac{Pc\ Vc\ \theta}{P\ \theta c} \qquad 6.1.-2.$$

Since the difference in pressure between the orifice of the filling tube and the gas within the cup was small, it was neglected, as was the slight change in top pressure during gas introduction. Table 6.1.-a. shows that the injected gas volume calculated using equation 6.1.-2. normally agreed within 6% of that measured by the constant volume technique (i.e. equation 5.2.-1.).

TABLE 6.1.-a.

Accuracy of Injection Technique

Given: $\theta c = 313^{\circ}K$, $\theta = 1293^{\circ}K$, $V' \equiv Vc \frac{\theta}{\theta c}$

$v_i = 730$ cc, $p_i = 1$ Atmos

Vc	$\therefore V'$	$(p_o - p_i)$	V_o	$\left[\frac{V' - V_o}{V_o}\right] 100$
cc	cc	$"H_2O$	cc	%
2.20	8.95	4.94	8.90	+0.6
2.06	8.39	4.54	8.20	+2.3
1.91	7.78	4.50	8.10	-4.0
2.45	9.98	5.20	9.35	+5.7
2.18	8.90	5.10	9.21	-3.4
1.75	7.14	4.05	7.30	-2.4
2.03	8.26	4.22	7.60	+8.0
0.76	3.10	1.68	3.06	+1.3
1.74	7.09	3.80	6.85	+3.5
2.81	11.44	5.88	10.52	+8.7
3.14	12.80	7.60	13.61	-5.9
3.23	13.15	6.82	12.22	+7.6
3.37	13.70	7.98	14.30	-3.5
3.72	15.15	8.52	15.30	-1.0

6.2. RISING VELOCITIES IN SILVER

Fig. 6.2.a. presents the results obtained on rising velocities of bubbles through silver. Both the velocities and equivalent radii, r_e, plotted in 6.2.a. represent arithmetic average values between the cup and surface.

The equivalent radius, r_e, was calculated from the average bubble volume during rise, whilst the velocity was calculated from the rising time of the bubble over the 53 cm to the surface. This time was taken to be between the initial and final instants of the slope change $\frac{dp}{dt}$ in the curves of the top pressure vs time. Thus, referring to Figs. 6.1.a. and 6.4.a., the time period between F and O represents the time of rise.

As seen, individual velocity results usually fell within $\pm$ 5% of the fitted curve in 6.2.a., being independent of mass transfer, and only a weak function of r_e.

In order to compare this method of velocity evaluation with true instantaneous velocities, the pressure-time curve presented in Fig. 6.1.a. for RUN 60 was used to evaluate instantaneous velocities.

In the case of inert bubbles, these may be calculated from a differential form of the expression

$$V = \frac{(p_o + \rho g H)\ V_o}{p\ + \rho g(H - h)} \qquad 6.2.\text{-}1.$$

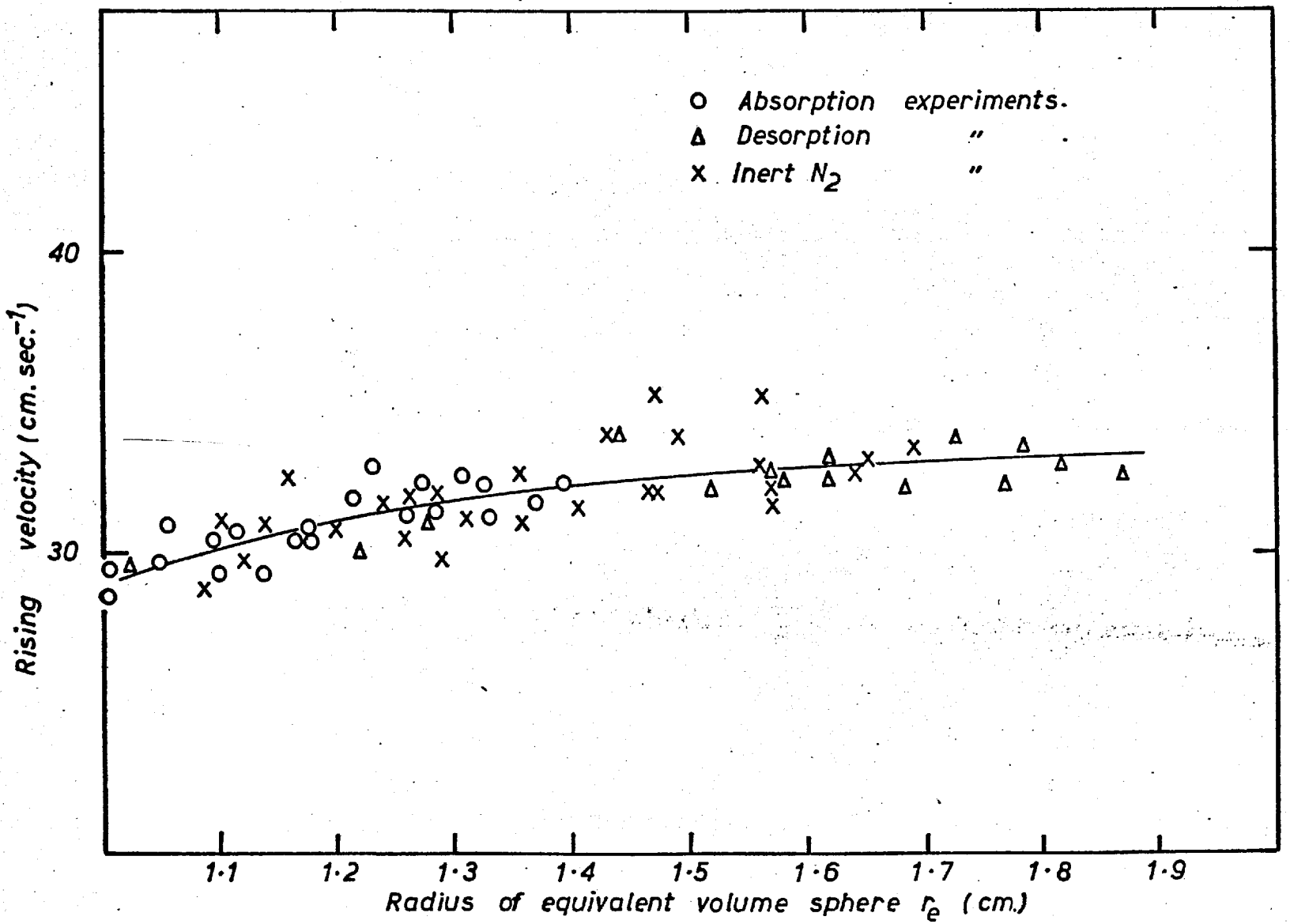

FIG. 6.2.a PLOT OF RISING VELOCITIES OF LARGE BUBBLES IN MOLTEN SILVER vs. r_e.

in differential form the velocity is

$$\rho g U = \left[\frac{\left[1 - \frac{p_i}{p_o}\right]\left[p_o + \rho g H\right] p_i}{(p - p_i)^2} + 1 \right] \frac{dp}{dt} \qquad 6.2.-2.$$

Calculations for RUN 60 based on the above equation are given in Table 6.2.-b., and these are plotted in Fig. 6.2.b. The bubble expanded from 13 to 19 cc approximately and as seen, within experimental error ($\pm$ 5%) the instantaneous velocity curve B, coincided with curve A, representing the average velocity (i.e. U = 53/1.615 = 32.8cm/sec.). The agreement indicated that the average velocity curve in Fig. 6.2.a. equally well represented the instantaneous velocity-diameter relationship, whilst it provided a further check on the reliability of the measuring system.

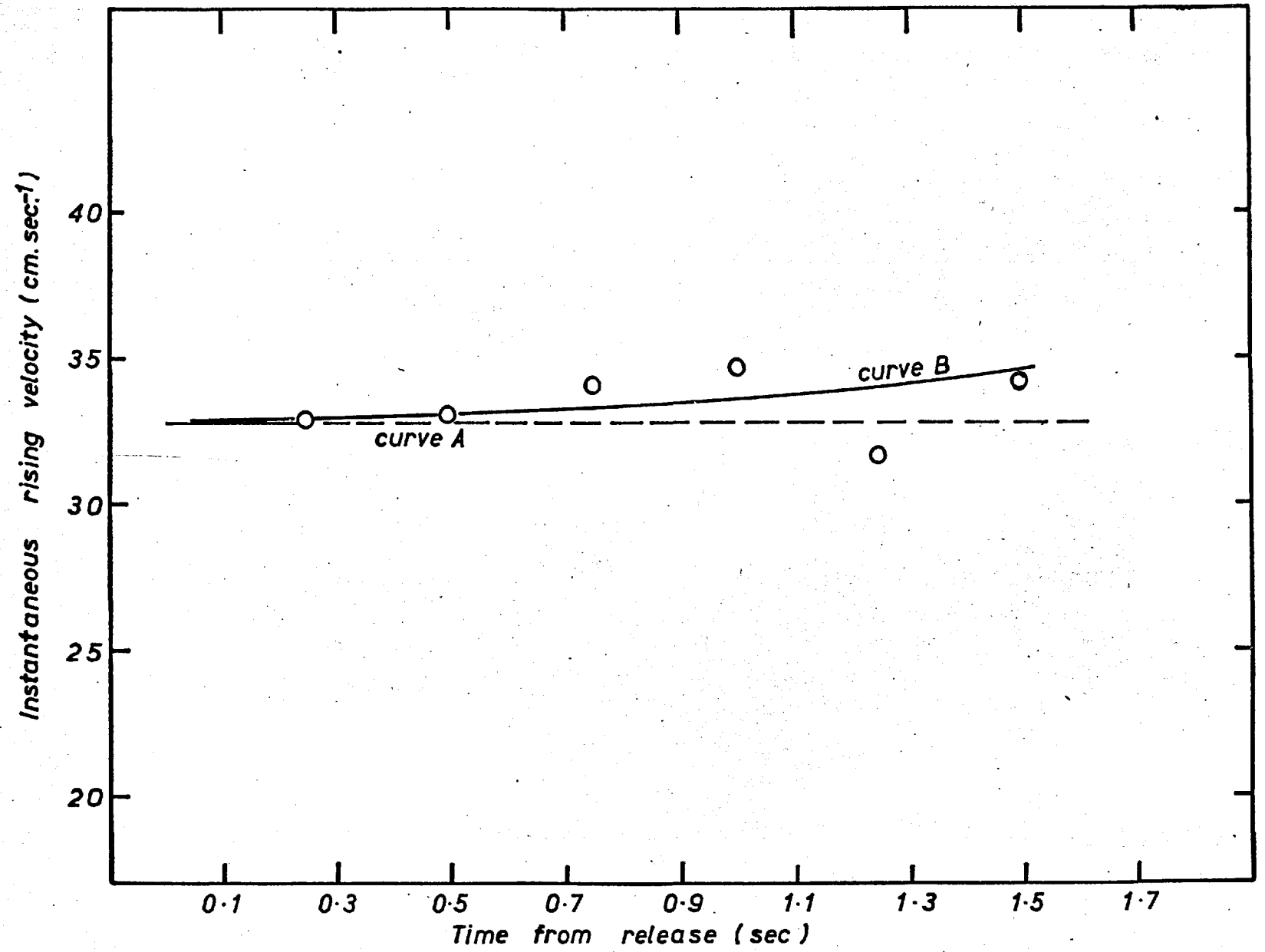

FIG. 6.2.b COMPARISON OF INSTANTANEOUS & AVERAGE VELOCITIES OF INERT BUBBLE IN SILVER. Run 60

TABLE 6.2.-b.

Calculation of Instantaneous Velocities by Equation 6.2.-2.

RUN 60

Given: $\rho = 9.52$ gm/cc, $H = 53 + 1$ cm.

$p_i = 407$" H_2O, $p_o = 407 + 7.2$" H_2O

$$\therefore \text{CONSTANT} = \left[1 - \frac{p_i}{p_o}\right](p_o + \rho g H) \quad p_i = 4324.14$$

TIME	$(p - p_i)$	$\frac{\text{CONST.}}{(p - p_i)^2} + 1$	$\frac{dp}{dt}$	$\therefore U$
sec.	"H_2O	-	"H_2O/sec	cm/sec
0.25	7.53	77.26	1.6	32.98
0.50	7.98	68.90	1.8	33.09
0.75	8.49	60.99	2.1	34.17
1.00	8.82	56.59	2.3	34.72
1.25	9.65	46.44	2.5	31.64
1.50	10.35	40.38	3.1	34.22

6.3. THEORY OF MEASUREMENT OF TRANSFER RATES

Rates of mass transfer of oxygen to and from S.C. bubbles rising through silver were interpreted by means of similar expressions to those developed in section 4.6.1.

a. Absorption from O_2 bubble rising through partially saturated silver

Since oxygen molecules dissociate at the gas/metal interface to dissolve in the form of atoms, it follows that

$$\dot{n}_{[O]} = 2\dot{n}_{O_2} \qquad 6.3.-1.$$

where $\dot{n}_{[O]}$ = no. of Gm Atoms of oxygen dissolving into silver/time.

$\dot{n}_{O_2}$ = no. of Gm Moles of oxygen lost from bubble/time.

It follows from the Gas Law that for isothermal solution of oxygen,

$$\dot{n}_{O_2} = -\frac{1}{R\theta}\left[P\frac{dV}{dt} + V\frac{dP}{dt}\right] \qquad 6.3.-2.$$

remembering that the partial pressure of oxygen, P_{O_2}, is equal to the total gas pressure, P, within the bubble for a pure oxygen bubble.

Assuming chemical equilibrium of oxygen at the gas/liquid interface, transfer rates may be interpreted in

terms of the customary equation for transport control in the liquid phase, i.e.

$$\dot{n}_{[O]} = k_L \, SV^{2/3}(C_I - C_B) \qquad 6.3.-3.$$

As previously mentioned oxygen solution in silver follows Sieverts Law. Hence,

$$(C_I - C_B) = q(P^{\frac{1}{2}} - P_B^{\frac{1}{2}}) \qquad 6.3.-4.$$

Substitution for $(C_I - C_B)$ from 6.3.-4. in 6.3.-3. followed by substitution for $\dot{n}_O$ and $\dot{n}_{O_2}$ in 6.2.-1. from 6.3.-2. and 6.3.-3. finally gives

$$k_L \, SV^{2/3} q(P^{\frac{1}{2}} - P_B^{\frac{1}{2}}) = \frac{-2}{R\theta}\left(P\frac{dV}{dt} + V\frac{dP}{dt}\right) \qquad 6.3.-5.$$

Since the constant volume technique was employed in high temperature studies, bubble volumes in 6.3.-5. are expressed in terms of top space pressures, p.

As shown in section 4.6.1.c.

$$V = v_i \, (1 - p_{i/p}) \qquad 6.3.-6.a.$$

$$\frac{dV}{dt} = \frac{p_i \, v_i}{p^2} \, \frac{dp}{dt} \qquad 6.3.-6.b.$$

where i = initial, i.e. before introduction of gas into dumping cup.

Similarly,

$$P = p + \rho g(H - \bar{U}t) \qquad 6.3.-6.c.$$

and

$$\frac{dP}{dt} = \frac{dp}{dt} - \rho g\bar{U} \qquad 6.3.-6.d.$$

Making the appropriate substitutions for V, $\frac{dV}{dt}$, P, $\frac{dP}{dt}$ in 6.3.-5. finally gives k_L in a convenient form for calculation

$$k_L = \frac{-2}{SqR\theta}\left[\left\{(v_i(1-p_i/p))^{\frac{1}{3}} + \frac{p+\rho g(H-\bar{U}t)}{(v_i(1-p_i/p))^{\frac{2}{3}}}\frac{p_i v_i}{p^2}\right\}\frac{dp}{dt} - \rho g\bar{U}(v_i(1-\frac{p_i}{p}))^{\frac{1}{3}}\right] \Big/ \left[(p + \rho g(H - \bar{U}t)^{\frac{1}{2}} - P_B^{\frac{1}{2}}\right] \qquad 6.3.-7.$$

b. <u>Oxygen Desorption from partially saturated silver into an O_2/N_2 bubble</u>

Considering the general case of desorption, in which a gas mixture containing oxygen and nitrogen is injected into the cup using the technique described in Chapter 5, section 5.4, the total number of moles of 'cold' gas injected into the inverted cup is given by

$$n = \frac{Pc\ Vc}{R\theta c}$$

whilst the number of moles of nitrogen injected is given by

$$n_{N_2} = \frac{X\ Pc\ Vc}{R\theta c} \qquad 6.3.-8.$$

where X = mole fraction of nitrogen in gas mixture injected,

c = cold, i.e. at room temperature.

During injection, oxygen will desorb from the silver into the gas mixture. At the instant of bubble release,

(t = 0) the total number of moles of gas in the cup is given by

$$n_o = \frac{P_o V_o}{R\theta}$$

whilst the total number of moles of oxygen is given by

$$n_{o,\,O_2} = \frac{P_o V_o}{R\theta} - \frac{X\ PcVc}{R\theta_c} \qquad 6.3.-9.$$

It follows from the Gas Law that the partial pressure of oxygen is given by

$$P_{o,\,O_2} = P_o - \frac{X\ PcVc\ \theta}{V_o\ \ \theta c}$$

whilst the oxygen partial pressure at time t after bubble release is

$$P_{O_2} = P - \frac{X\ PcVc}{V}\ \frac{\theta}{\theta c} \qquad 6.3.-10.$$

Also $$\frac{dP_{O_2}}{dt} = \frac{dP}{dt} + \frac{X\ PcVc}{V^2}\ \frac{\theta}{\theta c}\ \frac{dV}{dt} \qquad 6.3.-11.$$

Remembering that two oxygen atoms transported to the bubble interface combine to form one molecule of oxygen, it follows that

$$\dot{n}_{[O]} = 2\,\dot{n}_{O_2}$$

Substitution for $\dot{n}_{[O]}$ in terms of the mass transfer equation and for $\dot{n}_{O_2}$ in terms of the gas equation gives

$$k_L\ SV^{2/3}(C_B - C_I) = \frac{+2}{R\theta}\left[P_{O_2}\ \frac{dV}{dt} + V\ \frac{dP_{O_2}}{dt}\right] \qquad 6.3.-12.$$

The L.H.S. of 6.3.-12. is valid, provided the mass transfer coefficient of O_2 within the gas phase is much greater than in the liquid phase.

Substitution for P_{O_2} and $\frac{dP_{O_2}}{dt}$ from 6.3.-10. and -11. gives

$$k_L \, SV^{\frac{2}{3}} \, (C_B - C_I) = \frac{2}{R\theta} \left[P \frac{dV}{dt} + V \frac{dP}{dt} \right] \qquad 6.3.\text{-}12b.$$

Since O_2 obeys Sieverts Law (56), it follows that

$$(C_B - C_I) = q \, (P_B^{\frac{1}{2}} - (P - \frac{X \, PcVc}{V} \, \frac{\theta}{\theta c})^{\frac{1}{2}}) \qquad 6.3.\text{-}13.$$

Substitution for $(C_B - C_I)$ in 6.2.-12b., and making the substitutions for V, $\frac{dV}{dt}$, P, $\frac{dP}{dt}$ given in equations 6.3.-6a. to 6.3.-6d. finally yields

$$k_L = \frac{\frac{2}{SqR\theta} \left[\left[\frac{(v_i(1-p_i))}{p}^{\frac{1}{3}} + \frac{p+\rho g(H-\bar{U}t)}{(v_i(1-p_i/p))^{\frac{2}{3}}} \frac{p_i v_i}{p^2} \right] \frac{dp}{dt} - \rho g \bar{U} \frac{(v_i(1-p_i))}{p}^{\frac{1}{3}} \right]}{P_B^{\frac{1}{2}} - \left[p + \rho g(H-\bar{U}t) - \frac{X \, PcVc}{v_i(1-p_i/p)} \frac{\theta}{\theta c} \right]^{\frac{1}{2}}} \qquad 6.3.\text{-}14.$$

The above equation represents a generalised formulation for interpretation of all mass transfer systems studied. Thus, in the case of a pure O_2 bubble dissolving into partially saturated silver, substituting X = 0 in equation 6.3.-14. gives equation 6.3.-7. Similarly, in the case of absorption from an $(O_2 + N_2)$ bubble into unsaturated silver, the appropriate equation for calculation for k_L may be obtaining by substituting $P_B = 0$ in equation 6.3.-14

6.4. ABSORPTION FROM OXYGEN BUBBLES IN SILVER

Following the experimental procedure described in section 5.5., part of a typical curve of E.M.F. (or top space gauge pressure, 1 mV = 1" H_2O) vs time result is presented in Fig. 6.4.a. The Bulk Oxygen Partial Pressure during the experiments described below was maintained at 1.121 $\pm$ 0.025 Atmos. Since the value of q, the constant in Sieverts Law, is equal to 1.724 x 10^{-3} at 1020°C, this corresponds to a bulk oxygen concentration of 1.829 x 10^{-3} $\pm$ 0.024 x 10^{-3} gm Atoms O/cc. The observed pressure variations were most probably due to imperfect mixing within the column.

6.4.1. Measurements of Bubble Volume

In order to distinguish the effects of top space pressure changes due to oxygen desorption at the silver interface from those resulting from gas volume changes within the column, the initial linear rate of pressure rise within the top space was established before each experiment. Curve AB of Fig. 6.4.a. forms an extrapolation of the initial curve so obtained, and represents top pressure changes due to desorption during the formation and release of an oxygen bubble. The extrapolation is considered valid since:-

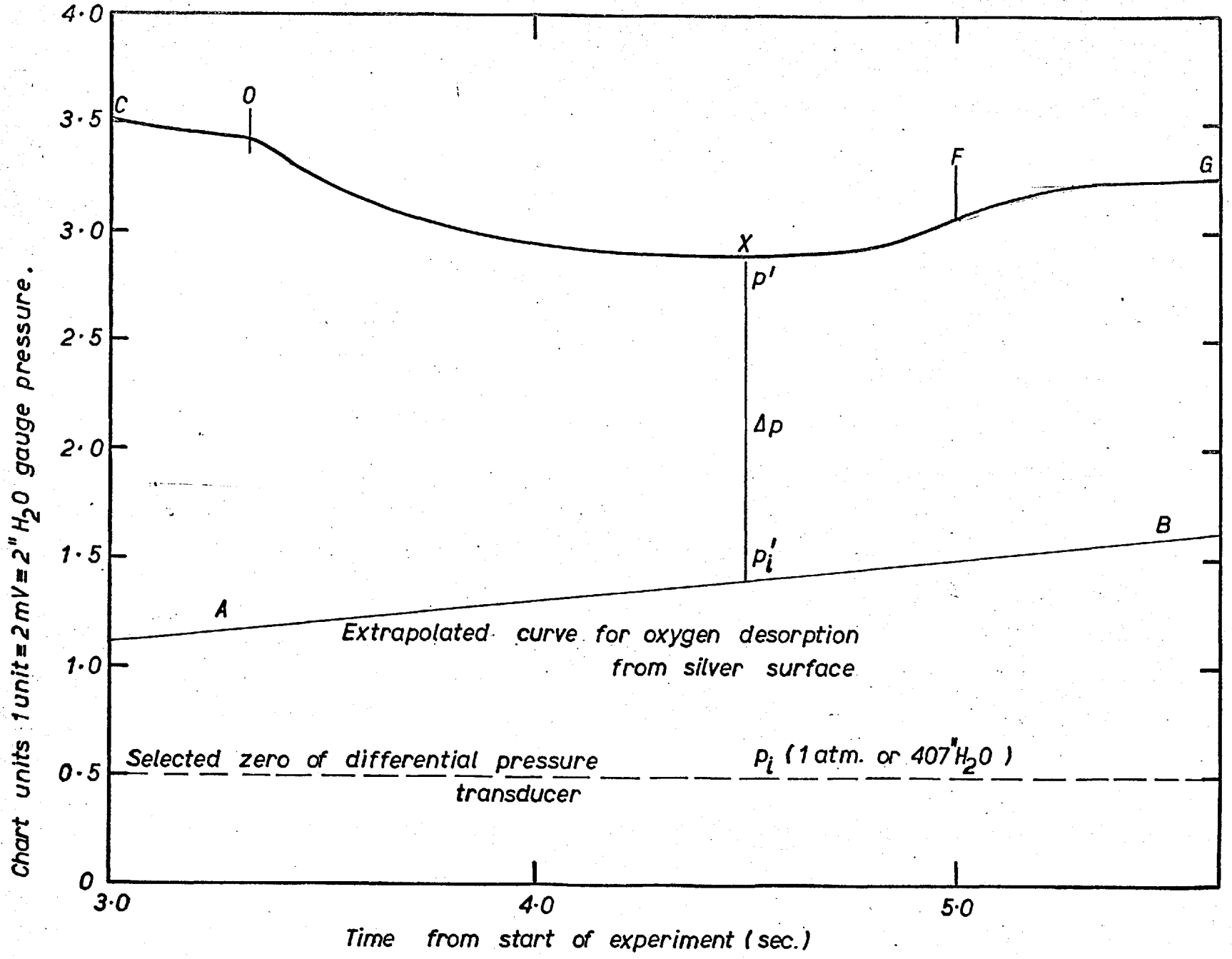

FIG. 6.4.a A TYPICAL GAUGE PRESSURE vs. TIME CURVE OBSERVED DURING THE RISE OF AN OXYGEN BUBBLE IN MOLTEN SILVER (1020°C). RUN 23.

a. Preliminary experiments on the rate of desorption of oxygen from the silver showed the rate to be constant and independent of top pressure over the relatively small differential pressure range used for measurements (i.e. 10" H_2O gauge). Thus Top Gauge Pressure increased linearly with time.

b. Gas volume changes within the apparatus during absorption experiments could have had little disturbing effect upon the silver surface, except when the bubble burst through, after which the final rate of desorption rapidly reverted to the initial rate prior to gas introduction.

Thus top gauge pressure variations resulting from gas volume changes were obtained by subtraction of Curve AB from the experimental curve (COXFG). Considering a typical case, the bubble volume at point X on the latter curve is related to the top space pressure and volume at time t by the equation

$$V^* = v_i \left(1 - \frac{p_i'}{p'}\right) \qquad 6.4.-1.$$

where

V^* = true volume of bubble

p_i' = top space pressure at time t without gas in apparatus

p' = top space pressure at time t with gas in apparatus.

This equation may be rearranged in terms of top gauge pressure

$$V^* = v_i \left(\frac{p' - p_i'}{p'}\right)$$

$$= v_i \frac{\Delta p}{p'} \qquad 6.4.-2.$$

where Δp = Differential Gauge Pressure resulting from volume of bubble.

Equation 6.4.-2. may be simplified by neglecting differences between p' and p, where (Fig. 6.4.a.)

$$p = p_i + \Delta p$$

$$p' = p_i' + \Delta p$$

Equation 6.4.-2. then becomes

$$V = \frac{v_i \Delta p}{p} \qquad 6.4.-3.$$

$$\text{or} \qquad V = v_i \left(1 - \frac{p_i}{p}\right)$$

The above equation was used in the calculation of bubble volumes throughout the absorption work. The percentage error involved may be represented by

$$\left(\frac{V - V^*}{V^*}\right) 100 = \left(\frac{p'}{p} - 1\right) 100 \qquad 6.4.-4.$$

Typical experimental values of p and p' at point X in Fig. 6.4.a. (408.8 and 411.8" H_2O respectively) may be inserted in 6.4.-4. which show the error to be approximately +1%. It follows that errors in $\frac{dV}{dt}$ are of the same order, so that the use of equation 6.4.-3. is justified.

6.4.2. Instantaneous Mass Transfer Coefficients

Between C and O on the pressure-time curve of Fig. 6.4.a., the top gauge pressure drops as the oxygen contained within the inverted cup steadily dissolves. At O, the bubble is released and dissolves rapidly at first, and then more slowly until a minimum is reached after approximately 1.3. seconds from release. Thereafter the bubble begins to expand until at F it bursts through the surface. Between F and G the rate of oxygen desorption initially observed is rapidly re-established.

An analysis of the concentration 'driving force' vs height above cup is presented in Fig. 6.4.b. Curve C represents the change in interfacial oxygen concentration of the bubble with height h above release point and has been calculated from the expression

$$C_I = q \; P_{O_2}^{\frac{1}{2}} = q \left[1 + \frac{\rho \, (H - h)}{13.6 \times 76}\right]^{\frac{1}{2}} \qquad 6.4.-5.$$

where H = height of silver above inverted cup (53 cm)

h = distance above cup (cm)

ρ = density of silver (9.26 gm/cc).

Curve D represents the bulk oxygen concentration which is assumed to be independent of height.

It is evident that $(C_I - C_B)$ is initially large and positive, decreases to zero and then becomes

negative. This explains the high initial rate of solution observed immediately after bubble release and also shows that the transfer direction reverses at h~ 40 cm, i.e. absorption changes to desorption. Possible errors in $(C_I - C_B)$ have been estimated in Fig. 6.4.b. and these result in an overall standard deviation in ΔC of $s \approx \pm 0.026 \times 10^{-3}$ Gm Atoms [O] /cc. Fig. 6.4.c. presents a plot of the relative error, S, vs height above cup, where the relative error in ΔC has been defined by the equation

$$S = \left[\frac{s^2}{(\Delta C)^2}\right]^{\frac{1}{2}} \qquad 6.4.-6.$$

As seen, S is initially small, but increases rapidly close to the cross-over point, tending to infinity when ΔC becomes zero at h = 40 cm. Consequently, instantaneous mass transfer coefficients calculated within this region are likely to be 'wild', and this is well illustrated by Fig. 6.4.d. which presents a typical plot of k_L vs time (RUN 23). In this case, the time taken to rise 53 cm was 1.7 seconds, giving an average rising velocity of 31.2 cm/sec. Thus, ΔC becomes zero approximately 1.24 seconds after bubble release, and this coincides with 'wild' values of k_L around that time. For this reason, calculated mass transfer coefficients over the first half of the column only have been

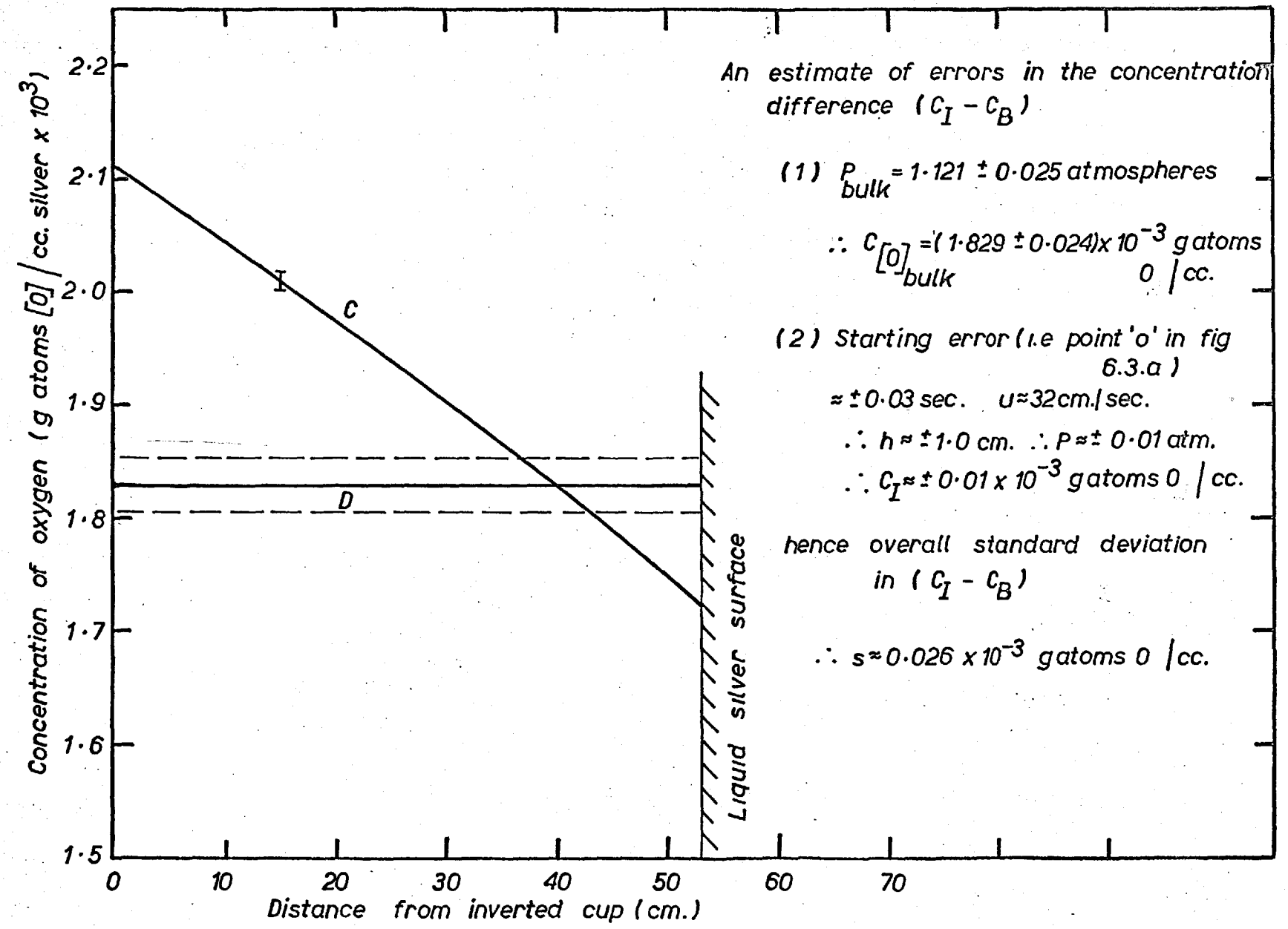

FIG. 6.4.b ESTIMATED OXYGEN CONCENTRATIONS AT BUBBLE INTERFACE AND IN BULK OF MOLTEN SILVER AT 1020°C.

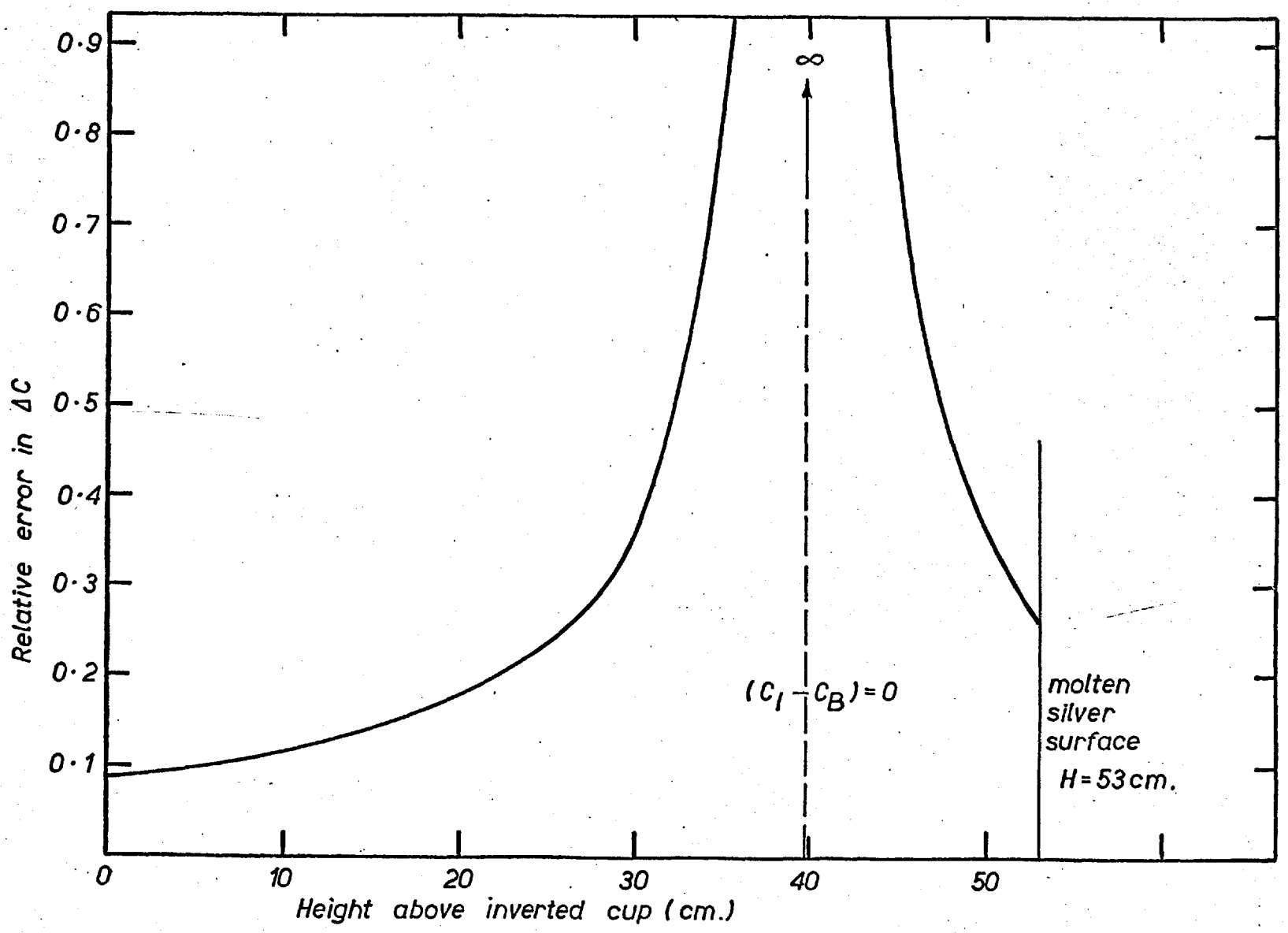

FIG. 6.4.c PLOT OF ESTIMATED RELATIVE ERROR IN $(C_I - C_B)$ WITH HEIGHT.

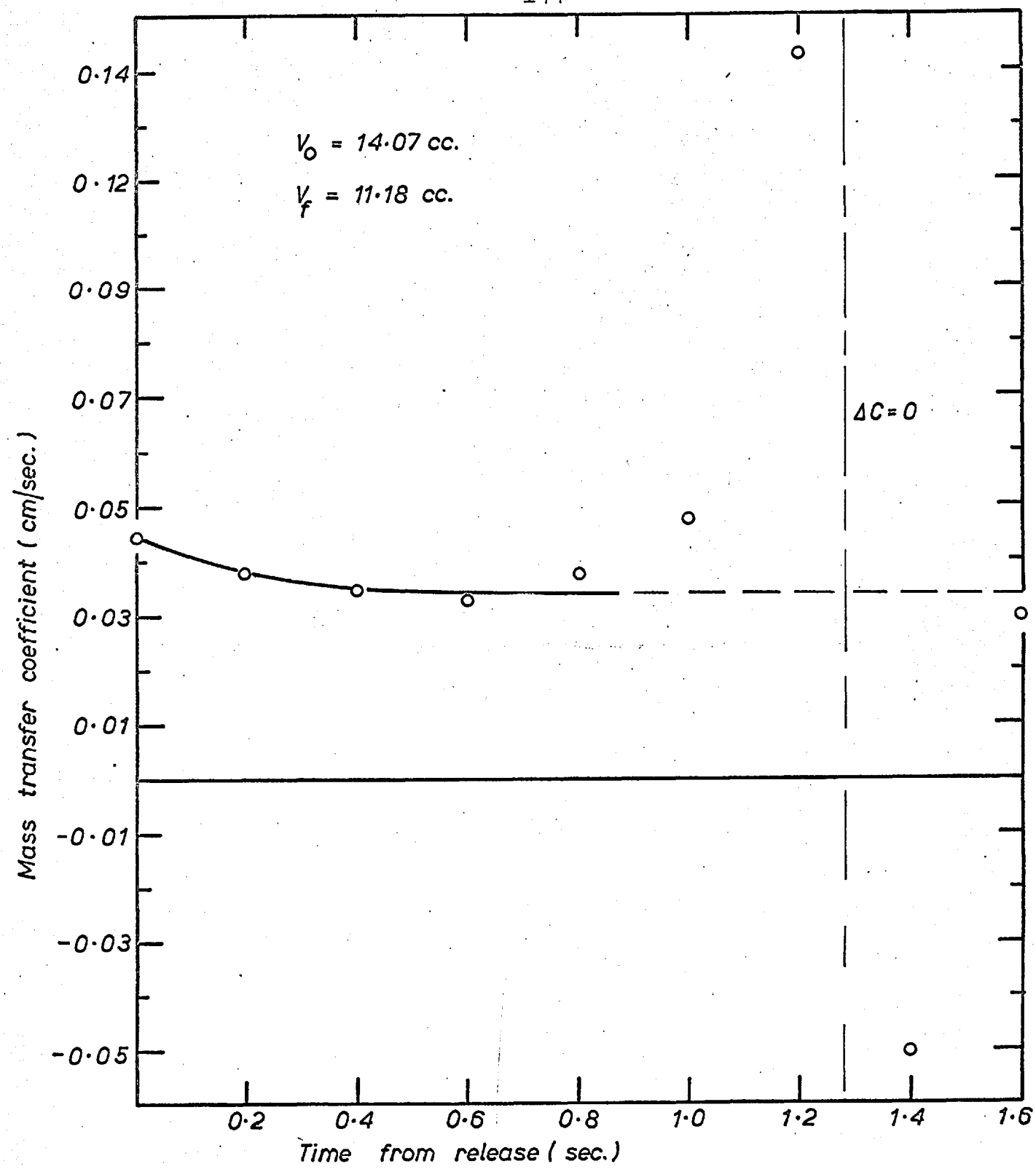

FIG. 6.4.d PLOT OF INSTANTANEOUS MASS TRANSFER COEFFICIENT vs. TIME. RUN 23.

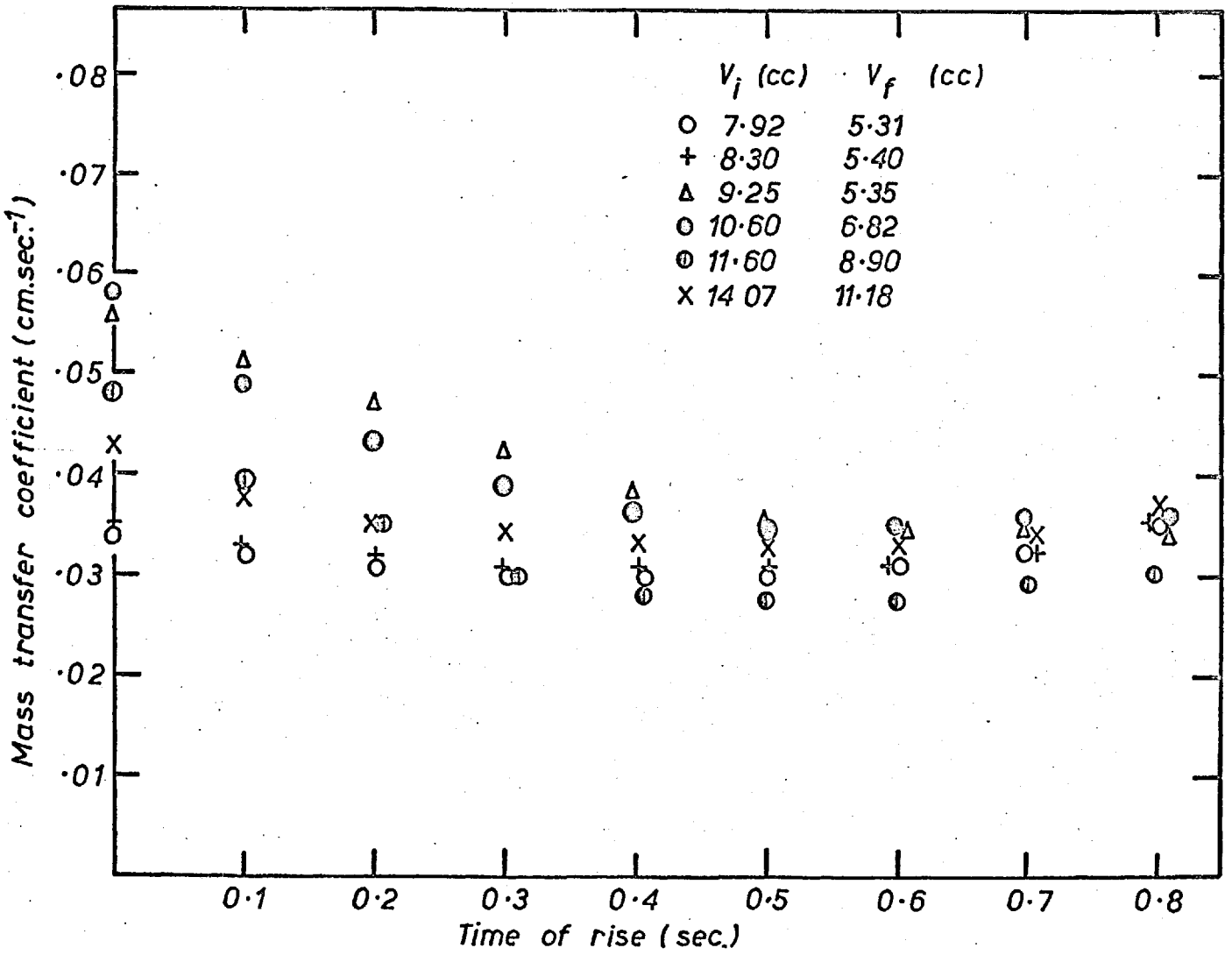

FIG.6.4.e PLOT OF INSTANTANEOUS MASS TRANSFER COEFFICIENTS FOR OXYGEN ABSORPTION INTO SILVER AT 1020°C

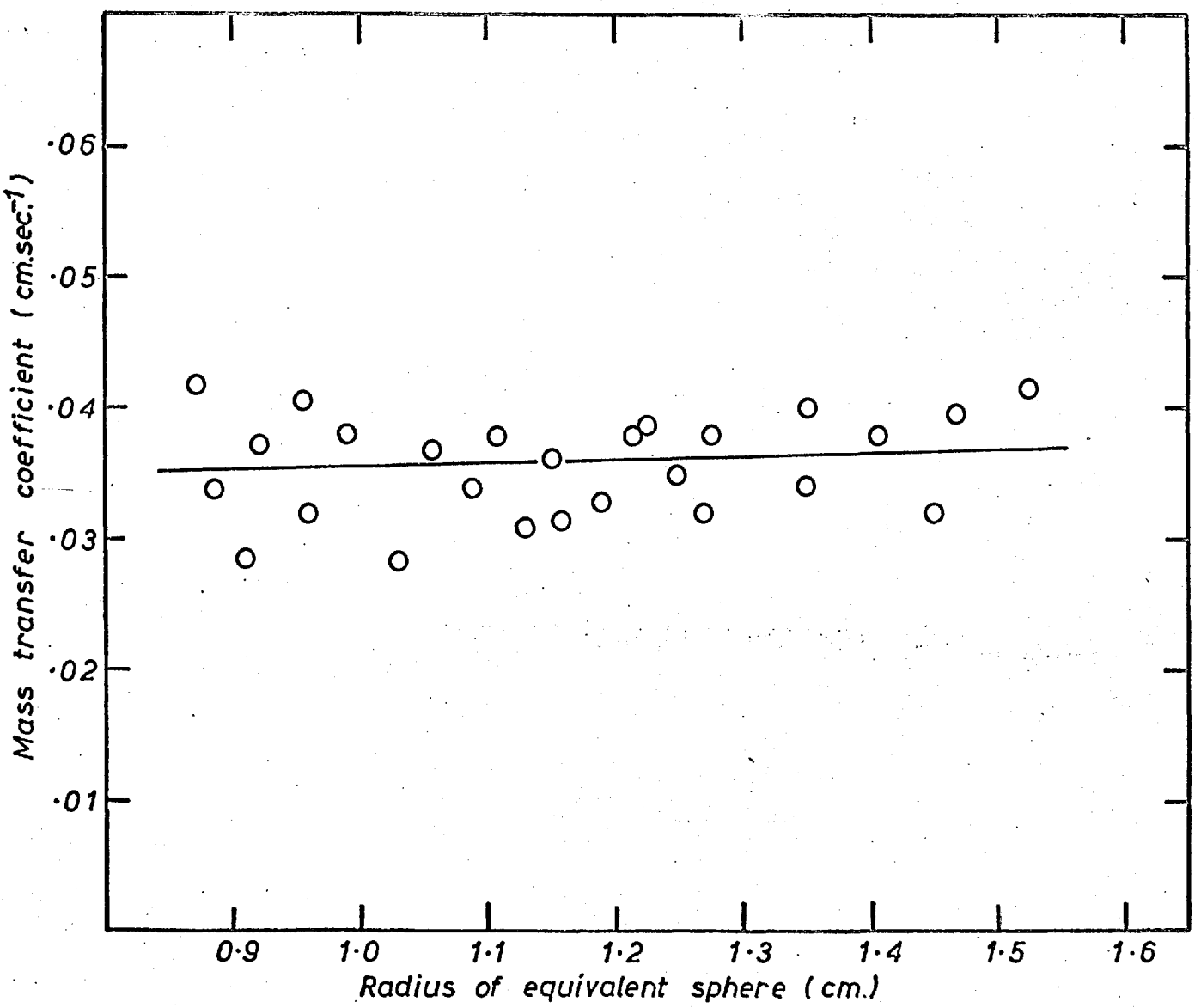

FIG.6.4.f PLOT OF OVERALL MASS TRANSFER COEFFICIENT vs. r_e FOR OXYGEN ABSORPTION INTO SILVER AT 1020°C

considered (i.e. 0 - 25 cms) and these are plotted in Figs. 6.4.e. and f. The method of calculation of k_L using equation 6.3.-7. follows the same procedure as that described in Chapter 4, section 4.6.2.,

It is considered that the accuracy of k_L with height will be of the order given in Fig. 6.4.c., so that mass transfer coefficients averaged over the first half of the column are accurate to $\pm$ 14% approximately.

6.5. ABSORPTION FROM OXYGEN/NITROGEN BUBBLES

Using the injection technique described in Chapter 5, section 5.4., known quantities of gas were bubbled into the inverted cup. The Mole Fraction of oxygen contained within the prepared O_2-N_2 mixture was 0.21, whilst the bulk oxygen concentration within the silver was maintained at zero by purging the column with nitrogen. Twenty-five experiments showed that, within experimental error, all the oxygen within the injected gas was completely absorbed before reaching the dumping cup. On release, the expansion of the bubble was equal to that observed for inert bubbles.

Since the accuracy of the injection technique was insufficiently high ($\pm$ 6%) to warrant further investigation with lower oxygen percentages, these experiments were abandoned. However, it is possible to make an

approximate assessment of the minimum transfer coefficient of the injected bubbles necessary to result in total oxygen absorption.

The bubbles were injected from the 1/4" I.D. filling tube and rose approximately 3 cm to the gas/liquid interface within the dumping cup. Neglecting changes in pressure within the silver, an average coefficient $\bar{k}$ is defined in equation 6.5.-1.

$$\bar{k} = \frac{\bar{\dot{n}}}{\bar{A}\left[\frac{C_I - 0}{2}\right]} \qquad 6.5.\text{-}1.$$

Assuming the bubble to be spherical, with an initial diameter, d_o, equal to 1/4", the final diameter after total oxygen absorption will be given by

$$d_f = d_o \left(1 - X_{[O]}\right)^{1/3} = 0.925\, d_o$$

Hence the mean diameter, $\bar{d}$, of the bubble is 0.61 cm. Taking a rising velocity, U, equal to 25 cm/sec, the average transfer rate of oxygen is given by

$$\bar{\dot{n}}_{[O]} \geqslant 2 \frac{PV}{R\theta}\left[\frac{X_{[O]}U}{h}\right] \qquad 6.5.\text{-}2.$$

where $\bar{\dot{n}}_{[O]}$ = average number of Gm Atoms oxygen dissolving/sec.

Also $C_I = q\,(PX_{[O]})^{\frac{1}{2}}$ 6.5.-3.

Substitution for $\bar{A}$, $\bar{\dot{n}}$, and C_I in 6.5.-1., finally gives

$$\bar{k} \geqslant \frac{2}{3} \frac{(PX_{[O]})^{\frac{1}{2}}}{q\,R\,\theta}\left[\frac{U}{h}\right]\bar{d} \qquad 6.5.\text{-}4.$$

Inserting appropriate values,

$$\bar{k} \geqslant \frac{2}{3} \quad \frac{(1.5 \times 0.21)^{\frac{1}{2}}}{1.7 \times 10^{-3} \times 82 \times 1293} \left[\frac{25}{3}\right] 0.61$$

$$\geqslant 0.01 \text{ cm/sec}^{-1} \text{ approx.}$$

R = Gas Constant Atmos cc/mole/^{o}K

6.6 DESORPTION INTO OXYGEN/NITROGEN BUBBLES

The results obtained for oxygen desorption from partially saturated silver into rising O_2/N_2 bubbles have not been included, owing to the large scatter in results ($\pm$ 100%). It was found that oxygen desorbed rapidly into the nitrogen injected into the cup, leading to low values of $(C_B - C_I)$. This, added to the effects of errors in Vc and C_B seems to render the system unsatifactory for mass transfer work. However, the desorption work proved very useful in extending the range of velocity measurements to high values of r_e. No allowance was necessary in bubble volume measurement, since the oxygen partial pressure was chosen so as to eliminate oxygen desorption from the top silver surface.

CHAPTER. 7.

7.0. DISCUSSION OF RESULTS

The results of shapes, velocities and mass transfer rates of bubbles rising in tap water, aqueous P.V.A. solutions and molten silver are discussed in the following sections.

7.1. RISING VELOCITIES OF LARGE BUBBLES

a. Low Viscosity Liquids

Present results obtained for terminal velocities of large bubbles rising in tap water and low viscosity aqueous P.V.A. solutions ($\not>$130 cp) confirm the experimental relationships proposed by Davies & Taylor (6) i.e.

$$U = K\ V^{1/6}$$

$$\text{or } U = C\ (g\ r_e)^{\frac{1}{2}}$$

Present values of K of 25.0 $cm^{\frac{1}{2}}sec^{-1}$ agree within one per cent of those obtained by Haberman & Morton (2) and Davies & Taylor, which were 25.2 and 24.8 respectively.

Although the present method of evaluating K involved mean values of U and V, it was shown in section 4.4.1. that velocity results were equivalent to those that would have been obtained from instantaneous measurements of U and V. The present experimental method allowed relatively long time intervals and distances to be used in velocity

determinations. This resulted in high accuracy and little experimental scatter around the curves in Figs. 4.4.a and b.

The Effect of Wall Proximity

As seen from Figs. 4.4.a and b, the velocities of bubbles rising in low viscosity liquids, depart from the values given by equation 4.4.-1. at bubble volumes in excess of 45 cc approximately. This may be attributed to the increasing influence of 'Wall Effect' in which liquid displaced by the rising bubble has to flow downwards through the annulus formed by the bubble and the column wall. The effect of wall proximity on U is predicted in the empirical expression obtained by Uno & Kintner (38)

$$\frac{U}{U_\infty} = \left[\frac{1}{b}\left[1 - \frac{d_e}{D}\right]\right]^{0.765} \qquad 7.1.-1.$$

(U, velocity of bubble in column; U_∞, velocity in an infinite fluid).

The authors found that the coefficient 'b' was a function of surface tension, σ, and column diameter, D. In the range of bubble sizes studied, ($0.2\ cm \leq d \leq 2.4\ cm$) they found that the value of 'b' increased with increasing D and decreasing σ. However, the effect of D and σ on b became much less marked at higher column diameters, tending towards a numerical value of 0.90 in all liquids.

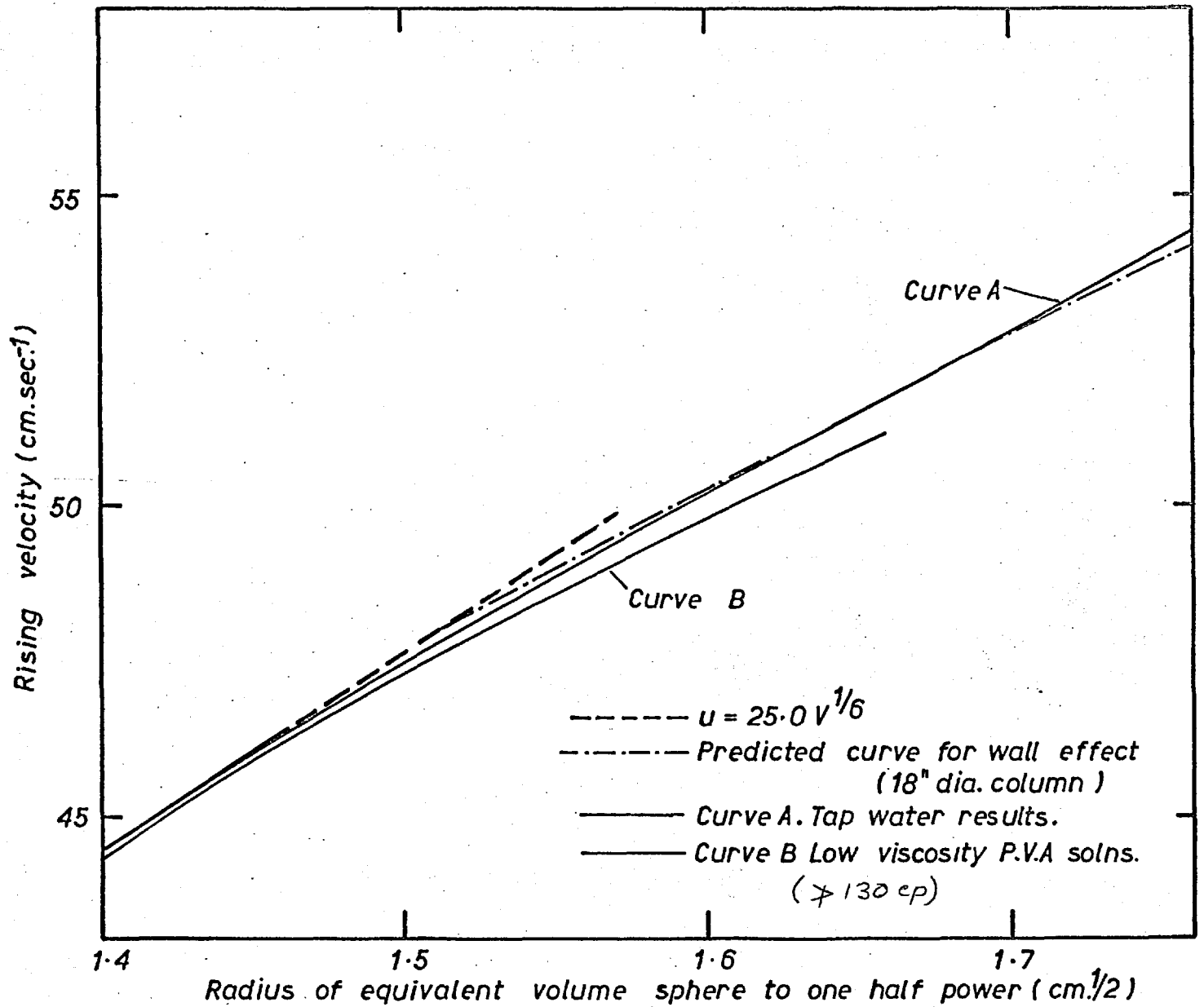

FIG. 7·1.a PLOT OF RISING VELOCITY vs. $r_e^{1/2}$ TO ILLUSTRATE EFFECTS OF WALL PROXIMITY.

Fig. 7.1.a. compared the velocity-radius curve predicted by equation 7.1.-1 (taking b = 0.90) with present experimental curves. As seen, good agreement is obtained, indicating that their empirical equation may be accurately extrapolated up to column diameters of 46 cm and equivalent spherical bubble diameters, d_e, of 5.0 cm. (Their maximum experimental values were 15.25 and 2.4 cm respectively).

High Viscosity Liquids

As seen from Fig. 4.4.b. the velocity-volume curves for highly viscous liquids fall below the common low viscosity curve, but tend towards it at higher bubble volumes. The reduced velocities cannot be attributed to Non-Newtonian behaviour, tests having shown (39) that viscosity of P.V.A. solutions were nearly independent of shear rate.

However, it is evident from the curves that at sufficiently high volumes, the rising velocities of bubbles in highly viscous liquids become virtually independent of liquid properties. A similar velocity-radius curve has been obtained by Astarita & Apuzzo (44) for nitrogen bubbles rising through a viscous aqueous solution of glycerol (440 cp).

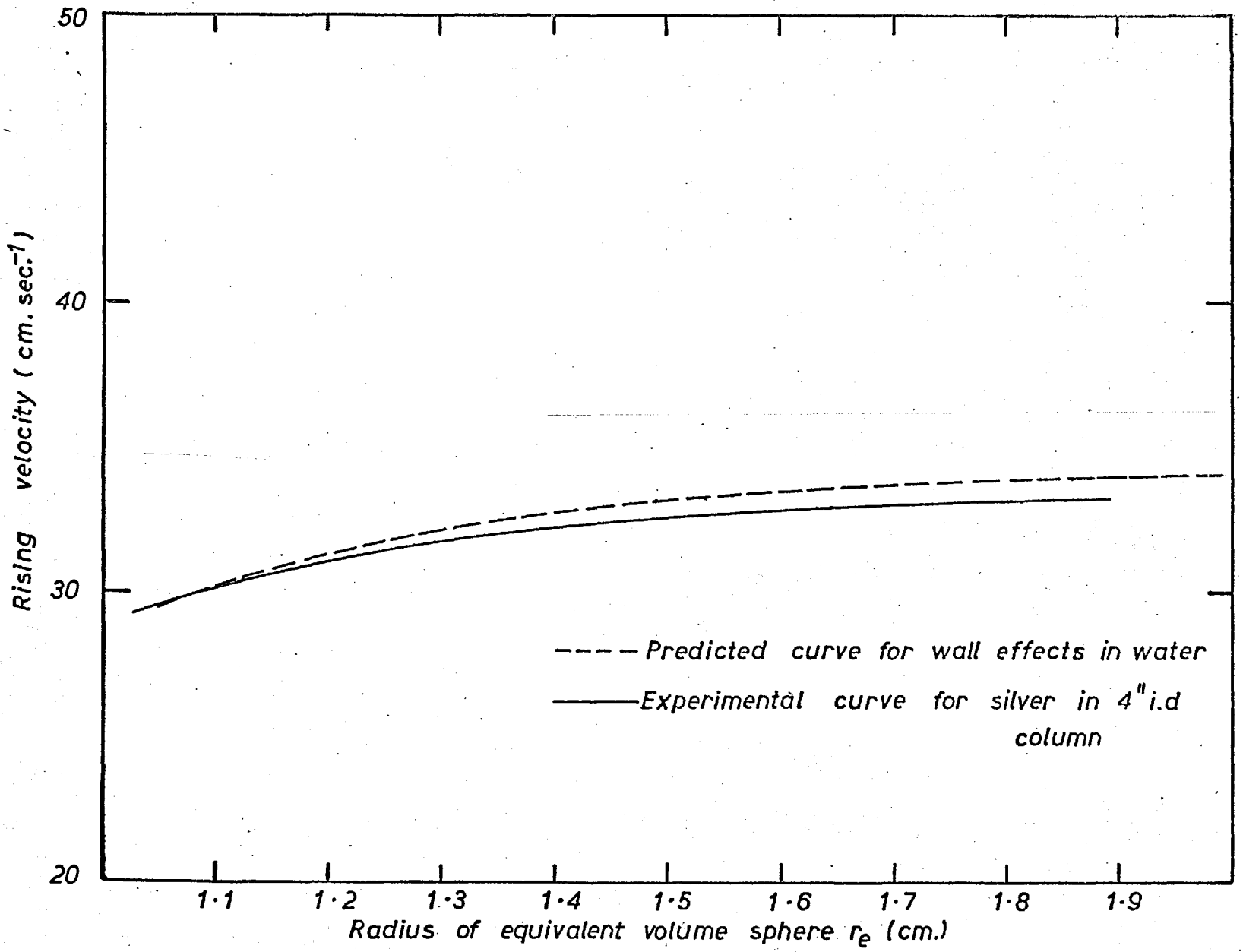

FIG. 7.1.b PLOT OF RISING VELOCITY vs r_e, TO ILLUSTRATE PREDICTED WALL EFFECTS

Bubble Velocities in Molten Silver

The results obtained for bubbles rising in molten silver (1020°C) showed that rising velocities were approximately independent of bubble volume. Fig. 7.1.b. compares the experimental curve obtained with that predicted by equation 7.1.-1. for bubbles rising in a 4" I.D. column of water. The close agreement between the two curves indicates that, within experimental errors stated the velocities of large bubbles are independent of liquid properties over the range between the two liquids (i.e. σ = 72 - 920 dynes/cm, ρ = 1.0 - 9.3 gm/cm^3, μ = 1 - 4 cp)

Effect of Mass Transfer

Mass transfer rates had no effect upon rising velocities for any of the systems investigated. This is not unexpected, since mass transfer coefficients were ~0.03 cm/sec^{-1} compared with bubble velocities of 30 - 50 cm/sec^{-1}. Thus the amount of transferring material across the gas/liquid interface is unlikely to distort the liquid flow pattern around the bubble.

7.2. SHAPES OF BUBBLES

The shape and rising velocity of a bubble, together with the rate of energy disipation within the wake are all interdependent. The complex interactions between

these three has so far prevented a complete analysis of bubble dynamics and bubble geometry.

However, on the basis of the work by Davies & Taylor (6), it was found that the bubble's shape was closely represented by a spherical segment, and that the observed rising velocity nearly agreed with that predicted by potential flow theory. As previously mentioned, the analysis was valid only for a region close to the front stagnation point of such a bubble shape. They obtained the relationship

$$U = \frac{2}{3}\,(gr)^{\frac{1}{2}} \qquad 7.2.\text{-}1.$$

From geometrical considerations, the radius of curvature may be expressed in terms of volume V, and height, b, of the spherical segment, according to

$$r = \left[\frac{V}{\pi b^2} + \frac{b}{3}\right] \qquad 7.2.\text{-}2.$$

Eliminating r from 7.2.-1. gives a relationship between the velocity and height of a bubble of volume V.

$$U = \frac{2}{3}\left[\, g\left[\frac{V}{\pi b^2} + \frac{b}{3}\right]\right]^{\frac{1}{2}} \qquad 7.2.\text{-}3.$$

Also, the basal radius of the bubble is related to V and b in the equation

$$V = \frac{\pi}{6}\,(3a^2b + b^3) \qquad 7.2.\text{-}4.$$

Since equation 7.2.-3. predicts b in terms of U (or vice versa), present experimental values of velocity may be

used to predict values of b (and a).

The velocity of rise in low viscosity liquids ($\not>$130 cp) was related to bubble volume according to the equation

$$U = 25.0 V^{1/6}$$

elimination of U in 7.2.-3. gives

$$\left(\frac{25 \times 3}{2}\right)^2 \frac{V^{\frac{1}{3}}}{g} = b\left[\frac{1}{3} + \frac{V}{\pi b^3}\right] \qquad 7.2.\text{-}5.$$

Use of equations 7.2.-5. and 7.2.-4. lead to solution of a and b in terms of bubble volume. Predicted curves of a and b in terms of r_e are shown in Fig. 7.2.a. These show close agreement with the experimental results plotted, although there is a slight tendency to over-estimate the basal radius (~4%).

It is concluded that a simple model based on potential flow around a spherical segment accurately relates the shape and velocity of large bubbles rising in low viscosity liquids.

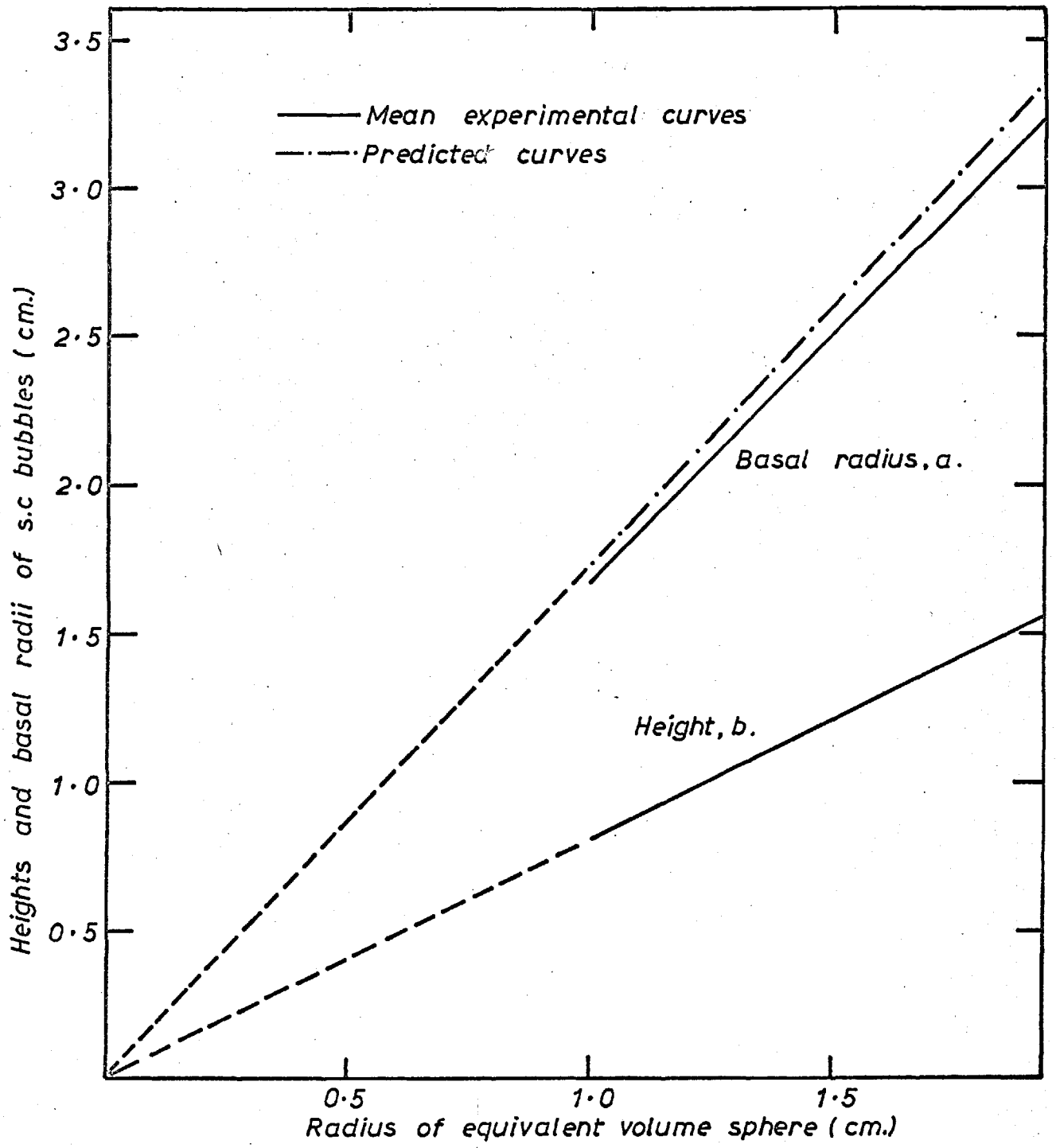

FIG.7.2.a COMPARISON OF PREDICTED & MEAN EXPERIMENTAL CURVES OF a & b vs. r_e FOR LOW VISCOSITY LIQUIDS ($\neq$130 cp.)

7.2.2. Effect of Viscosity on Bubble Shapes

Bubble rise through high viscosity slags has been simulated by the passage of bubbles through aqueous polyvinyl alcohol solutions.

As seen from Fig. 4.5.b, the shape of large bubbles changed significantly at high P.V.A. concentrations. Since the surface tension and density of the liquid remained nearly constant over the range of P.V.A. concentrations studied, these shape changes must be primarily a viscous effect.

For a given volume, increased viscosity (730 cp) led to a decrease in the basal radius, a, together with an increase in height, b, especially at low bubble volumes. As the bubble volume (or r_e) increased, departures from the predicted curve became less marked; the bubble shape tending to become independent of liquid properties. Since rising velocities in viscous liquids showed similar tendencies, it is concluded that U and r in viscous solutions become independent of liquid properties at sufficiently high volumes, and are then related by the Davies & Taylor Equation (7.2.-1.).

Davidson (59) has also observed a decreasing radius of curvature and reduced velocity of S.C. bubbles in very viscous media. He showed that viscous flow around a spherically capped bubble results in a different radial

pressure distribution within the fluid to that obtained for potential flow. In order to maintain constant pressure within the bubble, he calculated that the radius of curvature was decreased with increasing viscosity, and was related to the bubble's velocity by

$$r = \frac{9}{8}\frac{U^2}{g}\left[1 + \sqrt{\frac{128}{27}\frac{\mu g}{\rho U^3}}\right] \qquad 7.2.-6.$$

where

$$U = \frac{2}{3}\sqrt{gr - \frac{6\mu U}{r}} \qquad 7.2.-7.$$

Putting $\mu = 0$ in the above expression results in the Davies & Taylor relationship.

7.2.3. Wall Effects on Bubble Shapes

Since the present work on P.V.A. solutions was carried out in a large column, the effect of wall proximity on bubble shapes obtained in a 6" I.D. column (32) may be estimated.

Comparing mean curves of a and b vs r_e (Fig. 7.2.a.) for low viscosity liquids ($\not>$130 cp) with similar curves for the 6" I.D. column, close agreement is obtained between the two sets of results, up to bubble volumes of 20 cc approximately. Thereafter, deviations occurred which indicated that the radius of curvature, r, of the bubble was reduced in the 6" I.D. column due to wall proximity.

In order to test whether differences in radius of

curvature could be related to differences in bubble rising velocities within the two columns, predictions of r based upon the Davies & Taylor Equation (7.2.-1.) was made. It follows from equation 7.2.-1. that

$$r_{6"}/r_{18"} = (U_{6"}/U_{18"})^{\frac{1}{2}} \qquad 7.2.-8.$$

which may be rewritten as

$$r^* = U^{*\frac{1}{2}} \qquad 7.2.-9.$$

where r^* represents the ratio of the cap radius in the 6" I.D. column to that in the 18" I.D. column (similarly, U^*).

Table 7.2.3.-a. presents mean experimental values of r for the two column diameters, for various values of r_e. Experimental values of r^* have been calculated and these are compared with equivalent values of $U^{*\frac{1}{2}}$. Fig. 7.2.3.a. permits a comparison between the two curves. Since the agreement is reasonable, it seems likely that the relatively smaller values of r reported in the literature (21, 60), for bubbles rising in small diameter columns result from Wall Effects.

Table 7.2.3.a.

r_e (cm)	r 6"I.D.	r 18"I.D.	r^* -	$U^{*\frac{1}{2}}$ -
1.2	2.45	2.50	0.98	0.97
1.6	3.15	3.40	0.93	0.94
2.0	3.82	4.30	0.89	0.92
2.4	4.45	5.12	0.87	0.885

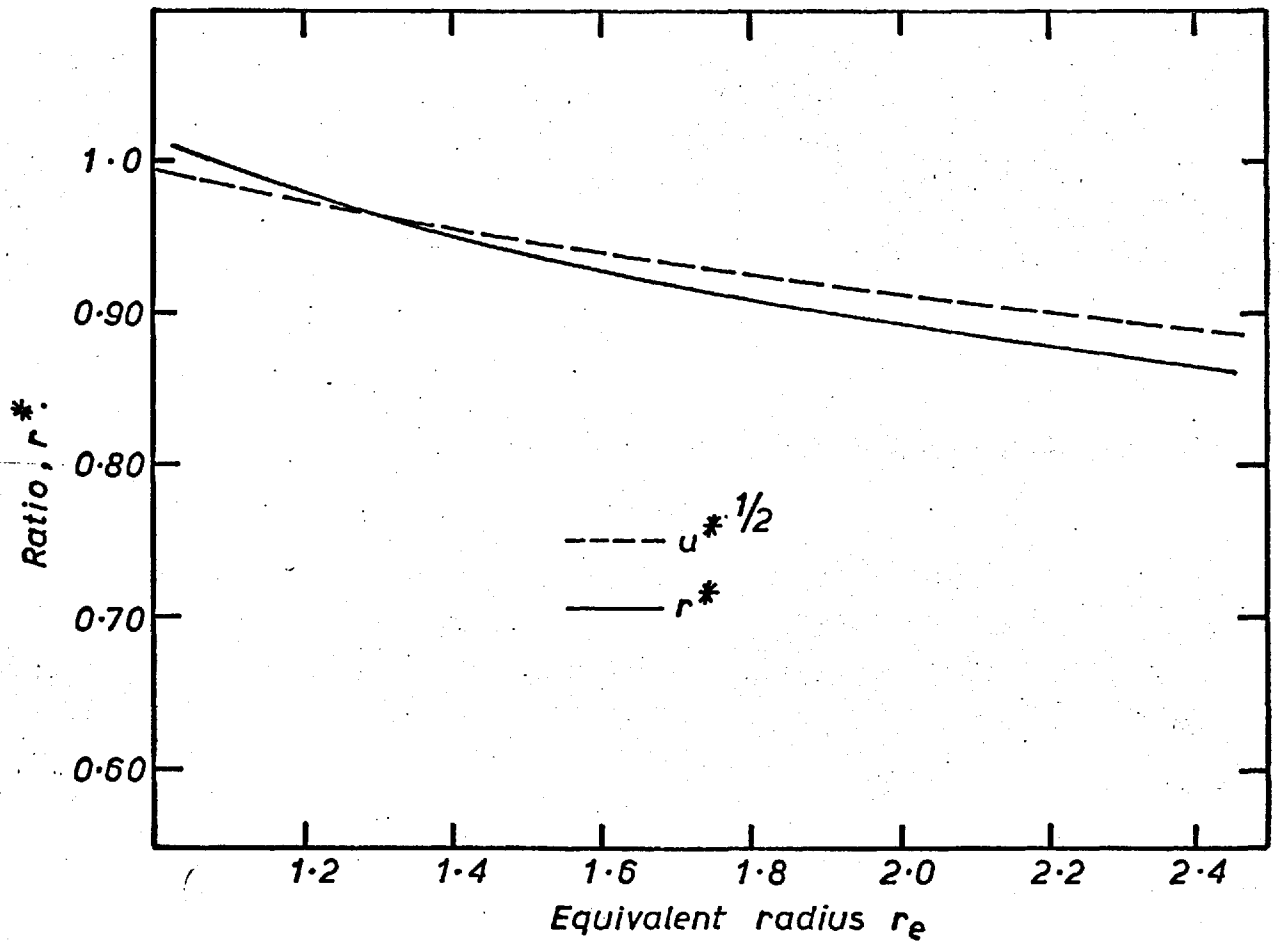

FIG. 7.2.3a VARIATION OF r^* vs. RADIUS OF EQUIVALENT VOLUME SPHERE COMPARED WITH PREDICTED RATIO FOR WALL EFFECTS.

7.2.4. Shape of Wakes behind S.C. Bubbles

The shape of wakes observed behind S.C. Bubbles have been described under section 4.5.2., of Chapter 4. The Reynolds Number of the bubbles ($\frac{\rho U d_e}{\mu}$) ranged approximately from 7 in 730 cp P.V.A. solution to 2.0×10^5 in water. The structure of the wake varied with Re, and passed through a series of transitions similar to those observed behind plates, discs and cylinders (section 2.1.1.)

In the case of bubbles rising in viscous P.V.A. solutions (>200 cp) trailing gas envelopes or 'skirts' were observed. These skirts apparently replaced the 'vortex sheath' observed behind solid bodies. The mechanism of formation and stability of these skirts are discussed later. The coloured wake experiments performed in water gave the required outlines for bubbles of high Re.

Low Reynolds Numbers Re 10 - 40

Over this range of Re, the shape or geometry of the enclosed wake altered. Thus, for S.C. bubbles in 730 cp P.V.A. solution, the eccentricity of the bubble and its wake increased with bubble volume, becoming approximately constant at volumes>35 cc (see Fig. 4.5.2.d.). This phenomenon may be explained by the growth of an annular vortex and would be analogous to the lengthening twin vortices observed behind cylinders over the range Re, 5-40.

Intermediate Reynolds Numbers 40 - 1000

For large bubbles in 730 cp P.V.A. (~50 cc), the lower parts of the gas envelope begins to waver. Similarly for bubbles rising in lower viscosity liquids, the skirt's stability is gradually decreased. The shape of the enclosed wake remains approximately independent of bubble volume, E = 1.1. Plate (a) of Fig. 2.1.b. provides a striking comparison with flow around a bubble at Re~820.

High Reynolds Numbers 1×10^3 - 2.0×10^5

From wake dimensions given for bubbles rising in water, it is evident that the shape of the enclosed wake remains similar. The blurred wake outlines in Figs. 4.5.2.a. and b. may be explained by the thickening of a 'vortex sheath', separating the wake from the bulk. Turbulent interactions between the bulk and the wake at these high Reynolds numbers rapidly result in an ill-defined zone of mixed material, especially towards the base of the enclosed wake. Plate (f) of Fig. 2.1.b. allows comparison of present results with those for flow past a flat plate at high Re, i.e. 1750.

The bubble wake remains approximately circular due to the wake underpressure causing actual streamlines to lie inside those predicted for inviscid flow(9). The

tortuous trail of discarded wake material is thought to result from a similar mechanism to that postulated for flow past spheres and discs at similar Re. i.e. periodic shedding of vortex loops, asymmetrically to the axis of rise of the bubble. However, the frequency and strength of the disturbances are insufficient to cause rocking motion at bubble volumes >5 cc.

7.2.5. Stability of Skirt Formation

Fig. 7.2.5.a. presents photographs of skirts trailing behind bubbles rising in 1000 cp glycerol solution in the 6" I.D. column. Photographic and visual observations suggest that the main bulk of the gas is contained within a spherical segment of similar proportions to those in low viscosity fluids.

It follows from Bernoulli's equation applied along the interface of the spherical cap, that the requirement of constant pressure is possible provided that the increase in static liquid pressure with depth is converted into an equivalent increase in kinetic energy. At $\theta' \sim 50^{\circ}$, this condition is evidently no longer possible and the characteristic planar rear surface of the bubble results, in low viscosity liquids . In high viscosity liquids, the trailing gas envelope may be approximated to a cylindrical shell. The increase in pressure along

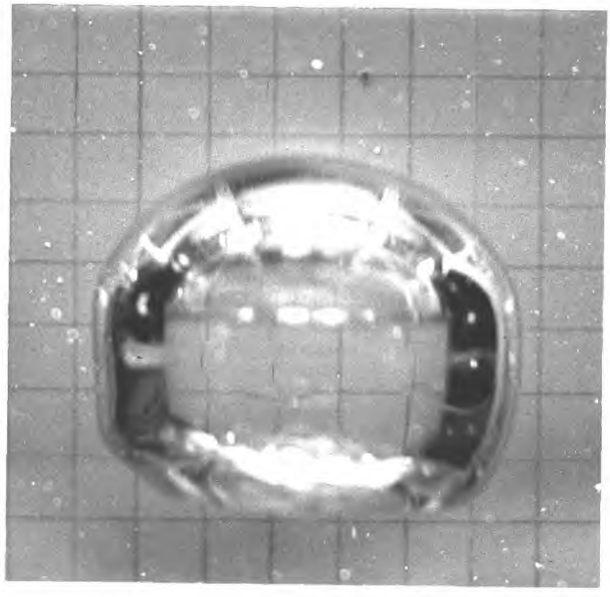

V = 25 cc.

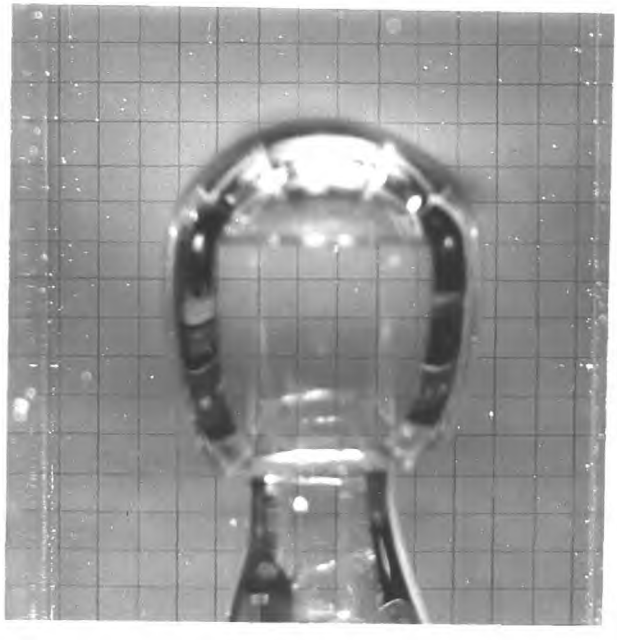

V = 50 cc.

Fig.7.2.5.a. Typical gas 'skirts' trailed by large bubbles in highly viscous liquids.

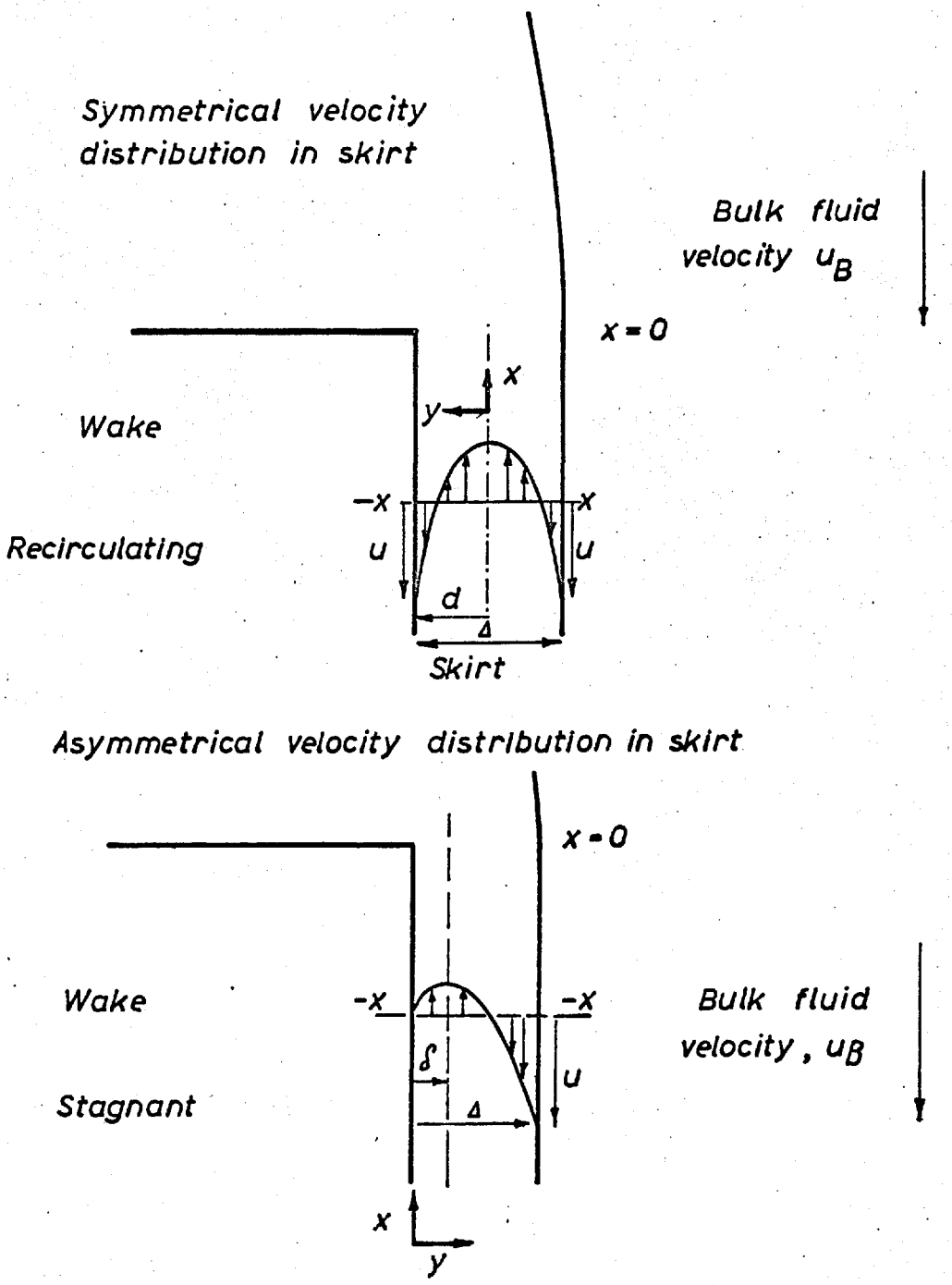

FIG.7.2.5.b POSSIBLE FLOW SITUATIONS TO EXPLAIN SKIRT STABILITY

the gas/liquid interface must equal the increase in static liquid pressure (for potential flow). It follows that an equivalent increase in gas pressure within the skirt is necessary for stability. The theory below shows that this is possible provided the gas within the envelope is in viscous flow. In addition, it predicts the requisite skirt thickness for the flow to occur.

Fig. 7.2.5.b. shows an enlarged cross-section of the skirt. Two possible gas velocity profiles have been considered, one symmetrical, the other asymmetrical due to the presence of a stagnant wake. Since $\mu_{gas} \ll \mu_{liquid}$, velocity profiles within the liquid phase remain undistorted. In the diagrams, a downward velocity, equal to the rising velocity of the bubble, has been superimposed on the system. Since the skirt thickness is much less than its width, curvature effects have been assumed to be negligible.

Considering one-dimensional incompressible gas flow under steady state conditions, the general equation of continuity in rectangular co-ordinates reduces to (42)

$$\frac{\partial v_x}{\partial x} = 0 \qquad 7.2.-11.$$

whilst the corresponding equation of motion (x component) reduces to

$$(\rho v_x) \frac{\partial v_x}{\partial x} = - \frac{\partial p}{\partial x} - \frac{\partial \tau_{yx}}{\partial y} + \rho g_x \qquad 7.2.-12.$$

Combining equations 7.2.-11. and 7.2.-12., and neglecting gravitational forces which are much less than viscous and pressure forces, yields the appropriate differential equation to be solved,

$$0 = \frac{dp}{dx} + \frac{d\tau_{yx}}{dy} \qquad 7.2.-13.$$

τ_{yx} represents the shear stress in the x direction exerted on a fluid surface of constant y, by the fluid in the lesser region of y, and is related to the velocity vector v_x by Newton's Law, ie.

$$\tau_{yx} = - \mu \frac{dv_x}{dy}$$

Symmetrical Velocity Distribution (see Fig. 7.2.5.b.)

Integration of 7.2.-13. w.r.t. y gives

$$\tau_{yx} = - \left[\frac{dP}{dx}\right]_x y + A$$

B.C.1. $\tau_{yx} = 0$, $y = 0$. Hence $A = 0$.

Hence, substituting for τ_{yx} gives

$$\frac{dv_x}{dy} = \frac{y}{\mu} \left[\frac{dP}{dx}\right]_x \qquad 7.2.-14.$$

Integration of 7.2.-14. w.r.t. y gives

$$v = \frac{y^2}{2\mu} \left[\frac{dP}{dx}\right]_x + B$$

B.C.2. $v = -U$, $y = d$,

hence, $$B = -U + \frac{y^2}{2\mu}\left[\frac{dP}{dx}\right]_x$$

which gives

$$v_x = \tfrac{1}{2}\left[\frac{dP}{dx}\right]_x \frac{(y^2 - d^2)}{\mu} - U \qquad 7.2.\text{-}15.$$

Under steady state conditions, the flow rate across any cross section of the skirt is zero.

$$\int_{-d}^{d} v_x dy = 0 = \int_{0}^{d} v_x dy \qquad 7.2.\text{-}16.$$

Substitution for v_x from 7.2.-15. in 7.2.-16. and integrating w.r.t. y from 0 to d , finally gives

$$d = -\sqrt{\frac{3\mu U}{\left(\frac{dP}{dx}\right)_x}} \qquad 7.2.\text{-}17.$$

As previously mentioned, the increase in pressure along the skirt is equal to the increase in static fluid pressure, i.e.

$$\left[\frac{dP}{dx}\right]_x = -\rho_L g$$

Hence substituting $\frac{dP}{dx}$ in 7.2.-17. gives a value for the skirt thickness.

Hence, skirt thickness $\Delta = 2d$

$$= 2\left[\frac{3\mu U}{\rho_L g}\right]^{\frac{1}{2}} \qquad 7.2.-18.$$

Asymmetrical Velocity Distribution (See Fig. 7.2.5.b.)

Integration of 7.2.-13. w.r.t. y yields

$$\tau_{yx} = -\left[\frac{dP}{dx}\right]_x y + A'$$

B.C.1. $\tau_{yx} = 0, \; y = \delta$

Hence $$\tau_{yx} = -\mu \frac{dv_x}{dy} = \left[\frac{dP}{dx}\right]_x (\delta - y) \qquad 7.2.-19.$$

Integration of 7.2.-19. w.r.t. y yields

$$v_x = -\frac{1}{\mu}\left[\frac{dP}{dx}\right]\left\{\delta y - \frac{y^2}{2}\right\} + B' \qquad 7.2.-20.$$

B.C.2. $v_x = 0, \; y = 0.$ Hence $B' = 0$

Also $v_x = -U$ at $y = \Delta$

Hence $$\frac{\mu U}{\Delta\left[\frac{dP}{dx}\right]_x} + \frac{\Delta}{2} = \delta \qquad 7.2.-21.$$

Also, at steady state $\int_0^{\Delta} v_x dy = 0$

Thus integration of 7.2.-20. ($B' = 0$) w.r.t. y from 0 to Δ yields

$$-\frac{\Delta^2}{2\mu}\left[\frac{dP}{dx}\right]_x\left[\delta - \frac{\Delta}{3}\right] = 0 \qquad 7.2.-22.$$

Substitution for from 7.2.-21. finally gives

$$\Delta = - \left[\frac{6\mu U}{dP/dx} \right]^{\frac{1}{2}}$$

Since $\left[\frac{dP}{dx} \right]_x = - \rho_L g$, the skirt thickness Δ becomes

$$= 2 \left[\frac{1.5\mu U}{\rho_L g} \right]^{\frac{1}{2}} \qquad 7.2.-23.$$

Equations 7.2.-18. and 7.2.-23. represent solutions for two possible flow configurations and predict skirt thicknesses differing by a factor of $\sqrt{2}$.

The theory indicates that:-

a. This model assumes an interfacial liquid velocity, U, which must be greater than zero and shows that if $U \leqslant 0$, skirt thickness, Δ, reduces to zero. A steady velocity profile around the enclosed wake's boundary may occur in highly viscous liquids (i.e. laminar flow) resulting in skirt stability. Turbulent velocity fluctuations at the wake's 'boundary' for bubbles rising in water indicate that skirts could not be stable in low viscosity liquids.

b. Provided $U \approx$ constant, the skirt thickness, Δ, is independent of height below the bubble's rear surface. Presumably the skirt terminates close to the stagnation region at the base of the enclosed wake since U tends to decrease.

c. The thickness, Δ, is proportional to $\left(\frac{\mu_{gas}}{\rho_{liquid}} \right)^{\frac{1}{2}}$

Inserting appropriate values of these properties into equations 7.2.-18. and 7.2.-23. leads to prediction of skirt thickness.

Taking μ_{N_2} = 0.0181 cp., ρ_L = 1.01 gm/cm^3 and g = 981 dynes/sec^2, values of Δ for different values of U are tabulated below.

U	Δ	Δ
cm/sec	Eqtn. 7.2.-18.	Eqtn. 7.2.-23
	cm	cm
40	9.35×10^{-3}	6.62×10^{-3}
4.0	2.96×10^{-3}	2.10×10^{-3}
0.4	9.35×10^{-4}	6.62×10^{-4}

Although quantitative measurements have not been obtained, observations made on the size of bubble formed when a stripped fragment of skirt 'rolls up' indicate a thickness, Δ, of approximately $10^{-2} - 10^{-3}$ cm. This provides some confirmation of the present theory.

Thus a nitrogen bubble of 30 cc would have a maximum skirt thickness of 9.35×10^{-3} cm, which would be reduced by a tenth if the velocity, U, were reduced by a hundredth (see Table). Accurate measurements of Δ would indicate whether or not the gas/liquid interface

is freely moving and so help in the understanding of mass transfer results.

The mechanism of skirt stability appears to be similar to that for inverse bubbles which may be observed in Surface Active Liquids (43).

Volume Measurements - End Effects

The effect of initial lags in dV/dt on k_L has been previously considered on page 107. Attempts were made to reduce the initial lag by decreasing the top space volume and length of tube to the soap film meter, but reductions to 1000 cc. and 30 cm., respectively, did not significantly improve the response (p. 57). Baird and Davidson (20) working on a smaller colume with top space volumes in the order of 200 cm^3. did not report such lags. However, these small top space volumes were not practicable in the 18" I.D. column.

It is thought that the present initial lag in dV/dt resulted from a lag in the movement of the soap film, i.e. it appeared that a small initial pressure in the top space had to be built up during the initial motion of the soap film. Taking a lag of 0.2 cm^3. in volume and an initial top space volume of 2500 cc. shows, by Boyle's Law, that this pressure was of the order of 0.1 cm. of water gauge pressure. It was noticed in addition, that if two soap films were placed in the burette and an inert bubble released, the lag in the measuring system was further increased, whilst inadequate lubrication of the burette had to be avoided due to extra resistance to the motion of the soap film through a dry burette.

7.3. MASS TRANSFER RESULTS

7.3.1. Comparison with Previous Work at Room Temperatures

As seen in Fig. 7.3.1.a., overall mass transfer coefficients for CO_2 absorption and desorption in tap water, and of CO_2 absorption in aqueous P.V.A. solutions show fair agreement with the results of a previous investigation by Davenport (32).

Also, the considerable decays in instantaneous transfer coefficients in tap water and surface active solutions at $d_e > 2.5$ cm reported by Baird & Davidson (20), are confirmed by the present results.

It is evident from Fig. 7.3.1. that small additions of surface active materials can result in considerable reductions in $\bar{k}_L$. Thus, higher levels of surface active impurity may explain the lower values of $\bar{k}_L$ in tap water, ($\sim$0.024 cm/sec^{-1}) compared with those reported by Baird (20) and Davenport (32) for absorption into distilled water ($\sim$0.026 cm/sec^{-1}). These results, in turn, were lower than those reported by Lochiel & Calderbank (31) ($\sim$0.033 cm/sec^{-1}), who used only specially purified distilled water which was changed at frequent intervals. The latter authors (31) made no mention of non-isothermal compression of the top gas space, and this may have influenced their results.

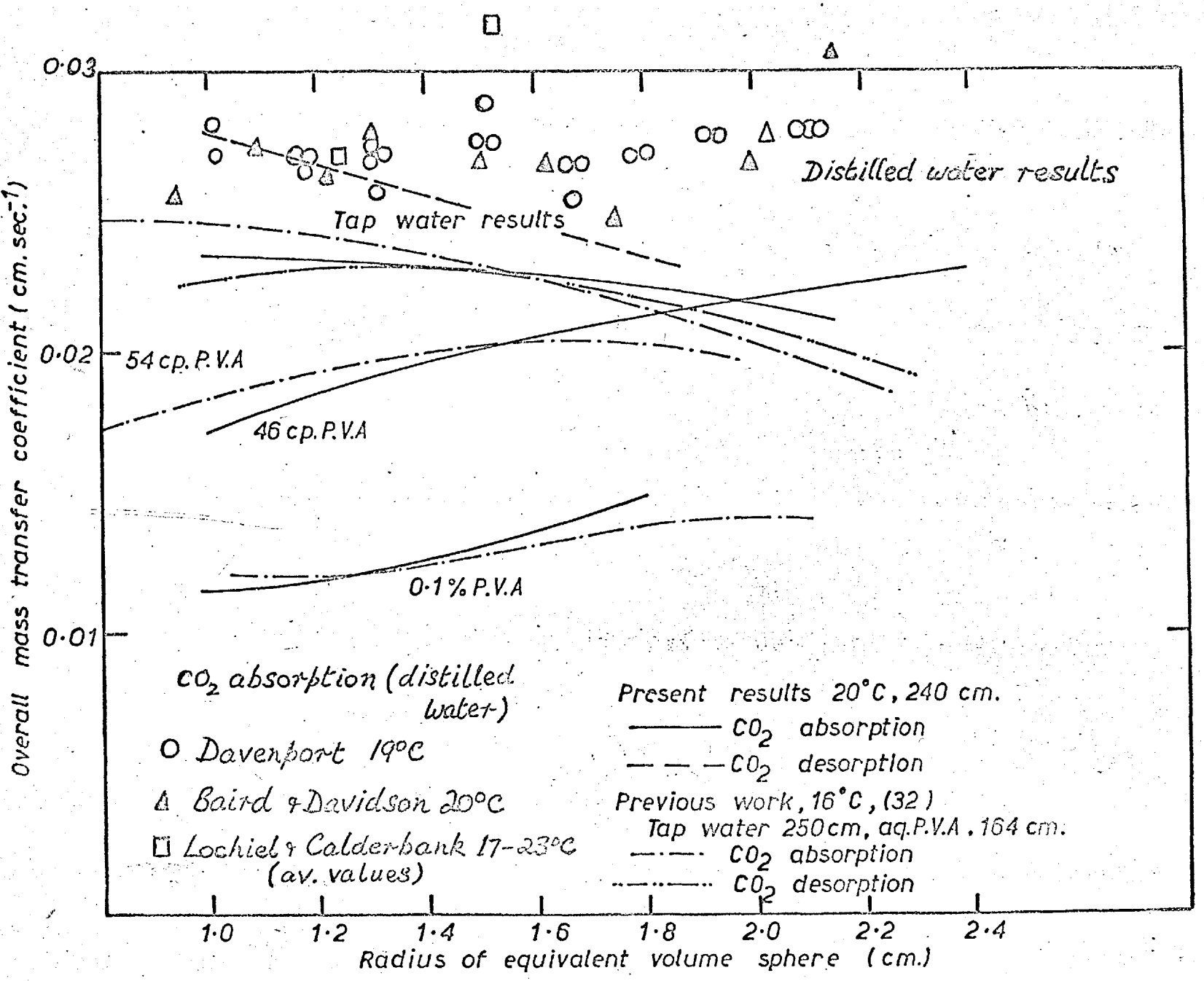

FIG.7.3.1.a COMPARISON OF $\bar{k}_L$ WITH PREVIOUS WORK (32) FOR CO_2 TRANSFER IN TAP WATER AND AQUEOUS POLYVINYL ALCOHOL SOLUTIONS.

The most notable feature of present tap water results is their scatter, and varying levels of impurity could explain the higher values of $\bar{k}_L$ obtained in a second series of experiments (Fig. 4.6.3.b.) compared with the first set. The column could only be cleaned by rinsing because of its size and materials of construction.

7.3.2. CO_2 Absorption and Desorption in Tap Water. Overall Coefficients, $\bar{k}_L$

As seen from Fig. 4.6.3.b., the results for CO_2 desorption compare satisfactorily with absorption results. In the case of absorption from a pure bubble of CO_2, gas phase resistance to transfer must be zero. Thus the reasonably close agreement between desorption and absorption results indicates that any resistance to transfer of CO_2 through N_2 on the gas side of the interface during desorption is very small.

The fact that k_L desorption$>k_L$ absorption may be partly attributed to the transport of CO_2 saturated water from the lower sections of the column whilst contained within the 'enclosed' wake of the bubble. Assuming a CO_2 distribution within the column according to Henry's Law, this transfer of liquid will result in a concentration difference $(C_B - C_I)$ at the rear surface of the

bubble, which is greater than that estimated. Another possibility is that the continued expansion of the interface during CO_2 desorption into rising bubbles could minimise the effects of possible accumulations of Surface Active material at the bubble interface, referred to subsequently.

Although the column was initially saturated with CO_2 by passing streams of small CO_2 bubbles up the column, the mixing effect of convection currents may have caused additional errors in the use of equation 4.6.-3.

Davenport's results (32) for desorption are lower than present results and also showed considerable scatter ($\pm$ 0.004 cm/sec^{-1}). This probably resulted from the cup filling technique employed, which involved bubbling N_2 through CO_2 saturated water into the dumping cup. Thus some mass transfer of CO_2 must have occurred prior to bubble release, resulting in a CO_2 concentration difference, $(C_B - C_I)$, less than that assumed in his calculations. The present method involving filling under mercury eliminated this error, but unfortunately, it could only be used for bubbles of less than 15 cc (in water), due to break-up at higher volumes when released from the hemispherical cup.

Instantaneous Transfer Coefficients, k_L

As seen from Figs. 4.6.3.c. and d, bubbles of 10 cc and less ($d_e \leq 2.7$ cm), showed little or no decay with time of rise for both desorption and absorption. In the case of absorption, initial rates then began to increase with size, decaying after 3 or 4 seconds to approximately constant values of 0.019 cm/sec^{-1}. For example, bubbles of d_e = 4.0 cm (33 cc) had initial transfer coefficients nearly twice the final values after 6 seconds of rise. This decay may be compared with results by Baird & Davidson (20), who reported a decrease in k_L from 0.051 to 0.026 cm/sec^{-1} for similarly sized bubbles over the same time period in tap water. In the case of desorption, k_L showed little decrease with time. The discrepancies between the shapes of curves for k_L at different bubble volumes probably resulted from uneven CO_2 distribution within the column.

Similar errors in previous investigations probably account for Leanard & Houghton (30) finding an increase in $\bar{k}_L$ with distance from release and Davenport (32) finding a decrease in $\bar{k}_L$. (for desorption).

7.3.3. CO_2 Absorption in Aqueous P.V.A. Solutions

Overall Transfer Coefficients

Fig. 4.6.3.e. shows that overall transfer coefficients

were markedly reduced below those in tap water with very small additions of P.V.A. (0.1%). This drop coincided with the elimination of rippling over the front surface of the bubble. (The larger scale rippling on the rear surface was not so markedly damped).

Thereafter, $\bar{k}_L$ began to rise as the P.V.A. concentration increased. Since the surface tension, density, and CO_2 diffusivity and solubility, remained nearly constant with P.V.A. concentration, this effect was probably due to the marked increase in viscosity. The increase in $\bar{k}_L$ was initially rapid (i.e. 1.4-46 cp) and continued rising up to 276 cp. In this solution, at $d_e \sim 4.0$ cm, $\bar{k}_L$ rose rapidly up to 0.028 cm/sec, and this increase coincided with the formation of skirts.

At the highest viscosity studied, 736 cp, $\bar{k}_L$ was practically equivalent to k_L, since little or no decay with time or rise was observed. Values of k_L were low at small bubble volumes and this coincided with low rising velocities. Thereafter k_L increased with bubble volume reaching 0.020 cm/sec at bubble volumes of 30 cc. Little or no scatter between individual results was found, but in view of the extra area available for transfer, coefficients were anamalously low.

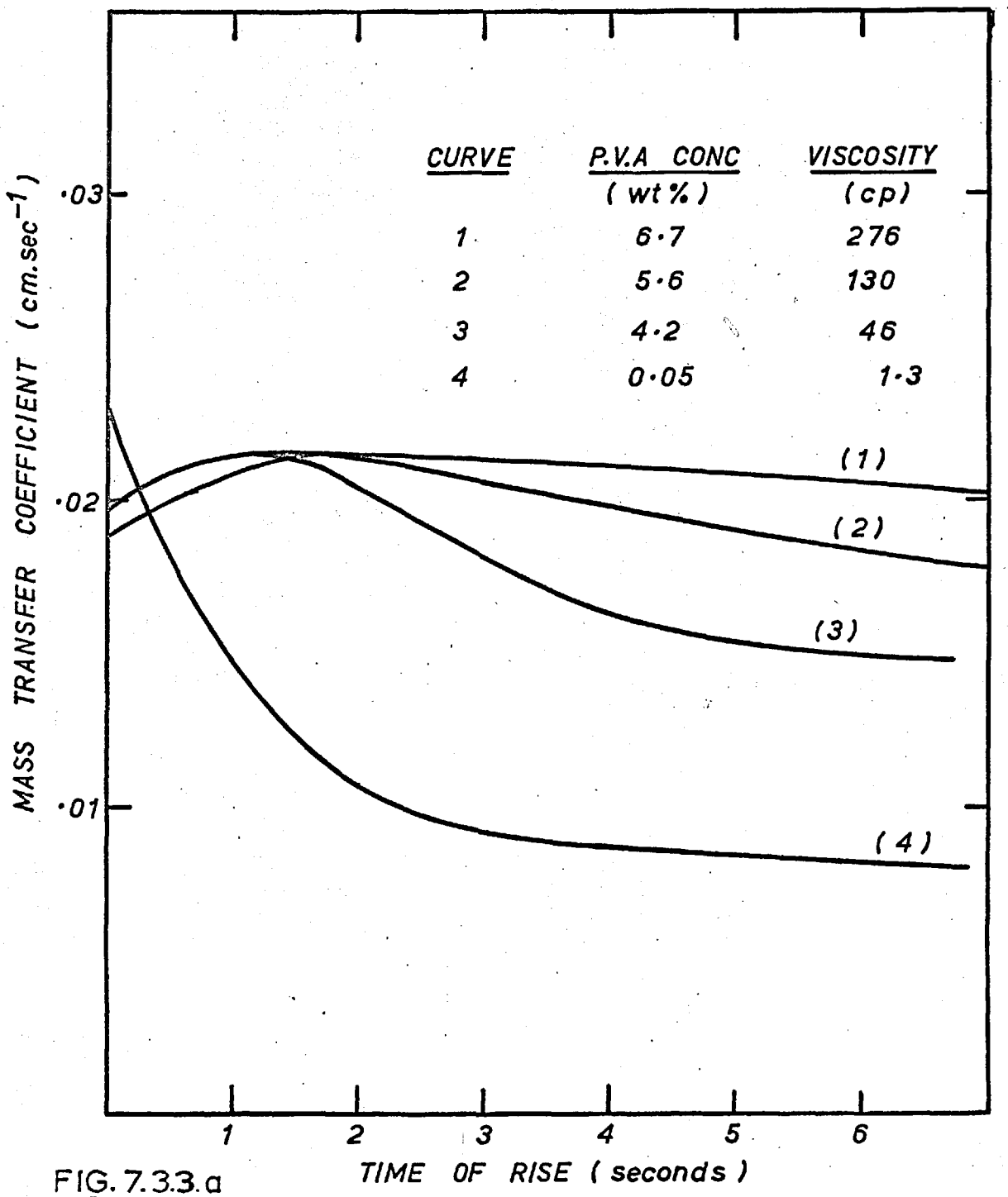

FIG. 7.3.3.a

EFFECT OF P.V.A CONCENTRATION UPON THE DECAY OF MASS TRANSFER COEFFICIENT WITH TIME FOR ABSORPTION OF CO_2 FROM 10 cc BUBBLES

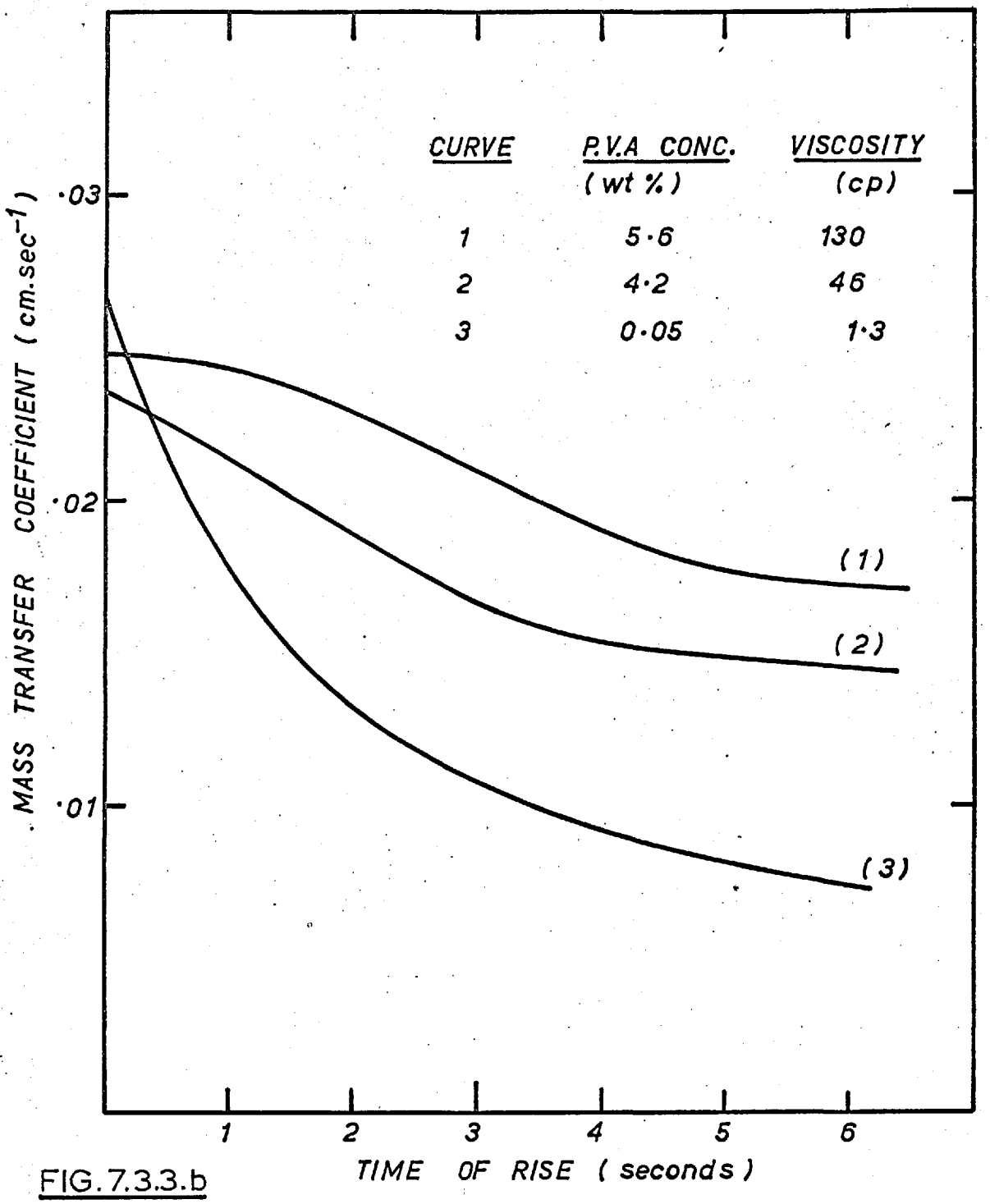

FIG. 7.3.3.b

EFFECT OF P.V.A CONCENTRATION UPON THE DECAY OF MASS TRANSFER COEFFICIENT WITH TIME FOR ABSORPTION OF CO_2 FROM 20 cc BUBBLES

Instantaneous Transfer Coefficients, k_L

In general, for a given P.V.A. concentration, initial transfer rates increased with bubble size ($d_e > 2.0$ cm), but decayed after 3 to 4 seconds rise to approximately constant values of k_L independent of time. Furthermore, it was found that this final value increased with increasing viscosity, and that the rate of decay in k_L to this final value decreased. Figs. 7.3.3. a and b compares instantaneous curves of k_L for 10 and 20 cc bubbles respectively, rising in various P.V.A. solutions, to illustrate this effect.

7.3.4. Effect of Liquid Surface Activity and Viscosity on Mass Transfer Coefficients

The damping of capillary waves ($\lambda < \frac{1}{2}$ cm in H_2O) by surface active agents has received considerable attention. Davies & Vose (50) studied the damping effect of soluble and insoluble S.A. materials on capillary waves in water. They found that the effect of extremely slight traces of contamination (much less than that required to form a monolayer of S.A. material at the gas/water interface) was very marked and lead to anomalously high damping.

They also showed that an optimum amount of S.A. material produced a maximum damping for waves of a given frequency. Van den Tempel (51) solved the relevant

hydrodynamic equations and showed that for the systems studied by Davies & Vose, maximum damping occurred at concentrations approximately half that required to form a monolayer on water. It is well known that the formation of ripples on liquid surfaces can considerably enhance rates of gas absorption, whilst rates of adsorption of S.A. impurities from very low concentrations within the bulk may be increased by up to seven times (52).

In addition, the formation of a film of S.A. impurities at moving gas/liquid interfaces is known to reduce rates of gas absorption by retarding liquid surface velocities. This effect is well known for wetted wall columns (53) and for CO_2 penetration into falling vertical jets of water (54). In the latter case, the addition of surface active agents (teepol) lead to the formation of an immobile monolayer around the lower part of the jet. This monolayer retained powder sprinkled on the surface and extended to such a distance up the jet that the spreading tendency was balanced by the shear stress between the monolayer and the moving liquid jet.

The above observations make it apparent that the lowering of $\bar{k}_L$ with small P.V.A. additions resulted partly from the suppression of rippling. However, mass transfer rates over the front surface should then coincide with values of k_L predicted by equation 2.2.-10.

In addition, since this equation only accounts for transfer from the front of the bubble, experimental values of k_L would be expected to be higher due to transfer from the rear surface.

Fig. 7.3.4.a. presents a plot of instantaneous transfer coefficients five seconds after release vs bubble volume for various P.V.A. solutions, and these are compared with those predicted. (D_{CO_2} was taken as 1.4×10^{-5} cm^2/sec). Values of k_L after 5 seconds rise were chosen as k_L then became approximately independent of time in all solutions. As seen from the results, transfer coefficients in 0.1% P.V.A. solution were significantly lower than those predicted. One explanation for these low values would be that a film of strongly adsorbed surface active material covered the rear and part of the front of the bubble, so reducing interfacial liquid velocities and resulting in low rates of absorption. The mechanism would then be similar to that described for wetted wall columns and water jets (53, 54).

The possibility of a true, non hydrodynamic interfacial resistance is unlikely, since Davenport (32) could detect no such resistance during diffusivity measurements of CO_2 in aqueous P.V.A. solutions, using the technique developed by Davidson & Cullen (45).

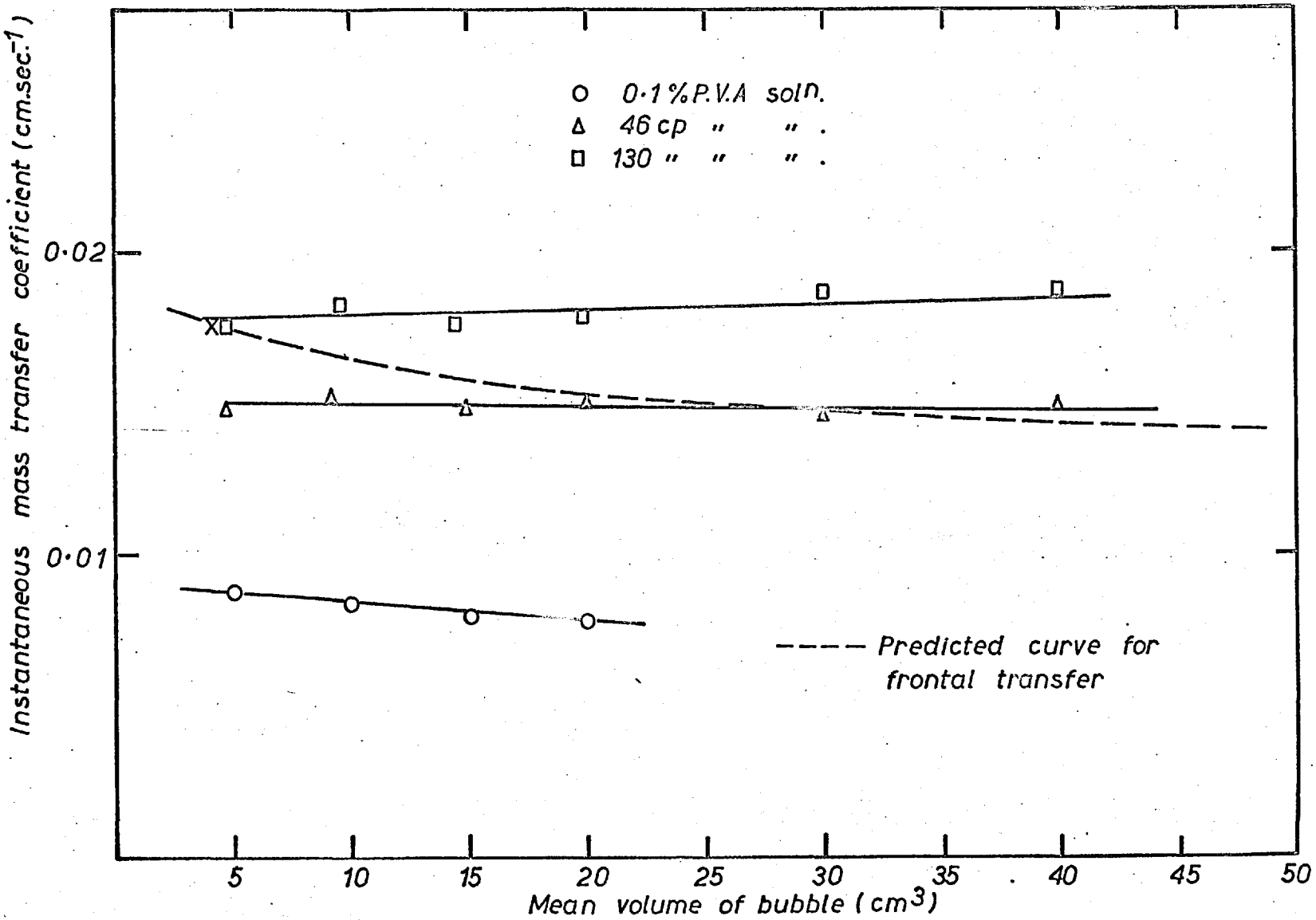

FIG. 7.3.4.a INSTANTANEOUS MASS TRANSFER COEFFICIENT 5 SECONDS AFTER BUBBLE RELEASE vs. VOLUME COMPARED WITH PREDICTED CURVE.

The close agreement of values of k_L for 46 cp and 130 cp solutions with those predicted for frontal transfer (Fig. 7.3.4.a.), would indicate that the rear surface of the bubble remained nearly stagnant, but that the front surface was freely moving. Presumably, the formation of a skin of surface impurity around the front would be prevented by the increased shear forces that would have resulted in these more viscous solutions.

Clarke (29) found a similar viscosity effect on small CO_2 bubbles dissolving in H_2O - glycerol solutions. Transfer coefficients in water and low viscosity liquids decayed with time, but became independent of time for liquids greater than 20 cp. He proposed that surface active agents were adsorbed during rise in low viscosity liquids, but that increased viscosity eventually prevented such adsorption.

7.3.5. Effect of Time on k_L

Baird & Davidson (20) considered that the unsteady value of k_L could probably be attributed to the fact that large rising bubbles carry behind them a turbulent wake (water). The rate of absorption by the wake was thought to decrease with time as the surface region under the bubble became saturated with CO_2. A somewhat oversimplified mathematical treatment based on

unsteady state diffusion gives the mass transfer coefficient of the rear surface as a function of time of penetration, t.

$$k_L \text{ (wake)} = \left[\frac{D_e}{\pi t}\right]^{\frac{1}{2}}$$

where D_e is an eddy diffusivity for the wake below the bubble. If one inserts values of D_e some hundred times that for molecular diffusivity i.e. 140 x 10^{-5} cm^2/sec, and combines resulting basal transfer coefficients with those predicted for the front surface, curves of k_L vs time may be constructed which are very similar to those found experimentally.

If this explanation is correct, one would expect turbulence to be damped in more viscous solutions, leading to lower values of D_e, and smaller experimental differences between initial and final values of k_L.

present dye experiments show that the main bulk of the wake was very turbulent in water, and lead to high values of K_w, the wake appeared to be well mixed. Thus any such stagnant film must be confined to a region in very close proximity to the surface. An alternative explanation of decay in k_L with time would be the diffusion of small concentrations of strongly adsorbed S.A. materials to the bubble interface during rise. Liquids of high viscosity would then presumably retard rates of adsorption and limit the area of surface finally covered.

Wall Effects

Within the limits of accuracy of k_L, mass transfer rates in water appear to be independent of column diameter. However, at $V > 20$, mass transfer coefficients for CO_2 absorption in P.V.A. in the 6" I.D. column decreased, whilst $\bar{k}_L$ continued increasing in the 18" I.D. column, providing some evidence that wall effects may lead to a reduction in k_L.

7.3.6. High Temperature Work

Mass Transfer from the bubble

Mass transfer between oxygen bubbles and molten silver can only be compared with mass transfer between CO_2 bubbles and water, provided that the hydrodynamics, bubble shape and controlling mechanisms are similar. Similarly, the theoretical equation developed by Baird and Davidson (Eqtn.22.-10, P20) may only be used for spherical cap bubbles in which the mass transfer is controlled by transport in the liquid phase. Their theory also assumes potential flow of liquid around the bubble cap i.e. viscosity is assumed to be unimportant.

Shapes - Although direct measurements of bubble shapes in silver were not made due to experimental difficulties, there is indirect evidence to show that bubbles adopt the spherical-cap shape in silver.

a) Over the same range of sizes covered in the silver work, (4 - 27cc), bubbles in low viscosity aqueous liquids ($\leq$130 cp) are spherically capped, their shapes and rising velocities being independent

of the liquids' surface tensions and densities. (p.150).

b) The velocity-equivalent radius relationship (p.155) for bubbles rising in silver is identical to that for spherical-cap bubbles rising through water in an equally sized column. (4" ID). (p.155). Since the rising velocities are independent of liquid properties over the range of the two liquids, it follows from a) that shapes are also likely to be independent of liquid properties, i.e. that bubbles in silver are spherically capped and that U may be related to the cap radius, $\bar{r}$, by equation 2.1.-5.

c) Work by Davenport (32) on nitrogen bubbles rising in mercury shows that for volumes $>$ 4 cc, bubbles are of the spherical cap shape, with dimensions similar to those of bubbles of equal volume in water. In addition, the velocity-equivalent radius relationship for S.C. bubbles rising in mercury was found to be identical to that for S.C. bubbles in water.

Since rising velocities have been used to justify bubble shapes in b), it is necessary to consider other possible bubble shapes that could have similar rising velocities. Haberman and Morton's results for low viscosity liquids (2), show that an ellipsoidal bubble is the only likely alternative. Rising velocities of ellipsoidal and spherical cap bubbles are similar at sizes at which shapes change from ellipsoidal to spherical cap. They found that the transition was completed at Re $>$ 5000, and at Weber Numbers, W, of approximately 20. Since typical values for bubbles in silver are

Re~14,000, W~18 (r_e = 1 cm), it is seen that, on this basis, the transition to the spherical cap shape is probably complete.

Mechanisms of Mass Transfer at the Gas/Liquid Interface

Although both the aqueous and silver systems were chosen so that transport control in the liquid phase should determine rates of gas solution, it is appreciated that the mechanisms of mass transfer at the interface are different in the two cases.

In the case of CO_2 absorption in water, molecules of CO_2 are adsorbed at the interface and then desorb from the interface into the bulk of the liquid without chemical dissociation. Evidence suggests (45) that the rate of gas solution is liquid phase transport controlled, so that equilibrium between gaseous CO_2 and dissolved CO_2 in a region very close to the interface (e.g. 50 A°)(66) may be assumed and Henry's Law may be applied. Furthermore, any reaction of dissolved CO_2 with water to form carbonic acid is negligible (65).

In the case of oxygen solution in molten silver, oxygen molecules dissociate and dissolve in silver in atomic form. Although little is known about the mechanisms of gas solution in molten metals, oxygen dissociation may be similar to that occurring during hydrogen adsorption on solid metals (64). In the latter case, there is evidence that the process of adsorption is accompanied by dissociation of the molecules on the surface, each hydrogen atom formed occupying a surface site. Thus, by analogy, it is possible that the dissociation mechanism for an oxygen molecule may be represented as

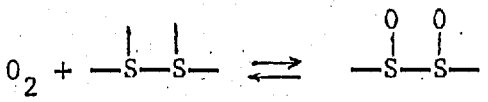

in which the process of adsorption is considered to be a reaction between the gas molecule and two surface sites, S, resulting in a chemisorbed layer of oxygen atoms at the silver interface. Oxygen atoms from the adsorbed layer then desorb from the interface into the silver and are transported by diffusion and convection through the bulk of the silver.

These steps are similar to steps 4, 3, 2 and 1 for the CO reaction in steelmaking, (Chapter 1, Section 1.1) except that in this latter case, two diffusing species are involved, C and O, resulting in the formation of a compound gas, CO, at the interface.

It has been found that rates of hydrogen absorption and effusion in alpha iron are controlled by the diffusion of hydrogen atoms through the iron, down to temperatures of 420°C. (63). This indicates that rates of adsorption, reaction and desorption at the interface are rapid compared to diffusion rates in the metal, so that equilibrium between gaseous and dissolved hydrogen, adjacent to the interface, can be assumed and Sieverts Law applied. Assuming that oxygen solution in silver follows a similar mechanism, and in the present case proceeds at a far higher temperature (1020°C) more rapid interfacial reaction rates may be expected on the basis of the Arrhenius law. In addition, Mizikar, Grace and Parlee (45) have studied the solution of oxygen in molten silver and have

determined diffusion coefficients of oxygen in silver, They found that oxygen solution was transport controlled in the liquid phase.

Thus, on the basis of previous work, the assumption of chemical equilibrium between gaseous oxygen and dissolved oxygen atoms close to the interface is justified, and Sieverts Law may be applied.

Experimental Results

Fig. 6.4.e. shows a plot of instantaneous mass transfer coefficients, k_L, vs time of rise, for a number of typical absorption runs. As seen, results were in good agreement, and apart from initial discrpancies which may have resulted from some bubbles breaking up, rates of decay were not generally marked, and were independent of bubble volume. Fig. 6.4.f. presents values of time averaged mass transfer coefficients, $\bar{k}_L$, taken over the first half of the column and plotted vs $\bar{r}_e$, the equivalent radius of the average bubble volume. Since differences between $\bar{r}_e$ and radii based upon integrated mean bubble volumes did not exceed 2%, the variations were small compared with maximum variations in $\bar{k}_L$ of $\pm$20%.

Values of $\bar{k}_L$ were approximately independent of $\bar{r}_e$, the mean value of $\bar{k}_L$ over the range studied being 0.036 cm/sec, with variations not exceeding $\pm$0.007 cm/sec. This value may be compared with that predicted theoretically by equation 2.2.-10 for frontal transfer alone. Taking a typical bubble diameter of 2.6 cm and a diffusion coefficient of oxygen in silver, $D_{[O]}$, at 1020°C, of 9.0×10^{-5}

$\pm 2.0 \times 10^{-5}$ cm^2/sec (61), gives $k_L = 0.04 \pm 0.005$ cm/sec. Thus, within experimental errors, the two values are in agreement.

Since values of $\bar{k}_L$, the mass transfer coefficient for the whole bubble, were close to those predicted for frontal transfer only, this indicates that transfer of oxygen through the rear surface of the bubble was small. It is also possible that the bubble surfaces were not rippling; it was observed, for example. that small additions of P.V.A. to tap water suppressed ripples and reduced rates of mass transfer. Although the effect of surface active agents is specific to the systems studied, and direct comparisons cannot be made, it is possible that oxygen may be surface active in silver, and may also inhibit rippling. It is known for example (58) that sulphur and oxygen in molten iron are highly surface active, and may reduce surface tensions from 1600 to 800 dynes/cm. Similarly, sulphur in molten copper reduces surface tensions from 1100 to 500 dynes/cm.

Comparison of High and Low Temperature Systems

Since average bubble volumes for oxygen solution in silver did not exceed 15cc, mass transfer coefficients for similarly sized bubbles in water may be used to predict values for oxygen absorption in silver. At bubble volumes less than 15cc, rates of decay in k_L were not marked in either the high or low temperature systems. The Baird and Davidson (20) and Lochiel and Colderbank (21) expressions

for mass transfer through the front surfaces of spherical cap bubbles show that rates of mass transfer of solute are proportional to the square root of the solute's diffusion coefficient in the liquid. Assuming that a similar relationship holds for transfer through the rear surface, and that hydrodynamic conditions are similar,

$$k_{L,Ag} = k_{L,H_2O} \left[\frac{D_{[O]}}{D_{CO_2}} \right]^{1/2}$$

Taking a typical value of 0.023 $\pm$0.002 cm/sec for k_L for CO_2 absorption in tap water (p.96), D_{CO_2/H_2O} = (1.6 $\pm$0.15)x10^{-5} cm^2/sec, 20°C, $D_{[O]/Ag}$ = (9.0 $\pm$2.0) x10^{-5} cm^2/sec, 1020°C, shows $k_{L,Ag}$ = 0.054 $\pm$0.008 cm/sec. This is somewhat higher than the measured value of 0.036 $\pm$0.007 cm/sec, but in view of the agreement between the measured value of k_L and that predicted for frontal transfer only by Equation 2.2.-10, the discrepancy could be due to differences in the transfer in the wakes between the two liquids, silver and water.

CONCLUSIONS

CO_2-Aqueous Systems

The rising velocities of spherically capped bubbles in low viscosity liquids ($\prec$ 130 cp) are proportional to $V^{1/6}$. In the 6" I.D. column, bubble velocities are reduced due to wall effects and, at higher volumes, i.e. 20 - 40 cc, the proximity of the walls cause a slight distortion of the bubbles. The walls have no appreciable effect on the overall mass transfer coefficient.

Instantaneous mass transfer coefficients decrease markedly with time, especially at large bubble volumes. This is probably caused by accumulation of surface active agents at the surface and/or unsteady rates of transfer from the rear surface of the bubble. The addition of surface active agents to water may result in a decrease of up to 50% in transfer rates. Increasing viscosity with solutions containing higher proportions of P.V.A. causes a rise in the mass transfer coefficient.

Trailing envelopes of gas (skirts) form behind spherical cap bubbles in highly viscous solutions of glycerol and P.V.A. These skirts become more stable at the higher viscosities and are not a result of wall effect. A theory has been developed which accounts for their stability, and the skirt thickness has been related to the gas viscosity and interfacial liquid velocities. The presence of skirts have no appreciable effect on mass transfer.

The wakes carried behind spherical cap bubbles are turbulent in low viscosity liquids and the rates of mixing with the bulk fluid are appreciable.

Oxygen-Silver Systems

The relationship between velocity and bubble volume for bubbles in silver is similar to that for bubbles in water. Mass transfer coefficients of oxygen bubbles in silver were found to be 0.036 cm/sec. The results show reasonable agreement with theoretical predictions for frontal transfer. Though transport in the liquid phase in likely to be the major controlling step some measure of chemical control at the interface cannot be ruled out.

LIST OF SYMBOLS

CAPITALS

A	surface area.
A_e	surface area of sphere of the same volume as the bubble.
C	concentration of solute or constant in U vs r_e relationship.
Cd	coefficient of drag.
D	solute diffusion coefficient.
E	eccentricity.
H	height of liquid above cup.
K	constant in velocity bubble volume relationship.
M	Morton number.
P	total pressure in bubble.
R	ideal gas constant.
Re	Reynolds number.
S	shape factor of sphere.
U	rising velocity of bubble.
V	bubble volume.
W	Weber number.
X	mole fraction of gas.

LETTERS

a	basal radius of bubble
b	height of bubble.
c	cold i.e. room temperature.

d diameter.

e equivalent value of pressure in E.M.F.

g acceleration due to gravity.

h height of bubble above inverted cup.

k mass transfer coefficient.

k_L instantaneous mass transfer coefficient of solute in liquid phase.

$\bar{k}_L$ overall mass transfer coefficient of solute in liquid phase.

p pressure of gas in top space above liquid.

Δp gauge pressure of gas in top space above liquid.

q Sieverts constant.

r radius of spherical cap of bubble.

r_e radius of an equivalent volume sphere.

t time from bubble release.

v top space volume.

SUBSCRIPTS

B bulk.

I gas/liquid interface.

G gas.

L liquid.

c condensation occurring.

e equivalent volume sphere.

i initial, prior to gas introduction into column.

o at instant of bubble release from tipping cup.

1 final.

t at time t secs. after bubble release.

ad adiabatic, *i.e. non-isothermal compression of top gas space.*

is isothermal.

GREEK SYMBOLS

β Bunsen solubility coefficient of CO_2 in liquid.

ρ density.

θ Absolute temperature.

μ viscosity.

σ surface tension.

π 3.142.

τ shear stress.

ξ constant.

APPENDIX 4.2.

Inert Bubble Results using Constant Volume Technique.

Specimen RUNS 1 and 2. (1 Unit = 0.4. "H_2O)

TIME FROM RELEASE (sec)	TOP GAUGE PRESSURE IN CHART UNITS RUN 1	RUN 2
0.0	5.14	5.15
0.4	5.16	'BLIP' t = 0.15
0.8	5.20	5.19
1.2	5.27	5.27
1.6	5.34	5.36
2.0	5.43	5.44
2.4	5.51	5.51
2.8	5.59	5.61
3.2	5.68	5.68
3.6	5.76	5.78
4.0	5.84	5.86
4.4	5.94	5.95 'BLIP' t = 5.00
4.8	6.02	6.03
5.2	6.12	6.11
5.6	6.23	6.23
6.0	6.33	6.33
6.4	6.43	6.44
6.8	6.52	6.52
7.0	6.54	6.55

APPENDIX 4.2.

Calculations based upon RUNS 1 and 2 assuming isothermal expansion of nitrogen bubbles

Given, $H = 271$ cm, $h_x = 6$ cm, $h_y = 202.3$ cm, $P_{At} = p_i = 14.71$"Hg

$p_{H_2O} = 1$ gm/cc, $g = 981$ cm/sec^2, $v_i = 3{,}400$ cc

1" H_2O = 5 mV

Hence, $p_i = 2020.28$ mV, and $p_o = 2020.28 + 2\,(5.14)$ mV

$$1 - \frac{p_i}{p_o} = 0.0050627$$

Hence, by 4.6.-6.

$$1 - \frac{2020.28}{p_y} = 0.0050627 \quad \frac{2030.56 + 533.46}{2030.56 + 135.20}$$

which gives $p_y = 2032.462 = 2020.28 + 2\,(6.091)$

Also, by 4.2.-5.

$$p_1 = 2030.56 + 533.5 \times 0.0050627$$
$$= 2020.28 + 2(6.491)$$

The Average Velocity between x and y = $\frac{202.3-6}{4.85}$ cm/sec

Hence, $t_1 = \frac{271}{40.47} = 6.70$ seconds

APPENDIX 4.3.

Calculations based on RUN W.23. V_o = 10.0 cm^3, θ = 20°C, H = 273 cm.

Time Increment	Time sec	Burette Reading cm^3	Bubble Volume cm^3	$\frac{\Delta V}{\Delta t}$ cm^3/sec	$\frac{dV}{dt}$ smoothed	V, Computor smoothed cm^3	dV/dt smoothed cm^3/sec	k_L Fictitious
0.	0.00	6.218	10.000	0.158		10.003	0.107	+0.008
1.	0.24	6.180	10.038	0.168	0.160	10.034	0.148	+0.006
2.	0.48	6.140	10.078	0.168	0.190	10.074	0.183	+0.005
3.	0.72	6.100	10.118	0.232	0.220	10.121	0.213	+0.0035
4.	0.96	6.045	10.173	0.274	0.238	10.176	0.239	+0.0025
5.	1.20	5.980	10.238	0.253	0.270	10.236	0.261	+0.0016
6.	1.45	5.920	10.298	0.295	0.298	10.301	0.280	+0.0010
7.	1.68	5.850	10.368	0.316	0.308	10.370	0.295	+0.005
8.	1.92	5.775	10.443	0.316	0.310	10.442	0.309	+0.000
9.	2.16	5.700	10.518	0.337	0.317	10.518	0.320	-0.0002
10.	2.40	5.620	10.598	0.358	0.328	10.596	0.330	-0.0004
11.	2.64	5.535	10.683	0.316	0.337	10.676	0.338	-0.0005
12.	2.88	5.460	10.758	0.337	0.342	10.758	0.345	-0.0006
13.	3.12	5.380	10.838	0.337	0.350	10.841	0.351	-0.0006
14.	3.36	5.300	10.918	0.421	0.357	10.926	0.357	-0.0006
15.	3.60	5.200	11.018	0.337	0.362	11.013	0.363	-0.0006
16.	3.84	5.120	11.098	0.400	0.369	11.101	0.369	-0.0006
17.	4.08	5.025	11.193	0.358	0.377	11.190	0.375	-0.0006
18.	4.33	4.940	11.278	0.421	0.383	11.281	0.381	-0.0006
19.	4.56	4.840	11.378	0.400	0.394	11.373	0.387	-0.0005
20.	4.80	4.760	11.458	0.400	0.399	11.466	0.394	-0.0005
21.	5.04	4.650	11.568	0.380	0.403	11.562	0.401	-0.0005
22.	5.28	4.560	11.658	0.421	0.411	11.659	0.408	-0.0005
23.	5.52	4.460	11.758	0.421	0.421	11.758	0.416	-0.0005
24.	5.76	4.360	11.858	0.421	0.426	11.858	0.423	-0.0006
25.	6.00	4.260	11.958	0.464	0.437	11.961	0.431	-0.0006
26.	6.24	4.150	12.068	0.464	0.441	12.065	0.439	-0.0005
27.	6.48	4.048	12.178	0.423	0.450	12.171	0.446	-0.0005
28.	6.72	3.938	12.280	0.480	0.457	12.280	0.454	-0.0005
29.	6.96	3.824	12.394	0.417	0.464			
30.	7.20	3.698	12.520	0.254	0.370			
31.	7.45	3.633	12.585	0.167	0.230			
32.	7.69	3.613	12.600		0.015			

Appendix 4.3 (cont).

The results of some inert experiments using the volume displacement technique are tabulated below. The W series of experiments were carried out using a top space volume of 2500 cc, the T series with a volume of 1000 cc and 30 cm length of connecting tube to the soap film meter.

The sequence of numbers for each set of results are; 1) Run identification no., 2) Initial Bubble volume (cc), 3) Time interval between successive readings (sec), 4) Soap-film meter readings (cc),

W9	15.0	0.48	11.50	11.35	11.15	10.99	10.68	10.39	10.15	9.90	9.62
	9.39	9.11	8.76	8.48	8.14	7.76	7.40				
W10	20.0	0.46	10.70	10.50	10.22	9.93	9.60	9.28	8.92	8.57	8.19
	7.79	7.39	6.97	6.50	6.04	5.58	5.28				
W21	10.00	0.48	5.835	5.798	5.718	5.597	5.475	5.335	5.195	5.040	4.900
	4.740	4.580	4.395	4.207	4.015	3.807	3.600	3.430	3.310		
W24	10.05	0.476	6.42	6.38	6.288	6.130	5.955	5.790	5.637	5.470	5.298
	5.120	4.930	4.740	4.540	4.317	4.108	3.880	3.690	3.670		
W25	10.0	0.48	6.260	6.160	6.020	5.850	5.685	5.524	5.365	5.205	5.040
	4.879	4.690	4.560	4.300	4.100	3.900	3.700	3.550	3.480		
W22	10.0	0.48	6.200	6.118	6.000	5.858	5.710	5.520	5.346	5.175	5.010
	4.838	4.670									
T30	15.0	0.54	11.45	11.30	11.05	10.80	10.50	10.20	9.90	9.60	9.30
	8.95	8.60	8.20	7.80	7.40	7.29					
T31	15.0	0.54	10.00	9.80	9.51	9.30	9.00	8.78	8.45	8.13	7.80
	7.40	7.00	6.65	6.23	5.90	5.88					
T18	20.0	0.54	6.00	5.70	5.40	5.00	4.60	4.22	3.85	3.42	3.00
	2.52	2.05	1.52	1.00	0.72	0.62					
T26	10.0	0.54	10.70	10.60	10.50	10.30	10.17	9.97	9.80	9.60	9.42
	9.20	9.00	8.75	8.50	8.23	8.13	8.10	8.08			
T27	10.0	0.56	7.90	7.80	7.65	7.50	7.30	7.13	6.97	6.80	6.62
	6.45	6.25	6.00	5.77	5.57	5.42	5.39	5.37			
T28	10.0	0.56	9.67	9.57	9.43	9.25	9.10	8.90	8.72	8.52	8.32
	8.10	7.87	7.63	7.37	7.10	7.00	6.97	6.96			
T19	20.0	0.54	6.20	5.90	5.62	5.24	4.85	4.42	4.01	3.59	3.14
	2.65	2.16	1.62	1.07	0.70	0.65					

APPENDIX 4.5

Dimensional Details of Nitrogen Bubbles Rising in Various Liquids

Volume (cm^3)	Equivalent Radius (cm)	Height (cm)	Basal Radius (cm)	Predicted Volume (cm^3)
4.2 percent Aqueous P.V.A. Solution. Viscosity 46 cp.				
6.05	1.13	0.925	2.10	6.90
6.05	1.13	0.925	2.02	6.41
24.18	1.80	1.30	3.20	21.4
24.30	1.80	1.45	3.15	23.4
12.20	1.43	1.15	2.45	11.6
12.18	1.43	1.15	2.55	12.5
36.4	2.06	1.55	3.50	31.6
36.4	2.06	1.60	3.40	31.2
48.5	2.27	1.90	3.80	46.5
48.5	2.27	1.80	3.87	45.5
72.6	2.59	2.00	4.30	65.1
72.6	2.59	2.10	4.5	71.8
5.6 Percent Aqueous P.V.A. Solution. Viscosity 130 cp.				
11.85	1.415	1.25	2.25	11.0
24.2	1.80	1.45	3.0	23.9
36.37	2.07	1.60	3.5	32.3
61.0	2.44	1.85	4.25	55.6

APPENDIX 4.5 (cont'd)

Volume (cm^3)	Equivalent Radius (cm)	Height (cm)	Basal Radius (cm)	Predicted Volume (cm^3)
73.4	2.60	2.10	4.50	72.0
73.4	2.75	2.10	4.50	77.0
48.8	2.28	2.05	3.88	52.95
24.4	1.81	1.43	3.03	22.2
12.4	1.43	0.95	2.25	9.2
12.2	1.42	1.10	2.20	9.1
48.5	2.26	1.90	3.75	45.5
24.6	1.82	1.50	2.95	22.3
8.4 Percent Aqueous P.V.A. Solution. Viscosity 735 cp.				
18.5	1.64	1.77	2.46	20.2
18.5	1.64	1.56	2.38	16.0
24.4	1.80	1.94	2.74	26.6
24.2	1.80	2.10	2.78	30.2
36.3	2.06	2.10	3.26	41.0
36.5	2.06	1.85	3.12	31.6
36.5	2.06	1.90	3.16	33.4
48.5	2.27	2.17	3.58	49.0
60.5	2.44	2.14	3.71	56.5
60.5	2.44	2.36	3.88	62.5

APPENDIX 4.5 (cont'd)

Volume (cm^3)	Equivalent Radius (cm)	Height (cm)	Basal Radius (cm)	Predicted Volume (cm^3)
72.5	2.59	2.44	4.21	75.8
85.0	2.73	2.44	4.23	77.7
108	2.96	2.65	4.85	108
Tap Water. Viscosity 1 cp.				
9.0	1.30	1.18	2.11	9.0
11.2	1.39	1.30	2.31	12.0
17.1	1.60	1.22	2.86	18.9
29.2	1.91	1.46	3.24	31.9
30.1	1.93	1.60	3.30	32.8
24.5	1.80	1.62	3.17	26.6
15.1	1.54	1.30	2.50	14.3
26.2	1.84	1.66	3.05	25.6
13.8	1.49	1.30	2.46	13.6
18.3	1.65	1.42	2.69	17.6
13.0	1.46	1.26	2.51	13.4

APPENDIX 4.6

General

Various programmes were developed on the Atlas computor (Univ. of London) for the calculation of instantaneous mass transfer coefficients.

The first section of the prepared programmes included the fitting of a polynomial of V (or Δp) in terms of t to experimental data of V at N time intervals, by the method of least squares A fifth degree polynomial in time was finally chosen, since the variance of the fitted curves were little improved when higher polynomials were used.

The second chapter involved solution of the relevant mass transfer equations developed in sections 4.6.1. and section 6.3. at chosen time intervals using an iterative method, and provided for the print-out of point values of V, dV/dt, t and k_L.

Incidentally, values of $\frac{dV}{dt}$ (or $\frac{dp}{dt}$) followed from differentiation of the fitted polynomial.

Tabulation of Results

Experimental details forming the basis of the instantaneous mass transfer coefficient vs time curves presented in section 4.6. are given below in terms of input data for the relevant computor programmes.

The absorption and desorption experiments of CO_2 in tap water and various aqueous P.V.A. solutions were carried out in the 18" I.D. column using the volume displacement technique. In these cases, the sequence of number for each experimental run had the following significance:-

Number in Sequence.	Meaning.	Units
1.	Total Number of burette reading photographically recorded during bubble rise.	-
2.	Bunsen Solubility Coefficient at θ^{o} K	-
3.	Temperature of liquid, θ.	^{o}K.
4.	Shape Factor of Sphere/273^{o}K.	$^{o}K^{-1}$
5.	Initial Pressure $P_o/\rho gK$.	$cm^{\frac{1}{2}}sec.$
6.	Degree of Polynomial used for smoothing of volume data.	-
7.	Bubble Volume of instant of release, V_o.	cm^3
8.	Time at instant of release, t_o i.e. 0 sec.	sec.
9.	Time interval between successive burette reading, Δt.	sec.
10.	Burette reading at instant of bubble release, t_o.	cm^3
11.	Burette reading at $t + \Delta t$.	cm^3
12.	Burette reading at $t + 2\Delta t$.	cm^3
13.	Burette reading at $t + 3\Delta t$.	cm^3
14.	etc.	

The instantaneous bubble volume at time, t, was obtained by subtracting the burette reading at time, t, from that at t_o and adding the resultant volume change, ΔV, to V_o. (In the case of CO_2 absorption in tap water, volume differences were divided by 2 to obtain true volume differences in cm^3).

In the highly viscous P.V.A. solutions requiring adjustment of the velocity equation, (see equation 4.6.-7a.) an additional number in the sequence (eigth number) was inserted which represented the numerical value of $\frac{\rho g A}{P_o}$ where A is the coefficient in the expression

$$U = A + K\bar{V}^{1/6}$$

CO_2 Absorption in Tap Water

18 0.9 292 0.0177 52.41 5 9.60 0 0.4033
14.6 14.8 15.0 15.23 15.45 15.65 15.85 16.0
16.17 16.30 16.42 16.60 16.73 16.80 16.92 17.05
17.20 17.30
17 0.90 292 0.0177 52.41 5 9.91 0 0.4315
18.40 18.45 18.70 18.85 19.08 19.22 19.37 19.44
19.60 19.70 19.80 19.90 20.00 20.10 20.20 20.25
20.37
16 0.9 292 0.0177 52.41 5 14.425 0 0.4325
10.05 10.25 10.48 10.60 10.70 10.80 10.82 10.90
10.98 11.10 11.20 11.22 11.22 11.22 11.22 11.22
18 0.9 292 0.0177 52.41 5 9.90 0.0 0.4033
20.60 20.60 20.73 21.0 21.1 21.2 21.3 21.4 21.5
21.6 21.65 21.75 21.80 21.85 21.85 21.85 22.0
22.05
18 0.9 292 0.0177 52.41 5 9.92 0.0 0.4033
13.80 13.85 13.80 13.90 14.05 14.25 14.45 14.65
14.80 [illegible] 5.03 15.19 15.24 15.33 15.40 15.42
15.50 15.60
17 0.9 292 0.0177 52.41 5 9.547 0.0 0.4315
14.82 15.00 15.20 15.40 15.58 15.66 15.85 16.10
16.22 16.40 16.55 16.55 16.65 16.85 17.00 17.00
16.95*
16 0.9 292 0.0177 52.41 5 14.625 0.0 0.4315
16.15 16.30 16.55 16.75 16.85 16.95 17.08 17.20
17.34 17.42 17.52 17.50 17.80 17.90 18.00 18.00

16 0.9 292 0.0177 52.41 5 14.50 0.0 0.433
13.30 13.40 13.65 13.92 14.10 14.26 14.38 14.50
14.60 14.67 14.73 14.85 14.90 14.99 14.99 15.05

16 0.9 292 0.0177 52.41 5 14.14 0.0 0.434
15.80 15.82 16.1 16.28 16.52 16.70 16.85 17.02
17.11 17.22 17.33 17.37 17.50 17.70 17.70 17.*70

20 0.9 292 0.0177 52.41 5 14.21 0.0 0.348
12.58 12.58 12.58 12.63 12.95 13.10 13.21 13.30
13.36 13.45 13.48 13.55 13.62 13.67 13.72 13.73
13.80 13.80 13.80 13.88

22 0.9 292 0.0177 52.41 5 4.99 0.0 0.390
8.00 8.00 8.00 8.08 8.25 8.40 8.55 8.62 8.78 8.94
9.08 9.22 9.38 9.43 9.59 9.66 9.70 9.88 9.98 9.16
9.22 9.20

23 0.9 292 0.0177 52.41 5 4.875 0.0 0.392
14.00 14.18 14.28 14.40 14.60 14.72 14.90 15.00
15.13 15.25 15.40 15.52 15.62 15.81 15.96 16.10
16.24 16.38 16.47 16.61 16.71 16.82 16.95

CO_2 Absorption in 6.7% P.V.A. Aqueous Solution

12 0.785 294.3 0.01177 42.41 5 19.27 -0.008067 0.0 0.618
16.23 16.36 16.50 16.58 16.64 16.70 16.74 16.76 16.78
16.78 16.74 16.68
12 0.785 294.3 0.01177 42.41 5 19.29 -0.008067 0.0 0.614
18.71 18.83 18.98 19.07 19.11 19.16 19.20 19.22 19.22
19.23 19.22 19.18
9 0.785 294.3 0.01177 42.41 5 39.45 -0.008067 0.0 0.614
15.95 15.95 16.00 16.00 16.00 15.97 15.89 15.79 15.63
13 0.785 294.3 0.01177 42.41 5 39.20 -0.008067 0.0 0.460
18.10 18.08 18.10 18.11 18.11 18.10 18.09 18.04 18.00
17.92 17.85 17.75 17.65
14 0.785 294.3 0.01177 42.41 5 39.20 -0.008067 0.0 0.411
20.70 20.69 20.72 20.72 20.72 20.72 20.70 20.68 20.66
20.60 20.55 20.50 20.40 20.30
9 0.785 294.3 0.01177 42.41 5 39.45 0.0 0.0 0.614
15.95 15.95 16.00 16.00 16.00 15.97 15.89 15.79 15.63
9 0.785 294.3 0.01177 51.86 5 39.45 0.0 0.0 0.614
15.95 15.95 16.00 16.00 16.00 15.97 15.89 15.79 15.63
13 0.785 294.3 0.01177 51.86 5 39.20 0.0 0.0 0.460
18.10 18.08 18.10 18.11 18.11 18.10 18.09 18.04 18.00
17.92 17.85 17.75 17.65
14 0.785 294.3 0.01177 51.86 5 39.20 0.0 0.0 0.411
20.70 20.69 20.72 20.72 20.72 20.72 20.70 20.68 20.66
20.60 20.55 20.50 20.40 20.30

CO_2 Absorption in 8.4% Aqueous P.V.A. (735 cp.)

$5 \leq V \leq 30$ cc.

16 0.853 291.3 0.01177 36.33 5 9.64 -0.01789 0.0 0.615
14.00 14.05 14.08 14.08 14.09 14.10 14.11 14.11 14.11
14.10 14.10 14.10 14.09 14.04 14.00 13.99
16 0.853 291.3 0.01177 36.33 5 9.71 -0.01789 0.0 0.630
14.49 14.50 14.51 14.51 14.56 14.57 14.59 14.59 14.60
14.59 14.58 14.56 14.54 14.51 14.50 14.46

APPENDIX 6.4.

Specimen results providing the basis for graphs 6.4. d, e and f, are given below, in terms of input data for the computor programme developed for the solution of equation 6.3.-7.

$$1\ mV = 1\ "H_2O = 0.5\ CHART\ UNITS$$

Number in Sequence	Meaning	Units
1.	Total Number of pressure readings taken from top pressure-time curve.	-
2.	Top space volume, v_i (730 cc)	cc
3.	$\frac{2}{Sq\theta R} \times \left[\frac{2.54}{76x13.6}\right]^{\frac{1}{2}} = (0.000112)$	$mV^{\frac{1}{2}}$
4.	$\frac{\rho \times \bar{K}}{2.54x1.0}$ (K corrected for Wall-Effects)	$mV/cm^{\frac{1}{2}}$ sec.
5.	$\frac{\rho \times H}{2.54x1.0}$	mV.
6.	Degree of polynomial used to smooth top gauge pressure vs time readings.	
7.	p_i, initial top pressure (1 Atmos = 407 mv)	mV
8.	$v_i^{1/6}$	$cm^{\frac{1}{2}}$
9.	$\frac{C_{[O]B}}{q} \left[\frac{76x13.6}{2.54}\right]^{\frac{1}{2}} = 20.17\sqrt{P_{O_2,B}}$	

Values of t_o and Δt together with successive readings of Δp (in terms of chart units, oxygen desorption allowed for) then follow.

O_2 Absorption in Ag (1020°C)

17 730 0.000112 85.7 202 5 407 3 21.4 0.0 0.1
1.35 1.23 1.15 1.10 1.04 0.99 0.95 0.90 0.87 0.83 0.80
0.78 0.77 0.76 0.77 0.76 0.78
15 730 0.000112 82.2 202 5 407 3 21.4 0.0 0.1
3.46 3.09 2.86 2.67 2.54 2.43 2.34 2.38 2.22 2.20
2.20 2.24 2.25 2.32 2.40
15 730 0.000112 83.6 202 5 407 3 21.4 0.0 0.1
2.61 2.36 2.14 1.98 1.86 1.77 1.70 1.66 1.61 1.57
1.54 1.51 1.51 1.50 1.50
15 730 0.000112 85.7 202 5 407 3 21.4 0.0 0.1
3.00 2.73 2.50 2.35 2.25 2.16 2.07 2.00 1.96 1.95
1.92 1.91 1.91 1.92 1.92
15 730 0.000112 83.9 202 5 407 3 21.4 0.0 0.1
2.60 2.40 2.22 2.05 1.90 1.80 1.74 1.70 1.66
1.63 1.60 1.70 1.70 1.71 1.72
15 730 0.000112 84.0 202 5 407 3 21.4 0.0 0.1
2.47 2.22 2.08 1.99 1.87 1.80 1.72 1.78 1.63 1.58
1.55 1.53 1.51 1.49 1.50
17 730 0.000112 84.0 202 5 407 3 21.4 0.0 0.1
2.50 2.28 2.19 2.07 1.99 1.91 1.86 1.80 1.75 1.71
1.68 1.66 1.64 1.64 1.67 1.70 1.78
17 730 0.000112 86.2 202 5 407 3 21.4 0.0 0.1
0.99 0.92 0.87 0.83 0.77 0.72 0.69 0.66 0.64 0.61 0.59
0.58 0.57 0.56 0.56 0.57 0.59
15 730 0.000112 84.5 202 5 407 3 21.4 0.0 0.1
2.07 2.01 1.94 1.89 1.84 1.80 1.76 1.76 1.75 1.77
1.77 1.79 1.82 1.89 1.96
17 730 0.000112 85.4 202 5 407 3.0 21.4 0.0 0.1
1.68 1.61 1.53 1.45 1.40 1.36 1.31 1.26 1.24 1.22

1.21 1.20 1.19 1.20 1.23 1.30 1.37
17 730 0.000112 84 202 5 407 3.0 21.36 0.0 0.1
2.59 2.48 2.29 2.22 2.13 2.07 2.01 1.97 1.92 1.89
1.86 1.87 1.87 1.91 1.99 2.09 2.24
17 730 0.000112 84 202 5 407 3.0 21.36 0.0 0.1
2.36 2.30 2.24 2.16 2.06 1.99 1.95 1.90 1.85 1.81
1.80 1.79 1.80 1.79 1.82 1.86 1.91
17 730 0.000112 84.5 202 5 407 3.0 21.36 0.0 0.1
2.23 2.11 1.98 1.89 1.81 1.74 1.67 1.73 1.57 1.53
1.50 1.48 1.46 1.45 1.45 1.47 1.49
17 730 0.000112 84.5 202 5 407 3.0 21.36 0.0 0.1
2.36 2.22 2.07 1.99 1.90 1.83 1.77 1.72 1.67 1.63
1.60 1.57 1.55 1.53 1.52 1.51 1.52
17 730 0.000112 81 202 5 407 3.0 21.36 0.0 0.1
4.01 3.72 3.59 3.43 3.30 3.22 3.15 3.09 3.07 3.02
2.99 2.97 2.96 2.95 2.98 3.08 3.16
17 730 0.000112 82.4 202 5 407 3.0 21.4 0.0 0.1
3.29 3.04 2.85 2.72 2.66 2.58 2.52 2.48 2.45 2.43
2.41 2.40 2.39 2.39 2.41 2.43 2.53

REFERENCES

1. Richardson F.D. - Iron and Coal Review 1961, p. 1105.
2. Haberman W.L. & Morton R.R. - Amer.Soc. of Civ. Engrs. No. 2799, p.227.
3. Moore D.W. - J. of Fluid Mech. 1959, 6, 113.
4. Moore D.W. - J. of Fluid Mech. 1965, 23, pt4, 749.
5. Hartunian R.A. & Sears W.R. - J. of Fluid Mech. 1957,3,27
6. Davies R.M., Taylor G.I. - Proc. Roy.Soc.A,1950,200,375.
7. Rosenburg B, Report 727, David Taylor Model Basin, U.S. Navel Dept. 1950.
8. Collins R.A. - Journal of Fluid Mech. 1966, 25 pt3, 469
9. Rippin D.W.T. - Chem.Eng.Sci. 1967, Vol.22, p217-228.
10. Davidson J.F. & Harrison D. - Fluidised Particles 1963 p.132.
11. Birkoff G. Zarantonello E.H. - Jets, Wakes and Cavities p. 290
12. Moeller W. - Phys. Zeit 1938, 39, 57.
13. Marshal D. Stanton T.E. - Proc.Roy.Soc.A, 1938,130,295.
14. Flachsbart O. - La. M.M. 15, 1935, 32-7.
15. Whitman W.G. - Chem. Met. Eng. 1923, 29, 146.
16. Whitman W.G. & Lewis W.K. - Ind.Eng.Chem. 1924,16,1215.
17. Higbie R. - Trans Am. Inst. Chem. Engrs. 1935, 31, 365.
18. Danckwerts P.V. - Ind. Eng. Chem. 1951, 43, 1460.
19. Harriott P. - Chem. Eng. SCI. 1962, 17, 149.
20. Baird M.H.I. & Davidson J.F. - Chem.Eng.SCI.1962,17,87.
21. Lochiel A.C. & Calderbank P.H. - Chem.Eng.SCI.1964,19,483

REFERENCES

22. Beek W.J. & Kramers H. - Chem.Eng.SCI. 1962, 16, 909.

23. Ledig P.G. & Weaver E.R. - J.A.C.S. 1924,46,650 and Ind. Eng. Chem. 1924,16,1231.

24. Guyer A. & Pfister X. - Helv. Chim Acta 29,1173,1946.

25. Datta R.L., Napier D.H. & Newitt D.M. - T.I.C.E.14,28, 1950.

26. Coppock P.D. & Meiklejohn G.T. - T.I.C.E., 75,29,1951.

27. Hammerton, D. & Garner F.H. - T.I.C.E. 32, 1954, S.18.

28. Deindorfer F.H. & Humphrey A.E. - Ind. & Eng. Chem. 53, No.9, 1961, 755.

29. Clarke - Ph.D. Thesis Birmingham 1962.

30. Leonard J.H.G. & Houghton - Chem.Eng. Sci.18.133,1963.

31. Calderbank P.H. & Lochiel A.C.-Chem.Eng.Sci.19,485,1964.

32. Davenport W.G. - Ph.D. Thesis London 1963.

33. Larsen B.M. & Sordahl L.O. - Int.Symp. on Phys.Chem of Pres.Met. 1959.

34. Darken L.S. & Gurry R.W. - Phys.Chem of Metals,McGraw Hill Book Co. 1953.p.480-485.

35. Szekely A.G. - Linde Co. Tonowanda, N.York, U.S. Private Communication.

36. Niwa, Shimoji, Kishida, Itoh. - The Physical Chemistry of Process Metallurgy. p.689.Ed.St.Piere

37. Pehlke, R.D. & Bement A.L. - Trans. A.I.M.E.224,1237,1962

38. Uno S. & Kintner R.C. - A.I.Ch.E.Journal, Vol2,No.3. 1956, 420.

39. Downey P.J. - Revertex Ltd., London. Private Communc.

40. Collins R. - Chem.Eng. Sci. 22, 89, 1967.

REFERENCES

41. Maxworthy T. - J. Fluid Mech.(1967) Vol.27,Pt2,pp.367-8.

42. Bird Stewart & Lightfoot - 'Transport Phenomena'

43. Baird M.H.I. - Trans.Far.Soc. 56,213,1960.

44. Astarita G. & Apuzzo G. - A.I.Ch.E.Jounral,11,No.5,p819.

45. Davidson J.F. & Cullen E.J. - T.I.C.E. 1957,35,p.51.

46. Hodgman C.D. - "Handbook of Chemistry & Physics" Chemical Rubber Publishing Co.

47. Smithells C.J. - "Metals Reference Book" Butterworth & Co. (Publishers) Ltd. London (1962)

48. Mizikar E.A., Grace R.E. & Parlee N.A.D. - Trans A.S.M. 56, 103, (1963).

49. Johnson Matthey & Co.Ltd. London. - Private Communication.

50. Davies J.T. & Vose R.W. - Proc.Roy.Soc.Ldn.A,1965,286,218

51. Van den Tempel,M. & Van de Riet,R.P. - J.Chem. Physics, 1965,42,2769.

52. Davies J.T. & Rideal E.K. - Interfacial Phenomena p.267 Academic Press 1961.

53. Lynn S, Straatemeier J.R. & Kramers H. - Chem.Eng.Sci. 1955,4,p.59.

54. Cullen & Davidson J.F. - Trans Far.Soc. 53,113,1957.

55. Seidell A. - Solubilities of Inorganic & Metal Organic D. Van Nostrand, New York, (1940).

56. Sieverts A. & Hagenacker J. - Zeit. Physik. Chem., 68, 115, (1909).

57. Davidson J.F. & Cullen E.J. - Chem.Eng.Sci. 1956,6,49.

58. Elliott J.F., Gleiser M. & Ramakrishna V. - Thermo Chemistry for Steelmaking Vol.2. p.631.

REFERENCES

59. Davidson J.F. - Cambridge University, Private Commn.

60. Tadake T. & Maeda S. - Chem.Eng. (Japan) 25.4.1961.p.260.

61. Masson C.R. & Whiteway S.G. - Atlantic Regional Lab., N.R.C. Halifax. N.S., N.R.C.0000.

62. Diaz C., Masson C.R. & Richardson F.D. - Min.Proc. and Extractive Metallurgy Vol.75,1966.

63. Carmichael, Hornaday, Morris, Parlee - Trans A.I.M.E. 218 1960, 826.

64. Laidler K.J. Chemical Kinetics. McGraw Hill p.260.

65. Berg, D, Patterson, A. J.Am.Chem. Soc. 1953 75 5197

66. Adamson A.W. Physical Chemistry of Surfaces, p.61 Interscience Publishers.

ACKNOWLEDGEMENTS

Sincere appreciation is extended to Professor A.V. Bradshaw for the encouragement and guidance given throughout the research project.

Discussions with members of the John Percy and Nuffield Research Groups have been both stimulating and useful, whilst the technical assistance of the Workshop Staff is gratefully acknowledged.

Finally, I would like to thank my wife for typing this thesis.

R. Guthrie.

APPENDIX 6.4 (cont.)

OXYGEN ABSORPTION IN SILVER (1020°C) cont.

```
I5  730  0.000II2  8I.0  202  5  407  3  2I.4  0.0  0.I
3.86  3.52  3.36  3.I7  2.94  2.83  2.75  2.70  2.62  2.60  2.6
2.64  2.65  2.72  2.80
I5  730  0.000II2  8I.0  202  5  407  3  2I.4  0.0  0.I
4.66  4.27  3.96  3.76  3.60  3.46  3.36  3.30  3.22  3.20  3.2
3.24  3.25  3.32  3.40
I5  730  0.000II2  85.7  202  5  407  3  2I.4  0.0  0.I
I.50  I.32  I.I9  I.08  I.0  0.9  0.82  0.76  0.72  0.70  0.70
0.7I  0.7I  0.72  0.73
I7  730  0.000II2  85.7  202  5  407  3  2I.4  0.0  0.I
I.56  I.43  I.29  I.I8  I.08  I.00  0.94  0.90  0.88  0.86  0.86
0.85  0.86  0.86  0.87  0.87  0.88
I7  730  0.000II2  85.0  202  5  407  3  2I.4  0.0  0.I
2.I2  I.98  I.80  I.68  I.56  I.47  I.37  I.29  I.25  I.22  I.20
I.I8  I.I7  I.I7  I.I8  I.20  I.25
I7  730  0.000II2  85  202  5  407  3  2I.4  0.0  0.I
2.I0  I.95  I.84  I.7I  I.60  I.52  I.42  I.33  I.26  I.24  I.22
I.20  I.I9  I.I8  I.I9  I.20  I.24
I7  730  0.000II2  84  202  5  407  3  2I.4  0.0  0.I
2.45  2.30  2.20  2.I0  2.00  I.92  I.85  I.80  I.75  I.72  I.70
I.66  I.65  I.65  I.65  I.66  I.70
I5  730  0.000II2  80  202  5  407  3  2I.4  0.0  0.I
5.25  4.9  4.6  4.35  4.I  3.9  3.7  3.55  3.45  3.4  3.4  3.45
3.55  3.75  3.80
I7  730  0.000II2  86  202  5  407  3  2I.4  0.0  0.I
I.I6  I.06  0.98  0.90  0.80  0.70  0.65  0.60  0.55  0.50  0.50
0.46  0.46  0.46  0.48  0.50  0.55
I5  730  0.000II2  86  202  5  407  3  2I.4  0.0  0.I
I.3I  I.20  I.08  0.96  0.90  0.85  0.80  0.76  0.72  0.7I  0.70
0.7I  0.72  0.73  0.74
```

CO_2 Absorption in Tap Water. (2nd. Set of Expts)

No correction reqd. for Volume Differences (see page 202)

```
12  0.855  294  0.0177  52.41  5  9.56  0.0  0.6682
12.2  12.37  12.51  12.67  12.80  12.94  13.07  13.18
13.29  13.39  13.50  13.59
12  0.855  294  0.0177  52.41  5  9.98  0.0  0.6773
14.11  14.32  14.50  14.63  14.77  14.92  15.05  15.18
15.30  15.42  15.50  15.60
12  0.855  294  0.0177  52.41  5  9.28  0.0  0.6727
13.17  13.40  13.62  13.75  13.90  14.07  14.19  14.29
14.43  14.50  14.61  14.67
11  0.855  294  0.0177  52.41  5  9.60  0.0  0.6663
12.60  12.86  13.00  13.17  13.30  13.45  13.60  13.71
13.82  13.91  14.10
11  0.855  294  0.0177  52.41  5  14.37  0.0  0.6805
13.10  13.34  13.48  13.58  13.66  13.76  13.81  13.88
13.90  13.90  13.90
10  0.855  294  0.0177  52.41  5  14.36  0.0  0.7200
14.00  14.18  14.41  14.51  14.60  14.66  14.69  14.75
14.78  14.80
10  0.855  294  0.0177  52.41  5  14.34  0.0  0.7500
16.10  16.30  16.50  16.62  16.75  16.77  16.90  17.00
17.04  17.08
10  0.855  294  0.0177  52.41  5  14.37  0.0  0.7114
14.12  14.42  14.66  14.82  15.00  15.13  15.27  15.37
15.48  15.55
10  0.855  294  0.0177  52.41  5  14.30  0.0  0.7200
13.07  13.10  13.39  13.66  13.86  14.04  14.20  14.38
14.50  14.58
***T
```

CO_2 ABSORPTION IN TAP WATER (1st set of expts.)

```
18 0.9 292 0.0177 52.41 5 9.60 0 0.4033
14.6 14.8 15.0 15.23 15.45 15.65 15.85 16.0
16.17 16.30 16.42 16.60 16.73 16.80 16.92 17.05
17.20 17.30
17 0.90 292 0.0177 52.41 5 9.91 0 0.4315
18.40 18.45 18.70 18.85 19.08 19.22 19.37 19.44
19.60 19.70 19.80 19.90 20.00 20.10 20.20 20.25
20.37
16 0.9 292 0.0177 52.41 5 14.425 0 0.4325
10.05 10.25 10.48 10.60 10.70 10.80 10.82 10.90
10.98 11.10 11.20 11.22 11.22 11.22 11.22 11.22
18 0.9 292 0.0177 52.41 5 9.90 0.0 0.4033
20.60 20.60 20.73 21.0 21.1 21.2 21.3 21.4 21.5
21.6 21.65 21.75 21.80 21.85 21.85 21.85 22.0
22.05
18 0.9 292 0.0177 52.41 5 9.92 0.0 0.4033
13.80 13.85 13.80 13.90 14.05 14.25 14.45 14.65
14.80 14.95 15.03 15.19 15.24 15.33 15.40 15.42
15.50 15.60
17 0.9 292 0.0177 52.41 5 9.547 0.0 0.4315
14.82 15.00 15.20 15.40 15.58 15.66 15.85 16.10
16.22 16.40 16.55 16.55 16.65 16.85 17.00 17.00
16.95*
16 0.9 292 0.0177 52.41 5 14.625 0.0 0.4315
16.15 16.30 16.55 16.75 16.85 16.95 17.08 17.20
17.34 17.42 17.52 17.50 17.80 17.90 18.00 18.00

16 0.9 292 0.0177 52.41 5 14.50 0.0 0.433
13.30 13.40 13.65 13.92 14.10 14.26 14.38 14.50
14.60 14.67 14.73 14.85 14.90 14.99 14.99 15.05

16 0.9 292 0.0177 52.41 5 14.14 0.0 0.434
15.80 15.82 16.1 16.28 16.52 16.70 16.85 17.02
17.11 17.22 17.33 17.37 17.50 17.70 17.70 17.*70

20 0.9 292 0.0177 52.41 5 14.21 0.0 0.348
12.58 12.58 12.58 12.63 12.95 13.10 13.21 13.30
13.36 13.45 13.48 13.55 13.62 13.67 13.72 13.73
13.80 13.80 13.80 13.88

22 0.9 292 0.0177 52.41 5 4.99 0.0 0.390
8.00 8.00 8.00 8.08 8.25 8.40 8.55 8.62 8.78 8.94
9.08 9.22 9.38 9.43 9.59 9.66 9.70 9.88 9.98 9.16
9.22 9.20

23 0.9 292 0.0177 52.41 5 4.875 0.0 0.392
14.00 14.18 14.28 14.40 14.60 14.72 14.90 15.00
15.13 15.25 15.40 15.52 15.62 15.81 15.96 16.10
16.24 16.38 16.47 16.61 16.71 16.82 16.95
19 0.9 292 0.0177 52.41 5 29.68 0.0 0.310
22.65
23.00 23.08 23.26 23.40 23.41 23.43 23.40 23.35
23.16 23.00 22.77 22.60 22.37 22.02 21.61 21.52
21.22 20.83
21 0.902 291.82 0.0177 52.41 5 19.86 0 0.299
13.00 13.16 13.18 13.20 13.22 13.22 13.20 13.18
13.10 13.07 13.02 12.98 12.95 12.90 12.80 [illegible]
12.70 12.58 12.48 12.39 12.26
21 0.902 291.82 0.0177 52.41 5 19.375 0 0.300
14.52 14.80 14.92 15.04 15.10 15.12 15.12 15.09 15.02
14.97 14.87 14.80 14.72 14.67 14.62 14.49 14.39
14.28 14.17 14.00 13.85
21 0.902 291.82 0.0177 52.41 5 19.395 0 0.304
17.41 17.63 17.80 17.99 18.02 18.18 18.24 18.36
18.40 18.41 18.42 18.42 18.40 18.35 18.25 18.18
18.08 18.01 17.94 17.85 17.80
20 0.902 291.81 0.0177 52.41 5 4.99 0 0.390
8.00 8.08 8.25 8.40 8.55 8.62 8.78 8.94 9.08 9.22
9.38 9.43 9.59 9.66 9.70 9.88 9.98 10.16 10.22
10.20
24 0.902 291.82 0.0177 52.41 5 5.0 0 0.390
10.82 10.94 11.07 11.02 11.60 11.53 11.68 11.85
12.00 12.20 12.33 12.48 12.63 12.80 12.93 12.98
13.13 13.22 13.20 13.43 13.55 13.65 13.75 13.85

24 0.902 291.82 0.0177 52.41 5 4.820 0 0.392
17.16 17.35 17.52 17.70 17.83 18.02 18.17 18.35
18.45 18.62 18.74 18.84 19.02 19.15 19.28 19.40
19.50 19.61 19.75 19.85 19.96 20.05 20.15 20.20

19 0.902 291.82 0.0177 52.41 5 29.73 0 0.3228
14.34 14.73 15.16 15.50 15.80 16.14 16.35 16.60
16.65 16.63 16.55 16.43 16.22 16.02 15.86 15.65
15.40 15.15 14.92

19 0.902 291.82 0.0177 52.41 5 39.50 0 0.3228
14.81 15.00 15.00 14.98 14.94 14.76 14.60 14.21
13.83 13.45 13.02 12.63 12.17 11.65 11.18 10.60
9.98 9.43 9.00

21 0.902 291.82 0.0177 52.41 5 19.56 0 0.302
23.75 24.02 24.18 24.41 24.56 24.67 24.73 24.81
24.86 24.90 24.93 24.90 24.92 24.89 24.86 24.84
24.79 24.78 24.68 24.62 24.59

21 0.902 291.82 0.0177 52.41 5 19.12 0 0.304
22.80 23.06 23.20 23.32 23.38 23.42 23.46 23.49
23.50 23.50 23.50 23.50 23.48 23.42 23.41 23.37
23.34 23.25 23.1 3.09 22.98

21 0.902 291.82 0.0177 52.41 5 19.62 0 0.308
21.58 21.78 21.85 21.95 22.08 22.10 22.19 22.17
22.17 22.16 22.08 22.00 21.93 21.84 21.76 21.72
21.65 21.56 21.40 21.28 21.00

22 0.902 291.82 0.0177 52.41 5 19.34 0 0.308
21.42 21.80 22.15 22.39 22.61 22.76 22.95 23.09
23.23 23.30 23.36 23.42 23.42 23.42 23.42 23.42
23.41 23.14 23.67 23.38 23.35 23.28

20 0.902 291.82 0.0177 52.41 5 29.54 0 0.309
21.92 22.02 22.06 22.02 22.02 22.02 22.01 22.01
22.00 21.95 21.80 21.65 21.55 21.42 21.20 21.00
20.75 20.55 20.22 19.88

20 0.902 291.82 0.0177 52.41 5 29.34 0 0.312
23.93 24.35 24.67 24.90 25.05 25.26 25.40 25.41
25.39 25.39 25.25 25.06 24.90 24.70 24.58 24.38
24.16 23.98 23.68 23.41

19 0.902 291.82 0.0177 52.41 5 39.12 0 0.312
20.18 20.40 20.70 20.92 20.98 20.82 20.62 20.47
20.26 19.98 19.62 19.22 18.78 18.37 17.90 17.40
16.84 16.36 15.80
```

CO_2 ABSORPTION IN 0.05% Aq. P.V.A Soln

```
12 0.88 292.6 0.0177 52.41 5 9.45 0.0 0.6245
16.60 16.69 16.72 16.72 16.71 16.64 16.55 16.50
16.41 16.36 16.26 16.16
12 0.88 292.6 0.0177 52.41 5 9.20 0.0 0.6273
19.70 19.78 19.78 19.76 19.70 19.65 19.59 19.52
19.43 19.30 19.20 19.09
11 0.88 292.6 0.0177 52.41 5 10.52 0.0 0.665
16.18 16.27 16.26 16.20 16.12 16.05 15.90 15.80
15.695 15.55 15.39
10 0.88 292.6 0.0177 52.41 5 10.2 0.0 0.761
17.30 17.41 17.41 17.38 17.29 17.19 17.085 17.00
16.82 16.675
12 0.88 292.6 0.0177 52.41 5 4.35 0.0 0.70
17.51 17.61 17.59 17.62 17.61 17.67 17.74 17.76
17.76 17.76 17.75 17.74
12 0.88 292.6 0.0177 52.41 5 4.58 0.0 0.692
17.30 17.40 17.46 17.50 17.50 17.50 17.50 17.58
17.58 17.58 17.56 17.57
12 0.88 292.6 0.0177 52.41 5 4.32 0.0 0.674
15.20 15.27 15.30 15.31 15.37 15.39 15.41 15.46
15.49 15.50 15.53 15.56
12 0.88 292.6 0.0177 52.41 5 4.58 0.0 0.690
16.11 16.18 16.20 16.21 16.21 16.21 16.21 16.21
16.19 16.18 16.15 16.11
10 0.88 292.6 0.0177 52.41 5 14.47 0.0 0.697
16.58 16.67 16.65 16.59 16.49 16.29 16.13 15.93
15.70 15.48
10 0.88 292.6 0.0177 52.41 5 14.05 0.0 0.725
16.80 16.93 16.91 16.86 16.72 16.54 16.35 16.16
15.92 15.68
11 0.88 292.6 0.0177 52.41 5 14.38 0.0 0.697
16.62 16.72 16.70 16.61 16.50 16.34 16.17 15.99
15.75 15.52 15.34
10 0.88 292.6 0.0177 52.41 5 19.49 0.0 0.694
17.06 17.15 17.08 16.99 16.75 16.58 16.28 15.99
15.60 15.21
9 0.88 292.6 0.0177 52.41 5 19.50 0.0 0.680
18.10 18.21 18.21 18.11 17.99 17.75 17.52 17.19
[illegible]
9 0.88 292.6 0.0177 52.41 5 19.37 0.0 0.691
17.33 17.50 17.50 17.33 17.11 16.88 16.60 16.28
15.92
9 0.88 292.6 0.0177 52.41 5 19.49 0.0 0.834
17.63 17.76 17.64 17.50 17.18 16.86 16.41 16.05
15.60
**
```

CO_2 ABSORPTION IN 4.2% Aq. P.V.A Soln (46cp)

```
10 0.815 293.1 0.0177 52.0 5 19.54 0.0 0.687
19.54 19.59 19.59 19.59 19.53 19.43 19.24 19.08
18.88 18.62
11 0.815 293.1 0.0177 52.0 5 19.53 0.0 0.636
19.42 19.49 19.51 19.44 19.39 19.28 19.13 18.99
18.80 18.63 18.40
9 0.815 293.1 0.0177 52.0 5 29.0 0.0 0.640
19.84 19.82 19.74 19.54 19.28 19.00 18.65 18.27
17.82
10 0.815 293.1 0.0177 52.0 5 29.30 0.0 0.648
17.02 17.05 17.01 16.78 16.58 16.27 15.96 15.54
15.13 14.65
9 0.815 293.1 0.0177 52.0 5 39.07 0.0 0.666
17.06 17.00 16.78 16.43 15.99 15.49 14.88 14.24
13.50
9 0.815 293.1 0.0177 52.0 5 39.14 0.0 0.666
19.86 19.80 19.63 19.21 18.78 18.29 17.73 17.09
16.38
9 0.815 293.1 0.0177 52.0 5 39.10 0.0 0.678
18.90 18.90 18.68 18.30 17.80 17.30 16.71 16.00
15.26
8 0.815 293.1 0.0177 52.0 5 38.04 0.0 0.765
19.41 19.40 19.15 18.69 18.24 17.62 16.94 16.16
9 0.815 293.1 0.0177 52.0 5 59.0 0.0 0.634
21.50 21.36 21.0 20.51 19.90 19.27 18.12 16.68
15.50
9 0.815 293.1 0.0177 52.0 5 58.9 0.0 0.685
20.50 20.30 20.00 19.50 18.90 18.19 17.37 16.58
15.45
12 0.815 293.1 0.0177 52.0 5 8.8 0.0 0.657
16.30 16.35 16.42 16.55 16.60 16.64 16.65 16.70
16.68 16.71 16.72 16.69
12 0.815 293.1 0.0177 52.0 5 9.0 0.0 0.687
18.00 18.10 18.17 18.28 18.32 18.36 18.37 18.37
18.37 18.36 18.34 18.30
12 0.815 293.1 0.0177 52.0 5 9.66 0.0 0.624
15.34 15.42 15.50 15.61 15.66 15.70 15.72 15.73 15.74
15.74 15.76 15.76
12 0.815 293.1 0.0177 52.0 5 9.95 0.0 0.636 15.85
15.92 15.98 16.02 16.06 16.08 16.12 16.13 16.08 16.05
15.98 15.94
12 0.815 293.1 0.0177 52.0 5 4.90 0.0 0.642
16.35 16.39 16.46 16.50 16.53 16.56 16.56 16.61 16.65
16.68 16.72 16.78
12 0.815 293.1 0.0177 52.0 5 5.0 0.0 0.648 17.10
17.21 17.26 17.30 17.34 17.38 17.42 17.46 17.50 17.51
17.53 17.55
11 0.815 293.1 0.0177 52.0 5 4.73 0.0 0.775 18.12
18.17 18.26 18.32 18.35 18.38 18.41 18.43 18.45 18.45
18.50
9 0.815 293.1 0.0177 52.0 5 58.5 0.0 0.680 19.46
19.28 18.94 18.30 17.40 16.40 15.30 14.14 12.65
*
```

CO_2 ABSORPTION IN 5.6% Aq. P.V.A Soln (130cp)

```
15 0.783 294.5 0.0177 51.9 5 4.92 0.0 0.556
15.38 15.48 15.50 15.54 15.59 15.64 15.68 15.74 15.74
15.76 15.80 15.82 15.86 15.86 15.88
15 0.783 294.5 0.0177 51.9 5 4.60 0.0 0.600
16.65 16.71 16.76 16.82 16.88 16.94 16.98 17.03 17.07
```

[illegible]
15.38 15.48 15.50 15.54 15.59 15.64 15.68 15.74 15.74
15.76 15.80 15.82 15.86 15.86 15.88
15 0.783 294.5 0.0177 51.9 5 4.60 0.0 0.600
16.65 16.71 16.76 16.82 16.88 16.94 16.98 17.03 17.07
17.10 17.14 17.18 17.22 17.24 17.28
14 0.783 294.5 0.0177 51.9 5 4.43 0.0 0.640
18.12 18.15 18.22 18.28 18.32 18.36 18.41 18.46 18.50
18.52 18.55 18.57 18.62 18.64
15 0.783 294.5 0.0177 51.9 5 4.53 0.0 0.606
13.62 13.68 13.73 13.79 13.84 13.90 13.96 14.02 14.08
14.13 14.19 14.24 14.29 14.32 14.38
15 0.783 294.5 0.0177 51.9 5 4.75 0.0 0.598
14.83 14.89 14.95 14.98 15.02 15.08 15.11 15.15 15.18
15.20 15.23 15.25 15.30 15.34 15.87
12 0.783 294.5 0.0177 51.9 5 9.94 0.0 0.670
16.59 16.69 16.67 16.73 16.80 16.86 16.91 16.97 17.00
17.02 17.05 17.09
12 0.783 294.5 0.0177 51.9 5 9.66 0.0 0.675
17.74 17.82 17.92 18.00 18.05 18.10 18.12 18.13 18.16
18.16 18.17 18.17
11 0.783 294.5 0.0177 51.9 5 14.37 0.0 0.625
16.93 17.00 17.06 17.12 17.16 17.16 17.15 17.11 17.08
17.01 16.95
12 0.783 294.5 0.0177 51.9 5 9.74 0.0 0.657
15.76 15.86 15.98 16.07 16.14 16.21 16.25 16.33 16.39
16.43 16.47 16.48
10 0.783 294.5 0.0177 51.9 5 19.42 0.0 0.665
17.48 17.54 17.60 17.63 17.64 17.61 17.55 17.45 17.30
17.14
10 0.783 294.5 0.0177 51.9 5 19.51 0.0 0.686
15.69 15.80 15.85 15.89 15.87 15.83 15.72 15.62 15.50
15.32
11 0.78 294.5 0.0177 51.9 5 19.50 0.0 0.618
16.72 16.78 16.81 16.84 16.84 16.81 16.76 16.65 16.51
16.39 16.22
12 0.78 294.5 0.0177 51.9 5 19.38 0.0 0.549
17.50 17.50 17.60 17.62 17.63 17.61 17.*60 17.55 17.47
17.34 17.20 17.07
11 0.78 294.5 0.0177 51.9 5 29**.47 0.0 0.600
15.01 15.09 15.08 15.00 14.91 14.77 14.58 14.31 14.08
13.73 13.39
11 0.78 294.5 0.0177 51.9 5 29.42 0.0 0.536
16.26 16.30 16.29 16.23 16.14 15.99 15.82 15.65 *15.38
15.09 14.76
11 0.78 294.5 0.0177 51.9 5 38.5 0.0 0.544
17.18 17.10 17.00 16.86 16.62 16.30 15.94 15.63 15.21
14.70 14.16
11 0.78 294.5 0.0177 51.9 5 39.45 0.0 0.562
17.47 17.41 17.34 17.20 16.99 16.69 16.34 15.99 15.54
15.06 14.50
11 0.78 294.5 0.0177 51.9 5 39.32 0.0 0.545
18.00 17.95 17.84 17.70 17.50 17.20 16.84 16.44 16.00
15.51 14.98
11 0.78 294.5 0.0177 51.9 5 39.40 0.0 0.572
17.60 17.50 17.42 17.29 17.09 16.78 16.43 16.08 15.60
15.10 14.50
12 0.78 294.5 0.0177 51.9 5 59.24 0.0 0.485
18.71 18.55 18.22 17.90 17.39 16.82 16.29 15.70 15.00
14.21 13.38 12.48
12 0.78 294.5 0.0177 51.9 5 59.15 0.0 0.480
17.70 17.58 17.30 16.91 16.49 15.92 15.28 14.50 13.76
12.90 12.01 11.14

CO_2 ABSORPTION IN 6.7% Aq. P.V.A Soln (300cp)

5 ≤ V < 400 cc.

14 0.785 294.3 0.0177 42.41 5 9.45 -0.008067 0.0 0.550
16.12 16.22 16.28 16.34 16.41 16.49 16.51 16.58 16.62
16.66 16.69 16.72 16.76 16.80
14 0.785 294.3 0.0177 42.41 5 9.50 -0.008067 0.0 0.565
18.10 18.14 18.21 18.27 18.34 18.41 18.50 18.56 18.60
18.66 18.71 18.76 18.80 18.83
14 0.785 294.3 0.0177 42.41 5 9.49 -0.008067 0.0 0.582
16.46 16.50 16.61 16.69 16.76 16.82 16.90 16.97 17.02
17.10 17.17 17.22 17.27 17.30
13 0.785 294.3 0.0177 42.41 5 9.48 -0.008067 0.0 0.644
18.12 18.20 18.27 18.33 18.42 18.50 18.58 18.63 18.70
18.76 18.81 18.86 18.90
11 0.785 294.3 0.0177 42.41 5 19.3 -0.008067 0.0 0.660
14.55 14.63 14.70 14.75 14.78 14.79 14.79 14.76 14.71
14.68 14.60
12 0.785 294.3 0.0177 42.41 5 19.27 -0.008067 0.0 0.618
16.23 16.36 16.50 16.58 16.64 16.70 16.74 16.76 16.78
16.78 16.74 16.68
12 0.785 294.3 0.0177 42.41 5 19.29 -0.008067 0.0 0.614
18.71 18.83 18.98 19.07 19.11 19.16 19.20 19.22 19.22
19.23 19.22 19.18
9 0.785 294.3 0.0177 42.41 5 39.45 -0.008067 0.0 0.614
15.95 15.95 16.00 16.00 16.00 15.97 15.89 15.79 15.63
13 0.785 294.3 0.0177 42.41 5 39.20 -0.008067 0.0 0.460
18.10 18.08 18.10 18.11 18.11 18.10 18.09 18.04 18.00
17.92 17.85 17.75 17.65
14 0.785 294.3 0.0177 42.41 5 39.20 -0.008067 0.0 0.411
20.70 20.69 20.72 20.72 20.72 20.72 20.70 20.68 20.66
20.60 20.55 20.50 20.40 20.30
9 0.785 294.3 0.0177 42.41 5 39.45 0.0 0.0 0.614
15.95 15.95 16.00 16.00 16.00 15.97 15.89 15.79 15.63
9 0.785 294.3 0.0177 51.86 5 39.45 0.0 0.0 0.614
15.95 15.95 16.00 16.00 16.00 15.97 15.89 15.79 15.63
13 0.785 294.3 0.0177 51.86 5 39.20 0.0 0.0 0.460
18.10 18.08 18.10 18.11 18.11 18.10 18.09 18.04 18.00
17.92 17.85 17.75 17.65
14 0.785 294.3 0.0177 51.86 5 39.20 0.0 0.0 0.411
20.70 20.69 20.72 20.72 20.72 20.72 20.70 20.68 20.66
20.60 20.55 20.50 20.40 20.30

CO_2 ABSORPTION IN 8.45% Aq. P.V.A Soln (735cp)

~~[illegible]~~) 5 ≤ V ≤ 30 cc

16 0.853 291.3 0.0177 36.33 5 9.64 -0.01789 0.0 0.615
14.00 14.05 14.08 14.08 14.09 14.10 14.11 14.11 14.11
14.10 14.10 14.10 14.09 14.04 14.00 13.99
16 0.853 291.3 0.0177 36.33 5 9.71 -0.01789 0.0 0.630
14.49 14.50 14.51 14.51 14.56 14.57 14.59 14.59 14.60
14.59 14.58 14.56 14.54 14.51 14.50 14.46
18 0.853 291.3 0.0177 36.33 5 4.52 -0.01789 0.0 0.644
14.80 14.84 14.86 14.90 14.90 14.94 14.97 15.00 15.01
15.01 15.06 15.09 15.11 15.12 15.15 15.16 15.18 15.20
20 0.853 291.3 0.0177 36.33 5 4.72 -0.01789 0.0 0.650
15.68 15.72 15.76 15.77 15.80 15.82 15.84 15.87 15.90
15.90 15.91 15.93 15.95 15.97 15.98 16.00 16.00 16.00
16.01 16.02
14 0.853 291.3 0.0177 36.33 5 14.8 -0.01789 0.0 0.636
16.20 16.27 16.29 16.30 16.30 16.30 16.30 16.28 16.23
16.18 16.11 16.02 15.99 15.88
13 0.853 291.3 0.0177 36.33 5 14.13 -0.01789 0.0 0.666
17.69 17.71 17.73 17.74 17.74 17.73 17.70 17.68 17.60
17.50 17.47 17.36 17.26
13 0.853 291.3 0.0177 36.33 5 14.70 -0.01789 0.0 0.660
18.20 18.20 18.21 18.21 18.21 18.20 18.16 18.10 18.03
17.95 17.86 17.76 17.64
12 0.853 291.3 0.0177 36.33 5 19.56 -0.01789 0.0 0.670
15.95 15.91 15.90 15.89 15.86 15.82 15.76 15.69 15.60
15.50 15.39 15.25
13 0.853 291.3 0.0177 36.33 5 19.71 -0.01789 0.0 0.655
15.49 15.495 15.50 15.48 15.44 15.40 15.34 15.29 15.21
15.11 15.06 14.88 14.74

30 ≤ V < 100 cc.

12 0.853 291.3 0.0177 36.33 5 29.84 -0.01789 0.0 0.634
16.82 16.80 16.77 16.69 16.595 16.480 16.32 16.16 15.93
15.69 15.41 15.10
12 0.853 291.3 0.0177 36.33 5 29.68 -0.01789 0.0 0.640
16.50 16.48 16.40 16.32 16.21 16.09 15.93 15.73 15.50
15.22 14.95 14.40
11 0.853 291.3 0.0177 48.64 5 39.32 -0.00550 0.0 0.663
15.68 15.51 15.35 15.11 14.86 14.56 14.23 13.86 13.45
12.97 12.50
11 0.853 291.3 0.0177 48.64 5 39.56 -0.00550 0.0 0.620
14.44 14.34 14.20 13.99 13.77 13.50 13.20 12.89 12.51
12.09 11.61
10 0.853 291.3 0.0177 48.64 5 49.69 -0.00550 0.0 0.617
18.16 17.68 17.00 16.26 15.44 14.55 13.53 12.50 11.40
10.10
10 0.853 291.3 0.0177 48.64 5 49.30 -0.00550 0.0 0.655
19.90 19.70 19.50 19.10 18.75 18.30 17.81 17.30
16.67 16.00
0

CO_2 DESORPTION FROM TAP WATER (1cp)

12 0.90 292 0.0177 52.55 5 8.95 0.0 0.524
14.80 14.39 13.88 13.41 12.95 12.50 12.04 11.53
11.03 10.50 10.00 9.43
14 0.90 292 0.0177 52.55 5 10.35 0.0 0.526
15.15 14.75 14.18 13.65 13.15 12.67 12.18 11.69
11.18 10.63 10.10 9.50 8.85 8.20
13 0.90 292 0.0177 52.55 5 12.85 0.0 0.530
17.55 17.00 16.33 15.68 15.08 14.49 13.88 13.25
12.40 11.90 11.20 10.46 9.66
13 0.90 292 0.0177 52.55 5 12.85 0.0 0.546
18.50 17.90 17.30 16.71 16.20 15.67 15.07 14.45
13.82 13.14 12.40 11.65 10.88
12 0.90 292 0.0177 52.55 5 12.0 0.0 0.546
19.75 19.18 18.52 17.90 17.30 16.78 16.20 15.60
15.00 14.30 13.62 12.90
12 0.90 292 0.0177 52.55 5 13.35 0.0 0.540
16.99 16.20 15.50 14.78 14.08 13.35 12.62 11.88
11.10 10.20 9.30 8.40
12 0.92 291 0.0177 52.55 5 9.0 0.0 0.540
16.50 16.09 15.59 15.16 14.70 14.23 13.75 13.29
12.79 12.26 11.73 11.17
14 0.92 291 0.0177 52.55 5 9.0 0.0 0.540
17.88 17.50 17.00 16.53 16.10 15.68 15.24 14.79
14.31 13.82 13.30 12.80 12.23 12.68
12 0.92 291 0.0177 52.55 5 14.35 0.0 0.544
18.8 18.15 17.30 16.52 15.80 15.10 14.33 13.53
12.75 11.95 11.00 10.10
13 0.92 291 0.0177 52.55 5 12.55 0.0 0.544
21.20 20.55 20.0 19.48 18.83 18.22 17.62 16.95
16.28 15.55 14.80 14.00 13.16
13 0.92 291 0.0177 52.55 5 12.35 0.0 0.544
21.42 20.79 20.19 19.60 19.00 18.42 17.82 17.20
16.52 15.85 15.14 14.40 13.62
13 0.92 291 0.0177 52.55 5 12.55 0.0 0.547
21.15 20.65 20.05 19.50 18.87 18.83 17.78 17.18
16.50 15.89 15.23 14.50 13.72
13 0.92 291 0.0177 52.55 5 12.0 0.0 0.547
21.2 20.52 20.04 19.50 18.88 18.34 17.80 17.20
16.55 15.90 15.25 14.55 13.75
15 0.92 291 0.0177 52.55 5 10.1 0.0 0.540
20.85 20.40 19.90 19.39 18.91 18.47 18.00 17.50
16.99 16.42 15.86 15.29 14.65 14.00 13.40
14 0.92 291 0.0177 52.55 5 10.60 0.0 0.54
19.55 19.02 18.50 17.87 17.30 16.78 16.26 15.65
15.06 14.45 13.77 13.16 12.42 11.73
14 0.92 291 0.0177 52.55 5 10.10 0.0 0.544
21.65 21.20 20.74 20.25 19.80 19.34 18.88 18.40
17.88 17.35 16.77 16.18 15.54 14.90
14 0.90 292 0.0177 52.55 5 7.25 0.0 0.552
19.55 19.15 18.72 18.32 17.94 17.50 17.09 16.69
16.24 15.79 15.33 14.83 14.30 13.78
14 0.90 292 0.0177 52.55 5 7.25 0.0 0.56
20.65 20.20 19.80 19.40 19.00 18.63 18.18 17.77
17.40 16.85 16.46 15.86 15.32 14.77
14 0.90 292 0.0177 52.55 5 7.25 0.0 0.566
18.80 18.40 17.97 17.54 17.14 16.74 16.32 15.90
15.44 15.03 14.50 14.00 13.49 12.87
15 0.90 292 0.0177 52.55 5 7.25 0.0 0.55
20.55 20.19 19.85 19.50 19.18 18.80 18.50 18.11
17.74 17.41 16.90 16.50 16.00 15.50 15.09
14 0.90 292 0.0177 52.55 5 7.25 0.0 0.555
19.87 19.50 19.10 18.75 18.40 18.01 17.65 17.24
16.81 16.40 16.00 15.56 15.09 14.60
15 0.90 292 0.0177 52.55 5 3.60 0.0 0.570
17.55 17.26 17.02 16.79 16.53 16.26 15.96 15.71
15.43 15.16 14.87 14.55 14.22 13.89 13.53
12 0.90 292 0.0177 52.55 5 3.60 0.0 0.570
19.95 19.80 19.58 19.33 19.13 18.88 18.65 18.44
18.30 18.12 18.00 17.78
15 0.90 292 0.0177 52.55 5 3.60 0.0 0.575
20.22 20.00 19.76 19.53 19.30 19.09 18.82 18.60
18.36 18.10 17.84 17.59 17.29 17.00 16.70
14 0.90 [illegible] 52.55 5 3.60 0.0 0.575
18.75 18.45 18.18 17.90 17.69 17.40 17.18 16.90
16.60 16.30 16.00 15.70 15.39 15.06
0
•••Z
***